Repair of Reinforced Concrete Bridge Columns via Plastic Hinge Relocation

Volume 2: Repair Using CFRP Materials

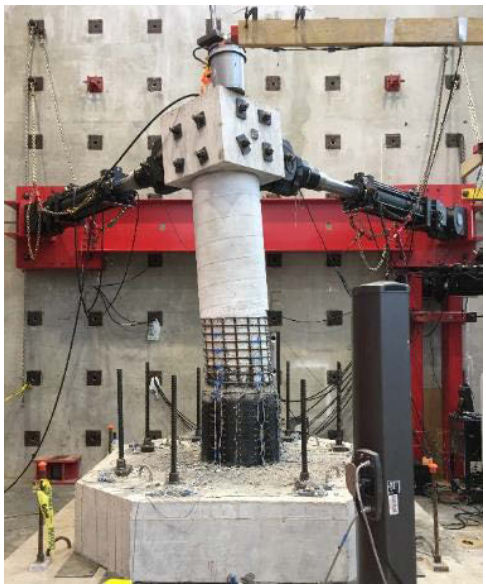

Photo of Plastic Hinge Relocation Test#2 taken by Emrah Tasdemir, June 2018

Prepared By:
Emrah Tasdemir, Ph.D. Candidate
Rudolf Seracino, Professor, Ph.D.
Mervyn J. Kowalsky, Professor, Ph.D.
James M. Nau, Professor, Ph.D.

Prepared For:
Alaska Department of Transportation & Public Facilities
Research, Development, and Technology Transfer
P.O. Box 112500
3132 Channel Drive
Juneau, Alaska 99811-2500

and

Federal Highway Administration
P.O. Box 21648
709 West 9th Street
Juneau, Alaska 99802-1648

REPORT DOCUMENTATION PAGE

Form approved OMB No.

1. AGENCY USE ONLY (LEAVE BLANK)	2. REPORT DATE	3. REPORT TYPE AND DATES COVERED
4000(142)	September 30, 2018	Final Report, May 2015 through September 2018

4. TITLE AND SUBTITLE

Repair of Reinforced Concrete Bridge Columns via Plastic Hinge Relocation
Volume 2: Repair Using CFRP Materials

5. FUNDING NUMBERS
Federal #: 4000(142)
IRIS #: Z839740000

6. AUTHOR(S)
Zachary F. Krish, Ph.D.
Mervyn J. Kowalsky, Professor, Ph.D.
James M. Nau, Professor, Ph.D.
Rudolf Seracino, Professor, Ph.D.

7. PERFORMING ORGANIZATION NAME(S) AND ADDRESS(ES)
Alaska Department of Transportation and Public Facilities
Research, Development & Technology Transfer
3132 Channel Drive
Juneau, Alaska 99811-2500

8. PERFORMING ORGANIZATION REPORT NUMBER
4000(142)

9. SPONSORING/MONITORING AGENCY NAME(S) AND ADDRESS(ES)

State of Alaska, Alaska Dept. of Transportation and Public Facilities
Research and Technology Transfer
3132 Channel Drive
Juneau, AK 99801-7898

10. SPONSORING/MONITORING AGENCY REPORT NUMBER
4000(142)

11. SUPPLEMENTARY NOTES

12a. DISTRIBUTION / AVAILABILITY STATEMENT
Copies available online at http://www.dot.alaska.gov/stwddes/research/search_lib.shtml

12b. DISTRIBUTION CODE

13. ABSTRACT (Maximum 200 words)
The goal of this report is to present a repair procedure for seismically damage reinforced concrete bridge columns via plastic hinge relocation. To repair the damaged columns, CF anchors were utilized. Thus, the behavior of CF anchors was studied through various testing method and design procedures were developed. In addition, the reliability of proposed design procedure was shown with large scale testing.

14- KEYWORDS :
Reinforced concrete bridges, Repairing, Earthquake resistant design, Plastic hinge relocation, Buckled reinforcement, Fractured reinforcement

15. NUMBER OF PAGES
191

16. PRICE CODE
N/A

17. SECURITY CLASSIFICATION OF REPORT	18. SECURITY CLASSIFICATION OF THIS PAGE	19. SECURITY CLASSIFICATION OF ABSTRACT	20. LIMITATION OF ABSTRACT
Unclassified	Unclassified	Unclassified	None

SI* (MODERN METRIC) CONVERSION FACTORS

APPROXIMATE CONVERSIONS TO SI UNITS

Symbol	When You Know	Multiply By	To Find	Symbol
		LENGTH		
in	inches	25.4	millimeters	mm
ft	feet	0.305	meters	m
yd	yards	0.914	meters	m
mi	miles	1.61	kilometers	km
		AREA		
in^2	square inches	645.2	square millimeters	mm^2
ft^2	square feet	0.093	square meters	m^2
yd^2	square yard	0.836	square meters	m^2
ac	acres	0.405	hectares	ha
mi^2	square miles	2.59	square kilometers	km^2
		VOLUME		
fl oz	fluid ounces	29.57	milliliters	mL
gal	gallons	3.785	liters	L
ft^3	cubic feet	0.028	cubic meters	m^3
yd^3	cubic yards	0.765	cubic meters	m^3
	NOTE: volumes greater than 1000 L shall be shown in m^3			
		MASS		
oz	ounces	28.35	grams	g
lb	pounds	0.454	kilograms	kg
T	short tons (2000 lb)	0.907	megagrams (or "metric ton")	Mg (or "t")
		TEMPERATURE (exact degrees)		
°F	Fahrenheit	5 (F-32)/9 or (F-32)/1.8	Celsius	°C
		ILLUMINATION		
fc	foot-candles	10.76	lux	lx
fl	foot-Lamberts	3.426	$candela/m^2$	cd/m^2
		FORCE and PRESSURE or STRESS		
lbf	poundforce	4.45	newtons	N
lbf/in^2	poundforce per square inch	6.89	kilopascals	kPa

APPROXIMATE CONVERSIONS FROM SI UNITS

Symbol	When You Know	Multiply By	To Find	Symbol
		LENGTH		
mm	millimeters	0.039	inches	in
m	meters	3.28	feet	ft
m	meters	1.09	yards	yd
km	kilometers	0.621	miles	mi
		AREA		
mm^2	square millimeters	0.0016	square inches	in^2
m^2	square meters	10.764	square feet	ft^2
m^2	square meters	1.195	square yards	yd^2
ha	hectares	2.47	acres	ac
km^2	square kilometers	0.386	square miles	mi^2
		VOLUME		
mL	milliliters	0.034	fluid ounces	fl oz
L	liters	0.264	gallons	gal
m^3	cubic meters	35.314	cubic feet	ft^3 m^3
	cubic meters	1.307	cubic yards	yd^3
		MASS		
g	grams	0.035	ounces	oz
kg	kilograms	2.202	pounds	lb
Mg (or "t")	megagrams (or "metric ton")	1.103	short tons (2000 lb)	T
		TEMPERATURE (exact degrees)		
°C	Celsius	1.8C+32	Fahrenheit	°F
		ILLUMINATION		
lx	lux	0.0929	foot-candles	fc
cd/m^2	$candela/m^2$	0.2919	foot-Lamberts	fl
		FORCE and PRESSURE or STRESS		
N	newtons	0.225	poundforce	lbf
kPa	kilopascals	0.145	poundforce per square inch	lbf/in^2

*SI is the symbol for the International System of Units. Appropriate rounding should be made to comply with Section 4 of ASTM E380. (Revised March 2003)

Table of Contents

List of Figures

List of Tables

Executive Summary

The capacity design approach is adopted in the design of the modern bridges. During a seismic event, seismic energy input in the bridges is mitigated at the top and bottom end of the columns in the form of plastic hinges. As the formation of plastic hinge result in bar buckling and bar fracture, most of the time replacement of bridges is assumed to be essential. The bridges, located on lifelines, should be kept open right after a major seismic event for emergency response. Therefore, development of rapid repair method is crucial.

The research study presented in this report is aimed to develop a rapid repair method using the plastic hinge relocation concept. The damaged bridge columns are repaired in such a way that the moment and displacement capacity of the original column can be achieved via plastic hinge relocation. As the bar buckling and bar fracture diminishes the tensile strength of the column, the provided repair must increase tensile strength of the damaged column to force the plastic deformation in undamaged location of the columns.

The current research work focuses on use of large diameter Carbon fiber (CF) anchors and the CFRP sheets to produce a robust repair solution. CF anchors are used to transfer forces from one concrete element to another through the anchor fan and the anchor dowel. Therefore, the role of each component in force transfer mechanism should be examined. Since the available data for large diameter CF anchors are limited, an experimental program is developed to investigate behavior of CF anchors. The first set of tests focuses on determining theoretical rupture capacity. Overall sixteen large diameter tests were conducted to find theoretical rupture capacity of large diameter anchors. The results of the test showed that as the anchor diameter increases, anchors become less efficient, meaning that the correlation between fiber volume fraction and capacity is not linear. As the goal of research is to use CF anchors to repair seismically damaged columns, three column tests with single CF anchor embedded on the extreme side of columns are conducted to study behavior of the CF anchors under column bending action through monotonic loading. Each column test lead to a different failure mechanism which is addressed in the following column test. The outcome of the direct tension and the column tests are used to develop repair scenarios which includes two large-scale columns. The repair design to relocate plastic hinge in undamaged region of column while the repaired region remains elastic. For the first column test, the strength of the column is restored but the failure of the CF anchors is observed. The second large-scale

column is repaired with larger CF anchors to ensure that the repair remains elastic. The plastic hinge is pushed in undamaged region of the column without inducing any damage to the repair region. A robust repaired design is achieved using the CF anchors and CFRP sheets.

Chapter 1: Introduction

The research work in this volume of the report represents the development of a repair method for seismically damage bridge columns using carbon fiber reinforced polymer (CFRP) anchors. A pilot study by Rutledge et al. [1] showed that CFRP composites could be used to relocate a plastic hinge in seismically damaged columns as shown in Figure 1.1.

Figure 1.1: Plastic Hinge Relocation Using CFRP Anchors[1]

In this volume, comprehensive research is presented with the aim of understanding the behavior of large CFRP anchors which can be used in seismic applications. The goal is to develop a repair method which can push plastic hinges into undamaged parts of a column by increasing flexural strength of the plastic hinges occurred in the column ends after a seismic attack. To have a section with a higher flexural capacity than the original column, the degraded tension capacity

of the longitudinal bars needs to be replaced by CFRP anchors as it was done by Rutledge et al (2014) [1]. Since CFRP anchors becomes the main load carrying member in the repair, it is essential to investigate and understand behavior of CFRP anchors to achieve reliable and robust structures that can resist seismic attacks without jeopardizing capacity design principles.

1.1 Background

Over the last three decades, experimental and field application has increased the confidence in using CFRP for strengthening or repair of reinforced concrete structures. Guidelines and specifications have been introduced regarding behavior, capacity and constructability. Carbon fiber (CF) anchors are one of the structural elements that can be used in externally bonded (EB) FRP applications. CF anchors are produced from loose carbon fiber bundles that are folded in half at the looped end to produce the anchor fan and dowel as shown in Figure 1.2.

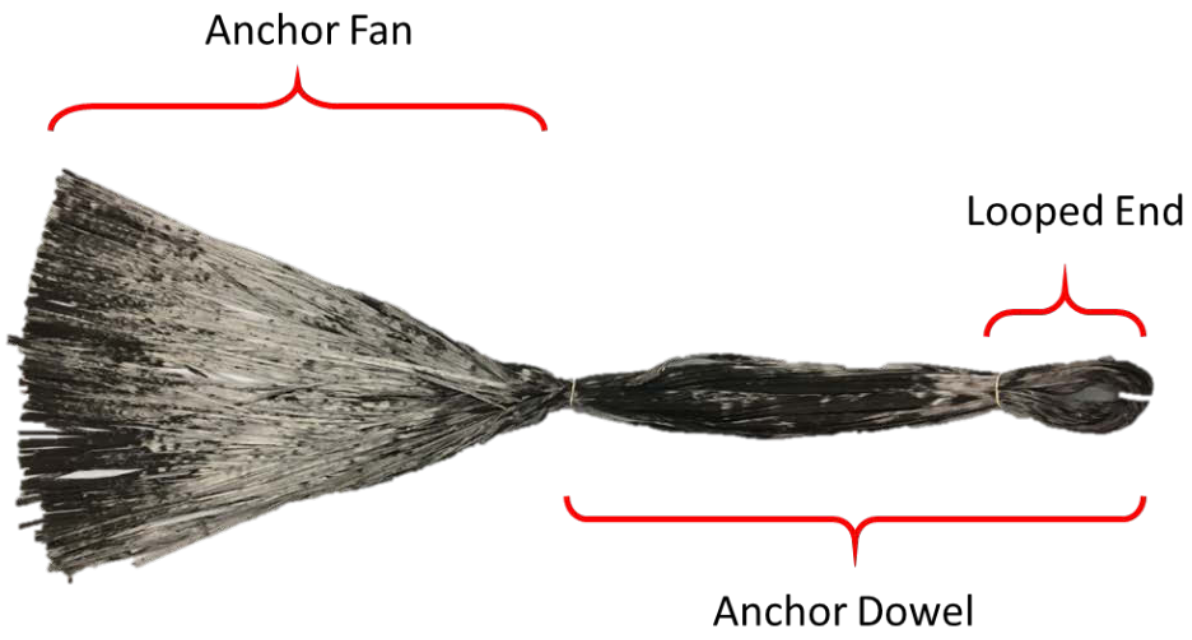

Figure 1.2: Parts of Carbon Fiber Anchor

CF anchors have been used to transfer forces from one concrete member to another one across an interface. As shown in Figure 1.3, tensile force developed in vertical CFRP sheets for flexural strengthening needs to be transmitted to the footing for continuity via the CF anchor. The

anchor fan provides the mechanism by which the force transfers to the CF anchor dowel which is epoxy bonded into a pre-drilled hole in the footing.

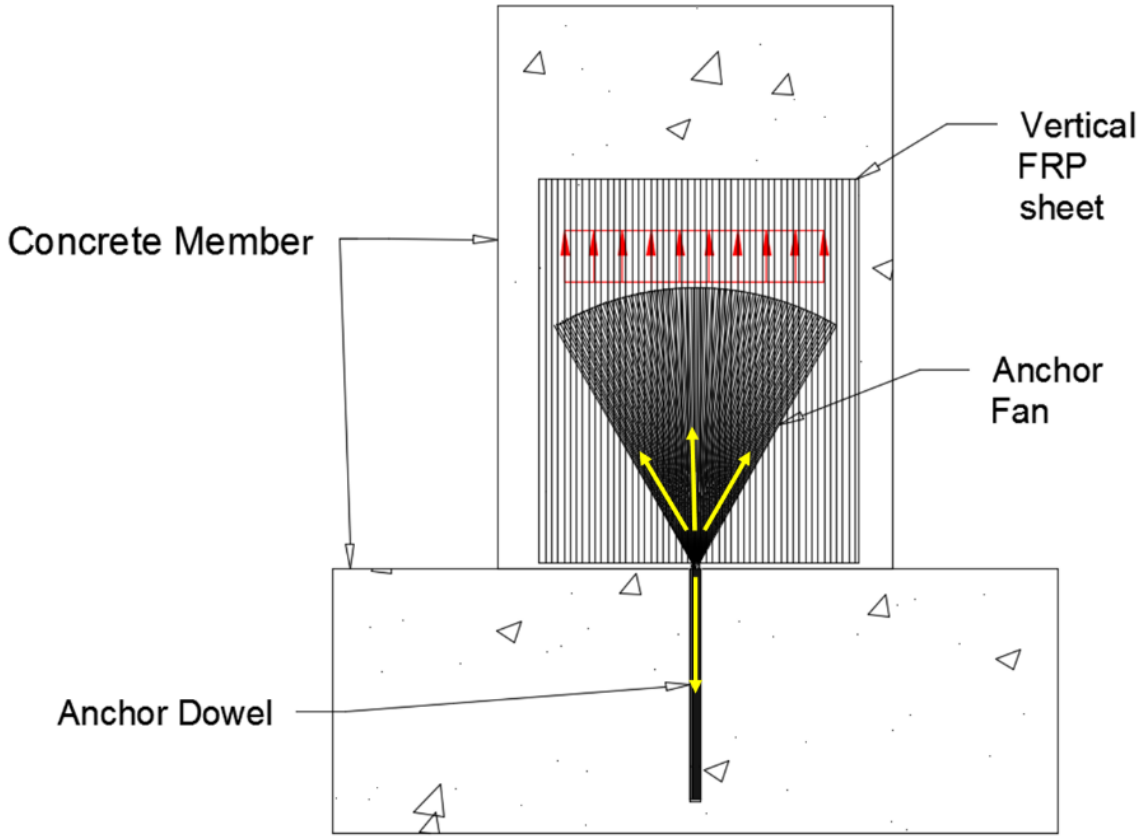

Figure 1.3: Force Transfer in Carbon Fiber Anchors

The literature provides different application of CFRP anchors for repair or retrofit of structural systems. If confinement of a column is necessary to increase ductility, for example, transverse layers of carbon fiber sheets are typically applied. However, the continuity of a transverse fiber wrap may be disrupted when a column, as shown in Figure 1.4a, has an obstruction such as concrete wing wall or masonry infill wall. In order to achieve the desired confinement, a continuous force transfer mechanism should be developed between the ends of the FRP wrap on either side of the wall. In this case, CF anchors have been used to provide the continuous force flow between the ends of FRP wrap[2].

In the flexural strengthening of reinforced concrete beams, CFRP sheets are typically bonded to the top or bottom soffits of the beam as shown in Figure 1.4b. Even though the flexural

capacity of the beams increases, premature debonding of the CFRP sheets is typically observed due to the propagation of an interfacial crack in the concrete at the bonded interface [3]. Carbon fiber anchors have been used to prevent or postpone premature debonding of the CFRP from the concrete substrate as shown in Figure 1.4b. Similarly, CFRP U-wraps, as shown in Figure 1.4c is used to increase the shear strength of beams. Due to the slab cast integrally with the beam, continuous wrapping is not readily possible. Again, premature debonding of the free ends of the U-wraps is typical [3], which can be prevented, or delay using CF anchors.

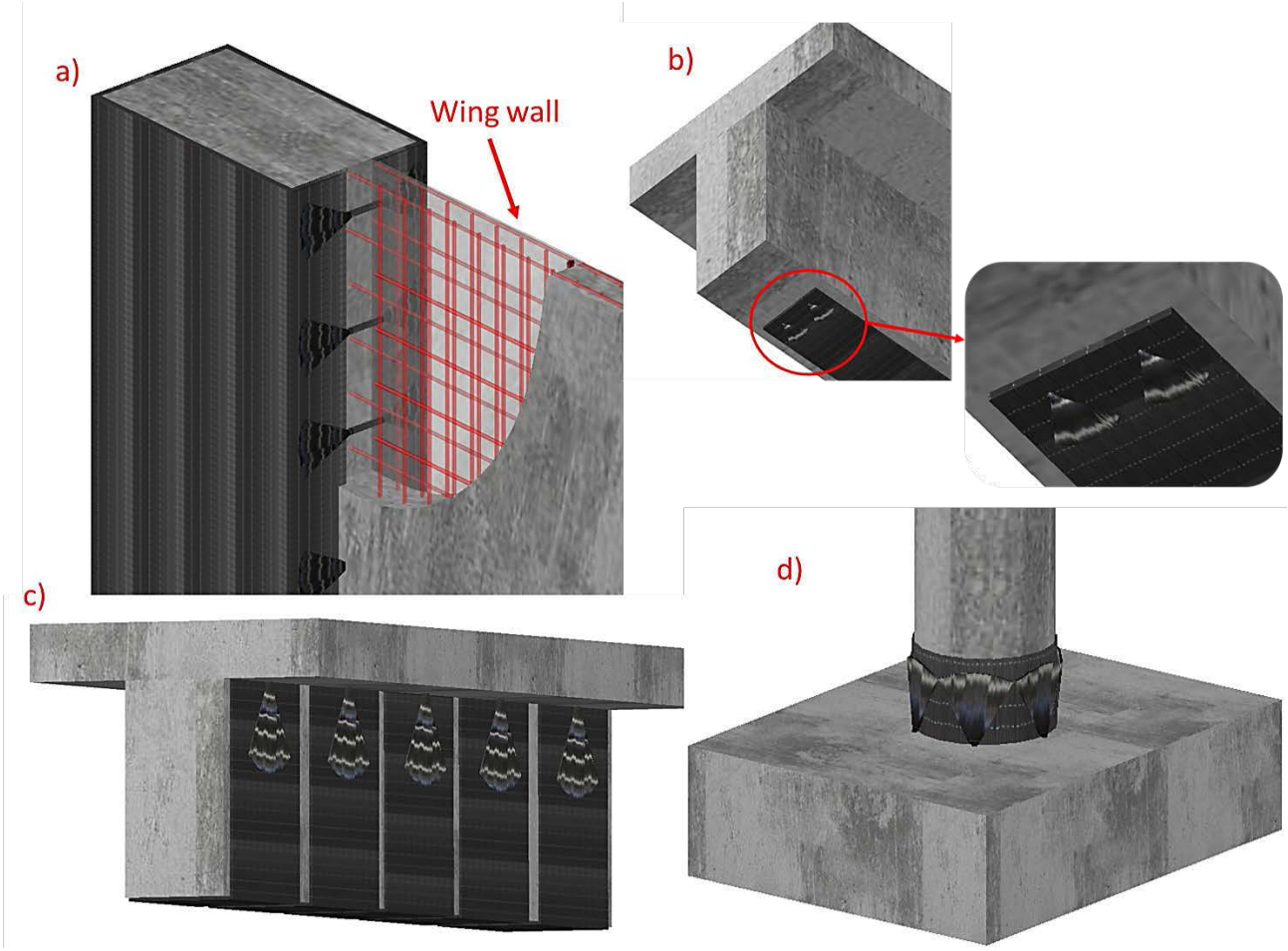

Figure 1.4: Various CFRP Anchor Applications

The FRP retrofit of substandard reinforced concrete columns has also been undertaken with the use of CF anchors [4]. The goal of adding CF anchors to columns is to increase moment

capacity of the column. Also, CFRP materials have been employed in the repair of reinforced concrete structural columns which were damaged by seismic activity [1], [5]–[8]. In one of the research studies, researchers utilized the plastic hinge relocation concept to restore moment and displacement capacity of the original column which required the use of CF anchors [1]. In this application, the purpose of CF anchors was to increase moment capacity of the repaired region to force the plastic deformations above the repaired region by transferring longitudinal tension from column to footing.

As discussed above, the use of CF anchors is becoming more common to address limitations of adhesively bonded FRP strengthening or repair systems. However, there is limited experimental data available for large diameter CF anchors of the type required in this research project. Consequently, there is a lack of robust recommendations and guidelines on the installation and design of such anchors. Therefore, there is a need to conduct a research study focusing on large diameter CF anchors to enable the goal of this research study which is to develop an all FRP repair method using plastic hinge relocation.

1.2 The Need for Research

While the use of CFRP has become more prevalent in the strengthening and repair of concrete, steel and wood structures, the lack of design and construction guidelines for CF anchors discourages widespread use of this specific structural component [9]. Establishing design and construction guidelines requires a sufficiently large experimental database, especially for composite systems due to the variable quality control of the in-situ installation. As the mechanical properties of the fibers and the resin are significantly different from each other, as shown in Figure 1.5 the composition of these two material forms a composite material with mechanical properties which may vary from one product to another due quality of installation and volume of resin used. Recognizing the variability of in-situ wet lay-up composites, it is necessary to quantify the variability of material properties to determine safe design limits for reliable applications.

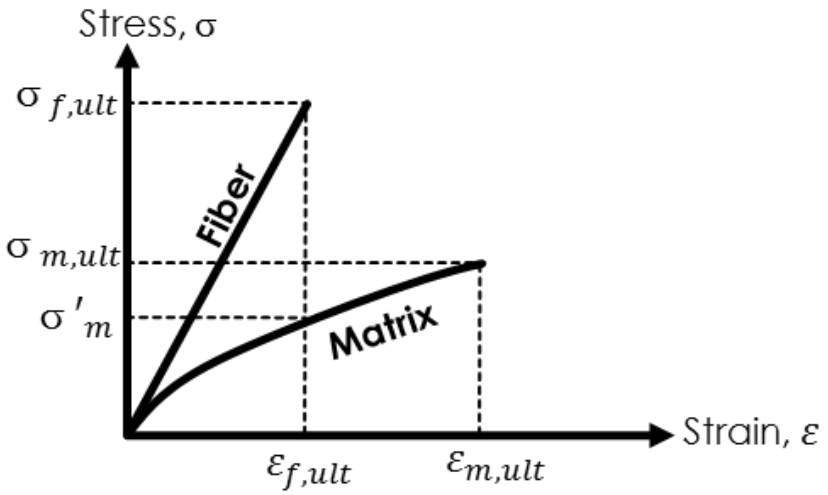

Figure 1.5: Stress-Strain Curves for Fiber and Resin

As CF anchors have become popular in structural applications, research needs have emerged to understand behavior and quantify potential failure mechanisms. Therefore, it is necessary to identify parameters that influence the behavior of CF anchors. Figure 1.6 illustrates all of the critical components of a CF anchor, including anchor diameter, fan angle, fan length and embedment depth.

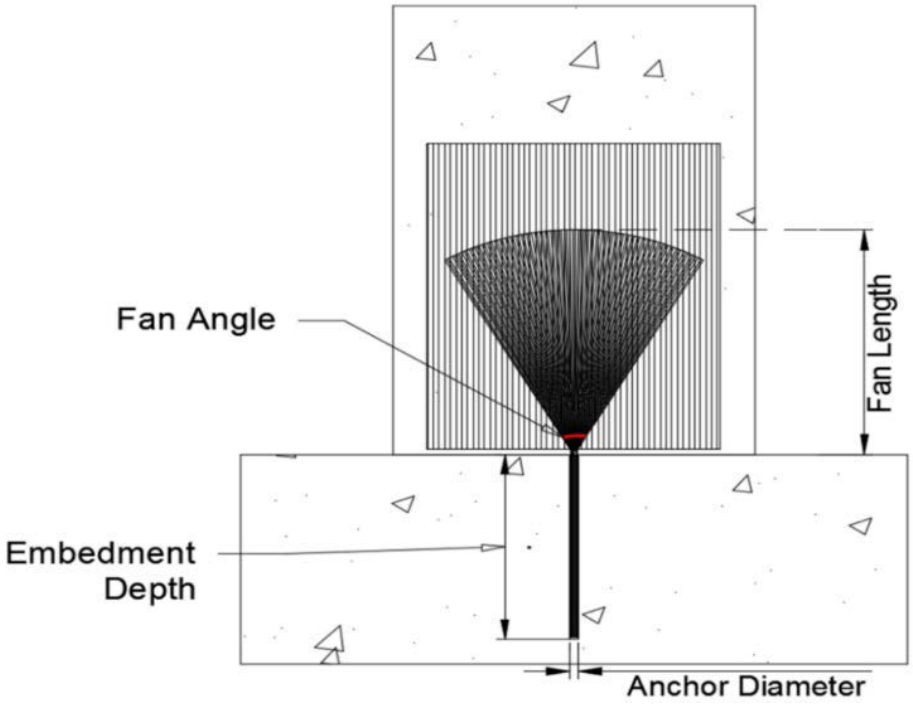

Figure 1.6: Details of Carbon Fiber Anchors

It is observed that the theoretical tensile rupture capacity of CF anchors is related to the anchor diameter [9]–[11]. This theoretical rupture capacity is often referred to as an efficiency ratio, defined by del Re Castillo et al.[11]. Efficiency is defined as the ratio of average stress developed in the bar/anchor to the manufacturer provided rupture stress of the anchor. Average stress is defined as the force developed in the bar divided by the nominal area of the anchor. The reason for the reduced efficiency with increasing diameter is attributed to the shear lag effect that plays a role in the force transfer mechanism of FRP composites bars [13]. When an FRP bar/anchor is installed in a drilled hole of concrete element, the applied tensile force is transferred to the bar/anchor by the epoxy bond developed between the concrete and the outermost fibers, as shown in Figure 1.7a. The fibers at the perimeter of the bar/anchor reach the maximum stress before the fibers towards the middle of the section. The fibers transfer force to the adjacent fibers through the softer resin matrix. Due to the shear lag effect, the stress across the section is non-uniform. The variation of stress is greater as the size of the anchor increases. That is, as the size of the anchor increases, efficiency decreases as shown in Figure 1.7b.

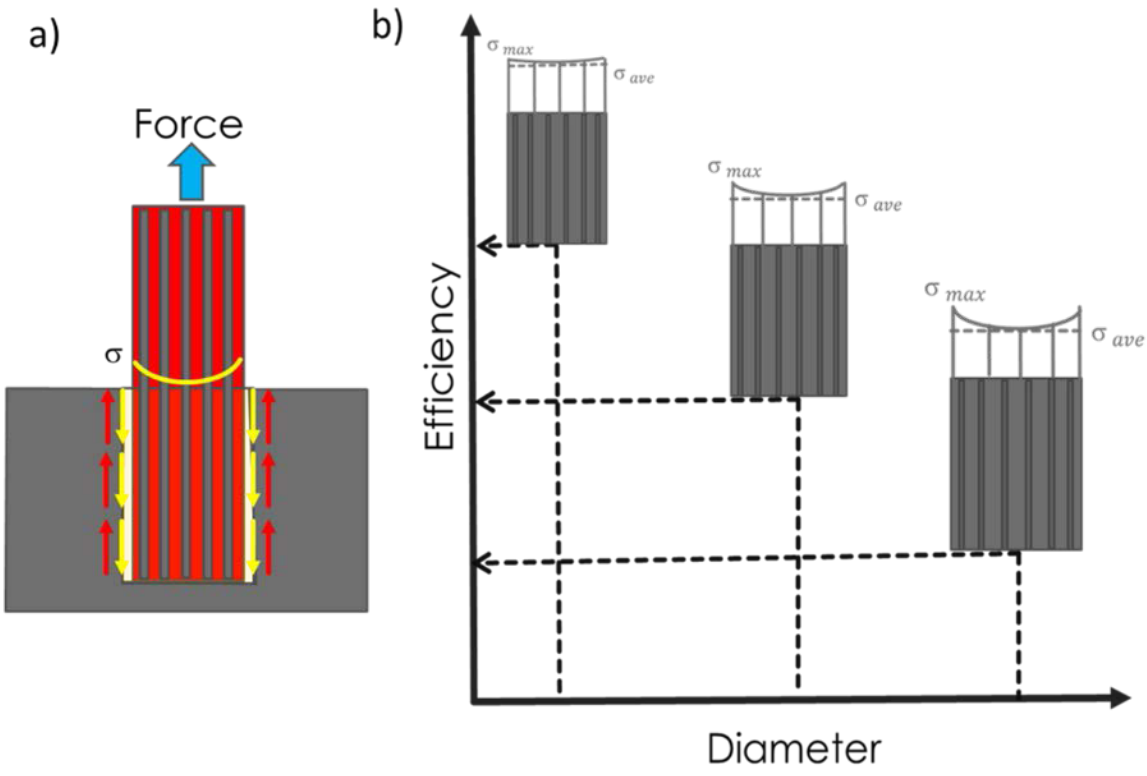

Figure 1.7: Efficiency Distribution of FRP Bar/Anchor

Because of this characteristic of fiber reinforced polymers FRP bars/anchors, it is required that the impact of anchor diameter on the capacity of the large diameter CFRP anchor should be investigated through experimental work, and statistically quantification should be done to determine reliable rupture limits for design purposes.

The anchor fan angle was another factor that has enormous influence on the capacity of carbon anchors [2], [9]–[11].It was shown that increase in fan angle resulted in reduction in the capacity of same diameter CF anchors [2], [9]–[11]. This reduction in the anchor capacity is stem from the intentional misalignment of the fibers due to transition of fiber from embedded part of the anchor to the anchor fan part. As shown in Figure 1.8, as the fibers in the fan are away from the center of fan, their contribution to the capacity of the anchor decreases as the angle (α) between the fiber and center of fan increases [2], [9]–[11]. Since distribution of the fibers in the fan part of the anchor is arbitrary regardless of the anchor fan angle, a statistical quantification is essential for a given fanning angle and anchor diameter. Again, it is required to determine the capacity of large diameter anchors since there is limited data available for large diameter CFRP anchors.

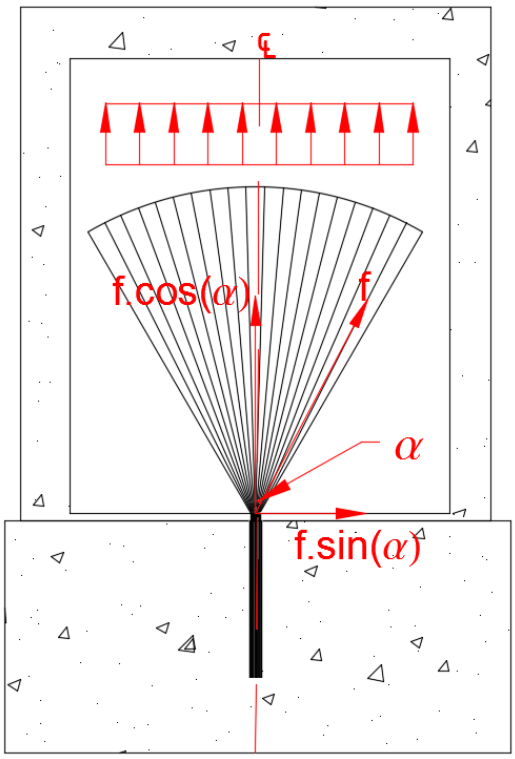

Figure 1.8: Force Components in CFRP Anchor Fan Fiber

As discussed above, for smaller fanning angles reduction in the capacity of the anchor decreases, and more efficient design can be achieved. Although smaller fanning angle may increase the capacity of the CFRP anchors, there is a reduction in the fan area which may cause debonding of anchor fan from the substrate due to smaller bonding area. In order to increase the bonding area of the fan part, a longer fan length may be needed. As the fan length increases, the area that transfers the tension force from column to anchor increases through interface shear developed between fibers and substrate. The increase in length may be required in order to develop rupture capacity of a CFRP anchor. Detailing of fan part becomes more critical when the number of available drilled holes is limited around the column. In order to resist the demand on the column, anchor fan may need to be splayed on a narrower but longer fan area for a reliable design. For instance, as shown in Figure 1.9, as the width of the anchor fan reduces from w1 to w2, anchor capacity increases due to increase in vertical force component of each fiber in the fan part. Therefore, bonded area may need to be increased by increasing length from L1 to L2.

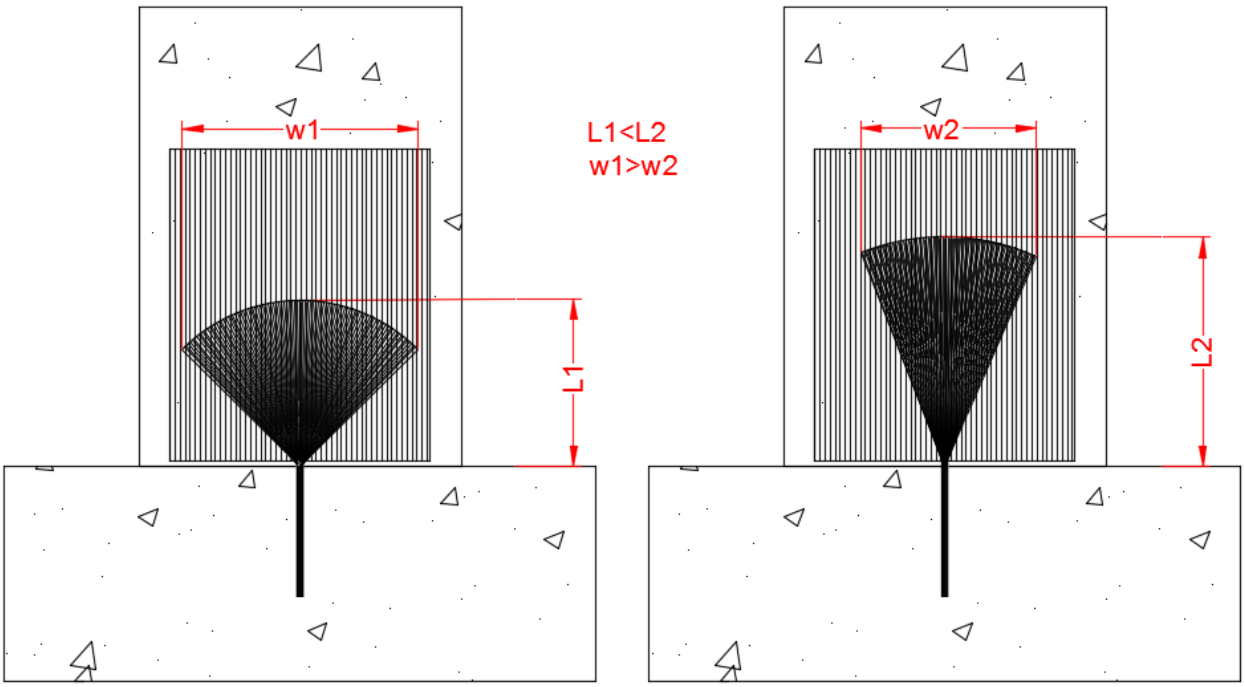

Figure 1.9: Anchor Fan Detail

Embedment depth of the anchor dowel is another factor that affects the failure mode developed in the CFRP anchors. In order to develop full rupture capacity of an anchor, embedment depth of the CFRP anchors should be long enough to prevent pull-out failure Even though there are research studies which developed methods for determination of embedment depth for CFRP anchors, the suggested method cannot be used due to size of the CFRP anchors used [12]. Developed methods to determine embedment depth for different construction material (e.g. reinforcing bars, GFRP bars) may be used to determine required embedment depth for CFRP anchors.

Available data on the large diameter CFRP anchors is not sufficient to make a capacity estimation for larger diameters due to the limited range of anchor sizes that have been tested. Therefore, there is a need for experimental work to quantify the capacity of large diameter CFRP anchors by considering parameters discussed above. Although a broad discussion on importance of this research was discussed, only a few aspects of large diameter CFRP anchors are studied.

1.3 Research Objectives

The primary objective of this research study is to develop a rapid repair method, which uses an all FRP solution to restore the lost strength and displacement capacity of the damaged column to that of the original column by plastic hinge relocation.

The specific objectives are:

- Develop test methods to examine the behavior of large diameter CF anchors.
- Determine the capacity of large diameter CF anchors which will be used in the design of the repair solution.
- Develop a design procedure for the repair of an all FPR solution.
- Develop recommendations for installation, handling, and durability FRP materials for seismic applications.

1.4 Work Plan

In order to accomplish the objectives listed above, several tasks are required:

- Investigate the rupture capacity of the CFRP anchors under direct tension
- Study impact of column bending on the CFRP anchor capacity

- Examine the effect of the fan angle and fan length on the capacity of CFRP anchors
- Develop proof of concept experiment for plastic hinge relocation

Task 1: Direct Tension Capacity of CFRP Anchors

A series of test was planned to determine rupture capacity of CFRP anchors. A critical parameter in these tests was the area (the amount of the fiber) of the anchor. The outcome of these test will help to better comprehend the impact of anchor area on the capacity of the anchor.

Task 2: The impact of Column Bending on the Capacity of the CFRP Anchors

In this task, it was intended to understand the influence of member (in this case, columns) bending on the capacity of the CFRP anchors. The tests were planned such that anchors are under tension due to column bending. A total of four column tests were planned to be conducted to investigate several parameters. Parameters were: Fan angle, fan length, and embedment depth. In addition to listed parameters, the requirement for transverse wrapping was also investigated.

Task 3: Proof of Concept Test

The main idea of this test is to develop a repair scenario using knowledge and experience which were obtained from tasks above. It was aimed to utilize plastic hinge relocation concept to restore moment and displacement capacity of the original column. Depending on damage level of the column, a repair method developed. A design procedure and construction sequence for this example were given to guide engineers.

1.5 Organization of the Report

This volume of the report contains the following chapters: Chapter 2 encompasses literature review on CFRP anchors; Chapter 3 contains experimental work conducted on determination of direct tension capacity of CFRP anchors; Chapter 4 focuses on effect of column bending on the capacity of the CFRP anchors; Chapter focuses on development of a repair design procedure and an experimental test to exhibit an example for repair via plastic hinge relocation; and Chapter 6 is the conclusions which are obtained from chapters of this volume.

Chapter 2: Literature Review

This chapter presents the literature review on FRP anchors. The purpose of the literature review is to identify parameters that were considered in past research studies and develop an understanding on how CFRP anchor has been used. The literature is arranged in historical order to provide the development done on CFRP anchors.

2.1 Advanced wrapping system with CF-anchors-Stress Transfer Mechanism of CF anchors (Kobayashi et al. 2001)

The anchors were used to generate a continuous force transfer for CFRP sheets wrapped around columns which were attached to wing walls, as shown in Figure 2.1. The direction of the force developed in the CFRP sheets changes when force is being transferred to the fan part of the anchor. Therefore, the stress transfer mechanism was studied. In order to investigate the behavior of the anchors, an experimental program was developed.

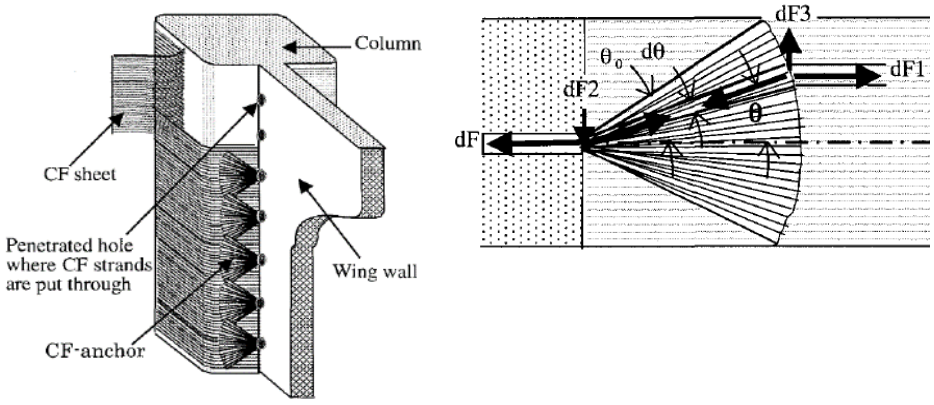

Figure 2.1: Stress transfer Mechanism in CFRP Anchors[2]

Two types of specimens were constructed as showm in Figure 2.2. The first type of specimens was constructed to investigate a single anchor with various fan lengths. The second type of specimens was built to examine multiple anchors with overlapping anchor fans. Fan length was

studied because as the length decreases, fan angle increases. The non-overlapping length was selected as one parameter because as the non-overlapping length decreases the opening of the fan part increases. For each parameter considered in the research, three different specimens were constructed.

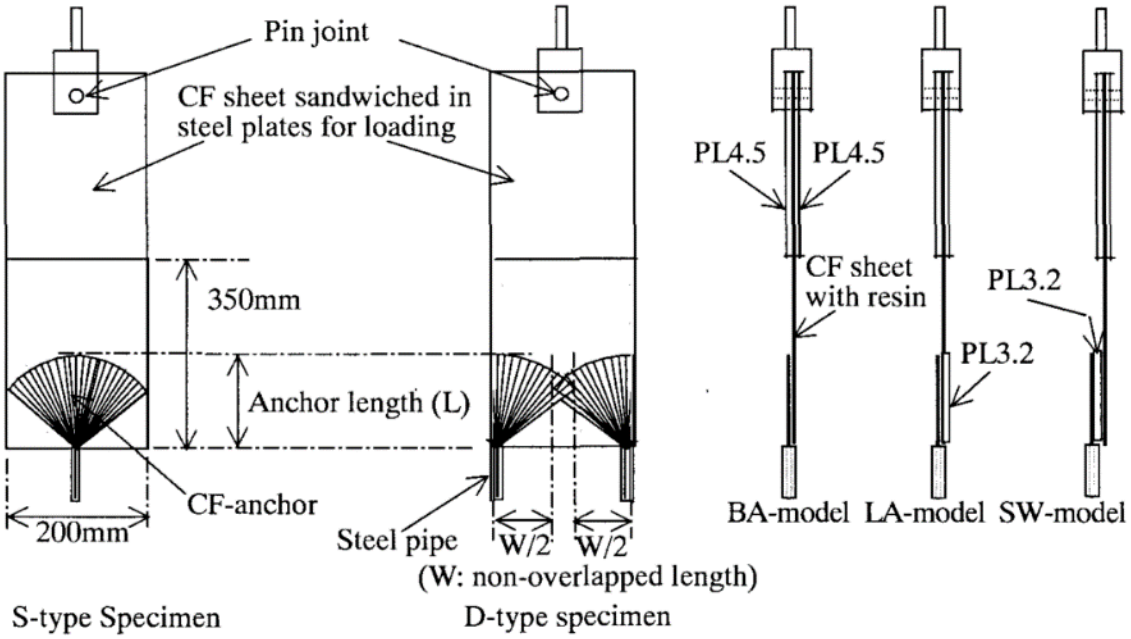

Figure 2.2: Prepared Specimen Types[2]

For the first specimen, the CFRP anchor was directly attached to CFRP sheets (BA-model) whereas for the second and third type specimens a steel plate was introduced into the setup to represent the bond between the CFRP sheets and the concrete. For one of the models, steel plate was attached to the back of the CFRP sheet (LA-model). In the setup, CFRP sheets were sandwich between steel plates (SW-model) to produce a uniform stress distribution on the anchors. The total area of the fibers in the anchor was the same as the CFRP sheet.

As the fan with for single type kept constant, an increase in capacity was observed as the fan length increased. This was attributed to reduced fan angle. When a plate was introduced between the CFRP anchor and the CFRP sheets, ultimate load became less. Similar behavior was observed in the specimens with a plate attached to the back of CFRP sheets. The reason for the

lower level of force was attributed to peeling of CFRP sheet caused by eccentricity which was produced by the plate. The developed ultimate load is shown in Figure 2.3. For all models with single anchor an increased observed for increased length. As the non-overlapping length increased, load capacity of the test specimen increased.

The strain distribution in the single anchor type specimen which was not attached to the plate was reduced as the fiber distance to center increased as shown in Figure 2.4. For the other type of single anchor, more uniform strain distribution was observed, but the magnitude of the strain was less than the ultimate strain of the CFRP sheet. This experimental work demonstrated that a significant amount of tensile force from the CFRP sheet could be transferred to the CFRP anchor as stress transfer mechanism of the key portion, which is the transition point of anchor fan fibers into anchor dowel, improved. Slightly overlapped CFRP anchors alleviated stress concertation at the center of the CFRP sheet even for the single type specimens with no plate attachment.

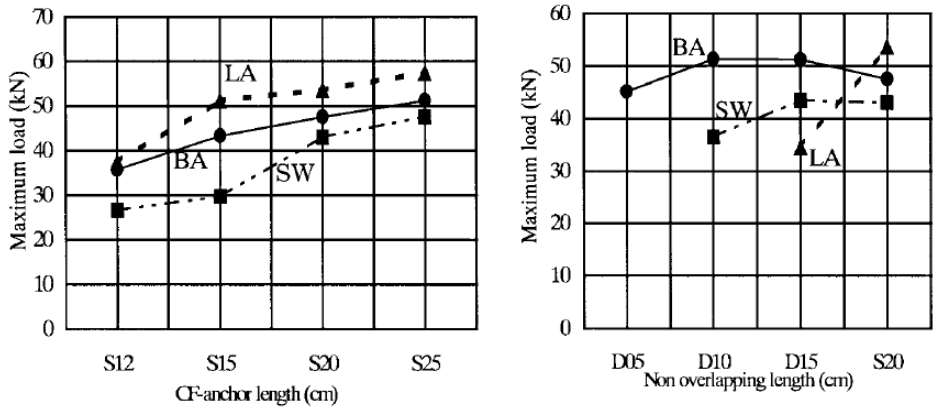

Figure 2.3: Developed Load in Anchors with Different Configuration [2]

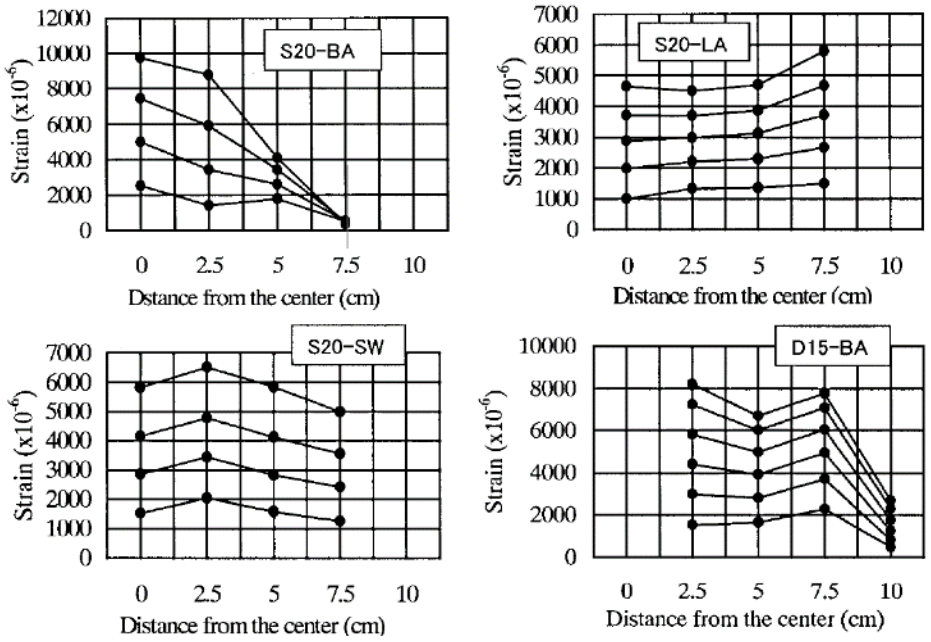

Figure 2.4: Strain Distribution in CFRP Sheets [2]

It was suggested that fan angle should be limited to an angle less than 90°. The anchor should be overlapped for better performance. A horizontal sheet should be provided, and the amount of the sheet should be more than half of the vertical CFRP sheet. Amount of fibers in the anchor should be more than the vertical CFRP sheet.

2.2 Tensile Capacities of CFRP Anchors (Ozdemir, & Akyuz 2006)

The tensile capacity of handmade CFRP anchors, meaning that a CFRP sheet was used to construct the anchors, was investigated in this research. The compressive strength of the concrete, diameter of the anchor, embedment length of the anchor and the number of fibers were parameters considered in the research. Unconfined concrete specimens were used to examine the behavior of the anchors. Two different sets of anchors were prepared by rolling CFRP sheets.

The main difference between the two sets of anchors was the preparation methods used. Figure 2-5 shows anchor preparation. The first set of anchors was prepared by rolling the CFRP sheets around itself, and the second set of anchors was prepared by rolling around a silicon rod to form a circular shape. For the first type of anchors, the widths of the CFRP sheets were 80 mm, 120 mm, and 160 mm. 120 mm CFRP sheets were used to form all the second types of anchors. Embedment lengths for the first type of anchors were 70 mm, 100 mm, and 150 mm. Concrete

strengths for the first type of anchors were 10 MPa, 16 MPa, and 20 MPa. The depth of embedment for the second type of anchor was 50 mm, 70mm, and 150mm. The concrete strengths were 10 MPa and 16 MPa for the second type anchors. The hole diameter for the first type of anchors was 12 mm, 14 mm, and 16 mm, and 20 mm was chosen for the second type of anchor.

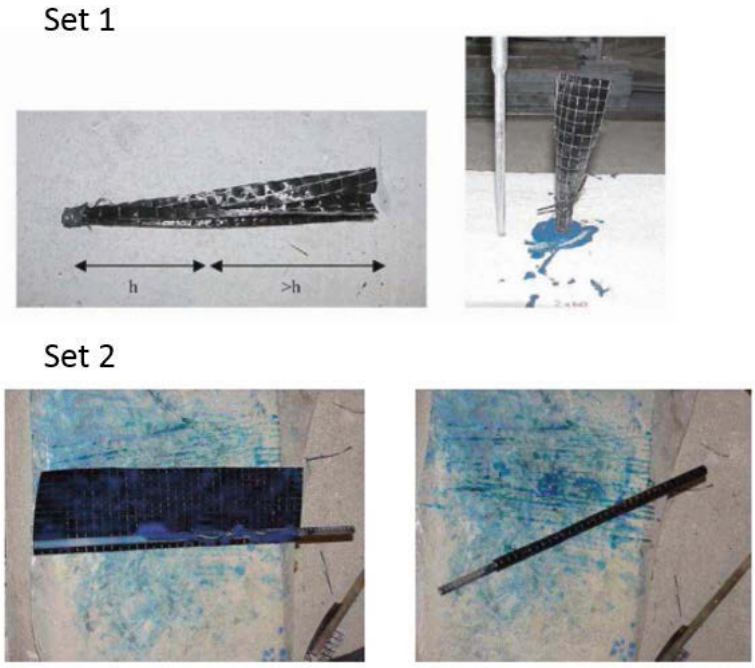

Figure 2.5: Anchor Preparation Method [13]

For the first test, results showed that the diameter of the hole did not have a substantial effect on tensile behavior. Moreover, the compressive strength of the concrete did not cause a considerable change in the behavior. As was expected, increasing the width of the CFRP increased tensile capacity, but the change was not linear. Figure 2.6 shows the nonlinear trend observed in the tensile capacity of anchors. The increase of the embedment length increases the tensile capacity, but at some point, the increase was almost constant. The results for the second set of anchors showed that for a given embedment length, the effect of concrete compressive strength was significant, and for an increased embedment length the capacity of the anchors was increased. After a certain embedment length, increase in the pull-out capacity reduced. For the parameters

that were considered in the research, the highest capacity was reached when the embedment length was 100 mm.

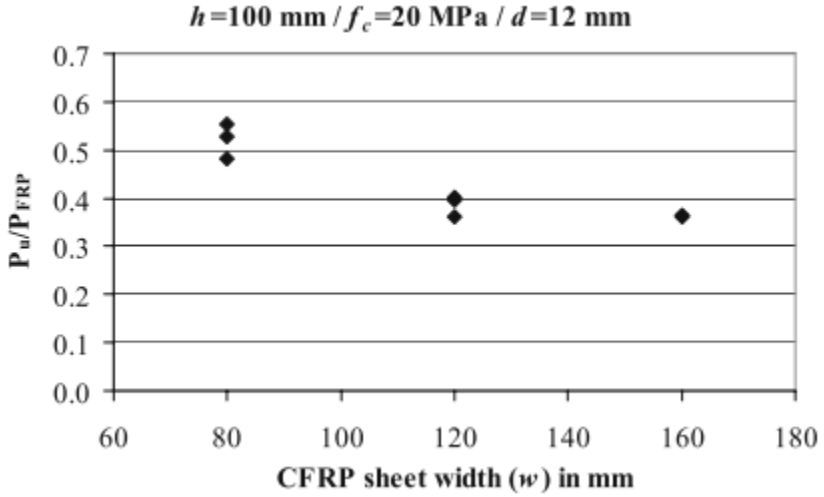

Figure 2.6: Effect of Fiber Content on Anchor Capacity [13]

2.3 Tensile Behavior of FRP Anchors in Concrete (Ozbakkaloglu and Saatcioglu , 2009)

This research focused on determining the tensile strength of the hand-made FRP anchors. In total, 81 FRP anchors were tested under applied tensile load. The anchor diameters were 12.7 mm, 15.9 mm and 19.1 mm. The embedment length was varied from 25 to 100 mm. Handmade anchors were made by rolling CFRP sheets. Two different concrete cylinders were used to examine anchor behavior. For the first set of anchors, 200 mm diameter concrete cylinders were used, but concrete splitting failure occurred. For the second set of anchors, the diameter of the cylinders was increased to prevent concrete splitting. Figure 2.7 shows the specimen tested in the study.

Figure 2.7: Prepared Test Specimen [14]

Three different failure modes were observed during the experiments. Figure 2.8 shows the failed specimens. Observed failure mode included: concrete splitting, anchor rupture, and anchor pullout. A total of 5 specimens experienced concrete splitting failure, whereas 68 specimens failed by anchor pullout. Moreover, anchor rupture took place in 8 specimens. Concrete pullout or combined cone-bond pullout was the primary failure modes observed in 68 specimens. It was observed that concrete cone failure only occurs in the specimen with the 25 mm embedment length. The remaining anchor failed by combined cone-bond failure.

The outcome of the experiments is summarized as follows. When the depth of embedment increased, the concrete cone depth decreased. The increase in the embedment depth also increased pullout capacity of the anchors. It was also observed that when the anchor diameter and the depth of embedment were increased, the average bond strength started decreasing. The reason was assumed to be Poisson's effect. Pullout force on the anchor caused a reduction in the diameter due to Poisson's effect. Increasing the depth of embedment reduced the bond strength. This showed that bond stress was non-uniform along the length of the FRP anchor. The effect of concrete strength was not significant on the bond strength of the anchors.

Figure 2.8: Observed Failure Mode in Tested Specimens[14]

For the 12.7 mm anchors with a 50 mm embedment length, the average bond strength were the same for the high strength and normal strength concrete. It was observed that the theoretical tension capacity of the anchors was larger than the actual tension capacities. This was attributed uneven strained fibers in the anchors due to the misalignment of the fibers. It was noted that when anchors were embedded with an angle, the pull-out capacity of the anchor was reduced.

2.4 Behaviour of Handmade FRP Anchors under Tensile Load in Uncracked Concrete (Kim & Smith 2010)

Tensile behavior of handmade CFRP anchors which were embedded into unreinforced concrete blocks was studied in this research. Additionally, the results from previous research projects were used to examine the behavior of the FRP anchors. Similar to previous studies (Ozdemir & Akyuz 2006 and Ozbakkaloglu & Saatcioglu 2009), the embedment depth of the anchor, the concrete strength of the block and the anchor hole diameter were selected as key parameters of the research. A total of 27 pull-out tests were conducted with these parameters mentioned before. Handmade anchors were embedded into 400 mm x 400 mm x 150 mm unreinforced concrete blocks. Figure 2.9 shows the specimens constructed and tested in the research. The anchor holes diameters were 12 mm, 14 mm and 16 mm with an embedment depth of 20 mm, 40 mm, and 60 mm, respectively. Sixty-millimeter, hundred ten-millimeter and hundred thirty-millimeter FRP sheets were utilized to generate a wide range of data. The anchor hole

diameter was selected as a parameter because constructing an anchor with exact dimensions was difficult. Therefore, anchor hole diameter was used to define anchor diameter. Concrete cone failure, anchor rupture, combined failure, and bond failure were the failure modes observed in the research.

Figure 2.9: Tested Specimens[14]

Based on the observed data, it was noted that when the embedment length was 20 mm, concrete cone failure took place. The concrete cone crack angle with respect to the concrete block surface was varied from 20 to 35 degrees. In addition, for the 12mm, 14 mm and 16 mm hole diameters, the forces that developed were 6.21 kN, 8.17 kN, and 7.43 kN, respectively. It was observed that anchors embedded into the 14 mm holes developed larger capacity than the anchors embedded into 16 mm holes. When the embedment length was 40 mm, several modes of failure were observed. These modes were concrete cone failure, combined failure, bond failure and FRP anchor rupture. The combined failure mode was mainly observed in the 12 mm hole diameter specimens. The concrete cone formed around the free end of the FRP anchors. When the anchor hole diameter was increased, the depth of the concrete cone also increased. Furthermore, anchor rupture failure was commonly observed in the anchors which had 60 mm embedment depth. It was observed that increase in the embedment depth resulted in an increase in the pull-out capacity of the anchor. The ratio of the anchor diameter to embedment depth was calculated to generate a clear relationship between pull-out force and failure modes. It was noted that for the low ratios,

the observed failure mode was mainly combined failure. As the ratio increased, concrete cone failure became the dominant failure mode. Based on the collected data from experiments and literature, there was no clear relationship between the concrete strength and pull out force. The tensile capacity of the anchors was found to be lower than the tensile capacities of the flat coupon counterparts.

2.5 Innovative Flexural Strengthening of Reinforced Concrete Columns using Carbon Fiber Anchors (Vrettos et al. 2013)

Strengthening of RC columns with the carbon fiber reinforced polymer (CFRP) anchors and sheets were examined in this research. The aim of the research was to increase the flexural capacity of RC columns by providing additional strength with FRP anchors and sheets. The behavior of strengthened RC columns was investigated under simulated seismic loading. The number of anchors and the diameter of the anchor were the critical parameters in the study. A total of four specimens, which had the same size, were prepared. Figure 2.10 shows the experimental setup and details of the columns. The first specimen was only strengthened with CFRP sheets at the plastic hinge region. The goal of wrapping CFRP sheets around the column was to increase confinement.

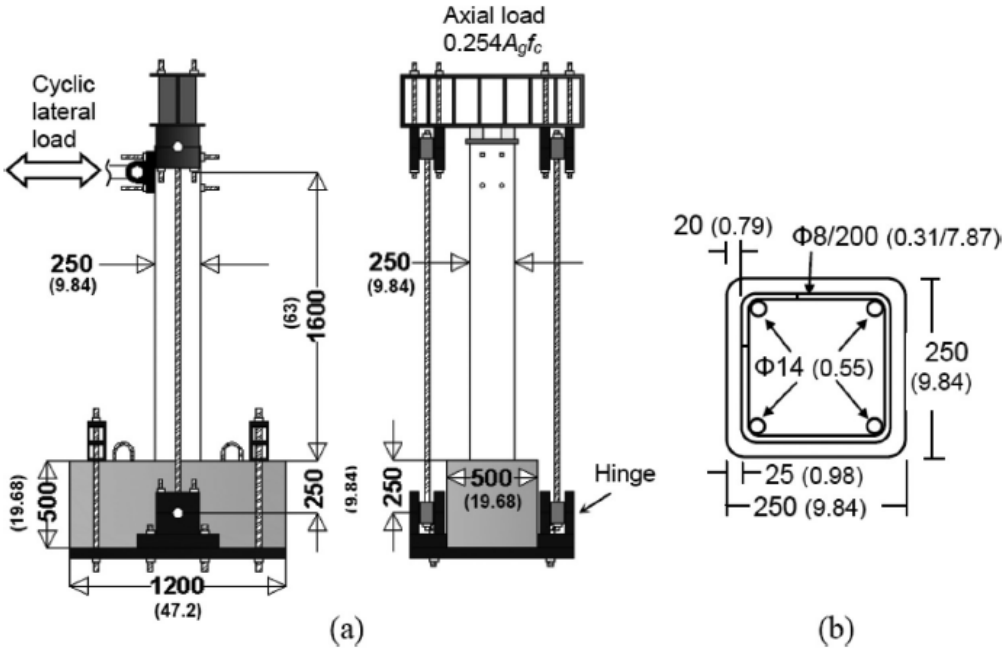

Figure 2.10: Experimental Setup and Column Details[4]

The other specimens were strengthened with CFRP sheets plus CFRP anchors. The second specimen (2_1.5) was strengthened with two anchors on each side of the column. The area of each anchor was 0.75 times the area of CFRP sheet which was bonded to the surface of the column. The third specimen (3_1.5) was strengthened with 3 anchors on each side. The area of each anchor was 50% of the CFRP sheet. The last specimen (2_1.0) was strengthened with two anchors. The area of an anchor was 0.5 times the area of CFRP sheet. The weight of the fiber for specimen 3_1.5 and 2_1.0 was 63 g/m whereas weigh of the fibers for specimen 2_1.5 was 94.5 g/m. The embedment length of each FRP anchor was 250 mm for all specimens. Table 2-1 shows the summary of results for all test.

Table 2-1: Results of Tested Specimen [4]

	Peak force P_{max}, kN (kips)		Column base moment at peak force, kN·m (kip·ft)		Drift ratio at peak force, %		Degree of strengthening ($P_{max,Specimen}/P_{max,Control}$)		Concrete cover in tension steel, mm (in.)		Effective strain in tension anchors, %	
Specimen	Push	Pull	Push	Pull	Push	Pull	Push	Pull	Push	Pull	Push	Pull
Control	37.91 (8.52)	–37.73 (–8.48)	62.53 (4.29)	–62.35 (–4.27)	3.67	–3.88	1.00	1.00	33	33	—	—
2_1.5	51.15 (11.50)	–50.66 (–11.39)	83.06 (5.69)	–82.25 (–5.64)	2.40	–2.35	1.35	1.34	25	36	0.53	0.52
3_1.5	47.49 (10.68)	–42.11* (–9.47)	77.40 (5.30)	—	2.79	—	1.25	—	32	31	0.43	—
2_1.0	45.04 (10.12)	–43.33 (–9.74)	73.32 (7.25)	–70.56 (–4.84)	2.48	–2.42	1.19	1.15	35	26	0.49	0.43

*Unreliable result (not used in further calculations) due to wrong positioning of one anchor.

Figure 2.11 shows the force-drift curves of all specimen. The results show that the flexural strengthening of the RC columns with FRP anchor and sheets was successful. The weight of the anchor has a linearly increasing impact on the effectiveness of the anchors Increase in number of anchors did not result in increased in force capacity. This was attributed to potential flaw in construction of the specimen.

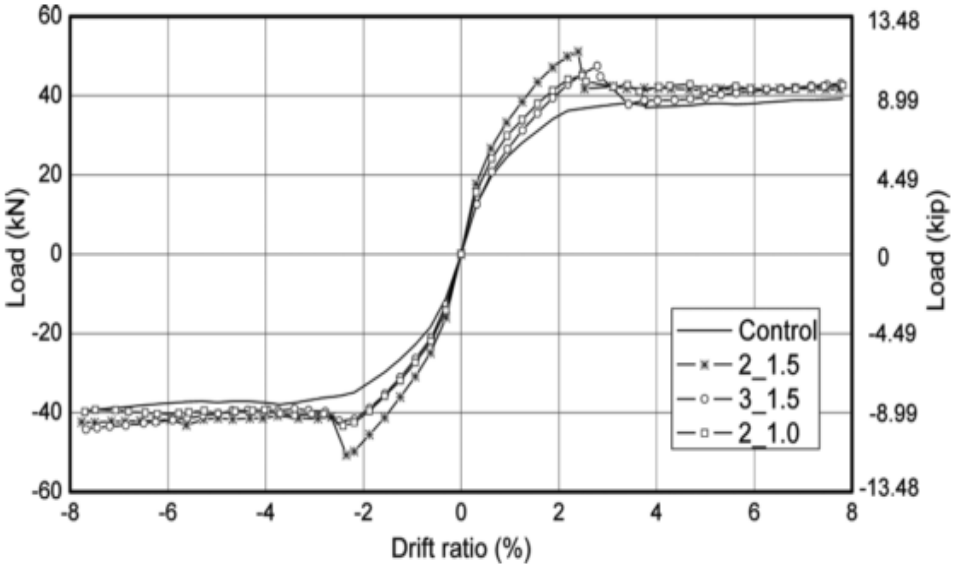

Figure 2.11: Force-Drift Curves for Tested Columns[4]

2.6 Tensile capacity of FRP Anchors in connecting FRP and TRM sheets to concrete (Bournas et al. 2014)

Direct tension capacity of CFRP spike anchors, which are generally close to a pen size, was studied by considering parameters such as the number of anchors, the nominal diameter of anchors, the fiber type and the bonding agent that was used to bind anchor fans to FRP or textile-reinforced mortar (TRM) sheets. The goal was to show effectiveness of this anchor on delamination of FRP or TRM sheets. Eight reinforced concrete (RC) columns with dimensions of 200 x 200 mm. were built. In addition to the RC columns, eight RC footing with dimensions of 400 x 400 mm. were built. Longitudinal steel bars in the columns were not continued into the footing in order to directly investigate the tensile capacity of the anchors. The only connection between the column and the foundation block was provided by FRP anchors which were fanned out from the holes drilled into the concrete footing. Two different bonding agents were used to bind anchor fans to the column face via FRP or TRM sheets. Detail of the experimental setup is shown in Figure 2.12. Table 2-2 shows details of the parameters.

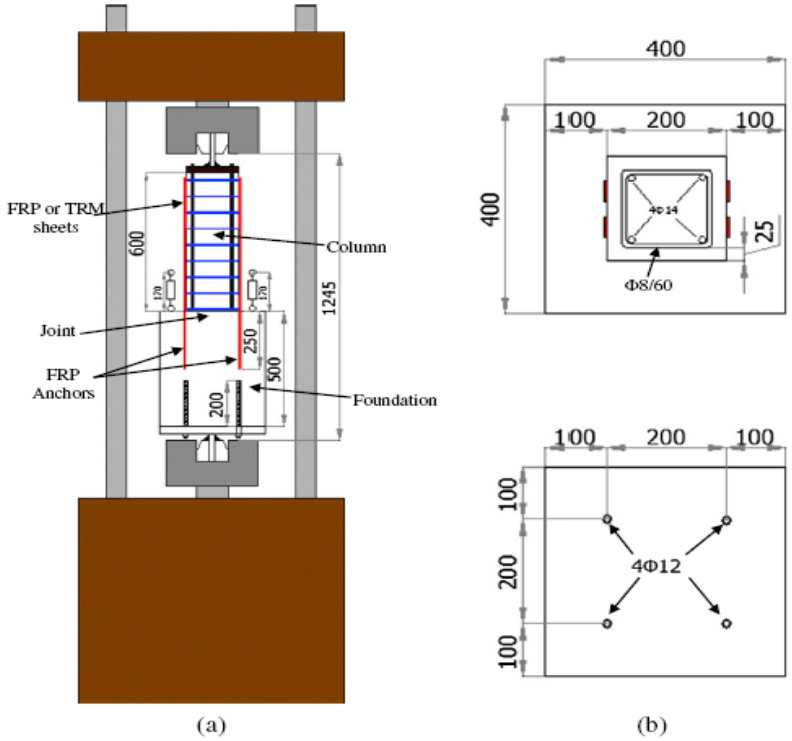

Figure 2.12: Test Setup and Column Details[15]

The embedment length of the anchors, which was not a parameter in the research, was taken as 200 mm. for all anchor sizes. The chosen depth was enough for preventing pull out of anchors from the concrete foundation. The columns were pulled up from the top by threaded longitudinal reinforcing steel bars which were connected to the MTS machine.

Table 2-2: Details of Tested Anchors [15]

Specimen notation	Column EB reinforcement		Bonding agent between anchors EBR	FRP anchors				Total anchor area (mm^2)	Area of vertical fibers of the EBR (mm^2)
	Type of carbon fiber	No. of layers per side		Number per side	Diameter (mm)	Area of each anchor (mm^2)	Weight of each anchor (gr/m)		
F2_2Φ6	Unidirectional sheet	2	Resin	2	6.25	30.67	56	122.7	136
F2_1Φ9	Unidirectional sheet	2	Resin	1	9.25	67.2	121	134.4	136
F4_1Φ12	Unidirectional sheet	4	Resin	1	12.7	126.7	228	253.3	272
F4_2Φ9	Unidirectional sheet	4	Resin	2	9.25	67.2	121	268.8	272
T4_2Φ6_R	Bidirectional textile	4	Resin	2	6.25	30.67	56	122.7	152
T4_2Φ6_M	Bidirectional textile	4	Mortar	2	6.25	30.67	56	122.7	152
T7_2Φ9_RJ	Bidirectional textile	7	Resin	2	9.25	67.2	121	268.8	304
T7_2Φ9_MJ	Bidirectional textile	7	Mortar	2	9.25	67.2	121	268.8	304

A summary of the results is presented in Table 2-3. The results show that the anchors have an effect on postponing early delamination of FRP or textile-reinforced mortar (TRM). When the same amount of CFRP anchors bonded to columns with FRP and TRM sheets, increase in total tensile capacity was 70% and 50% for columns with FRP and TRM sheets, respectively. The effective strain, which is given as the ratio of the average strain of anchors at the failure to the ultimate strain, indicated that CFRP anchors which were utilized to connect FRP uniaxial sheets to concrete have more capacity than the CFRP anchors that were utilized to connect the textile fiber sheets (TRM).

Table 2-3: Experimental Results[15]

Specimen notation	(1) Peak force (kN)	(2) Displacement at peak force (mm)	(3) Tensile capacity of each anchor		(4) Tensile strain of the FRP Anchor, (–)			(5) Failure Mode
			Force, (kN)	Stress, $f_{anc,eff}$ (MPa)	(i) Calculated, $f_{anc,eff}/E_f$	(ii) Measured with SGs	$\varepsilon_{anc,eff}/\varepsilon_{fu}$	
F2_2Φ6	79.97	3.18	19.24	627	0.0066	Unreliable recordings	0.66	Anchors rupture
F2_1Φ9	97.12	3.85	48.55	722	0.0075	0.00445	0.75	Anchors rupture
F4_1Φ12	135.83	4.99	67.92	535	0.0060	0.0073	0.60	Anchors rupture
F4_2Φ9	167.7	3.97	41.93	623	0.0065	0.0053	0.65	Anchors rupture
T4_2Φ6_R	44.67	2.00	11.17	365	0.0038	Unreliable recordings	0.37	Anchors rupture
T4_2Φ6_M	38.36	1.25	9.59	313	0.0032	0.0038	0.32	Debonding and slip of anchors from the textile
T7_2Φ9_RJ	70.1	6.20	17.51	260	0.0027	0.0034	0.27	Rupture of the anchors one by one successively
T7_2Φ9_MJ	58.3	4.02	14.60	217	0.0023	0.0022	0.23	Debonding and slip of anchors from the textile

2.7 Tensile Strength of Straight CFRP Anchors (Castillo et al. 2015)

In this research study, the focus of the authors was to experimentally examine the failure mode developed in the key portion of the FRP anchor due to fiber rupture. In addition to the key portion failure mode, debonding of FRP sheet from concrete substrate was the second failure mode. Two parameters were determined to examine the behavior of the anchor under direct tension. The first parameter was the amount of fiber used in the FRP anchors. The second parameter was the concrete compressive strength, which was believed to have an influence on the bond strength developed between the FRP sheet and the concrete substrate.

An experimental setup was developed to represent real structural applications as shown in Figure 2.13. In the setup, a rectangular beam was connected to a concrete slab via an FRP sheet and an FRP anchor. One end of the FRP anchor fan was splayed onto the FRP sheet, which was bonded to the concrete substrate. The other end was inserted into pre-drilled holes to ensure a force transfer mechanism of the system. The embedment length in the study was not mentioned. The angle of the fan was set at 60 degrees, and the area of the fan was set large enough to avoid anchor fan de-bonding from the FRP sheet. In the study, the fiber area of the FRP anchors was varied from 28 mm^2 to 168 mm^2. The setup was built such that eccentricity due to the loading could be minimized.

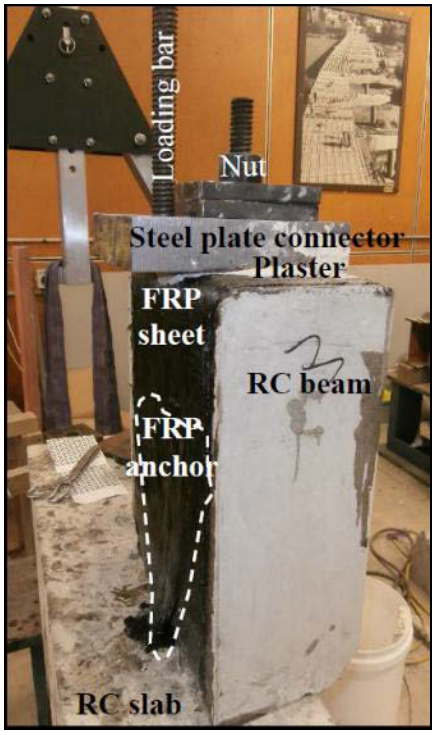

Figure 2.13: Test Setup and Specimen [9]

The efficiency of the FRP anchor was defined as the ratio of the force developed by the FRP anchor to the load that was calculated by using producer-specified material properties. This was the main focus of this experimental work. It was observed that as the amount of fiber increased, the capacity of the anchor also increased but the correlation between these two was not linear. It was also observed that the efficiency reduced, as shown in the Figure 2.14, when the amount of the fiber increased. For the smallest anchor size, an average of 92.2 % efficiency was reached whereas for the largest size anchor the efficiency dropped down to 43.4%. When the concrete compressive strength was 24.9 MPa, de-bonding of the FRP sheet from the concrete substrate occurred, but it did not affect the ultimate load developed by the FRP anchors.

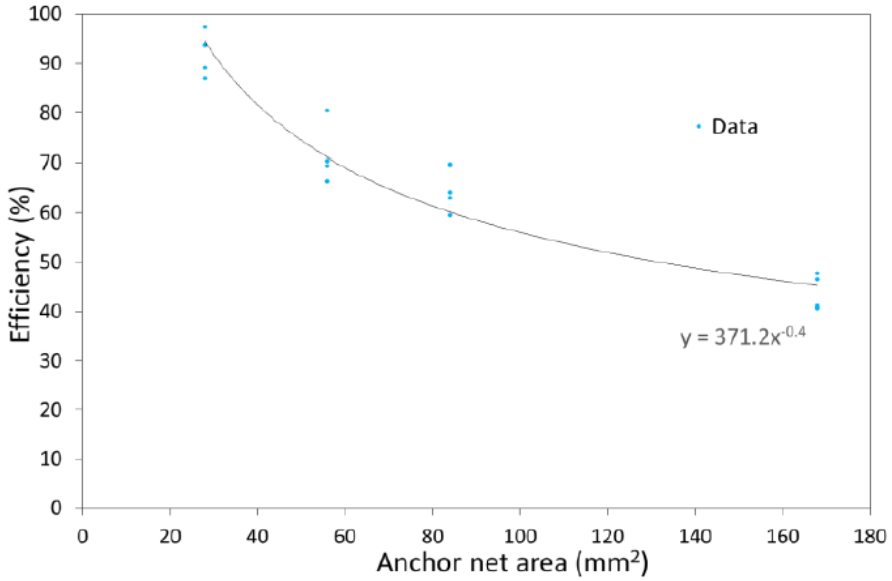

Figure 2.14: Efficiency Distribution[9]

2.8 Force-based Model for straight FRP anchors exhibiting fiber rupture failure mode (Castillo et al. 2016)

The goal of the research was to understand the force transfer mechanism of the anchor and develop an empirical equation to determine anchor capacity. Fan angle and net cross-section area of the anchor were two main parameters used in the research. In the study, the fan angle was varied from 15 º to 60 º, and the number of bundles to produce the anchors was varied from half bundle to six bundles. A bundle Fan angle of 15 º and 60 º were not tested for large size anchors (6 bundle) due to the limitation of test set-up. A total of 72 FRP anchors were tested. Figure 2.15 shows the fan angle and components of the anchors studied in the research. Digital Imaging Correlation (DIC) method was used to measure strain at the failure of the anchor. In the research, the load developed at each failure mode was reported.

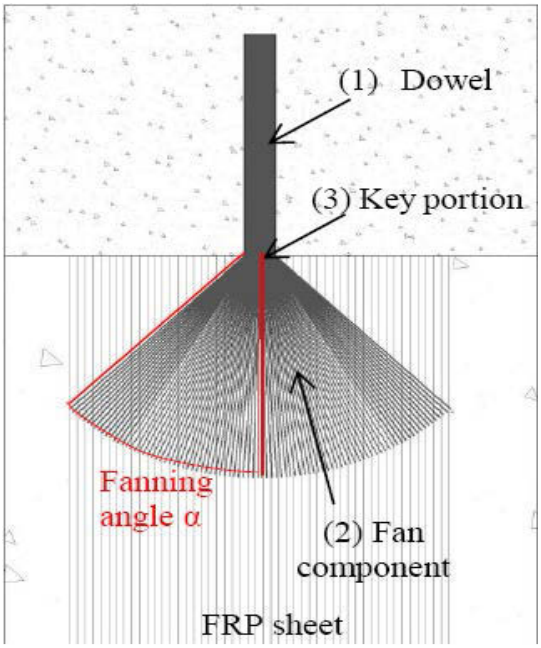

Figure 2.15: Graphic Representation of Fanned Anchor[11]

The failure modes reported in the study were: failure of the key portion, failure of the anchor at the middle height of the fan and failure of the anchor at the top of the fan. Figure 2.16 shows the failed anchors. It was found that as the fan angle increased, the capacity of the anchor reduced. It was observed that the anchor efficiency increased with the decreasing anchor fan angle. The standard deviation of anchors was studied for each parameter considered in the study. The following equation was suggested as a lower bound equation to determine the capacity of the anchor.

$$Nfr = 2.9\sigma_{frp}\, cos(0.57\alpha_0)\,(2.9Adowel^{\frac{2}{3}} - 1.2Adowel^{\frac{2}{3}}) \qquad \text{Equation 1}$$

Figure 2.16: Ruptured Anchors[11]

Chapter 3: Direct Tension Capacity of Large Diameter CF Anchors

3.1 Experimental Program

An experimental program was developed to examine the behavior of large diameter carbon fiber anchors under direct tensile loading. Testing parameters in this part of the experimental program were determined based on the information collected from the literature review. Ozdemir and Akyuz [13] showed that ratio of the experimentally developed force in the anchor to theoretical rupture force calculated from manufacturer provided design stress reduces, as the amount of the fiber increases. It was noted that this reduction was not linear. Similar observations also were made by Castillo et al. [9].

It was concluded that for a given anchor diameter, which is determined by finding fibers that can fit into a hollow pipe with a given diameter, the rupture capacity of large CF anchors should be investigated as the available data is very limited.

3.1.1 Test Matrix

Three different anchor diameters were considered in this experimental program, based on the literature review. To date, the largest tested CF anchor was 1-1/4 in. [16] which was selected as the largest diameter CF anchor for this experimental program. It was decided that in order to cover wide range of anchor sizes, ¾ in. and 1 in.-diameter anchors were added to test program. In total, 16 anchors were tested, as described in Table 3-1 which summarizes the test parameters considered, namely anchor diameter, embedment depth, anchor hole diameter, and preparation the method.

Table 3-1: Test Matrix

# Test	Nominal Anchor Diameter (in)	Embedment Depth (in)	Anchor Preparation Method
1	1-1/4	$10*d_{hole}$	A
2	1-1/4	$10*d_{hole}$	A
3	1-1/4	$11*d_{hole}$	B
4	1-1/4	$11*d_{hole}$	B
5	3/4	$10*d_{hole}$	A
6	3/4	$10*d_{hole}$	A
7	3/4	$12*d_{hole}$	B
8	3/4	$13*d_{hole}$	C
9	3/4	$13*d_{hole}$	C
10	1	$12*d_{hole}$	B
11	1	$12*d_{hole}$	C
12	1	$12*d_{hole}$	C
13	1	$12*d_{hole}$	C
14	1	$12*d_{hole}$	C
15	1	$13*d_{hole}$	C
16	1	$13*d_{hole}$	C

Based on published literature[1], it was assumed that $10d_{hole}$ embedment depth will be sufficient enough embedment depth to reach the rupture capacity. Thus, the provided embedment length was larger than $10d_{hole}$ for most of the tested anchors in this program to observe the rupture failure mode and determine the theoretical capacity of the anchors. In all but one case, the anchor hole diameter was taken as ¼" greater than the anchor diameter to avoid possible shear failure through the epoxy layer. Selection of the preparation method varied during testing and was based on experimental observations. Details of preparation methods considered are discussed in section 3.1.5.

3.1.2 Experimental Setup

A testing method for CFRP and GFRP bars, which are used as internal reinforcement in reinforced concrete structures, is suggested by ASTM D7205 [17] to determine tensile properties of composites bars. The maximum bar size that can be tested using ASTM D7205[17] is limited to 1-1/4 in. for GFRP bars , and 3/4" for CFRP bar. As the bar diameter increases, the length of the pipe to embed the ends of bars increases. Thus, for larger CFRP bar sizes, very long pipes may be needed. Therefore, ASTM D7205 testing method which may not be appropriate for testing large diameter CFRP anchors due to expected level of force developed by large diameter CF anchors.

A testing method that can carry large tensile forces was developed. The schematic view and the general view of the experimental setup developed for this testing program is shown in Figure 3-1 and Figure 3.2, respectively. The testing setup includes from top to bottom: a disposable tube to bond CFRP anchors; a loading tube to transfer load from hydraulic check to disposable tube; a load cell between hydraulic jack and loading tube to measure load at failure; a hydraulic jack to load anchors; and reaction frames to create a self-reacting mechanism. As expected loads at rupture is high, safety chains were used to constrain the hydraulic jack and a plywood board was provided to prevent disposable tube from becoming a projectile after sudden energy release at failure of the anchors.

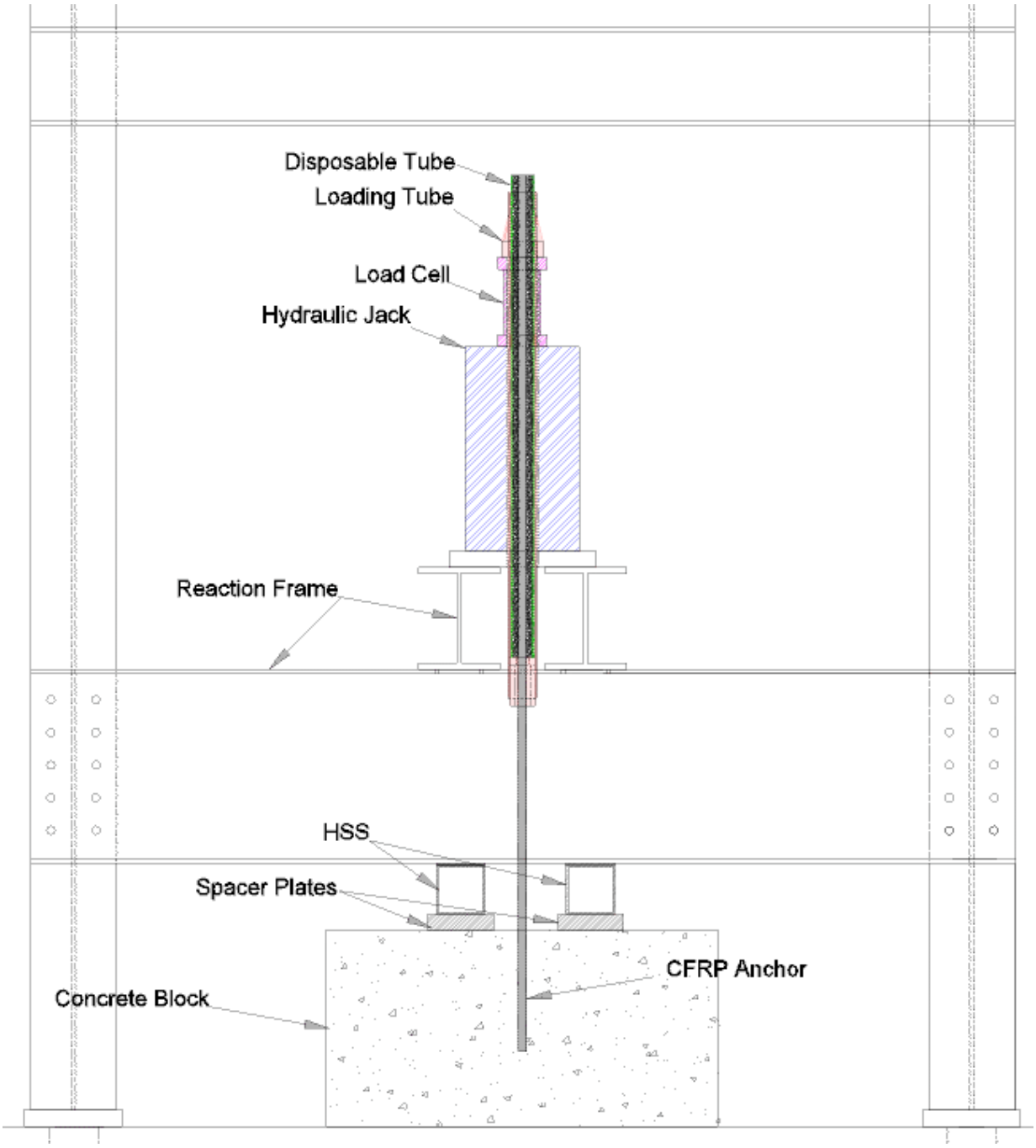

Figure 3.1: Schematic View of Test Setup

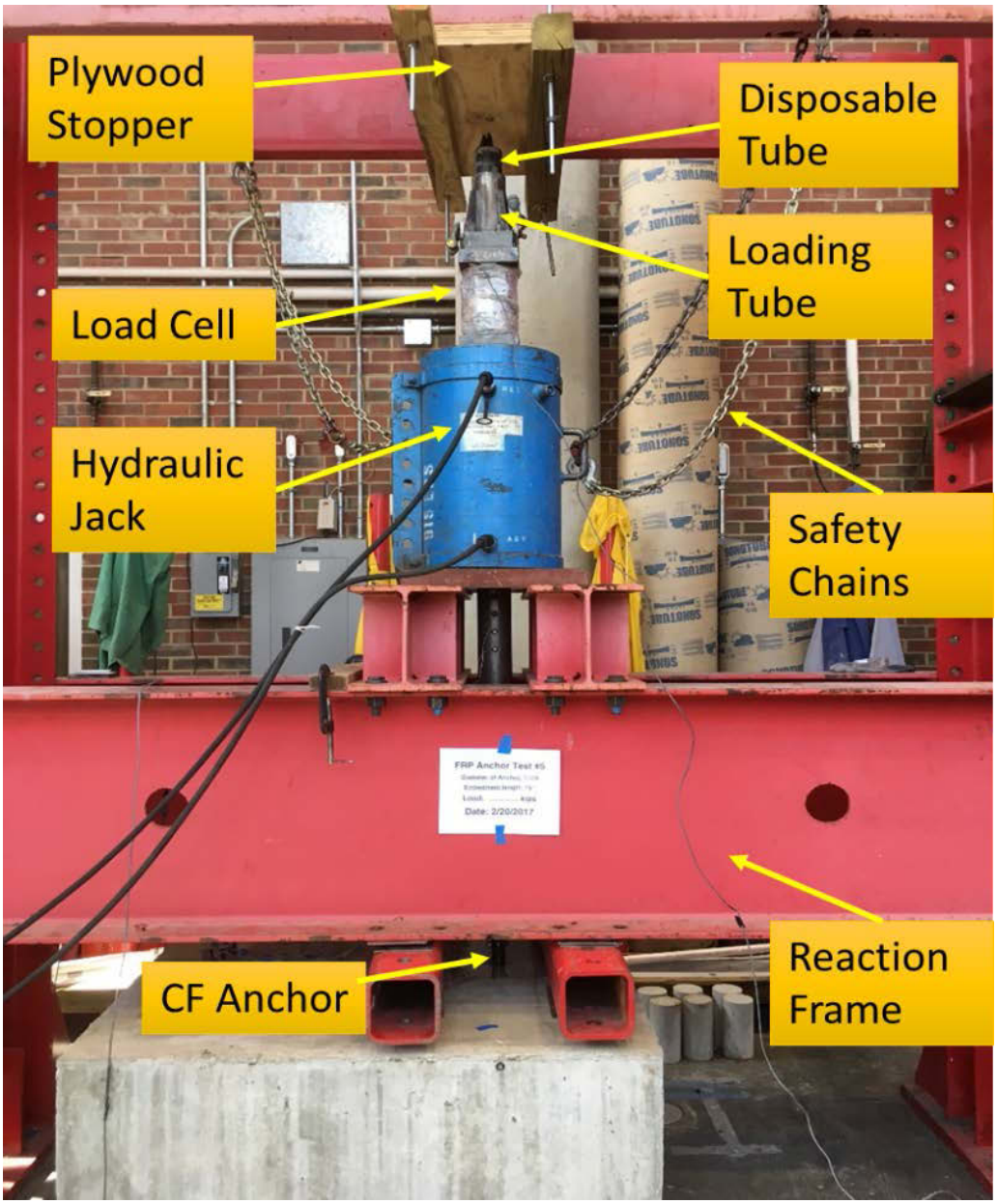

Figure 3.2: General View of the Experimental Setup.

The setup was developed such that a CF anchor can be pulled from the concrete block. To pull the CF anchor from concrete block, a gripping mechanism was required. ASTM D7205 [17] suggests a testing method in which a gripping mechanism can be developed through anchoring both ends of CFRP or GFRP bars into steel pipes via epoxy or cementitious grout. A similar approach was used to grip the free ends of the. As shown in Figure 3.3, a 3 inch-nominal-diameter

steel pipe (disposable tube) was used to anchor top of the CF anchors via non-shrink grout. Due to the magnitude of the expected loads, the length of the disposable tube was 5 ft to provide enough development length to prevent slip of the anchor from the disposable tube. The disposable tube was placed into a loading tube, which was design in a way that force from the hydraulic jack can be transferred to the disposable tube through the load cell. To transfer force from the hydraulic jack, a two-inch-thick plate was welded around the top of the loading tube. Four gusset plates were also welded at the top of the loading to prevent bending of the welded plate.

Although load measurement in this experimental set-up could be done by placing a load cell at various locations, it was decided that the most accurate load data would be obtained when the load cell is between the loading tube and the hydraulic jack. Therefore, a custom load cell was manufactured in house to allow the loading tube to pass through, as shown in Figure 3.3. To transfer force in the loading tube to the disposable tube, a bearing plate was placed on top of a smaller tube, which was welded at the bottom end of the loading tube with plug welds, as shown in Figure 3.3.

Moreover, to hold the concrete block in place during loading of the CF anchor, two hollow structural sections (HSS) were added to the setup with four spacer plates as shown in Figure 3.4. The purpose of the spacer plates was to prevent compression stress in the concrete block around the anchor hole. This configuration enables a self-reacting system. The concrete block did not have to be tied to the strong floor and could be moved for multiple tests. The spacer plates allowed enough the length of the CF anchor to be exposed for placement of LED markers to monitor strain at failure of the CF anchors.

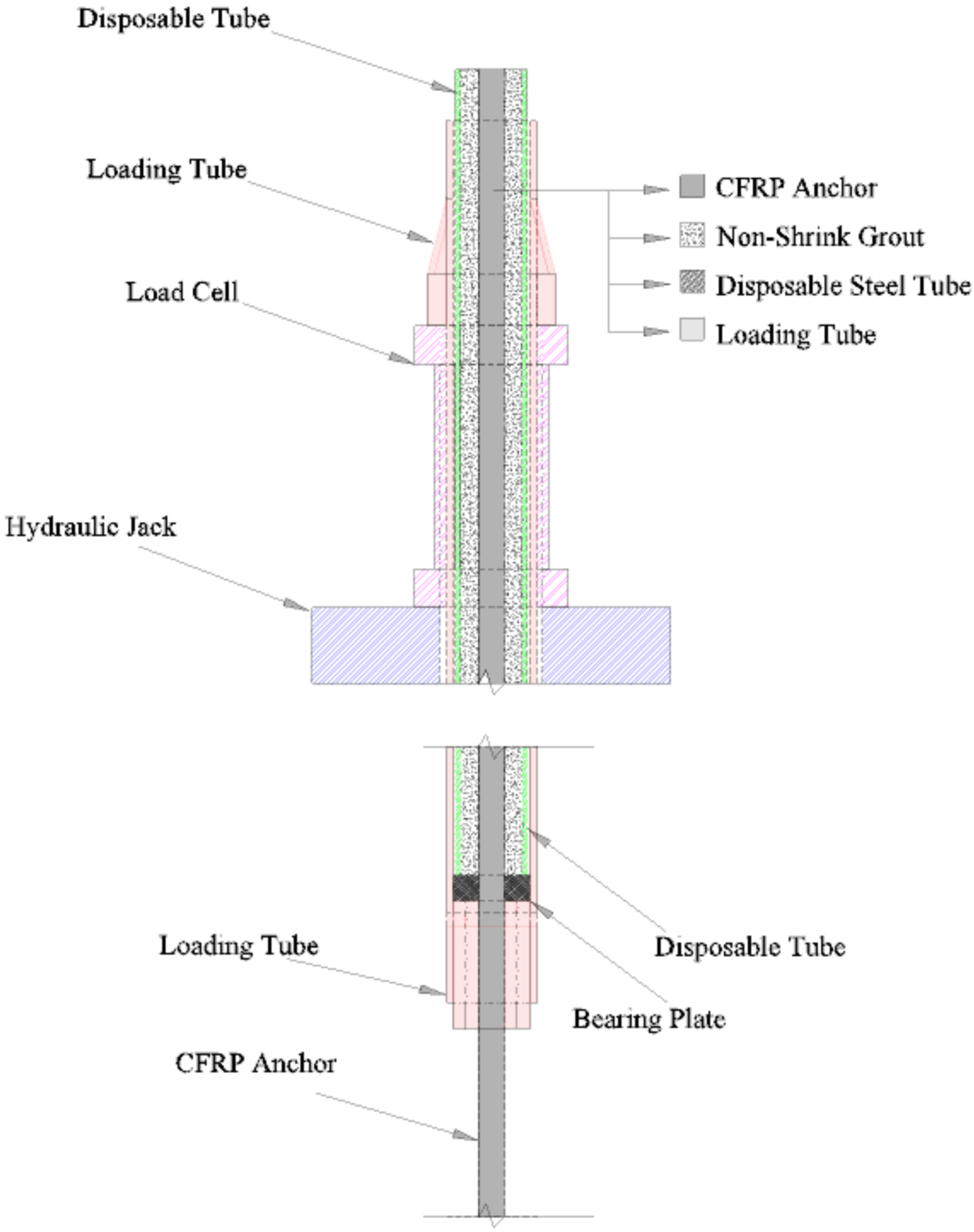

Figure 3.3 : Cross Section View of the Loading Setup

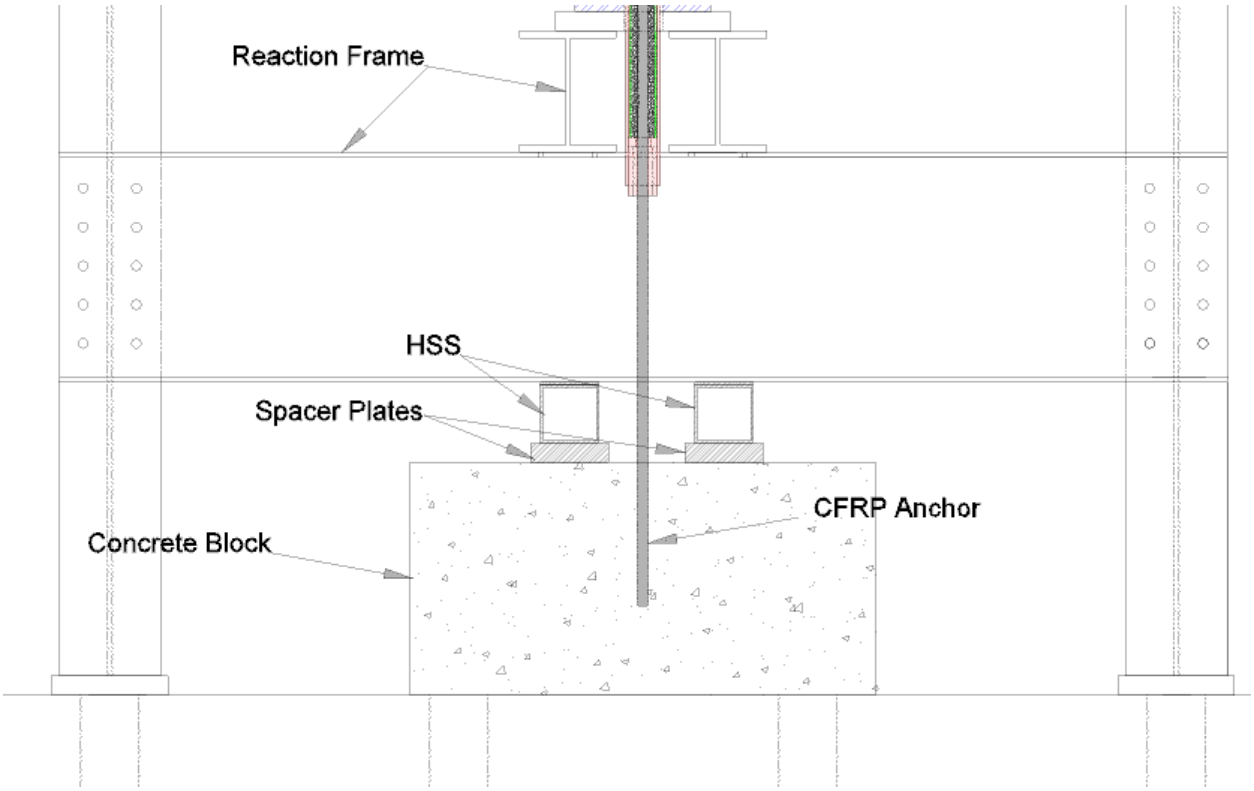

Figure 3.4: Elevation View of Bottom Half of Experimental Setup

A schematic of the force flow in the experimental setup is shown in Figure 3.5. The force in the hydraulic jack is transferred to the load cell as shown in Figure 3.5. The force in the load cell is transmitted to the top part of the loading tube through the welded plates as shown in Figure 3-4b. Then, the load is transferred to the inner tube, which is welded to the loading tube with a plug weld. The load in the inner tube is then transmitted to the disposable tube through the bearing plate. As the CFRP anchor is anchored in the disposable tube using non-shrink grout, load in the disposable tube is transmitted to the CFRP anchor through the bond developed between the anchor and the non-shrink grout. The concrete block is restrained by the HSS, which is placed between the reaction frame and the concrete block.

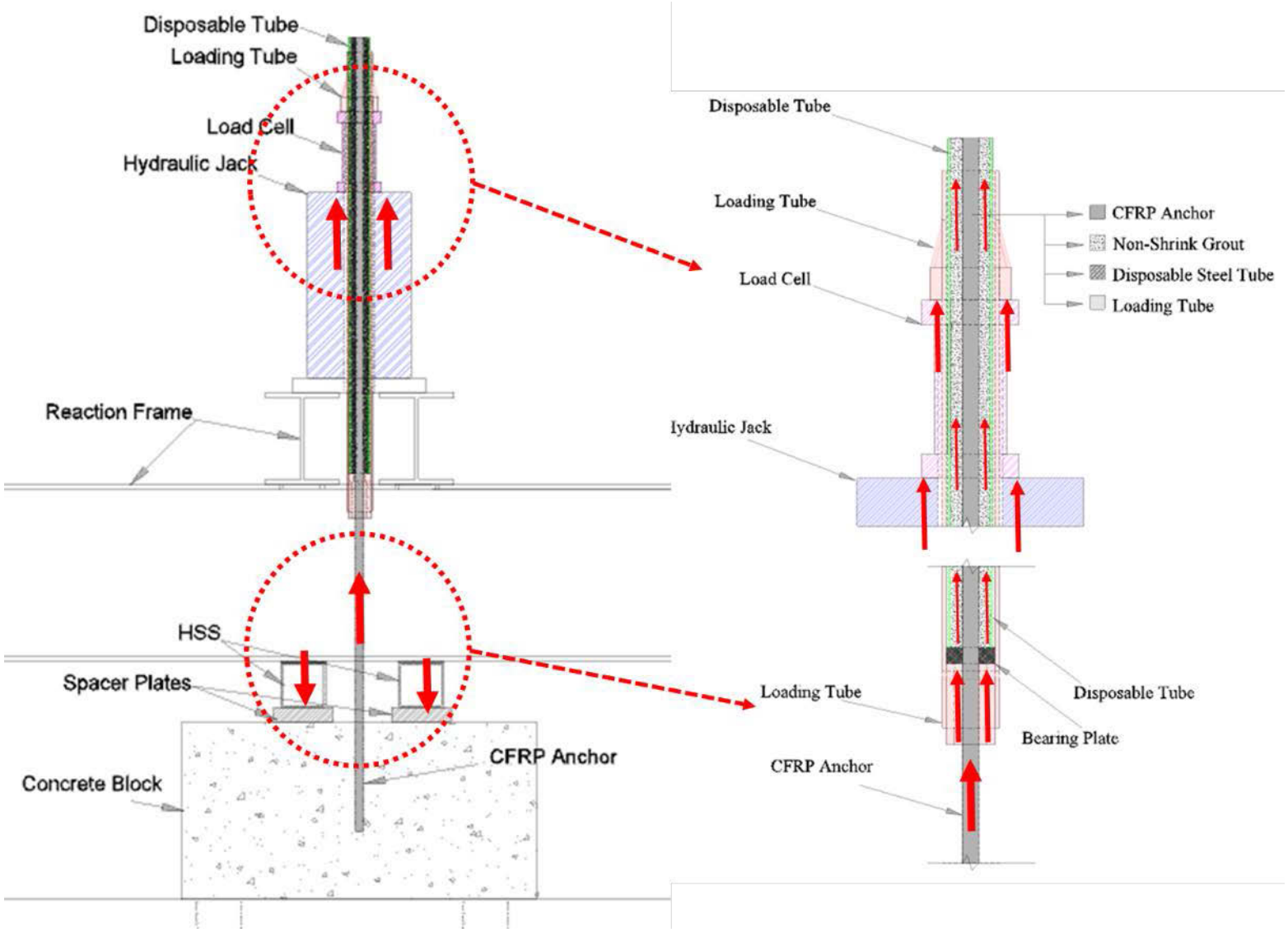

Figure 3.5: Schematic of Force Flow

3.1.3 Material Properties

Tyfo® SCH Fiber anchors were used in this phase of the experimental program. These anchors were constructed from carbon fiber rovings. The composite gross laminated properties provided by company are 143000 psi for ultimate tensile strength in primary fiber direction, 1.2% elongation at break, 13.9x106 psi tensile modulus. Dry fiber properties for CFRP anchors are also provided by company. Tensile strength is 550000 psi in primary direction, 33.4x106 psi tensile modulus, and 1.7% elongation at break. The laminated properties of CFRP anchors are produced through experimental testing of certain anchor diameter. As it was discussed before, material properties vary as the diameter of the anchor changes. Therefore, a given laminated properties is specific to certain CFRP anchor sizes, but dry fiber properties is similar for any given CFRP anchor size. The ultimate tensile strength of laminated CFRP anchor was used as theoretical tensile capacity when efficiency of the anchors was calculated.

Two different concrete blocks were built with different reinforcing details. In addition, two different concrete strength was used to build concrete blocks. Initially, embedment depth was one of the testing parameters. Later, due to observed experimental results, focus of the experiment shift to determination of design stress limits. Therefore, concrete compressive strength, which has impact on embedment depth, was removed from parameter lists. The experiments were conducted on concrete blocks where specified concrete compressive strength was 4 ksi, but cylinder tests resulted in an average concrete compressive strength of 7.2 ksi.

3.1.4 Instrumentation

The instrumentation objective was to collect enough data to quantify mechanical properties of the CF anchors. For collecting load data, a load cell was built. The first phase of building load cell was to weld two 6 in. x 6 in. x 1-1/2 in plates with a 4 in diameter hole to the top and bottom of a 6 in long steel pipe, which has an inside diameter (ID) of 4-1/2 in, as shown in Figure 3.6. The reasoning behind the given details of the load cell was to permit loading tube to be pass through the load cell. The second phase of the load cell was to locate strain gauges to produce a Wheatstone bridge as shown in Figure 3.7a. Four strain gauges were placed around column with same distance from each other, as in Figure 3.7b. Later, to protect the strain gauges from any environmental effect, putty strips were applied onto strain gauges as shown in Figure 3.7c. The last phase of the preparation was to calibrate the load cell for the expected ultimate load. In this setup, the load cell

was utilized to measure only tensile load in the CF anchors by locating the load cell at the location where compression forces developed. The prepared load cell was placed in a Universal Testing Machine (MTS) for calibration as shown in Figure 3.7d.

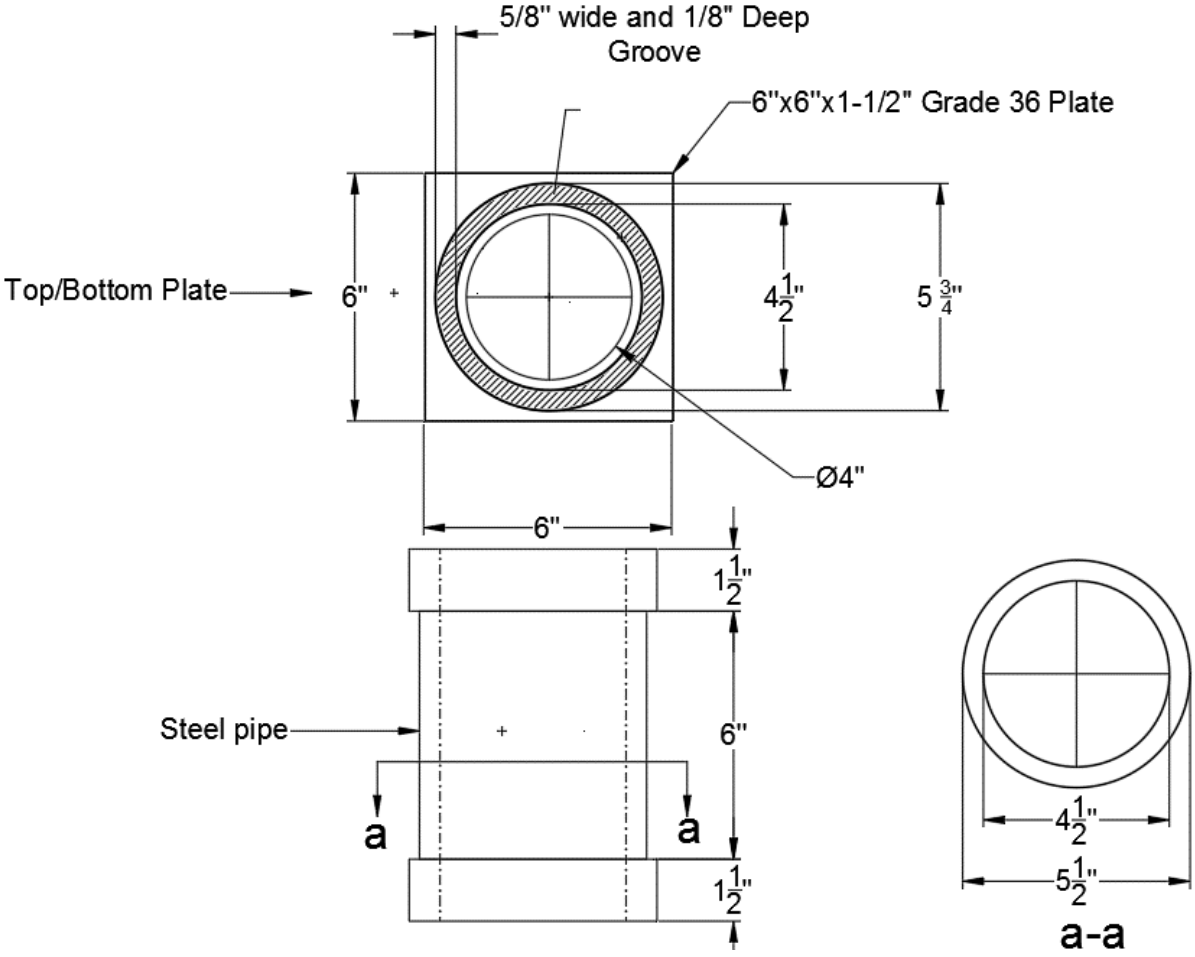

Figure 3.6: Schematic of Load Cell

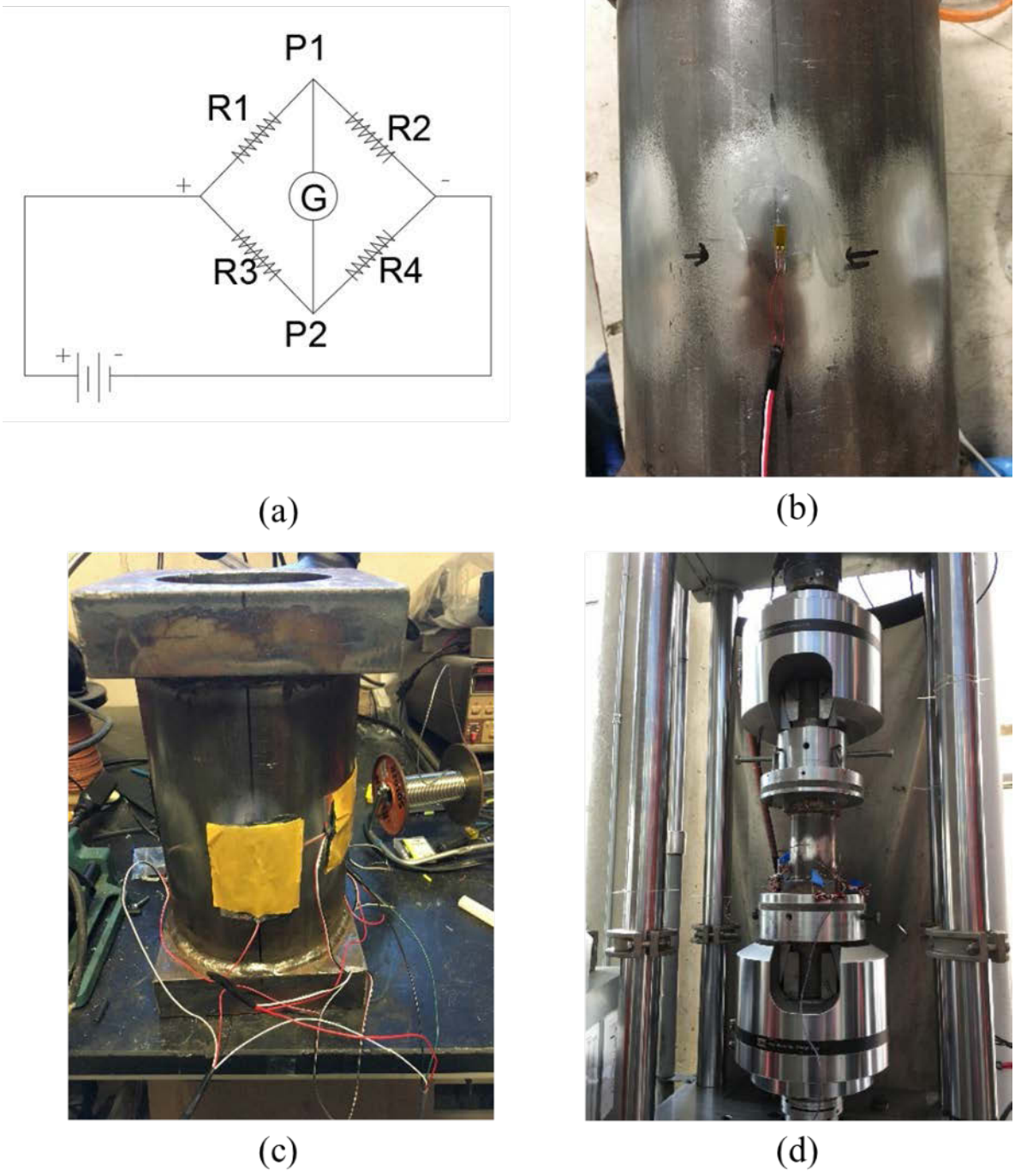

Figure 3.7: a) Wheatstone Bridge Schematic, b)Strain Gauge application, c) Protection of Strain Gauges, d) Calibration of Load Cell

As shown in Figure 3-7, a load increment of 20000 lb was applied until reaching 150000 lb which was the anticipated ultimate load for the largest tested CF anchor in the experimental program. The load reading from the UTM and Load Cell were in good agreement as shown in Figure 3-7. An error of 2 %, which was small compared to the magnitude of the applied ultimate load, was calculated.

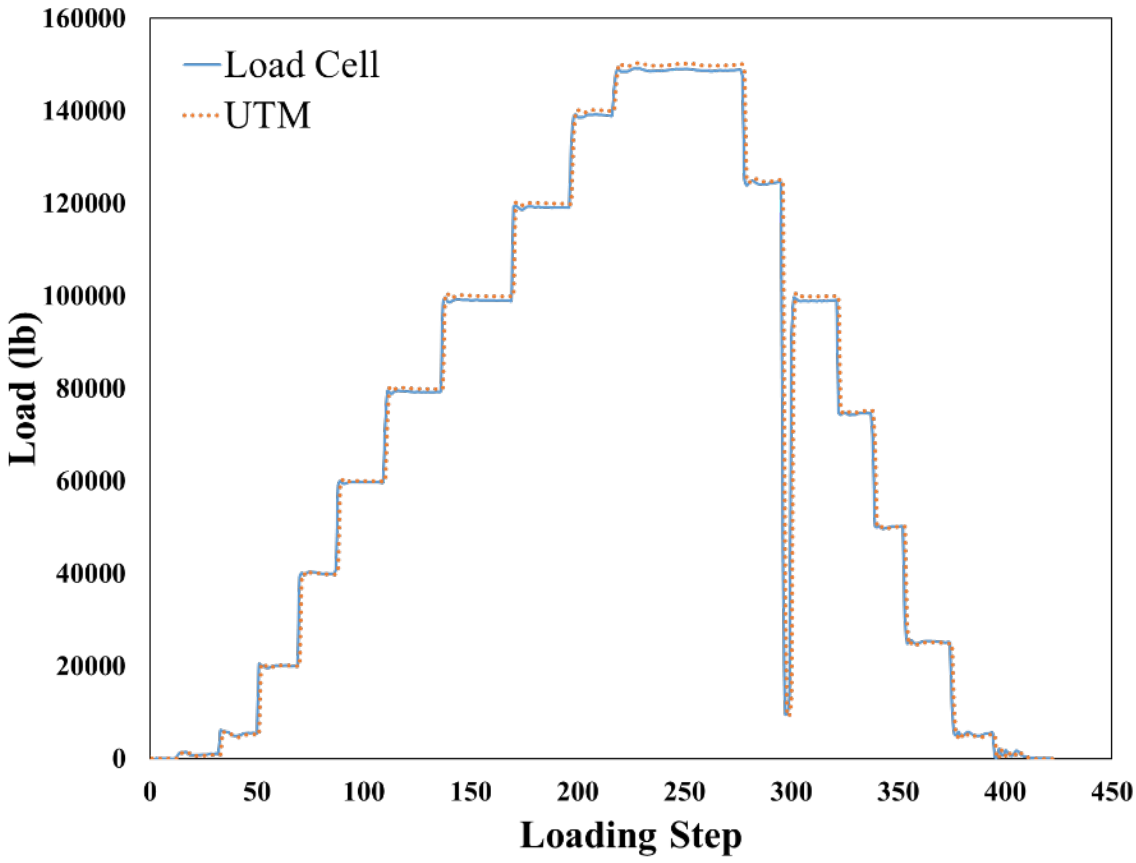

Figure 3.8: Calibrated Data of the Load Cell

A 3D optical measuring system (Optotrak Certus HD 3D) was utilized to obtain real-time strain data for the tested CF anchors via the Optotrak Camera shown in Figure 3.9a. LED target markers were placed on the CF anchor surfaces as shown in Figure 3.9b. The system can read the location of the LED target markers in three-dimensional space during a test. To calculate the strain in the tested specimen, the final distance of two LED target markers relative to each other should be calculated. The ratio of the final distance between two LED target markers to initial distance

between the same markers gives an average strain between these two LED target markers. A detailed discussion on this 3D optical system can be found in Goodnight et al. [18].

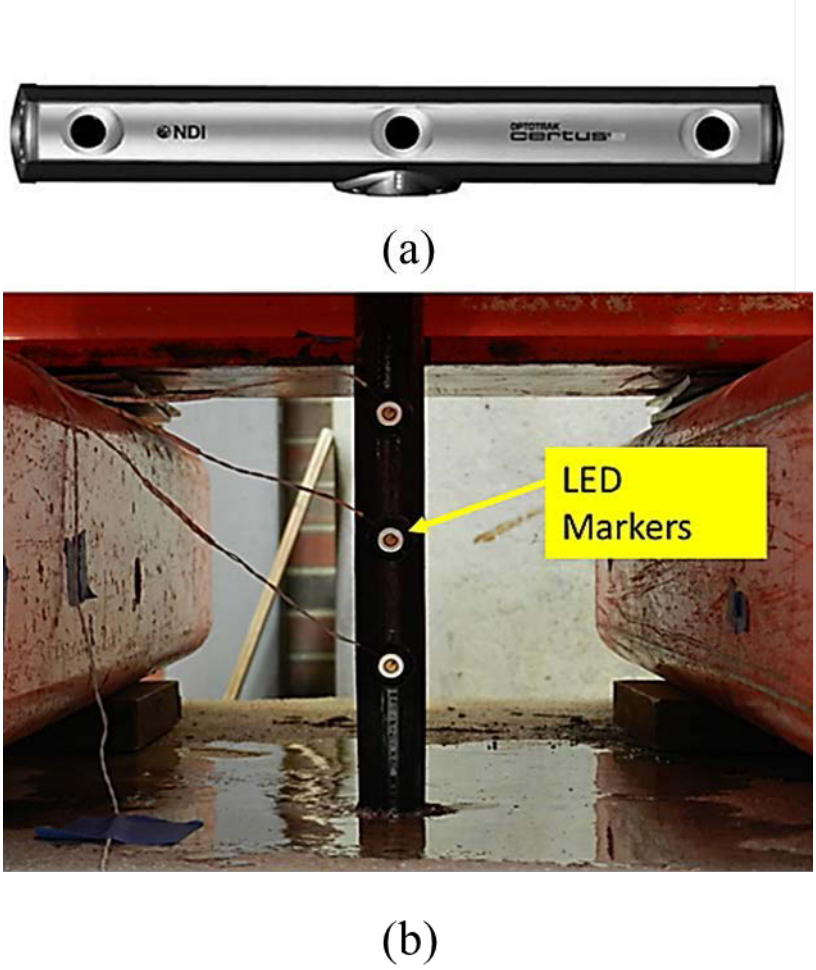

Figure 3.9: a) Optotrak Camera; b) LED Target Markers

3.1.5 Loading Protocol

A 600-kip hydraulic jack was used to apply tensile load to the CF anchors. Although ASTM D7205 suggests a testing method for CFRP and GFRP bars, there is no suggested loading protocol in the standard [17]. All anchors were monotonically loaded until a failure mode reached. The load rate was not controlled during testing. Therefore, the impact of loading rate on the capacity of the CF anchors was not examined in this research program.

3.1.6 Anchor Preparation

The recommended preparation of CF anchors varies from one manufacturer to another. In this research program, a preparation method was followed after discussion with the CF anchor manufacturer. Since the investigation on the impact of anchor diameter on the capacity of the CF anchor is the goal, the applied preparation method required formation of a circular cross-section. A circular PVC pipe, which had smaller inside diameter than the anchor hole, were used to form circular cross-section. Three different anchor preparation methods were followed due to the obtained test results. Due to the developed testing setup, 9 ft.-long CF anchors were used in the testing program. Details of the preparation methods are given in the following sections.

3.1.6.1 Anchor Hole Preparation

The preparation of anchor holes is important in order to reach the rupture capacity of the CF anchors.

The steps followed for the preparation of anchor hole are:

1. 1-Anchor holes drilled to the required depth and diameter as shown in Figure 3.10a.
2. 2-A steel brush used to move loose debris from hole surface shown in Figure 3.10b.
3. 3-Dust removed from the hole using pressurized air in conjunction with a vacuum as shown in Figure 3.10c.

Figure 3.10: a) Drilling Concrete b) Brushing inside the Hole c) Removing dust via Pressurized Air

3.1.6.2 Preparation Method- A

The idea behind this preparation method was to imitate a real field application where after saturation of the CF anchors, shown in Figure 3.11a, a steel rod is used to install the anchor via its looped end, as shown in Figure 3.11b.

The preparation steps for the first method was as follows:

1. CF anchor was set on a table, which was covered with a plastic sheet. Then, the fibers were gently spread on the table as shown in Figure 3.12a.
2. The two-component epoxy was mixed following the instructions provided by the manufacturer, shown in Figure 3.12b.
3. Using a squeezed bottle, carbon fibers were gentled saturated as shown in Figure 3.12c. It should be noted that over saturation of fibers may cause swelling of the anchor, which may later be an issue when the anchors are installed in the drilled holes.
4. A PVC pipe used to form circular cross-section of the CF anchor as shown in Figure 3.12d. The anchor was pulled inside the PVC pipe with a long wire. The length of the PVC pipe was chosen based on the required embedment length for a CF anchor.

5. Later, the anchor with the PVC pipe was hung and a steel rod used to install the anchor into the drilled hole as shown in Figure 3.12e. The reason for hanging CFRP anchors to have good vertical alignment of the anchor.
6. After curing of the CF anchor, the PVC pipe was removed. The cured CF anchor is shown in Figure 3.12f.

Note: Due to the results of the several tests, an improved construction process was adopted. The reason is discussed in the results and discussion section of this chapter.

Figure 3.11: Example of a simulated Field Application[16]

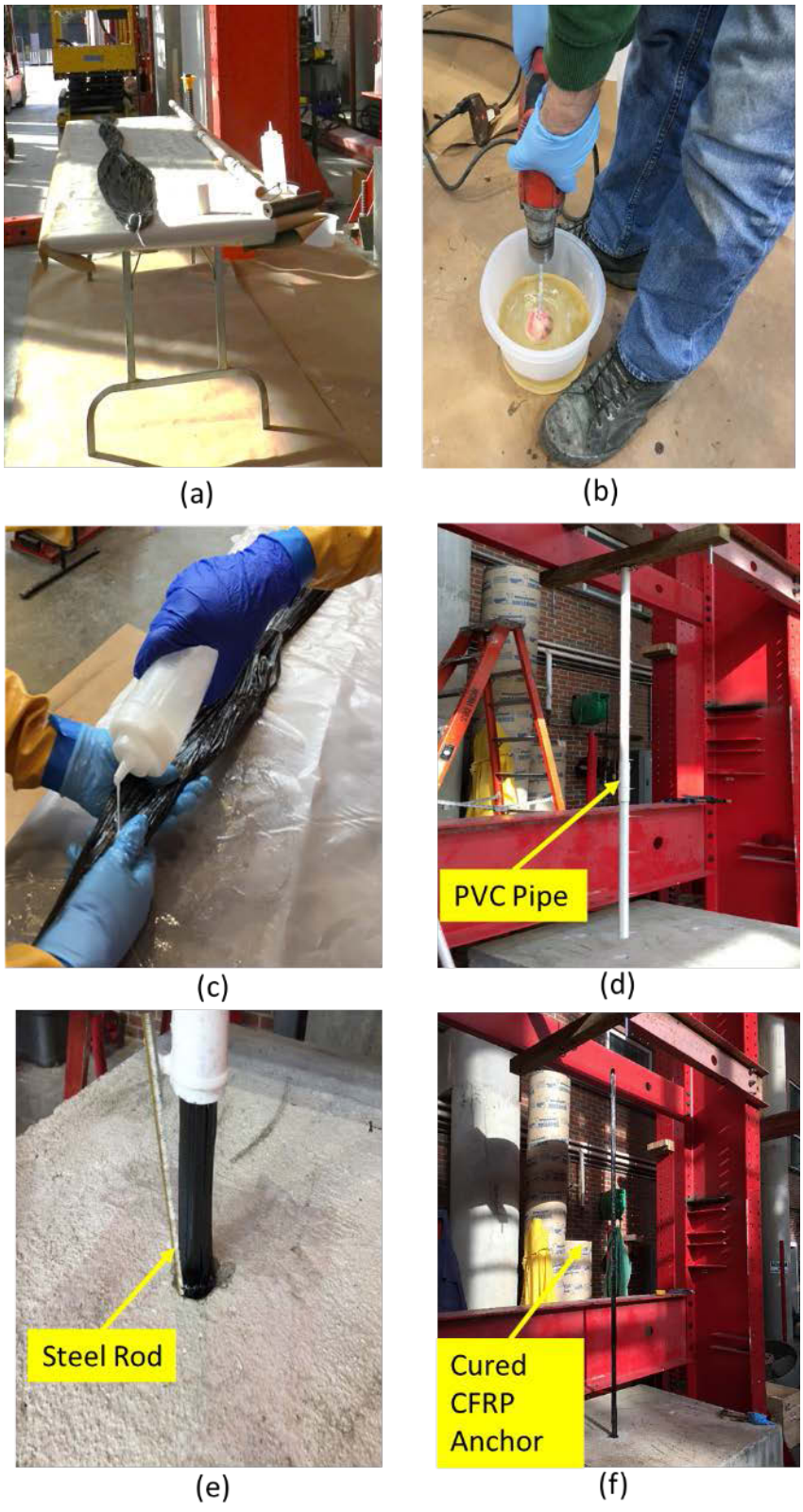

Figure 3.12: Anchor Preparation Method-A

3.1.6.3 Preparation Method-B

Due to the results of the first couple of anchor tests, the preparation method for the CF anchor was slightly changed to increase the efficiency of the anchors. The discussion on anchor efficiency was presented in the introduction chapter of this report.

The steps for the preparation method as follow:

1. The CF anchor was set on a table, which was covered with a plastic sheet. Then the fibers gently spread on the table as shown in Figure 3.13a.
2. The two-component epoxy was mixed following the instructions provided by the manufacturer, shown in Figure 3.13b.
3. Using a squeezed bottle, carbon fibers were gentled saturated as shown in Figure 3.13c. It should be noted that over saturation of the fibers may cause swelling of the anchor, which may later be an issue, when the anchors are pulled into the PVC pipe.
4. A 9ft.-long PVC pipe was used to form a circular cross-section as shown in Figure 3.13d. The saturated carbon fiber bundles were pulled into a PVC pipe and vertically hung until cured.
5. The anchor hole was filled with the epoxy before installing the cured anchor.
6. Later, the cured anchor was inserted into the drilled hole without utilizing a steel rod, as shown in Figure 3.13e.

Note: Improvement in the efficiency was observed, but upon a carefully examination of the produced anchors, misalignment of the fibers was observed**.** Thus, a further change in the preparation method was adopted to reduce the misalignment of the fibers the anchors.

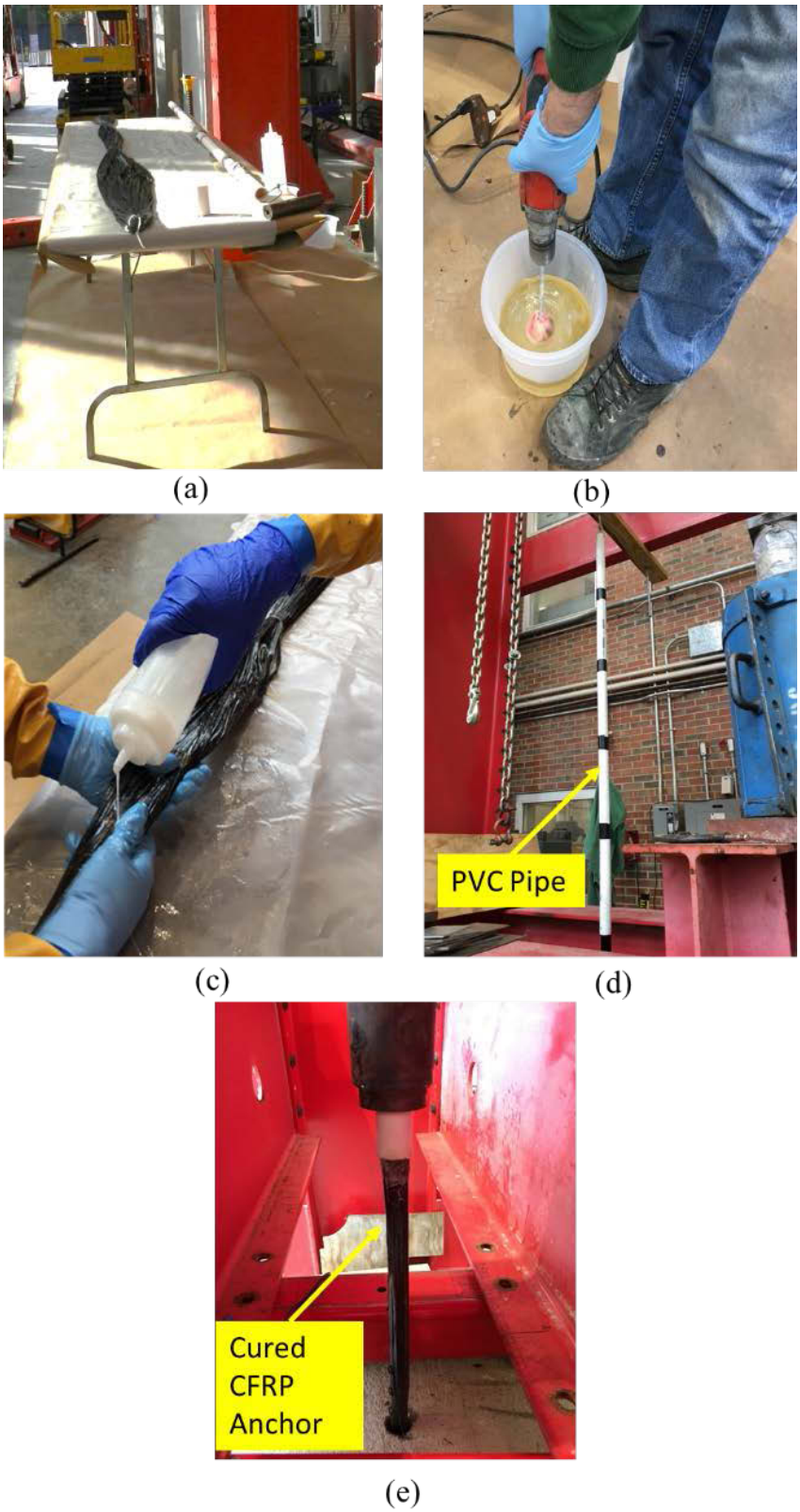

Figure 3.13: Anchor Preparation Method-B

3.1.6.4 Preparation Method-3

As mentioned above, although preparation Method-B resulted in an improved efficiency, the second preparation method was slightly modified to improve the alignment of the carbon fibers.

The steps for the third preparation method were as follows:

1. The CF anchor was set on a table, which was covered with plastic sheet. Then the fibers gently spread on the table as shown in Figure 3.14a.
2. The two-component epoxy was mixed following the instructions provided by the manufacturer, shown in Figure 3.14b.
3. Using a squeezed bottle, the carbon fibers were gentled saturated as shown in Figure 3.14c. It should be noted that over saturation of the fibers may cause swelling of the anchor, which may later be an issue, when the anchors are pulled into the PVC pipe.
4. The saturated CF anchor was pulled in a 4 ft.-long PVC pipe and hung as shown in Figure 3.14d. Later, the fibers were aligned by hand. Figure 3.14e shows an anchor example for the preparation Method-C. A more uniform circular cross-section was obtained.
5. The drilled hole was filled with epoxy before installation.
6. Later, the cured anchor was installed into drilled hole without utilizing a steel rod, as shown in Figure 3.14f.

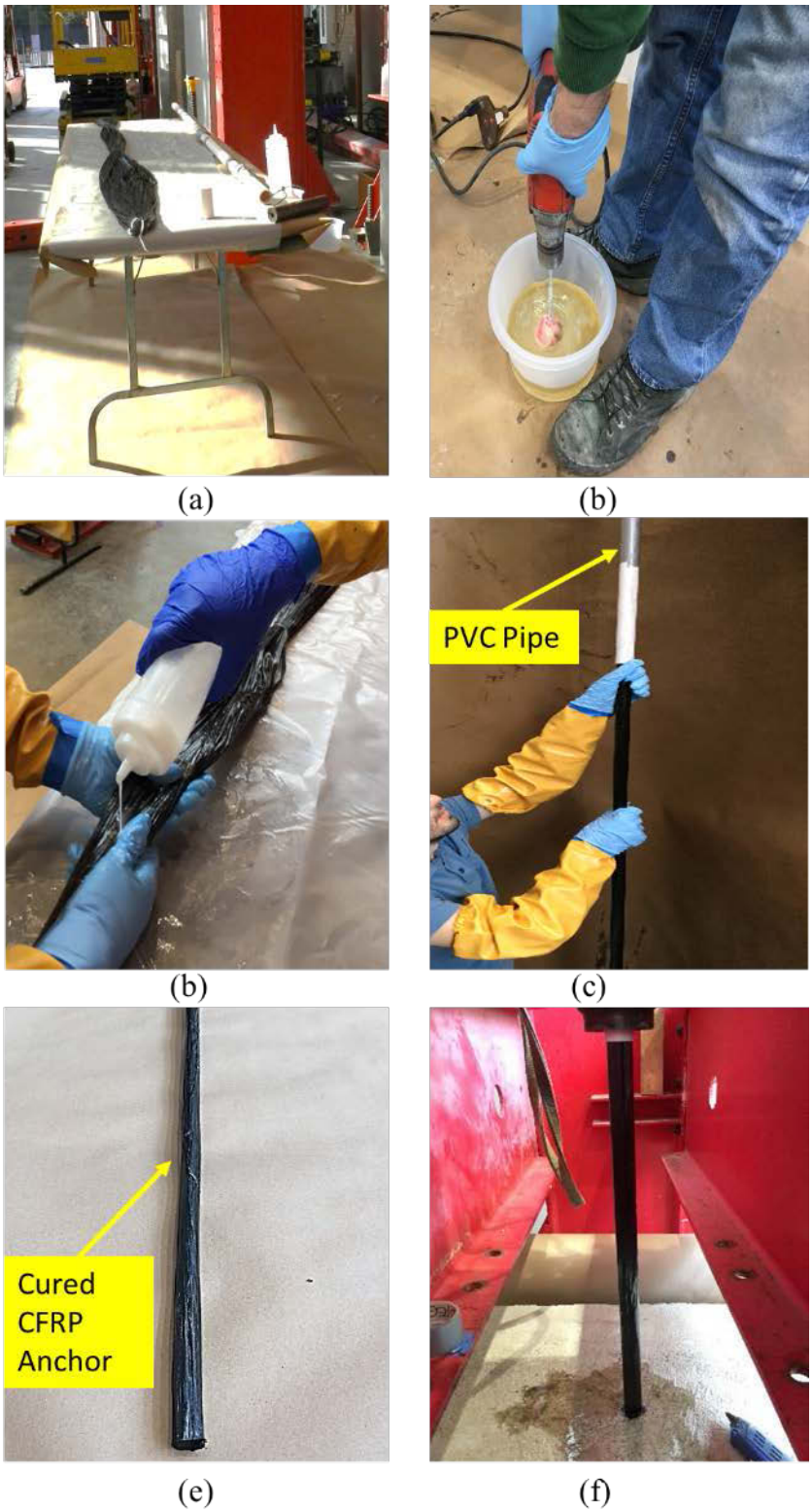

Figure 3.14: Anchor Preparation Method-C

3.2 Results and Discussion

Results for all anchor tests are summarized in Table 3-2. The table shows the anchor diameter, embedment depth, observed failure mode, average stress developed in the anchor, strain at failure of the anchor, and efficiency.

Table 3-2: Results of Tested Anchors

No. Test	Nominal Anchor Diameter (in)	Embedment Depth (in)	Failure Mode	Calculated Average Stress (ksi)	Max. Measured Strain	Efficiency (%)	Anchor Preparation Method
1	1-1/4	$10*d_{hole}$	Rupture	83	0.009	58	A
2	1-1/4	$10*d_{hole}$	Rupture	44	0.004	31	A
3	1-1/4	$11*d_{hole}$	Pull-out	87	0.007	61	B
4	1-1/4	$11*d_{hole}$	Pull-out	65	0.0054	46	B
5	3/4	$10*d_{hole}$	Rupture	68	0.005	47	A
6	3/4	$10*d_{hole}$	Rupture	44	0.005	31	A
7	3/4	$12*d_{hole}$	Rupture	131	0.01	92	B
8	3/4	$13*d_{hole}$	Rupture	166	0.012	116	C
9	3/4	$13*d_{hole}$	Rupture	168	0.013	117	C
10	1	$12*d_{hole}$	Pull-out	73	0.005	51	B
11	1	$12*d_{hole}$	Pull-out	127	0.01	89	C
12	1	$12*d_{hole}$	Rupture	117	0.01	82	C
13	1	$12*d_{hole}$	Rupture	119	0.01	83	C
14	1	$12*d_{hole}$	Pull-out	128	0.01	90	C
15	1	$13*d_{hole}$	Pull-out	138	0.012	96	C
16	1	$13*d_{hole}$	Pull-out	139	0.011	97	C

Average stress was calculated by dividing the max force developed in the experiment to nominal area of the anchor. Calculating an average stress is a rational choice as it is known that the stress in the anchor is non-uniform through the section due to the interaction between the fibers and the epoxy. The efficiency [9][10], as discussed before, was calculated as the ratio of the average stress obtained to the theoretical rupture capacity provided by manufacturer. This quantity can be interpreted as the performance of the anchor under tensile load. Moreover, for anchors failed in rupture, it can be thought that the efficiency increases, as the quality of the anchor increases.

3.2.1 Overserved Failure Modes

Several failure modes were observed in this experimental program. Figure 3.15 shows the observed failures modes. Brooming rupture was only observed in one of the ¾ in. diameter anchors as shown in Figure 3.15a. Most of the anchors, which failed by rupture, display the failure mode shown in Figure 3.15b. Some of the anchors exhibited pull-out failure, as shown Figure 3.15c.

Figure 3.15: ***Observed Failure Modes of CFRP Anchor: a) Brooming Rupture b) Rupture c) Pull-out***

It was observed that the pull-out failure became the main failure mode as the preparation method of the anchor improve. The reason is attributed to insufficient embedment depth of the anchors, as the theoretical capacity increase due to the better fiber alignment and manufacturing process.

3.2.2 The impact of Preparation Method, Anchor Hole Diameter and Embedment Depth on the Behavior of the Anchors

One of the key factors impacting the anchor efficiency was found to be the anchor preparation method. The impact of the preparation method can be seen in the efficiency distribution. Figure 3.16 shows the efficiency distribution of all tested anchors. Each preparation method in the graph was represented by different geometrical shape. Method-A, Method-B and Method -C are designated by diamond, triangle and circular shapes, respectively. An effective comparison can be done by looking at the efficiency distribution of the ¾ in diameter anchors, since all preparation methods were utilized, and the all tested anchors failed by rupture. As the anchor preparation method improved so did the efficiency. It was observed that preparation Method-C gave higher capacity than the other two preparation methods. Again, this was attributed to the improved fiber alignment in the direction of loading, as the quality of the preparation method was improved.

Figure 3.17 shows the anchors prepared by using Method-A and Method-C. Fibers bulged at the top of the drilled hole when preparation Method-A was used. This was attributed to use of the steel rod when installing the saturated anchor in the drilled hole. As the anchors were pushed into holes through the looped end by a steel rod. The steel rod caused misalignment of the fibers as shown in Figure 3.18. As the steel rod was removed, epoxy moved into the gap created by the steel rod. Therefore, fibers were remained misaligned which resulted in a reduction in the capacity. This shows that sensitivity of the alignment must be considered.

For ¾ in. diameter anchors, it was observed that an anchor hole diameter of 1 in. was appropriate regardless of the preparation method. As the preparation method varied to improve quality of the anchors, embedment depth was increased to make sure that the rupture capacity of the anchor could be achieved. For an anchor diameter of ¾ in., an appropriate embedment depth is 13 in, or $13d_{hole}$.

For 1 in. diameter anchors, only two preparation methods were used. Only one anchor was prepared by Method-B, and the rest of the anchors were prepared using Method-C. The anchor, which was prepared using Method-B, failed by pull-out with a lower level of efficiency. The reason for such a lower efficiency was because of the oversized anchor hole diameter. Due to the available drill bit at the time of drilling, a hole diameter of 1-1/2 in. was used. Because of the oversized hole, the resulting layer of epoxy at the interface between the anchor and concrete block was thicker. Due to the subsequent shear failure through the thick layer epoxy, a less efficient anchor capacity was obtained. Anchors with anchor hole diameter 1-1/4 in. were more efficient. Therefore, for 1 in. diameter anchors, 1-1/4 in. anchor hole diameter was found to be appropriate. Moreover, although Method-C was used for the rest of the anchors, two different failure modes were observed. Only two anchors were failed by rupture with an efficiency lower than the anchors failed by pull-out. It is believed that the amount of epoxy used to impregnate the anchors was inadequate. For the 1 in. diameter anchors, the embedment depth was slightly increased as the preparation method was modified to make sure that rupture capacity of the anchor could be reached. It was observed that slight change in embedment depth resulted in a small increase in the efficiency. This suggests that the provided embedment depth for 1 in. diameter anchors should be increased above $12d_{hole}$.

For the 1-1/4 in. diameter anchors, only preparation Method-A and Method-B was used. It can be seen in Figure 3-15, an improvement was observed as the method improved but there is a need for more testing to confirm the improvement in the anchor quality. For anchors prepared by Method-A, rupture failure was observed, but a huge stress variation was observed due to flaw caused by the preparation method. As the preparation Method-B used, embedment depth increased to resist the increased capacity and the failure mode changed from rupture to pull-out. But it was concluded that the provided embedment depth ($13d_{hole}$) was inadequate to rupture the anchors. Using 1-1/2 in. diameter hole was assumed to be enough, as the intention was to have least amount of epoxy around the embedded anchor.

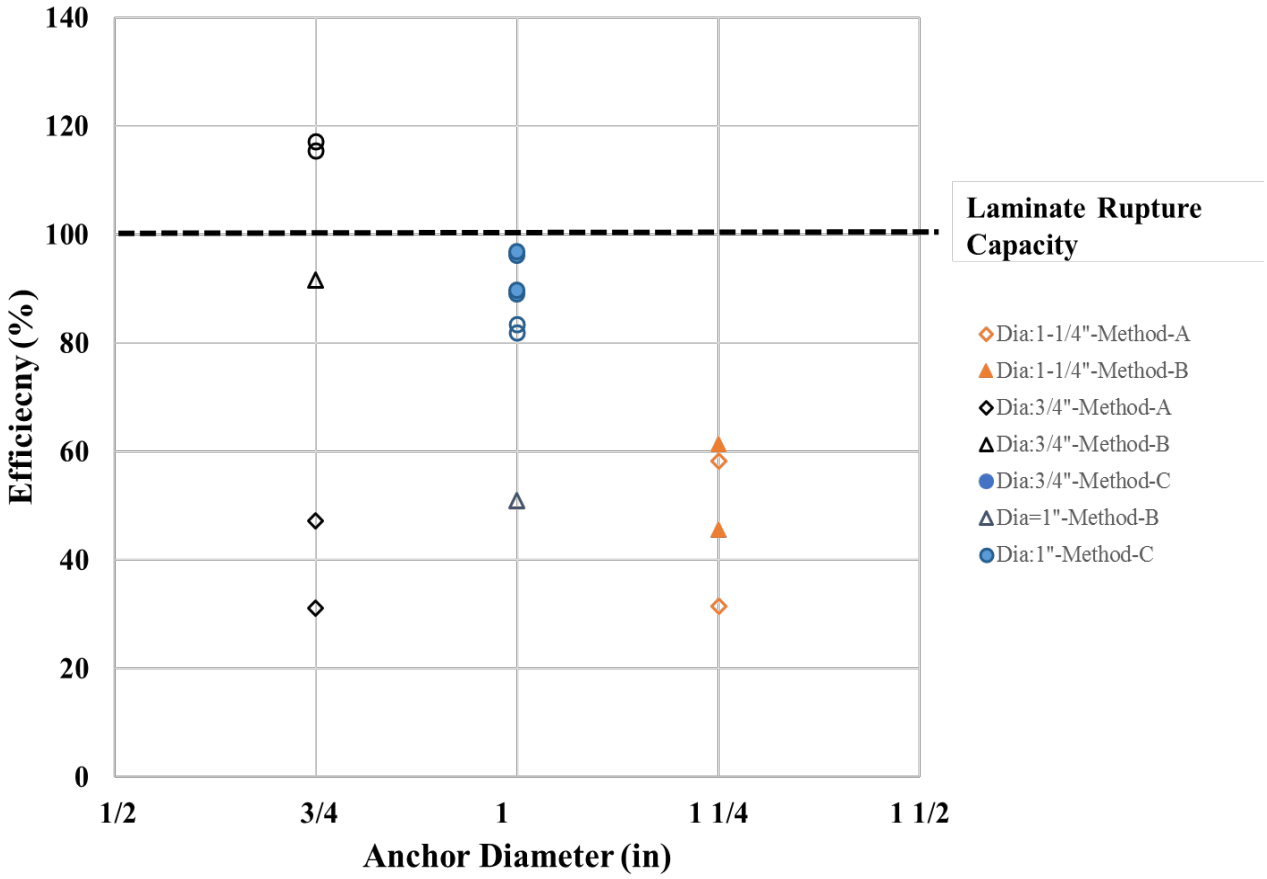

Figure 3.16: Efficiency Distribution of Tested Anchors

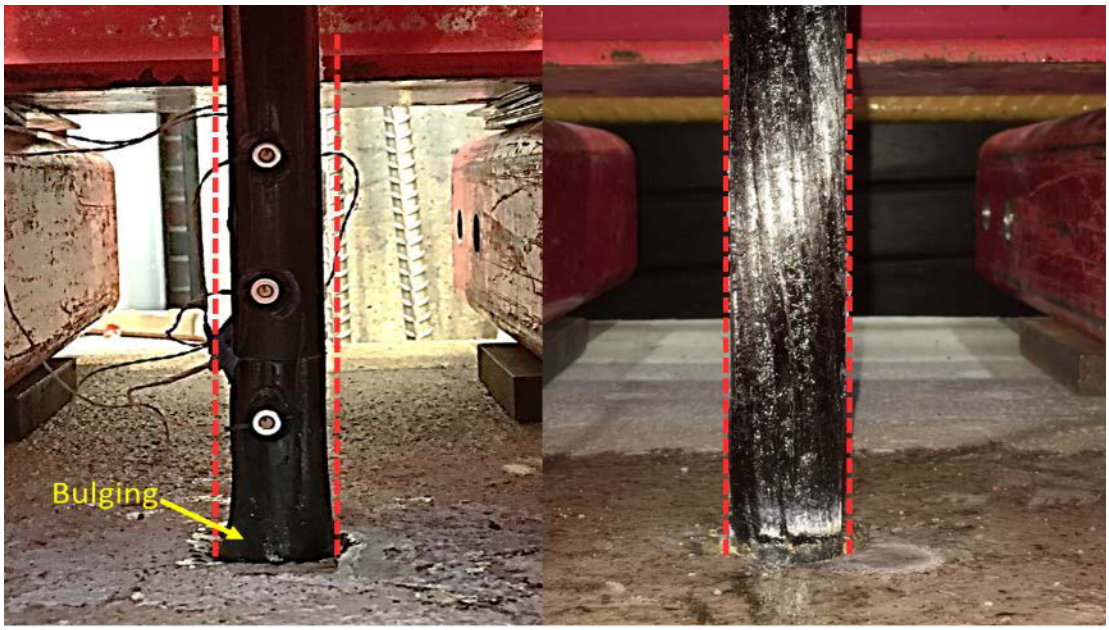

Figure 3.17: Anchors Prepared by Different Methods a) Method 1 b) Method 3

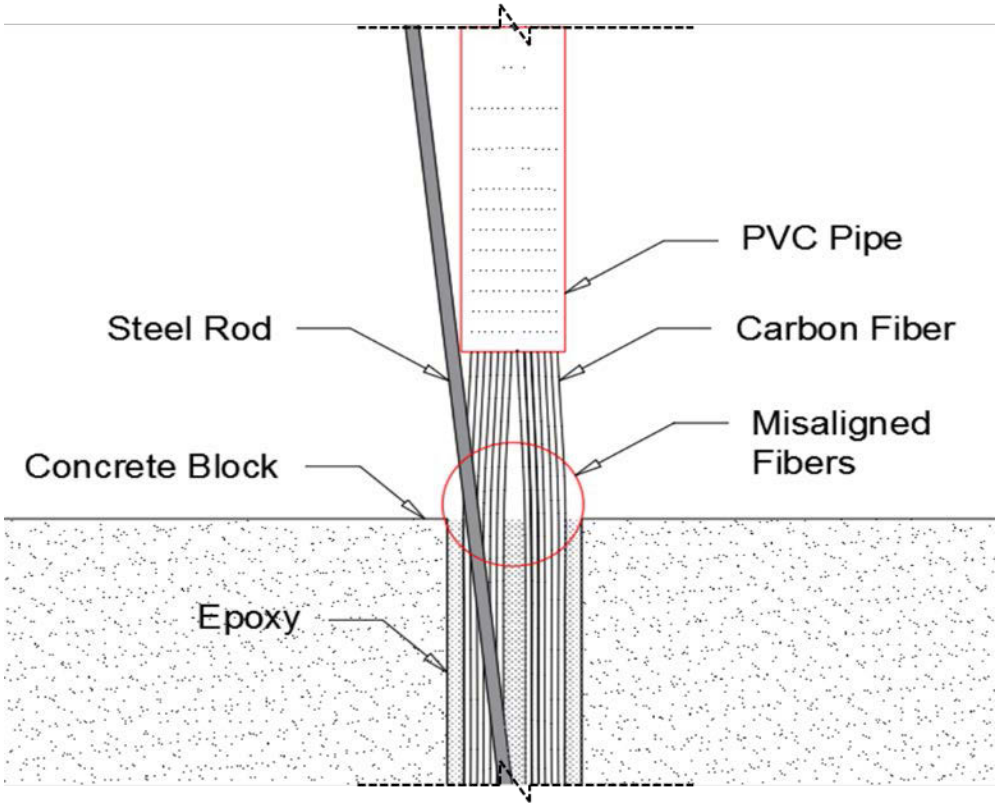

Figure 3.18: Schematic for Preparation Method-A

3.2.3 Impact of Anchor Diameter on the Capacity of Anchor

As discussed in Chapter 2, the main reason for not having a linear increase in the capacity of CF anchors similar to steel reinforcing bars were attributed to force-transfer mechanism developed in anchor cross section. The stress in the fibers were transferred from one fiber to another through epoxy, which is relatively softer material. Due to the epoxy in the cross section, a shear lag effect causing a non-uniform stress distribution in the anchor occurred [19] . As the size of the anchor increases, shear lag effect became more profound. Therefore, efficiency of the anchor decreases as the anchor diameter increases [9].A similar trend was observed for the tested anchor diameters, although failure mode for some anchors was not always rupture. Recall Figure 3.16 which shows the efficiency of the tested anchors.

3.3 Conclusion and Future Work

As the idea behind the testing program is to determine design stress limits for anchor size ¾ in, 1 in and 1-1/4 in, several anchor tests were conducted. Due to stress variation observed in some of the test results, a better understanding on the behavior of large diameter CFRP anchors under direct tension was aimed to develop. Although the number of test results was not sufficient to developed design stress limits, which were not directly used in this research study, testing program enabled to better understand impact of the preparation method and the anchor diameter on the capacity of the CFRP anchors.

3.3.1 Conclusion

Results obtained from this experimental program provided the following conclusions:

- The number of the tests were not sufficient to statistically quantify the theoretical upper and lower bond capacity of the anchors due to initially unforeseen issues such has the impact of preparation method on the capacity of the CFRP anchors.
- Quality control of the anchors is a crucial factor which affected the capacity of the anchors.
- More efficient anchors were constructed using preparation Method-C which is not suitable for real field applications.

- Provided embedment depths of $16d_b$ and $14d_b$ for anchor diameter 1 in and 1-1/4 in, respectively, was not sufficient.
- Diameter of drilled anchor holes of 1 in, 1-1/4 in and 1-1/2 in were appropriate for ¾ in, 1 in and 1-1/4 in diameter CFRP anchors, respectively.

3.3.2 Future Work

The following future works are essential to better understand behavior of CF anchors under direct tension.

- Perform more tests to statically quantify the theoretical rupture capacity of the anchors.
- Perform more tests to determine required embedment depth larger than used in this testing program for each anchor diameter.

Chapter 4: Behavior of Large Diameter CF Anchors under Column Bending

4.1 Experimental Program

Use of large-diameter CFRP anchors for seismic repair of columns with buckled bars was studied, including the effectiveness of CFRP anchors for relocating plastic deformations by Rutledge et al. [1]. But, specific design details for CF anchors were not reported. It is essential for practicing engineers to have specific guidelines to develop robust designs. Therefore, each factor, which has an impact on the capacity and behavior of large-diameter CFRP anchors should be investigated. As discussed in Chapter 1of this report, fan angle, fan length and embedment depth of the anchors are among the parameters which impact the capacity of the anchors. The goal of the testing program is to utilize CF anchors to repair severely damaged columns by plastic hinge relocation. Thus, using column elements to investigate the above-mentioned parameters for a single anchor is more realistic.

The following includes three column tests using column obtained from another research study [20].

The aim of the testing program was to answer the following question:

- What should be the length of the anchor fan to develop the full rupture capacity of the CF anchor?
- What should be the optimum fan angle?
- How many layers of vertical fibers is needed?
- If the provided fan length is not sufficient, what approach should be followed to improve the bond between fan part and the concrete substrate?

4.1.1 Condition of Tested Columns

As stated before, the columns used in this phase were obtained from another research study which focused on the use of Gr.80 steel for seismic reinforcement. In total, four columns were obtained. The columns are 24 in. in diameter and have 16 No.6 bars evenly distributed around the column. Three out of the four columns have three fractured and two buckled bars at both extreme faces the columns. Figure 4.1 shows the typical damage level in one of the columns. The reason for using these columns for testing anchors was the damage level observed in the columns. The idea was to install anchors on both extreme face of the columns where bars were fractured so that the CF anchors can be placed under direct tension. In this way, it was hoped that the force resisted by the CF anchors could be determined using equilibrium.

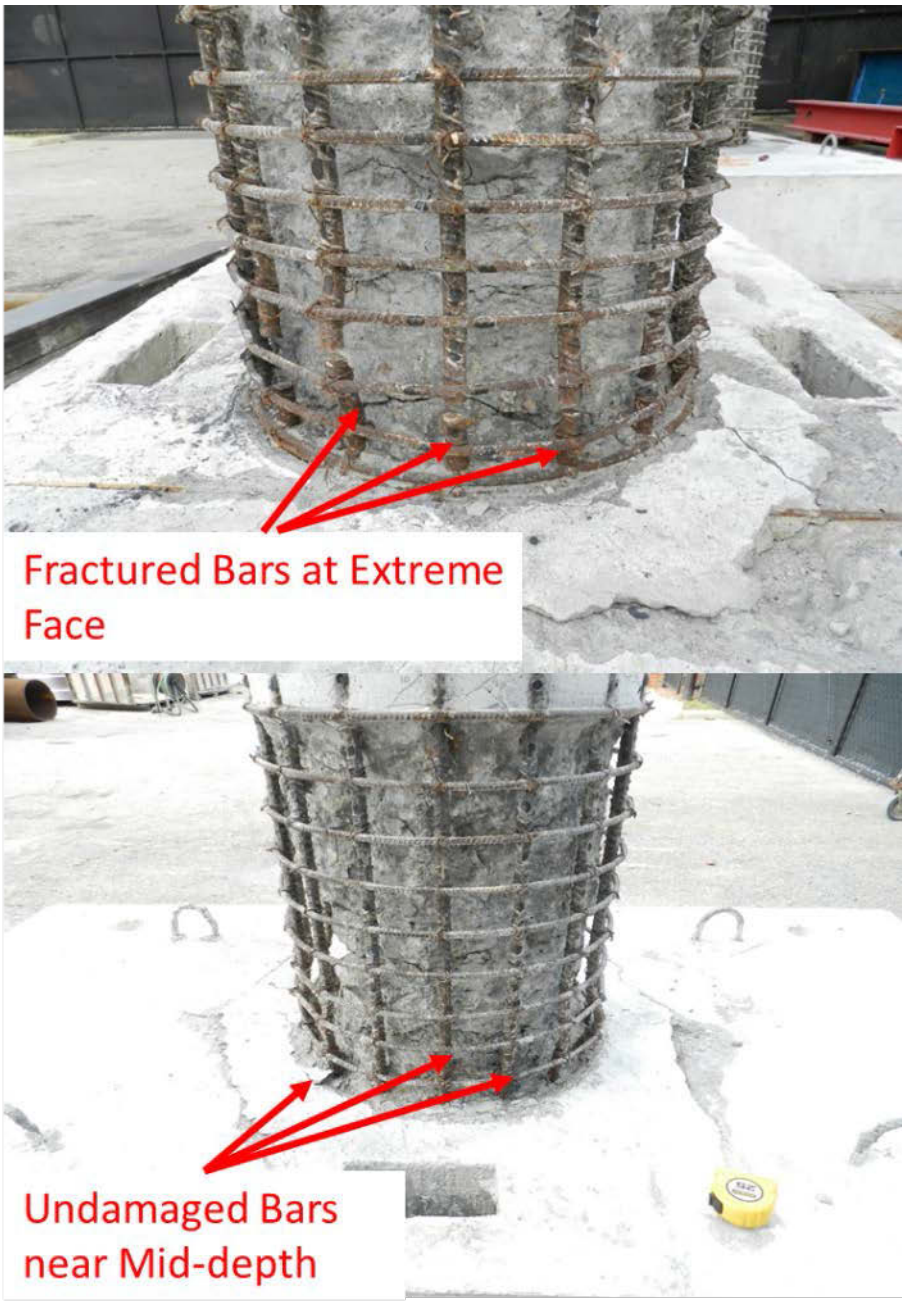

Figure 4.1: Condition of Tested Columns

4.1.2 Preparation of Tested Columns

4.1.2.1 Restoration of Concrete Section

It is necessary to repair any damaged concrete and restore the cross-section. The longitudinal bars were exposed in the previously tested columns to collect data via the Optotrak

system, and the damage was in form of bar buckling, bar fracture and core concrete crushing in the plastic hinge region. High strength non-shrink grout was used to restore the circular concrete section. Any loose and damaged core concrete was removed but nothing was done to the steel reinforcement. To create a good bond between the non-shrink grout and the reinforcing bars, concrete from behind the bars was also removed as shown in Figure 4.2. Later, to clean dust and debris from the core concrete, pressurized water was applied to the concrete surface.

Figure 4.2: Removal and Cleaning of Loose Core Concrete

As shown in Figure 4.3, foam blocks were placed on the straight bars near the mid-height to block out the high-strength grout so that strain gauges could be attached to the bars. The damaged columns were 24 in. in diameter, but a 26 in. circular cross-section was created using the grout. The reason for using a larger diameter cross-section was to make sure that all the longitudinal steel reinforcing bars had enough concrete cover. Due to the buckled bars at the plastic hinge region, a larger cross-section was needed. A flexible board, shown in Figure 4.4, was placed around the column to serve as the form for the high-strength grout repair. After removing the form, a smooth surface was obtained as shown in Figure 4.5.

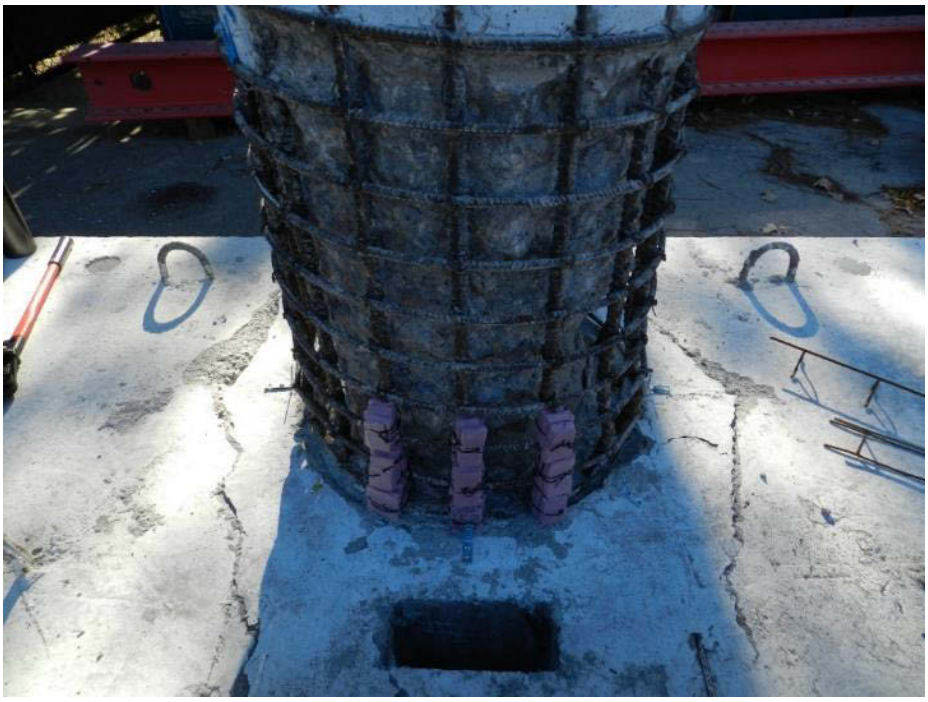

Figure 4.3: Foam Board to Bloc-out Grout on Straight Bars

Figure 4.4: Form Work and High-Strength Grout

Figure 4.5: Restored Circular Concrete Section

Once the column section is restored, the footing was drilled for required diameter and depth of the anchor as shown in Figure 4.6a. To remove any sharp edges that may damage the FRP, the edge of the drilled hole was rounded using a drill bit provided by CF anchor manufacturer Figure 4.6b. The restored grout surface was later roughened to prepare the surface for the externally bond the FRP. A needle gun was used according to the manufacturer recommended installation procedure as shown in Figure 4.6c. Finally, the hole was cleaned using a steel brush, which had the same diameter as the hole Figure 4.6d. The brush was used to remove loose concrete debris due to drilling. Later, compressed air was blown into anchor hole to remove dust.

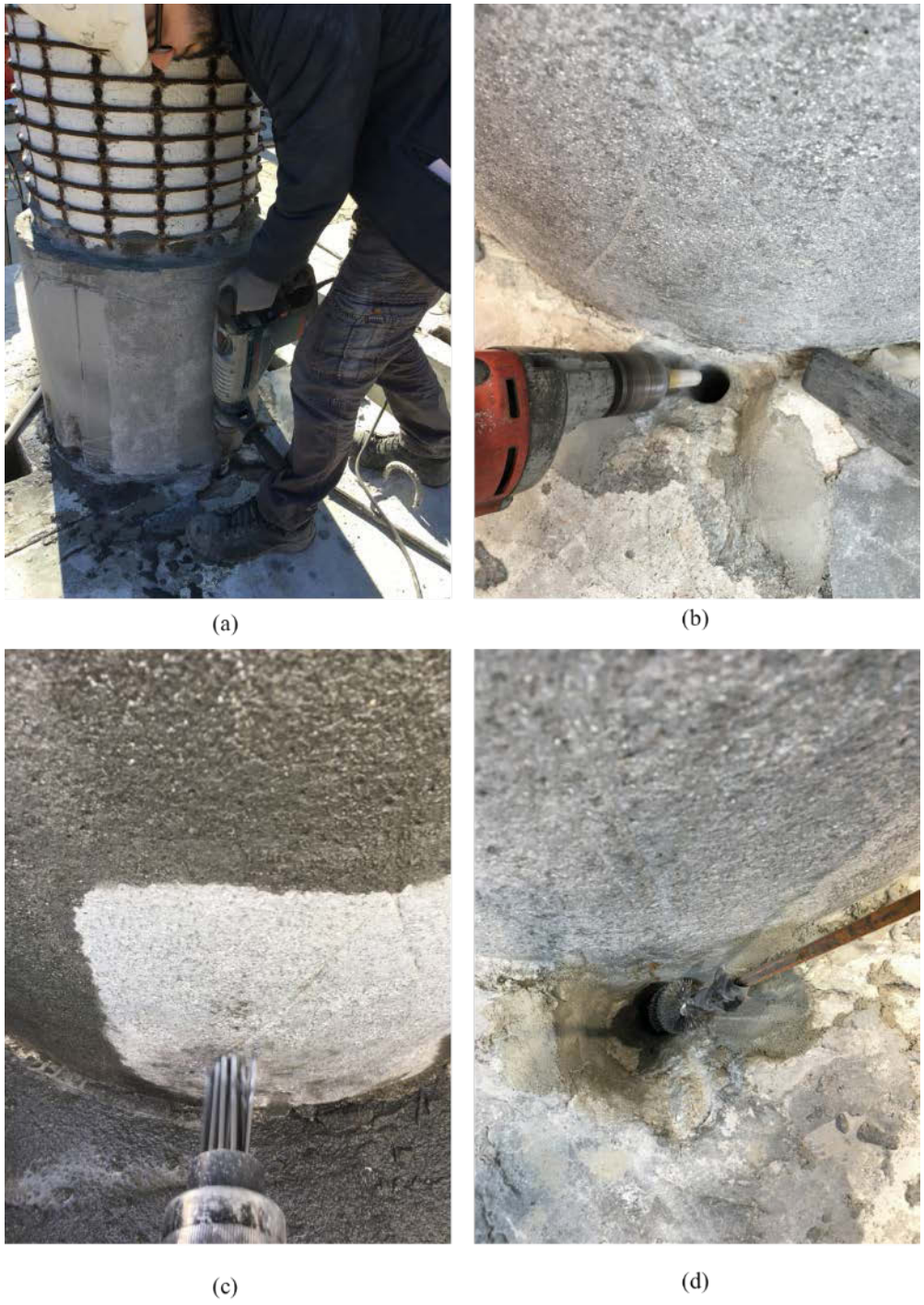

Figure 4.6: Preparation Steps

4.1.2.2 CF Anchor Application

Once the RC elements are prepared, the following steps were followed to install the CF anchors and CFRP sheets:

- A two-component epoxy was mixed according to manufacturer recommendations.
- The CFRP sheet was saturated using a roller brush to ensure that CFRP is well saturated as shown in Figure 4.7a.
- Dust free grout surface was saturated using the same roller brush, shown in Figure 4.7b.
- The saturated sheet was attached to concrete surface, shown Figure 4.7c. It should be noted that every epoxy has a different working-time, the application of CF anchors and CFRP sheets should be completed within working-time of the epoxy.
- More epoxy was applied to the attached CFRP sheet, shown Figure 4.7d.
- CF anchor was cut to the right length, and the loop end of the anchor cured a day before application to ease installation, as shown in Figure 4.7e.
- Dowel part of the anchor was saturate with epoxy, shown Figure 4.7f.
- Later saturated dowel part inserted in drilled hole which was filled with.
- Dry fan fibers were splayed on CFRP surface following the recommendations of the manufacturer, shown Figure 4.7g.It should be noted that the application of CF anchor is different for each CF anchor manufacturer.
- A bristle brush was used to saturate dry fibers, as shown in Figure 4.7h.
- A putty knife was used to stretch saturated fibers to form the fan part for a given angle, shown in Figure 4.7i. As observed in previous phase of experimental testing, bulging of the anchor fibers must be prevented to achieve expected capacity of the CF anchor.
- In addition to putty knife, a roller handle was used to remove air bubbles as shown Figure 4.7j.

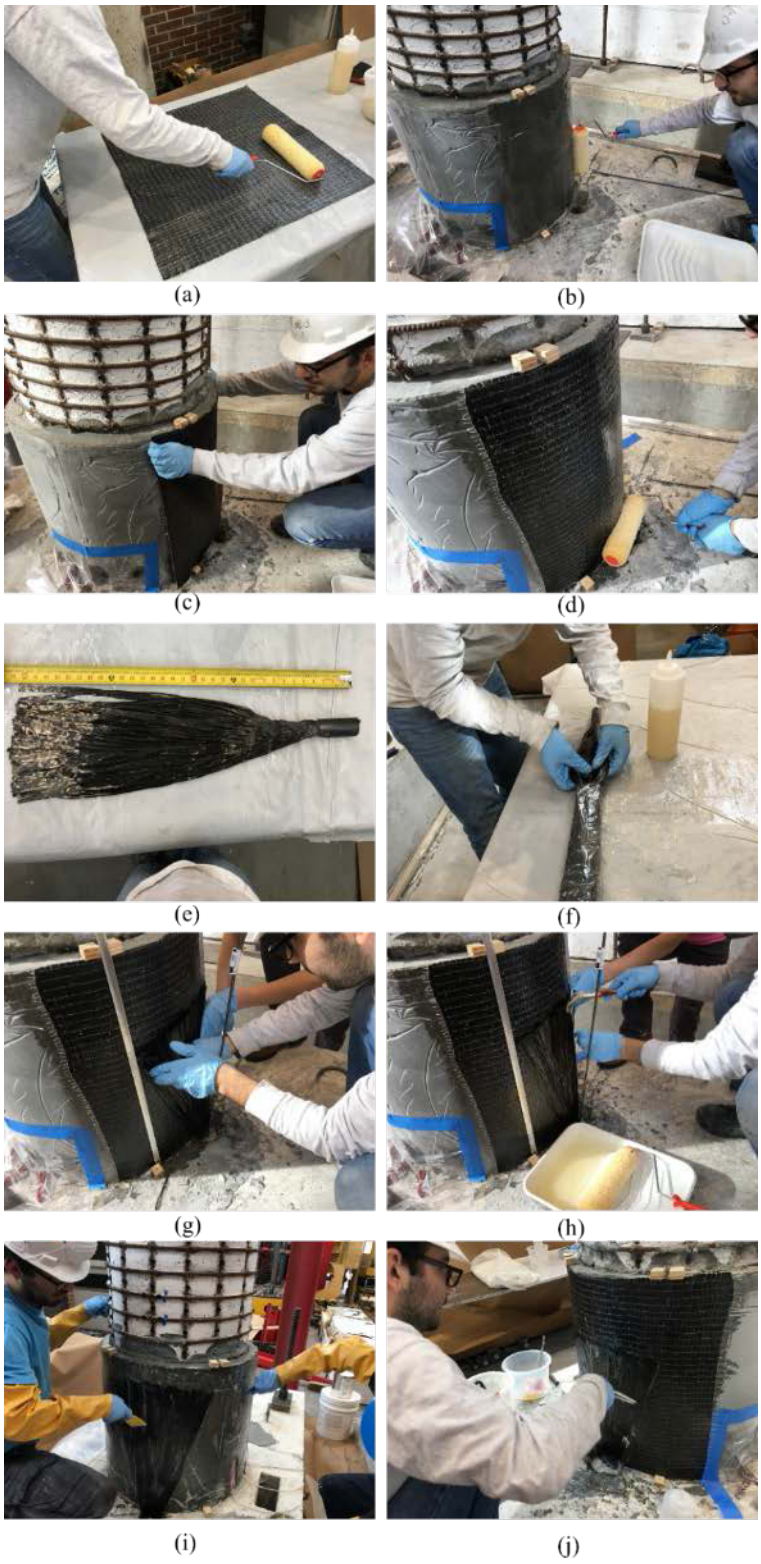

Figure 4.7: Anchor Preparation Process

4.1.3 Test Setup

As the goal of this testing program was to investigate behavior of CF anchors under column bending action, an experimental setup that was used in the previous research study was used. A schematic of the setup is shown in Figure 4.8. The lateral load is applied to the columns through a 110-kip capacity actuator with a ± 10 in. stroke capacity. Axial force was not applied to the columns, as only the column bending effect is of interest. The column is tied down to the strong floor via post-tensioning bars, and a half-inch-thick hydro stone layer was provided under the footing to secure it to the strong floor.

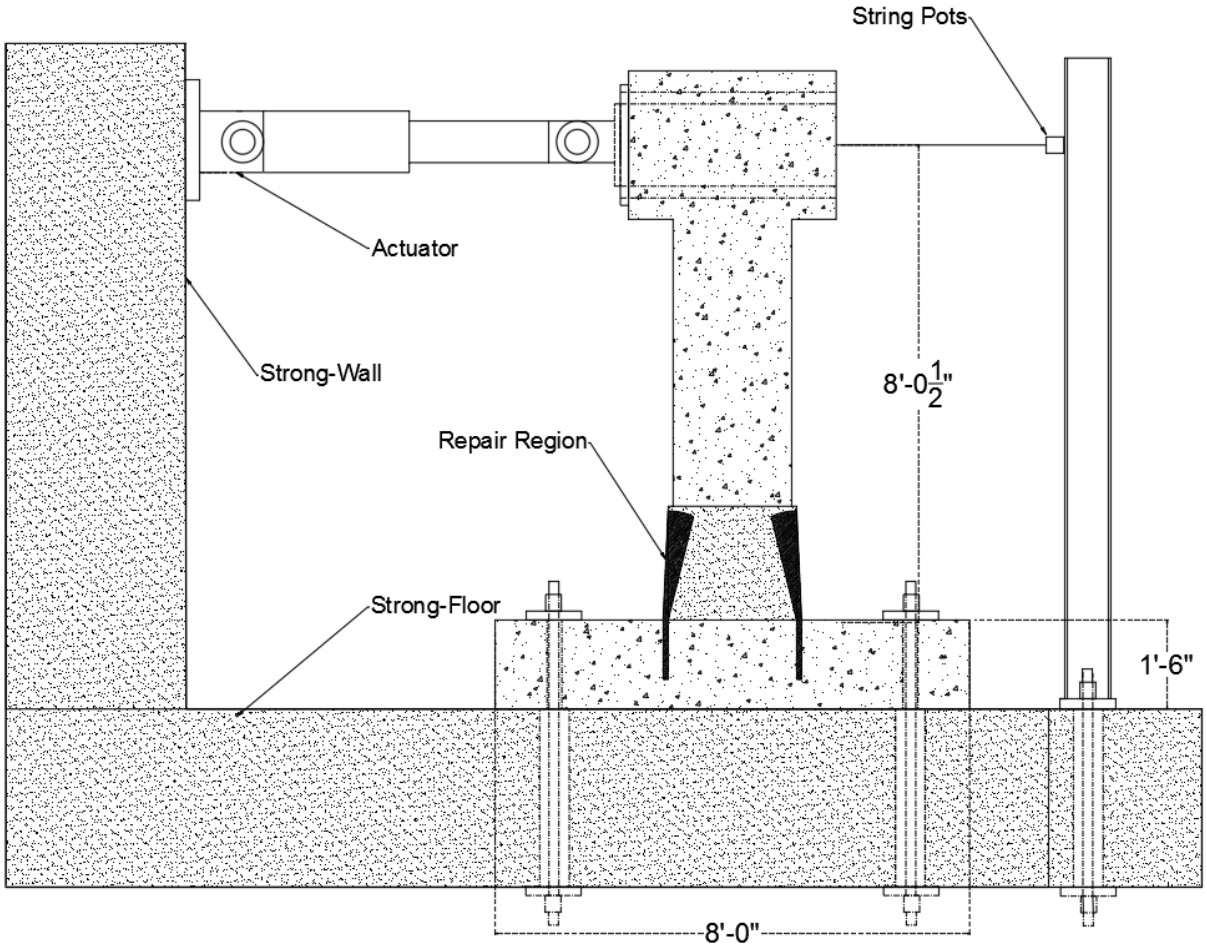

Figure 4.8: Schematic for Experimental Setup

4.1.4 Instrumentation

To experimentally measure the axial strain profile at the column, Optotrak LED target markers, shown Figure 4.9a, were applied on the reinforcing bars. Moreover, to check the accuracy of the strain data from the Optotrak system, strain gauges were also applied as shown in Figure 4.9b. Optotrak LED markers were also placed on CF anchor to collect strain data during loading. Digital image correlation (DIC) was also implemented to obtain strain field data for the CF anchor fan, as shown in Figure 4.9c. In addition to LED markers, a strain gauge was also applied at the bottom of the CF anchor, shown in Figure 4.9d. String pots were attached to the cap beam to collect global displacement data. The applied force was recorded via the actuator load cell.

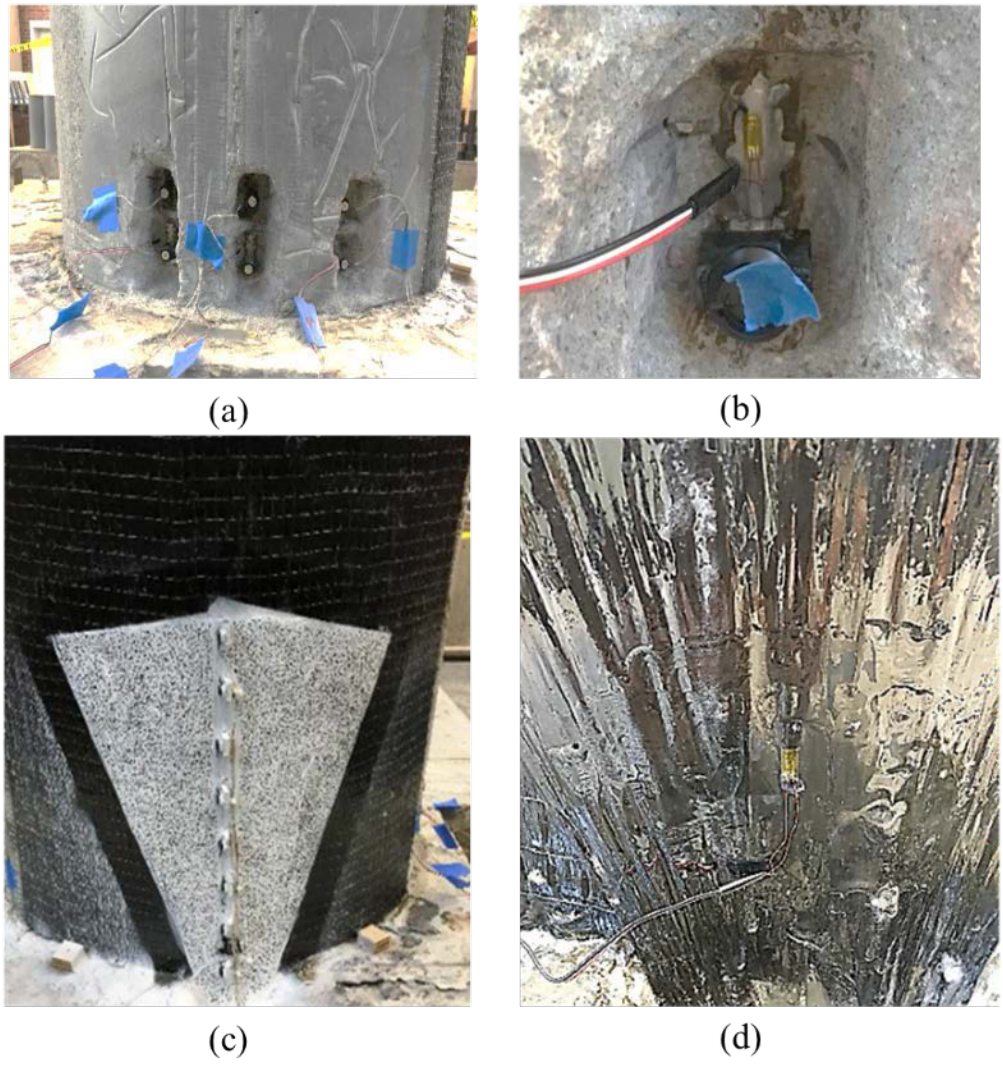

Figure 4.9: Instrumentation

4.1.5 Material Properties

Tyfo® SCH-41 composite sheets were used in this phase of the experimental program. The composite gross laminated properties provided by the manufacturer were 143000 psi ultimate tensile strength in the primary fiber direction, 1.0% elongation at break, 13.9x106 psi tensile modulus. CSS-CA anchors were used in this experimental program. Laminate properties of this anchors were128000 psi for tensile strength, 0.9% elongation at break 14200 ksi tensile modulus in primary fiber direction. This anchor properties slightly different than the ones that used in the first phase of testing. Most of the time dry fibers properties of each manufacturer is similar, but epoxy varies from manufacturer to manufacturer. Although there are dissimilarities in properties, overall behavior of the anchor is expected to be same. The non-shrink concrete strength at test day was 8.3 ksi, 8.5 ksi and 8.6 ksi for column 1, column 2 and column 3, respectively. It was aimed that the repair grout should have at least the compressive strength of the original column concrete.

4.1.6 Large-Scale Column Test

As mentioned before, all the column tests were conducted in this phase aimed to investigate behavior of CF anchors under bending action. Depending of the outcome of each anchor test, the next test was slightly modified to improve behavior of the anchor.

4.1.7 Column 1

For the first column, two separate anchor tests were conducted. For the first anchor test, the CF anchor was directly applied on concrete substrate as shown in Figure 4.10a. The fan width was about 15 in and the fan length was 22 in. After observing the results of the first test, a single layer of CFRP sheet was applied onto concrete substrate before installing CF anchor as shown in Figure 4.10b. The idea was to improve bond between the column and the CF anchor. As the vertical CFRP sheet added to the repair region, the fan length was kept shorter than the first anchor test due to expected increase in the bond capacity. The embedment depths were 13 in and 14 in for the first and the second anchor tests, respectively. The anchor hole diameter was 1-1/4 inches for both holes.

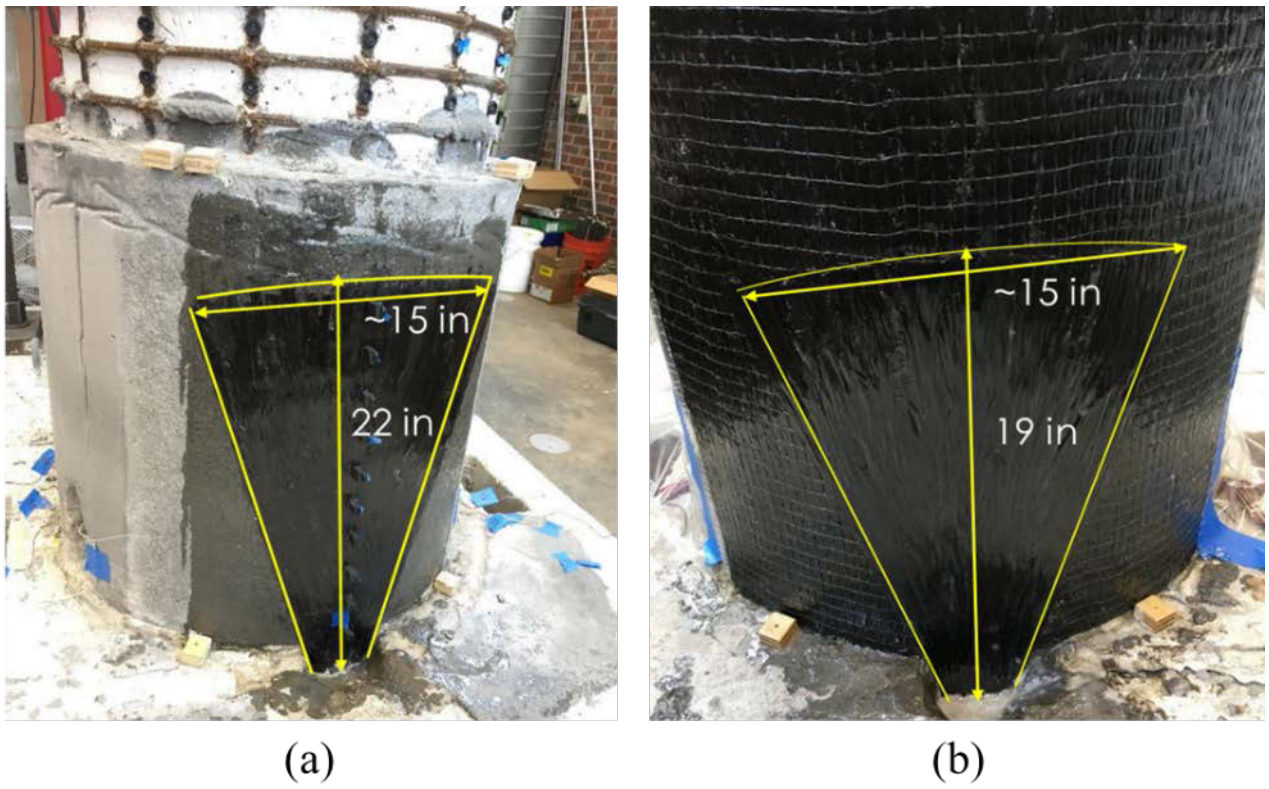

Figure 4.10: Column1 a) Test1 and b) Test2

4.1.7.1 Test Results

The column was tested under monotonic loading. A displacement-controlled loading was applied for both tests. Tests started by applying ¼ in. displacement and an increment of ¼ in. was applied until failure took place. The column reached 23 kips load at 0.75 in. top column displacement for both anchor tests as shown in Figure 4.11. For both anchor tests, debonding from the column grout substrate was the failure mode.

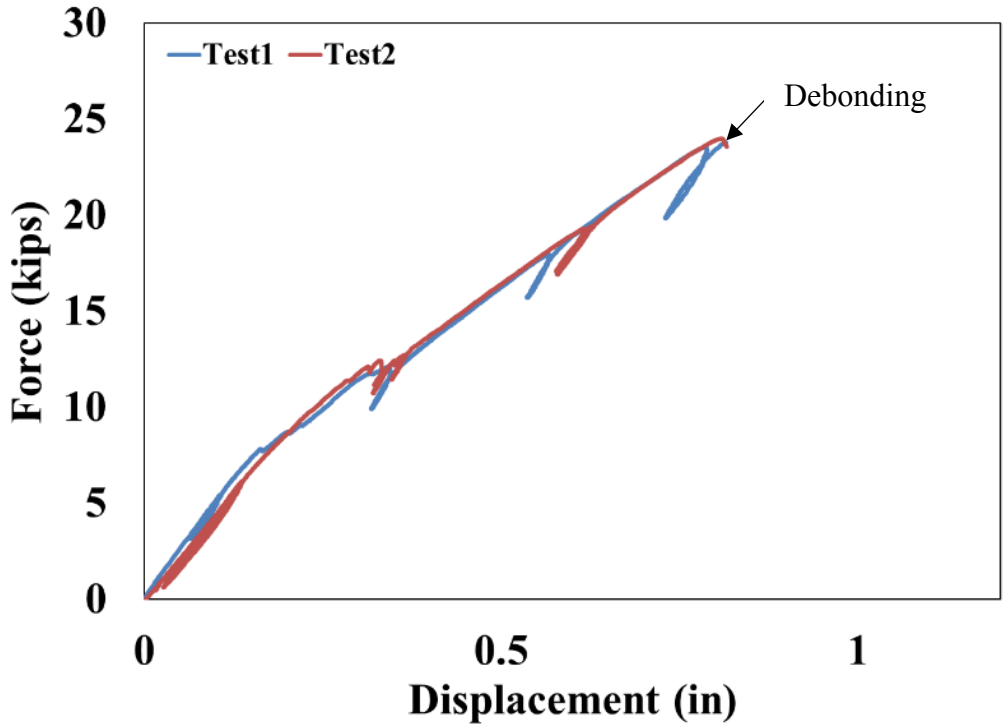

Figure 4.11: Force-Displacement of Column 1

The reason for the debonding failure was because of the interfacial crack propagation close to column base where the ruptured bars are located. Once the concrete cracks, interfacial cracking between the epoxy and grout substrate develops to accommodate the crack widening leading to debonding of CFRP sheet or the CF anchor as shown in Figure 4.12.

A typical strain distribution in an ideal anchor should be maximum at the column-footing interface were the anchor fibers enters the drilled anchor hole and should be close to zero at the tip of the anchor fan. This trend was observed in the anchor test with a slight difference. Due to cracking of the concrete, strain distribution showed different behavior. Figure 4.13 shows the strain distribution obtain from DIC and Optortrak data. Strain at the tip of anchor fan right before failure was close to zero as expected. A gradual increase in strain took place close to bottom part of the anchor. A sudden dropped in the strain was observed at 5 in. above the footing. This location was at a cracked plane of the concrete section.

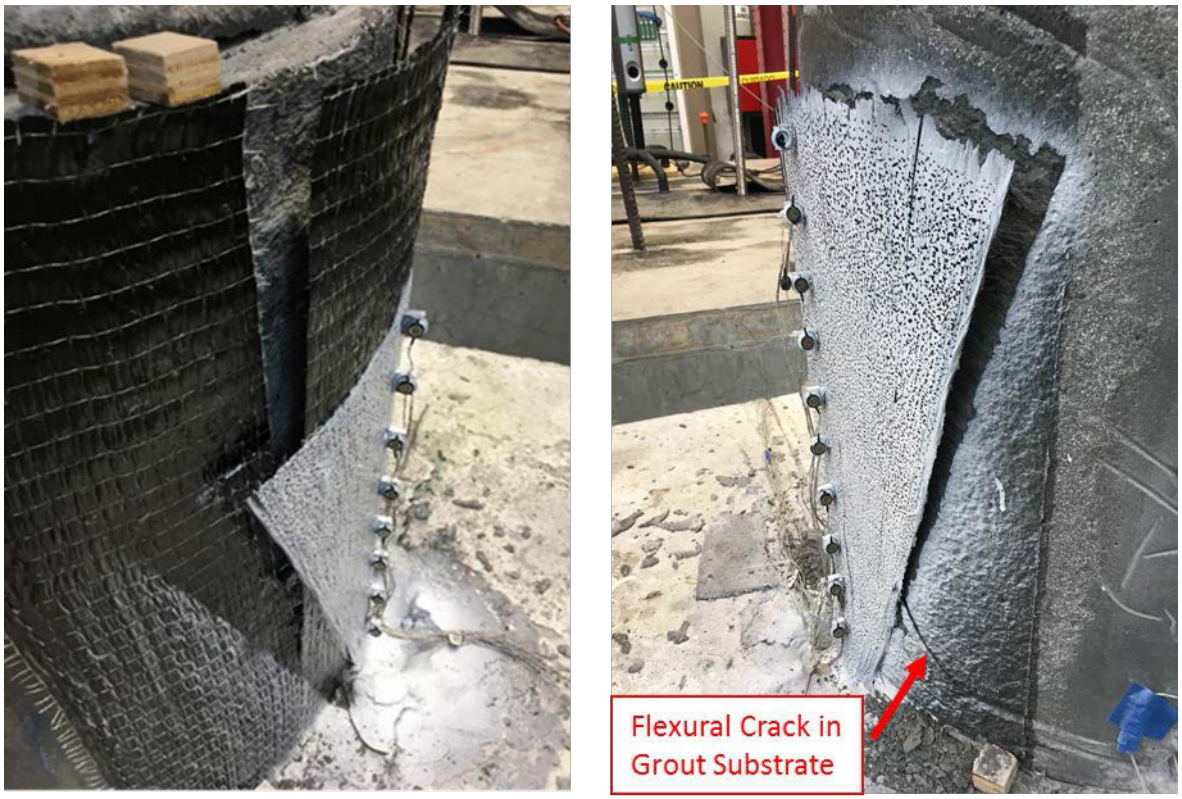

(a) (b)

Figure 4.12: Debonding Failure Observed in Experiments

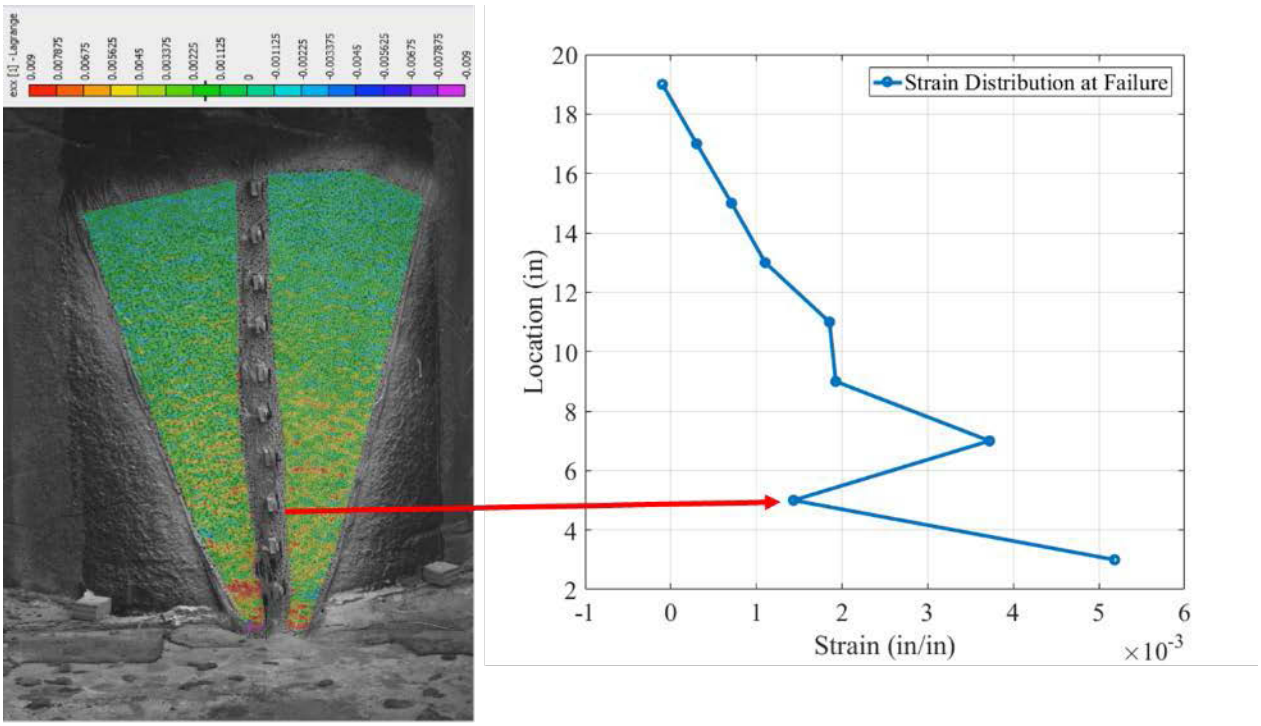

DIC

(a)

OPTOTRAK

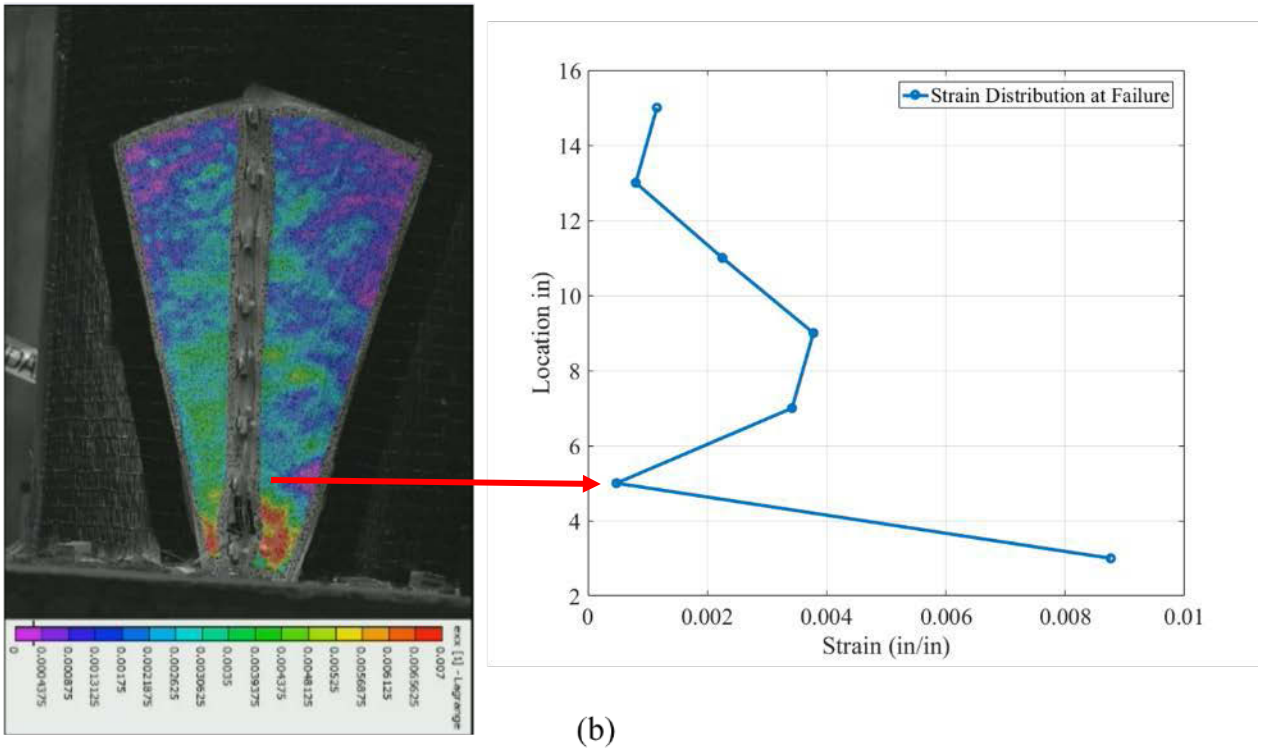

(b)

Figure 4.13: Strain Distribution in a) Anchor Test 1 b) Anchor Test 2

It was concluded from these anchor tests when CF anchors are bonded to concrete substrate with or without vertical CFRP sheets, due to the crack propagation close to the bottom of the column, debonding of attached material was the dominant behavior. This failure mode can be prevented or delayed by increasing the fan length. But due to the plastic hinge relocation concept, the length of the fan must be limited. The repair height for this testing program was taken as one column diameter. This was shown as a proper height by Rutledge et al. [1] Due to the repair height, the maximum fan length could be 24 in. As shown in the first column test, provided length was not adequate to develop rupture capacity of the anchor. Thus, an additional measure should be taken to prevent debonding of the anchor fan.

4.1.8 Column 2

As discussed before, there is a need to prevent the debonding of the CF anchor fan from the column grout substrate. Providing a longer anchor fan length was not option as the repair height was limited 24 in. Thus, wrapping anchor fan with CFRP hoop fibers was the only practical option. Design concept proposed by Rasheed et al. [21] was utilized to prevent debonding of the anchor fan from the column grout substrate. In the suggested design concept, the U-wraps were used to create clamping force to prevent debonding of FRP plates that were bonded beam bottom soffits. In order to develop full capacity of FRP plates to increase flexural capacity of a beam section, a strain limit was set for the U-wraps. Later, based on the friction developed between the concrete and the FRP sheet, the required force was calculated when the full strain capacity of U-wraps reached.

A similar approach was adopted in this research study. The assumption was that the provided transverse CFRP sheets should produce a confinement pressure (f_l) on the CF anchor fan as shown in Figure 4.14. The confinement pressure should produce a force level such that friction between the CF anchor fan and the concrete substrate can resist full rupture capacity (F) of the anchor. The required number of transverse CFRP sheet layers was determined based on the assumption that transverse CFRP sheet should developed its full capacity at strain level of 0.0058. This strain level was obtained from ACI 440.2R-17[22]. A coefficient friction of 1.4 was used by Rasheed et al. [21] for reinforced concrete structures. Since the size of the aggregates for non-shrink grout is smaller than the regular concrete, the coefficient friction was assumed to be 1.

Based on these assumptions, the required number for transverse CFRP sheet layers was determined.

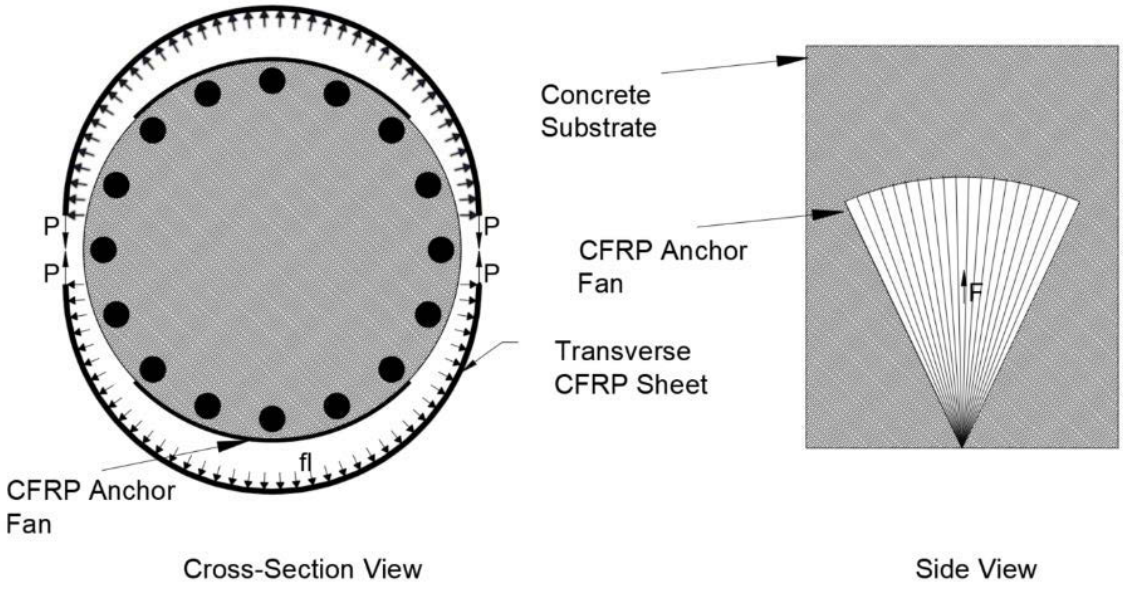

Figure 4.14: Design Concept of CFRP Wrap

4.1.8.1 Installation of CF Anchors and CFRP Sheets

A similar preparation process, which was used in the first column test, was followed for this column test as well. But for this column, two anchors were installed at same time. Details of the anchor were kept same as the first column test. The reason for installing two anchors at the same time was to investigate anchor behavior under compression and tension cycles. Both anchors were directly bonded to concrete substrate. Later, three layers of CFRP sheets were applied. The CFRP sheets were staggered around the column. Each transverse CFRP sheet had 10 in overlap region. Figure 4.15 shows the tested specimen. The embedment depth for the anchor installed at the strong wall side of the column was 15 in and for the opposite was 10 in. The anchor hole diameter was 1-1/4 inches for both holes.

Figure 4.15: Wrapped Column

4.1.8.2 Test Results

Similarly, Column 2 was tested under monotonic push and pull cycle. A displacement-controlled loading protocol that was used for Column 1 was adopted for this test. A quarter inch displacement applied to the top of the column until a failure mode occurred. The column was pulled in the direction of the strong wall to fail anchor on the opposite side. The lateral force reached 38 kips and displacement was 1.45 in, as shown in Figure 4.16. Figure 4.16 also shows the force-displacement curve of Column 1. Provided wrapping enable the CF anchor to resist more force that the anchor installed on the first column. A sudden drop was observed when a strong rupture noise heard from the anchor. Once rupture of the anchor took place, the restored concrete section lifted. Figure 4.17 shows the failure in the anchor. Moreover, due to ruptured bars at the bottom of the column, a crack occurred in the concrete section. This crack caused splitting of CFRP wrap as shown in Figure 4.18. The propagation of splitting stopped at a location where the CF anchor was attached to concrete substrate. Due to improper saturation of the anchor on the compression side of the column, full capacity of the CF anchor was not reached, and a splitting was observed in CFRP wrap as shown in Figure 4.19.

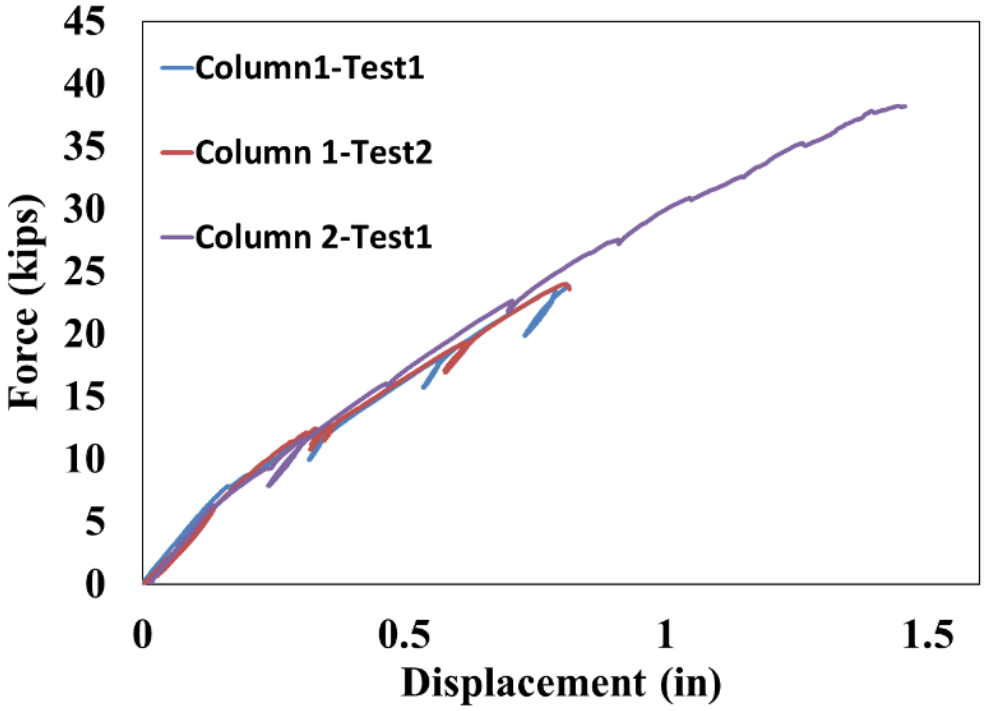

Figure 4.16: Force-Displacement Curve for Column 1 and Column 2

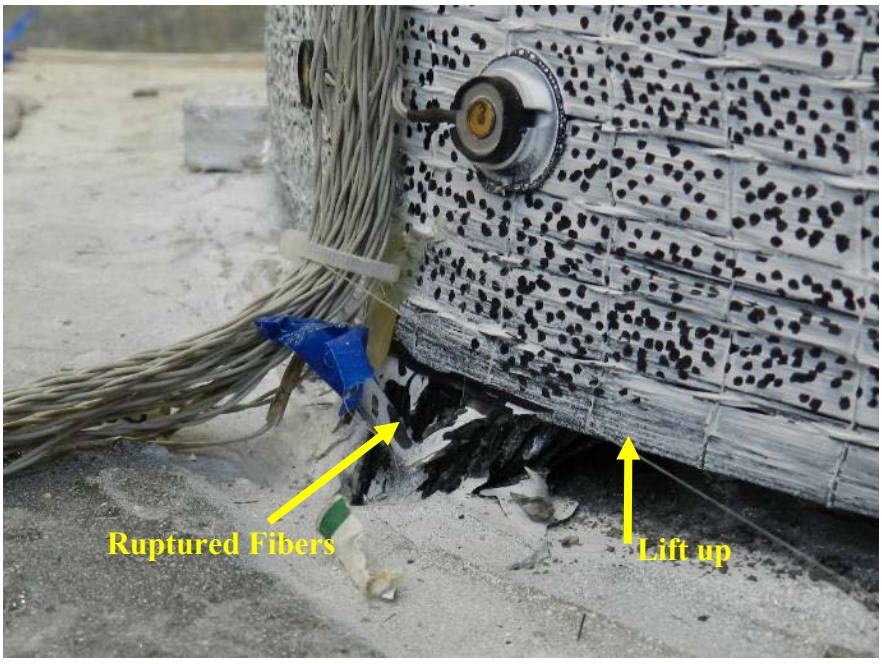

Figure 4.17: Failure in the Anchor

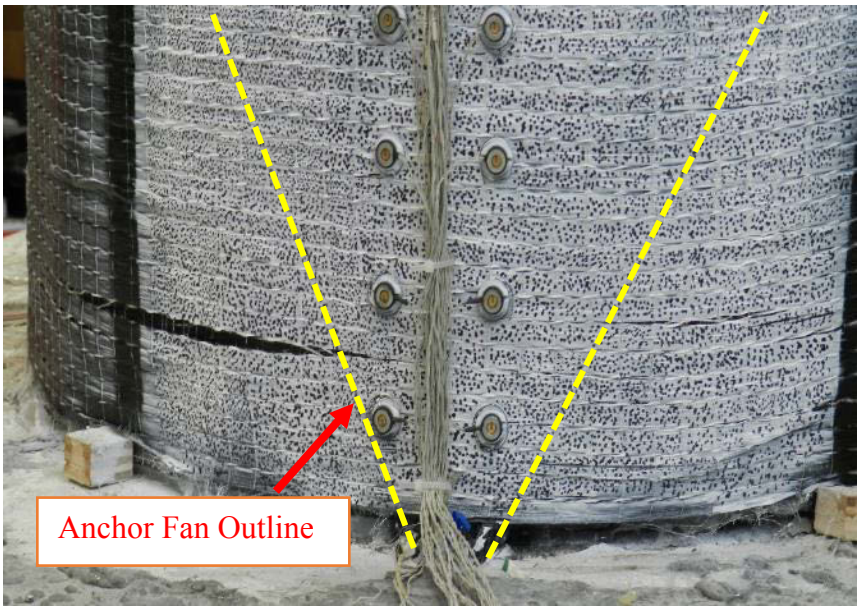

Figure 4.18: Splitting Failure in Column 2 Wrap

Figure 4.19: Splitting Failure in the Anchor on the Compression Side

As the aim of CFRP wrap was to improve the bond between the column grout substrate and the CF anchor fan, vertical strain development in the fan area was examined. DIC and OPTOTRAK systems were used to collect data. Figure 4.20 shows the strain distribution on CFRP

wrap. Although anchor rupture was achieved in the test, a strain concertation was observed at 22 in above the footing where the anchor fan tip is located. The strain increase was captured by DIC and OPTOTRAK systems. It was concluded, although the fiber rupture observed in the anchor, there was slight debonding.

In addition to vertical strain distributions in CFRP wrap, hoop fiber strains were also checked to see if the assumed design strain level for transverse CFRP sheet was reasonable. Figure 4.21 shows the hoop fiber distribution in the repair. The average strain at the bottom end of the column was 0.007 which was larger than the design strain, but no damage was observed in the hoop fiber due to the larger strain demand. The reason for observing larger hoop strain was attributed to the splitting observed in the CFRP wrap. It was concluded that design strain of 0.0058 and a coefficient of friction equal to 1 was reasonable for design. It should be noted that more experimental tests are needed to provide a more accurate design strain and a coefficient of friction.

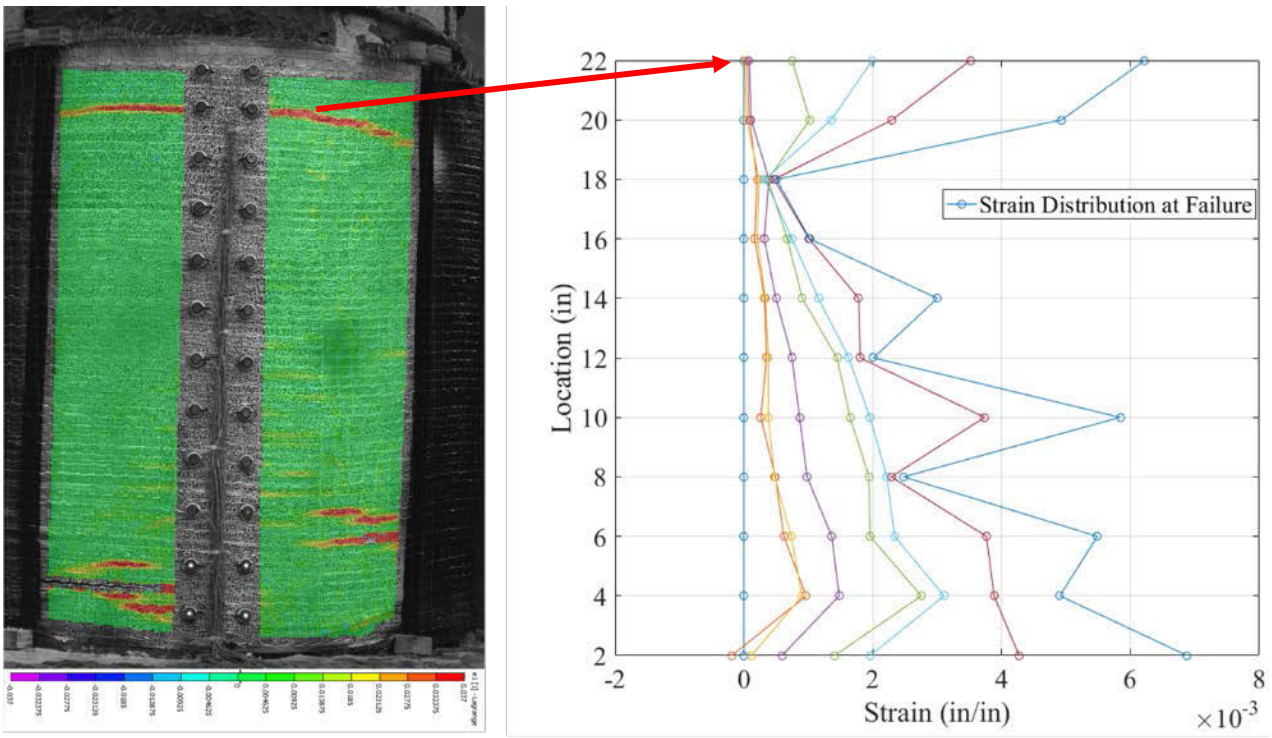

Figure 4.20: Vertical Strain Distribution in CFRP Wrap

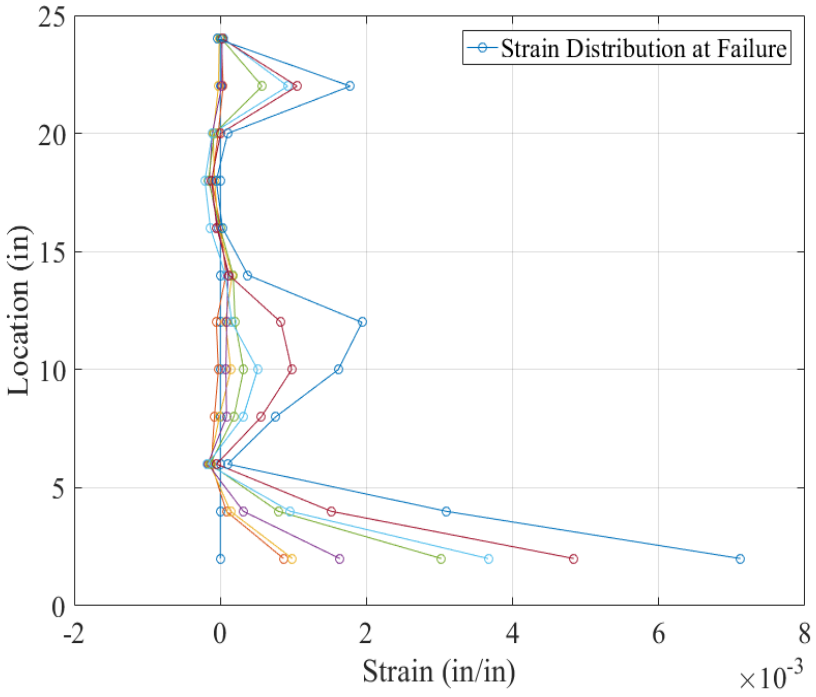

Figure 4.21: Hoop Fiber Strain Distribution in CFRP Wrap

4.1.9 Column 3

Although the anchor fibers were ruptured, the debonding of the CF anchor fan was observed through strain distribution data obtained from the DIC and the OPTOTRAK. In order to prevent debonding of CF anchor fan, the CF anchor fan was sandwich between two vertical CFRP sheets. This allows a uniform stress transfer between the CFRP sheet and the CFRP anchor. The anchor fan width and the anchor fan length were 15 in and 22 in, respectively. The drilled hole depth was 13 in for the anchor installed at the strong wall side of the column, and for the anchor installed on the opposite side, the drilled hole depth was 11 in. The anchor hole diameter was 1-1/4 inches for both holes. The column was tested under a displacement-controlled loading protocol same as the first two column tests.

4.1.9.1 Installation of CF Anchors and CFRP Sheets

The installation process began with bonding the first layer of the vertical CFRP sheet on grout substrate. The size of the vertical CFRP sheets was 24 in x 24 in. Later, the CF anchor fibers

were splayed on the vertical CFRP sheet for the given details. Finally, the second layer of vertical CFRP sheet bonded onto the CF anchor. As mentioned before, CFRP hoop fibers were added to increase bond capacity of the anchors. In total, three layers were calculated adopting the assumption adopted for Column 2.

4.1.9.2 Test Results

The top of the column was loaded with ¼ in displacement increments until the rupture of the CF anchor occurred. Figure 4.22 shows the force-displacement response of the all column tests conducted in this research program. As the top of the column was displaced, the anchor fibers began gradually rupturing. It can be seen in Figure 4.22 that Column 3 reached 26 kips lateral force capacity at a displacement of 1.2 in. The drop in the lateral load capacity was attributed to damage level in the column and distribution of fibers within the anchor. In addition, any change in the drilled hole geometry may lead a lower anchor capacity.

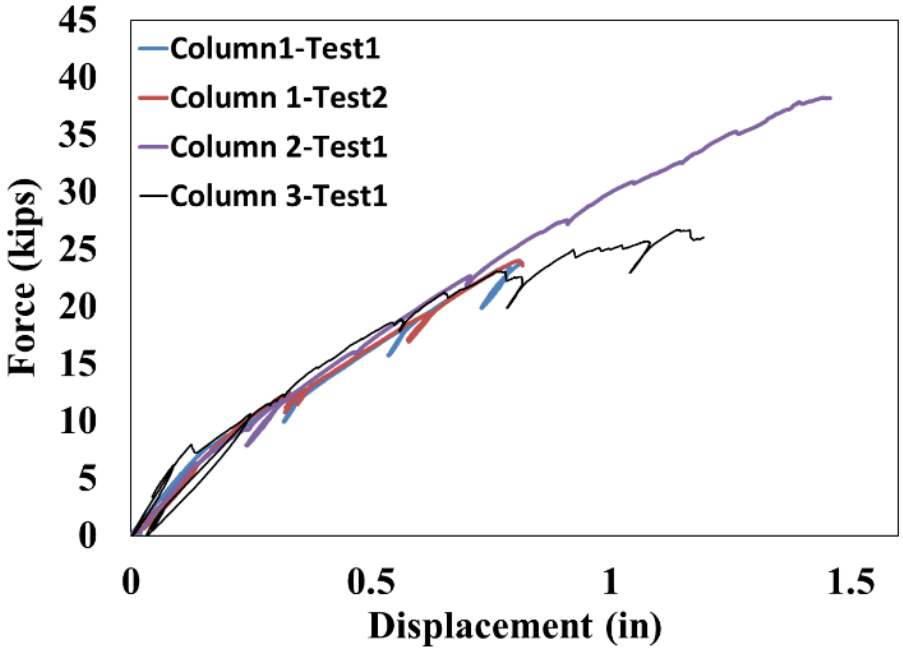

Figure 4.22: Force-Displacement of Tested Columns

Figure 4.23: Fiber Rupture in the CF Anchor

Axial and hoop strain data were collected throughout the loading of the column with the DIC and the OPTOTRAK systems. Figure 4.24 shows the axial strain distribution from both data acquisition systems. It was observed that axial strain distribution was lower at the top and increases towards the bottom of the column as expected. No strain concentration was observed. Thus, debonding of the CFRP sheet from grout substrate was prevented. The hoop fiber strain distribution is given in Figure 4.25. The hoop fiber strain increases towards the bottom end of the column as expected. The hoop fiber strain at the bottom of the column was less than 0.004 which was lower than the design strain limit. The crack developed across the grout plane was not propagated due to the vertical CFRP sheets. Thus, no splitting was observed in the CFRP hoop fibers. The addition of vertical CFRP sheets was an improvement as the strain limits was less than the design strain limit. Capacity of the anchor could not be predicted due to strain distribution obtained in the reinforcing steel bars and the grout cross-section.

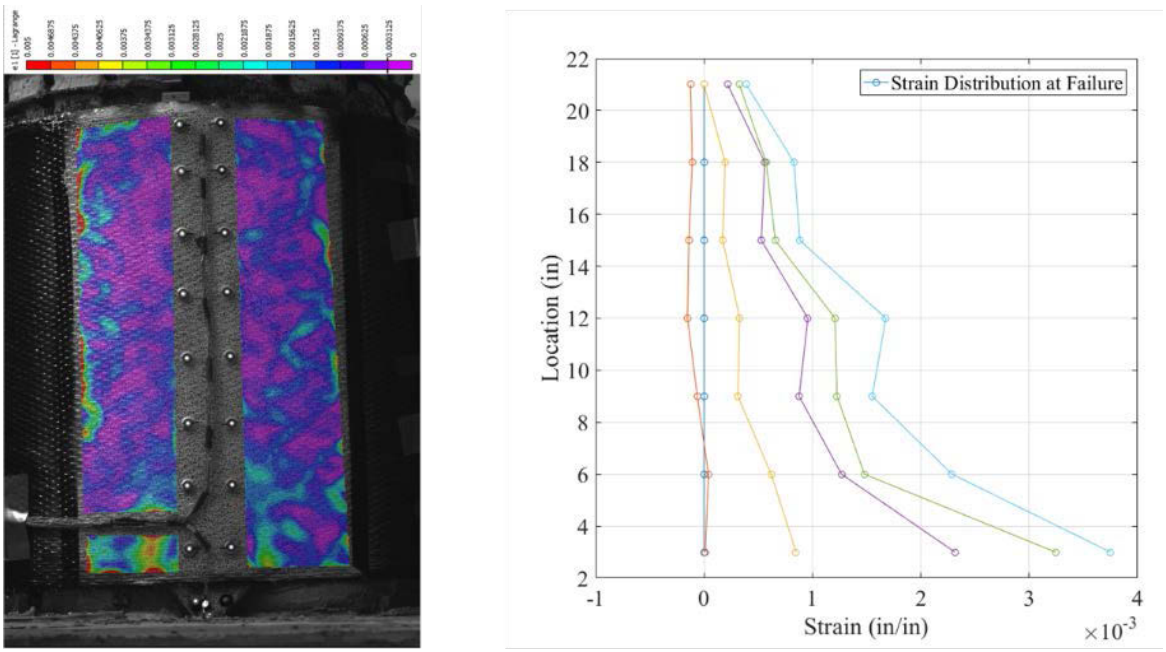

Figure 4.24: Axial Strain in Distribution in Column 3

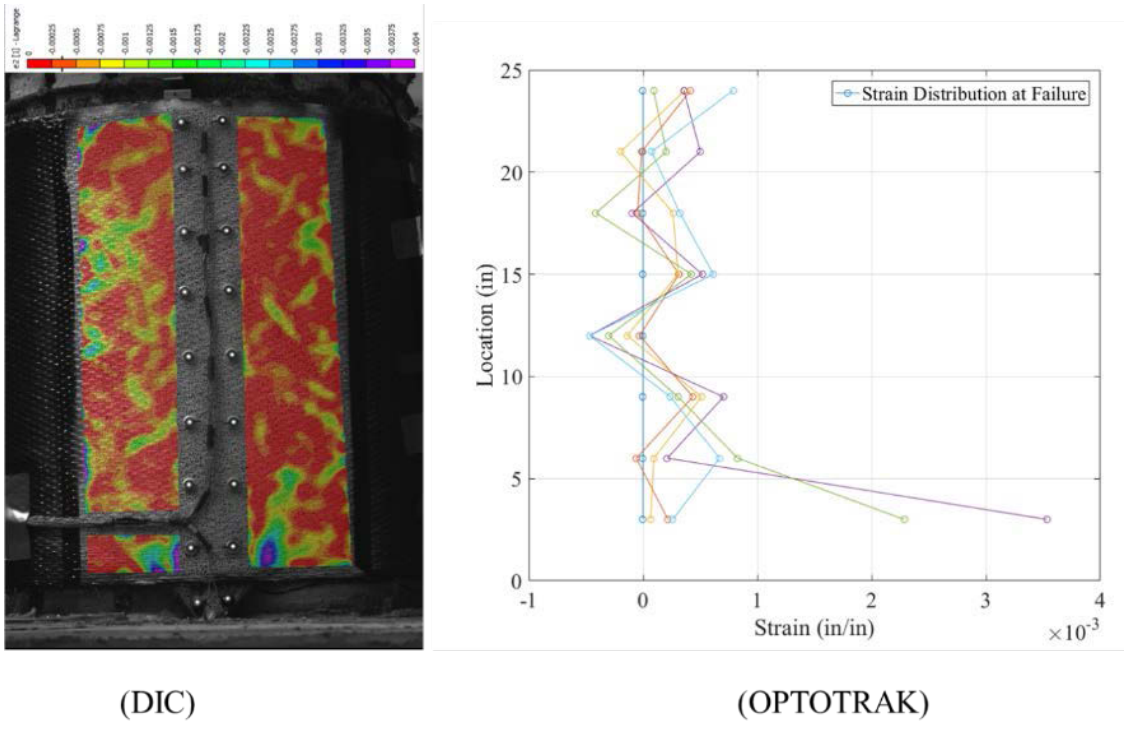

Figure 4.25: Hoop Fiber Strain in Distribution in Column 3

4.1.10 Conclusion and Future Work

Each iteration of column test provided a unique failure mechanism that was addressed in the subsequent columns. Although the capacity of the CF anchors could not be predicted, a design and construction method were developed.

4.1.10.1 Conclusion

The following conclusions were drawn from this experimental program:

- If the length of the fan part is not long enough, debonding failure takes place.
- Providing single layer of vertical CFRP sheet did not affect the failure mode.
- Using a shear friction model to determine number of hoop fiber layers is appropriate.
- A coefficient of friction value of 1 can be used for non-shrink grout.
- Sandwiching the CF anchor fan between two vertical CFRP sheets reduces help wit

4.1.10.2 Future Work

The following works need to be done to better understand behavior of the CF anchors.

- More test should be conducted to quantify capacity of the anchors.
- Overlapping of the fan part for multiple anchors should be examined to see impact of overlapping.

Chapter 5: Repair of RC Columns by Plastic Hinge Relocation Using CF Anchors

5.1 Overview

The goal of the research study is to develop a repair method for reinforced concrete columns using CFRP anchors. In order to develop a robust solution using CFRP anchors, several experimental works, which was mentioned in the previous chapters, were conducted. From the knowledge obtained in the previous experimental work of this research program, a design methodology is developed to guide design engineers. Two large-scale columns with different reinforcing details were repaired and tested to prove plastic hinge relocation concept. These two columns were obtained from another research work [23]. The original columns were tested under simulated quasi-static cyclic loading to reach bar buckling limit state. Two different anchor size were employed to restore moment and displacement capacity of the original columns by the relocation of plastic deformation into the undamaged location of the columns. This chapter discussed the design methodology for the reinforced concrete circular columns.

5.2 Experimental Program

5.2.1 The condition of Original Columns

An experimental program was developed to repair columns with substantial damage, meaning that columns have fractured or buckled longitudinal reinforcing bars. Two reinforced concrete columns with different construction details were tested to investigate the effect of various parameters. Columns are labeled as C1 and C2. Both C1 and C2 columns were 24 inches diameter with the concrete compressive strength of 6.29 ksi and 6.24 ksi, respectively. The height of both columns were 109 inches from top of to the center of loading. The longitudinal reinforcing ratio was 1.6% for C1 and 2.1% for C2. The column C1 was built using 16 #6 bars where C2 had 16 #7

reinforcing bars. Both columns were built using #3 reinforcing bars at 2.75 in. spacing. The axial load which was applied to columns was 191 kips, approximately corresponds to the axial load ratio of 7.3%. The detail of each column is given in Table 5-1.

The columns were tested utilizing the test setup shown in Figure 5-1. The goal of the testing was to investigate load path under the bidirectional loading. The details of the test setup can be found in Goodnight et al. [23]

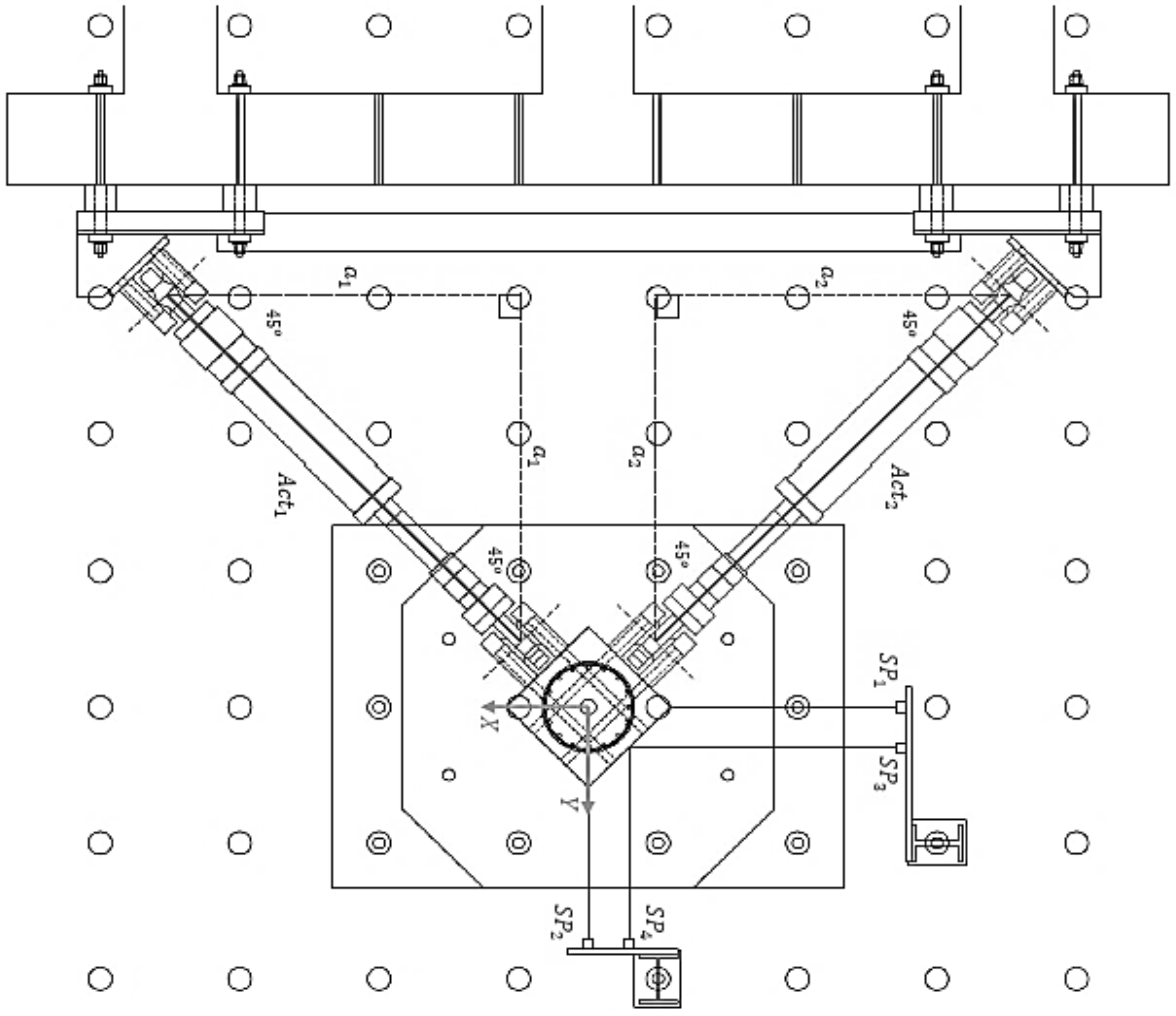

Figure 5.1: Test Setup [23]

The columns were tested in both x and y-direction under displacement control loading protocol shown in Figure 5-2b. The columns were pushed and pulled from their top in +y and –y directions, then same displacements were applied in +x and –x directions. This protocol was repeated two times for each ductility level. The loading protocol was applied until the expected limit state was reached. In this case, both columns were tested until the rupture of a single longitudinal bar took place. The level of the damage in both columns was quite similar. The damage occurred in the plastic hinge region of the columns are shown in Figure 5-3. The columns were reached fractured of a longitudinal reinforcing bar at different ductility level. C1 was reached fracture of the first longitudinal reinforcing bar at ductility level of 5 whereas the first longitudinal reinforcing bar was fractured at ductility 6 for C2.

Table 5-1: Details of Original Columns

ID of Specimen	Diameter (in)	Concrete Strength (ksi)	Long. Steel Ratio (%)	Transverse Steel Ratio (%)	Damage Level
C1	24	6.29	1.6	0.7	Mostly Buckled Bars and one Ruptured Bar
C2	24	6.24	2.1	0.7	Mostly Buckled Bars and one Ruptured Bar

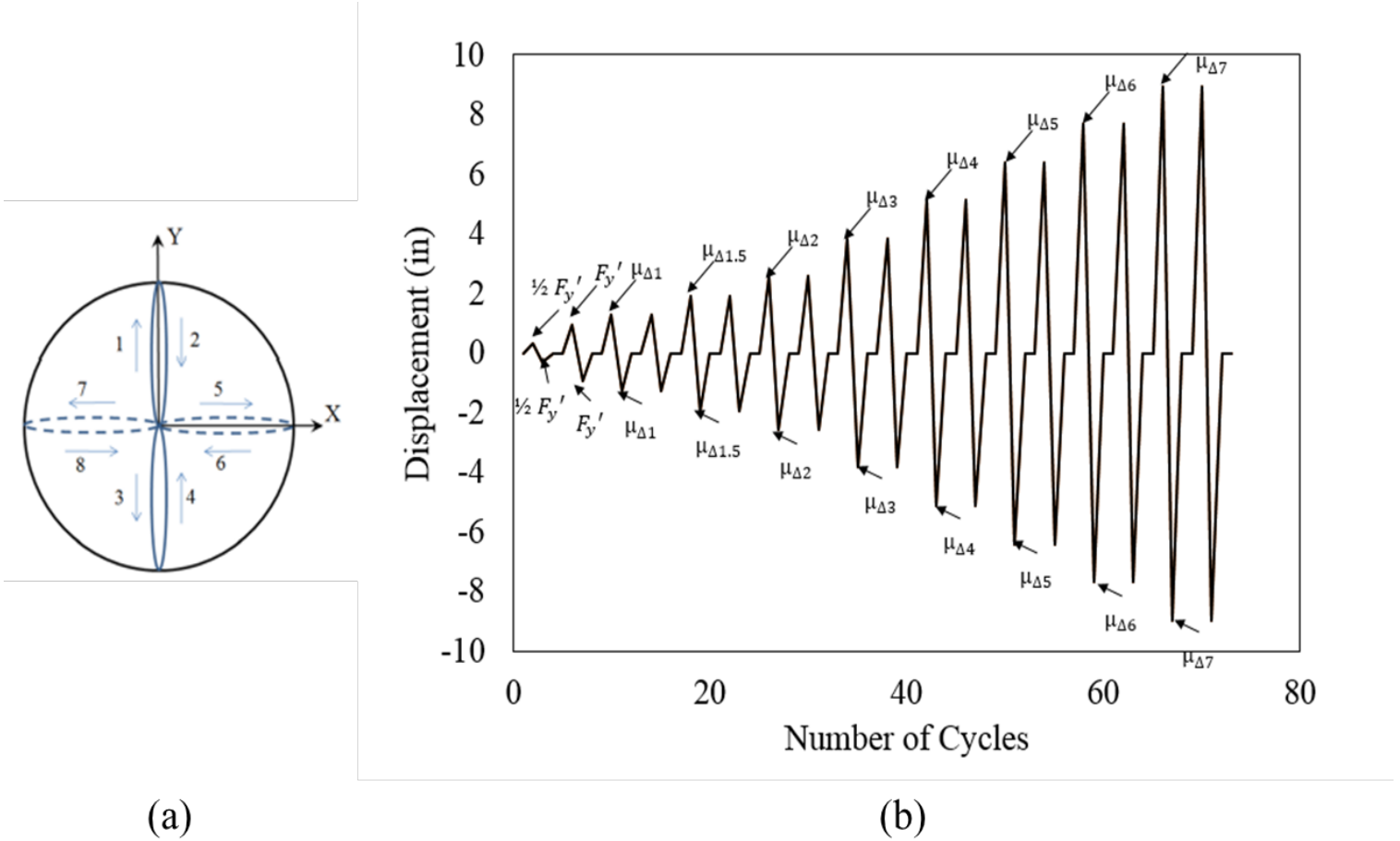

Figure 5.2: a) Load Path b) Loading Protocol [23]

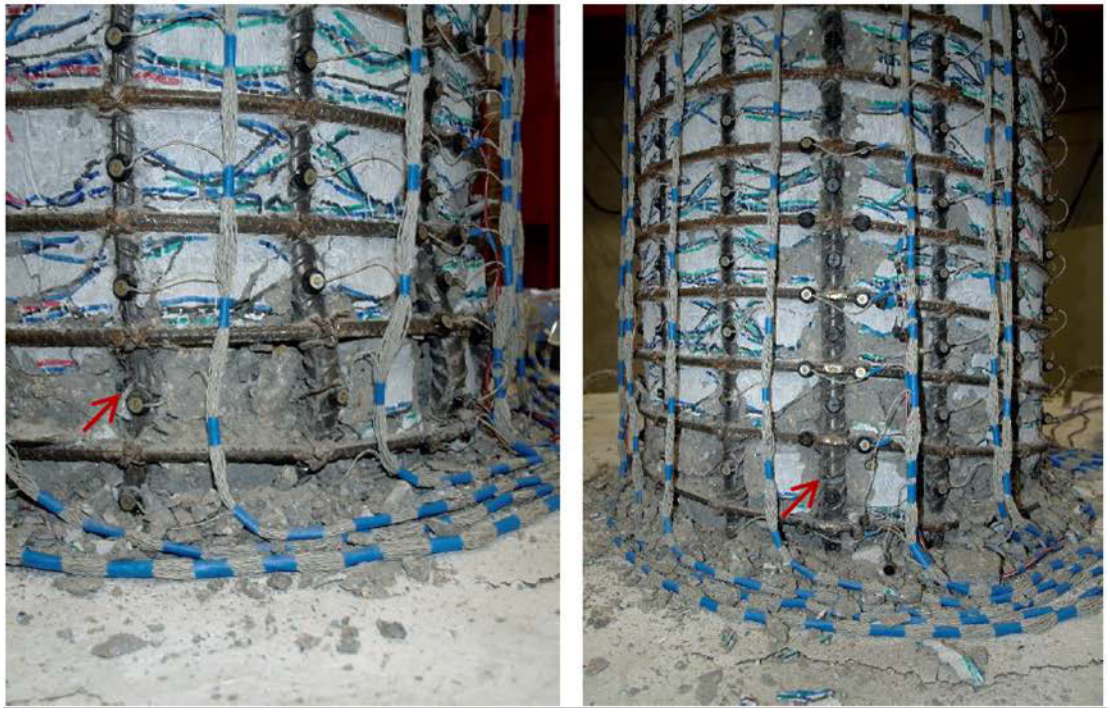

(a)

(b)

Figure 5.3: a) Damage in C1 b) Damage in C2 [23]

5.2.2 Design Consideration of Repair

As the plastic deformation takes place at column top and bottom ends during the main shock, tension capacity of the longitudinal reinforcing bars degrades. Therefore, for the period of the following aftershock, bridges may not perform well enough to resist demand induced by the earthquake. As state in previous chapters, the goal of the repair is to restore moment and displacement capacity of seismically damaged columns via relocation of the plastic hinge into undamaged parts of the columns. To reach this goal, loss tension capacity of the columns needs to be increased by the repair provided to the column. A CFRP solution similar to Rutledge et al. [1] research work is adopted in this study.

5.2.3 Determination of Base Demand

As the details of the repair design are dictated by the base shear force developed due to the relocation of the hinge, determining the location of the new plastic hinge is the first step of the design. It should be noted that the new location of the plastic hinge should be a distance above the damage region where relocation of the plastic hinge enables restoration of moment and displacement capacity of the original column. If the hinge location is selected near to the damage region, due to the spread of plasticity, moment capacity may not be restored. In the case of a higher repair height, demand at the column base increases. Thus, it may require a repair detail which may not be cost-effective.

In order to determine the location of the new plastic hinge, the thought process followed by Rutledge et al. [1] was adopted for this research work. The plastic hinge was relocated one column diameter length above the footing. The reason for locating plastic hinge one column diameter above footing was that the strain in the longitudinal reinforcing bars was less than the half of the buckling strain observed in the original column experiments. Even though Rutledge et al. [1] use a repair height of one column diameter length, anchor fan length was equal to plastic hinge length of the original column. With the given anchor fan length, the plastic hinge was relocated at 24 in. length above footing. It was shown that one column diameter length of repair was appropriate. It should be noted that in the design vertical CFRP sheets were provided. The vertical CFPR sheets were bonded the full height of the repair region. It can be concluded that regardless of the height of the anchor fan the new location of the plastic hinge is determined by

the height of the vertical CFRP sheet. Even though the length of the fan was less than the height of the

In this research, 24 in. length of the column above footing was also repaired, but anchor fan length was chosen to be longer than the plastic hinge length of the original column. Typically, a 60 degree or lesser fan angle is suggested for CFRP anchor applications. [24] However, in the literature, the suggested fan angle was based on CFRP spike anchor.

Moreover, the recent study by Castillo et al. showed that as the fan angle reduces, the capacity of the anchor increases. Therefore, a narrower fan angle (~33 degrees) was selected in this research work to reach larger anchor capacity for a given diameter. The fan length was 22 in. for this research for anchor diameter of 1 and 1-1/4 in due to available experimental data. The experiments on CFRP anchors showed that 22 in. fan length is appropriate when the anchor fan is confined using transverse wrapping. The details of the confinement of anchor fan were discussed in Chapter 4 of this report.

Moreover, since plastic hinge length is a function of the clear height of the column and reinforcing bar diameter, taking anchor fan length equal to plastic hinge length may not be appropriate because plastic hinge length may not be long enough to develop anchor rupture capacity. Also, vertical CFRP sheet was bonded at the full height of the repair. Therefore, the moment at column base determined using one column diameter height. As it can be seen in Figure 5.4, demand at the column base can be calculated by extrapolating demand at the new plastic hinge region using Equation 2.

$$\mathbf{M_d} = \mathbf{M_{oc}} \cdot \frac{\mathbf{Hc}}{\mathbf{H_c - H_r}} \qquad \text{Equation 1}$$

The column can now be designed for the calculated demand. Since a capacity design approach is conducted, a safety factor (S_f) can be added to determine the required repair capacity due to unexpected material properties. Thus, Equation 3 can be used to determine required capacity.

$$M_{rc} = S_f . M_d$$ Equation 2

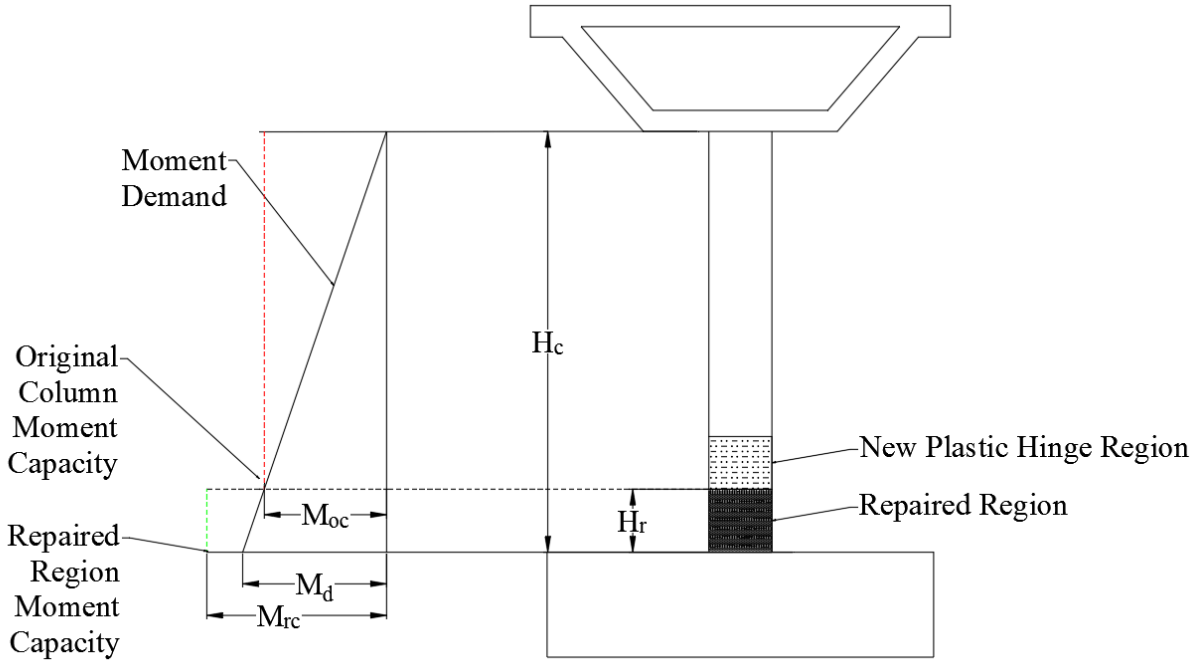

Figure 5.4: Moment Demand Distribution

As the moment demand increases due to the relocation of the plastic hinge, shear demand at the column base also increases. Thus, shear capacity of the column at any location should also be checked to prevent brittle shear failure in the column. The shear demand at any location of the column can be calculated using Equation 4 where L is the distance from the top of the column to the point of interest.

$$V_d = \frac{S_f . M_d}{L}$$ Equation 3

5.2.4 Determination of Details of the Repair Design

The aim of the repair design is to develop a fully flexural column behavior when the plastic hinge is relocated above the repair region. Therefore, a simple moment-curvature analysis should be enough to design the repair. By utilizing a moment-curvature analysis, the required number of anchors and the required number of vertical CFRP sheet layers can be determined.

5.2.4.1 Material Properties for Repair Design

It is required to determine the level of the damage at the plastic hinge region before running a moment-curvature analysis. Specifying the level of damage is crucial, as the material properties, which are used in the moment-curvature analysis, dictates the capacity and details of the repaired section. For the concrete material in the column cross-section, material properties were assumed to be the same. It should be noted that depending on the level of damage, transverse steel may reach its yield strength. Therefore, confined concrete material properties degrade. This change in the material properties should be considered in the moment-curvature analysis as the repaired region is designed to remain elastic during the seismic attack. In this study, confined concrete properties were assumed to be the same as the original column. The reason for such an assumption is that as the debonding issue of the CFRP anchor fan was emerged in the experimental tests, discussed in the fourth chapter, the CFRP transverse sheets were used to prevent debonding of the CFRP anchor fan from concrete substrate. As the CFRP wrap is attached around the repaired region to prevent debonding of the CFRP anchor fan, confined concrete properties are also. However, confined concrete properties were determined assuming that the confinement only provided by the stirrups.

Since an externally bonded CFRP application is conducted in this study, damaged concrete needs to be restored either by patching or forming a new cross-section as shown in Figure 5-5. The moment-curvature analysis of a column-cross section, shown in Figure 5-5, becomes complicated as the distribution of concrete/grout in the cross-section is non-uniform. To simplify the moment-curvature analysis process, concrete/grout that restored cross-section was assumed to have the same material property as the core concrete. The material properties of the confined core concrete for C1 and C2 specimens are given in Table 5-2. The values given in the Table 5-2 were calculated using Mander confined concrete model[25].

Table 5-2: Confined Concrete Material Properties for C1 and C2

ID of Specimen	f_{cc}' (ksi)	ε_{cc}'	f_{cu}' (ksi)	ε_{cu}'
C1	7.7	0.0057	6.09	0.02
C2	7.8	0.006	6.18	0.022

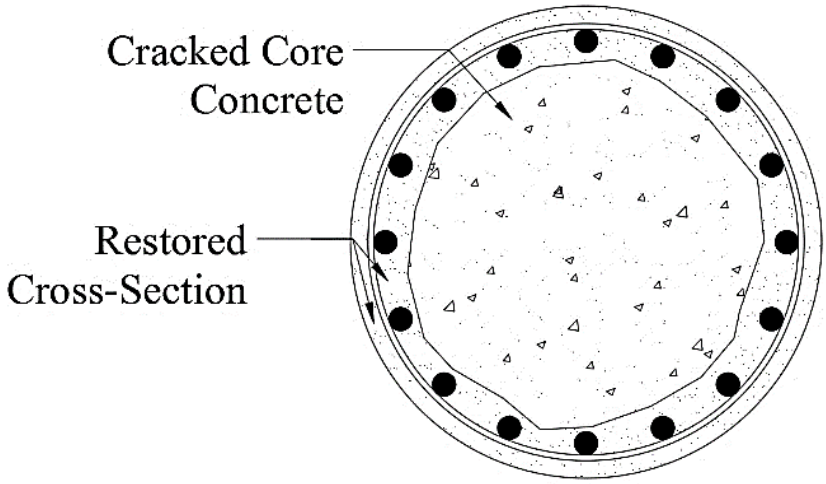

Figure 5.5: Restored Column Cross-Section

If the demand on the column is high, it is probable to have fractured or buckled bars at the plastic hinges of the column. If a reinforcing bar is ruptured, the ruptured bar is removed from the cross-section when the moment-curvature analysis is conducted. For a buckled reinforcing bar in the cross-section, there is a residual strength, but it is unclear how the degree of buckling determines the strength. Therefore, modification factors suggested by Vosooghi and Saiidi (2013) was used to determine material properties of reinforcing bars at the original plastic hinge. The factors were based on the apparent damage occurred in the column plastic hinge region. The reduction in the strength of the bars were represented by a reduction factor which corresponds to damage level observed. Five damage level, which were flexural cracking (Damage Level 1), slight spalling and possible shear cracks (Damage Level 2), wide crack and spalling (Damage Level 3), noticeable lateral or longitudinal bars (Damage Level 4), compressive damage of the core concrete

edge (Damage Level 5 -this also includes several buckled bars), were considered in the study. Table 5-3 shows the damage and corresponding modification factors.

Table 5-3: Observed Damage and Modification Factor [7]

Damage Level	Observed Damage	Modification Factor (ζ)
Damage Level 1	Flexural Cracks	No Modification
Damage Level 2	Slight spalling and Possible Shear Cracks	0.67
Damage Level 3	Wide Cracks	0.5
Damage Level 4	Noticeable Long. Reinforcing Bar	0.3-0.4
Damage Level 5	Compressive damage of the core concrete edge	0.2

The material property of the original longitudinal reinforcing steel is given in Table 5-4. Initial stiffness of the stress-strain curve was modified by the factor that corresponds to the observed damage level. In this research, as it is mentioned in the previous section, damaged section in both columns was a fracture of a single reinforcing bar and buckling of the several other bars in the cross-section. A factor of 0.2 was used to modify the behavior of the buckled bars.

To repair the columns, two different unidirectional CFRP sheets with the following properties were used. Two different unidirectional CFRP sheets were used due to the availability of unidirectional CFRP sheets at the time of the repair of the columns. Table 5-5 shows the laminated (cured) material properties of the unidirectional CFRP sheets used in the repair of the columns. Same unidirectional sheets were also used for wrapping of the repaired region of the columns.

Table 5-4: Material Properties of Longitudinal Reinforcing Steel

ID of Specimen	f_y' (ksi)	ε_{cy}'	f_{su}' (ksi)
C1	70.3	0.0028	98.68
C2	71.2	0.0025	97.9

Table 5-5: Material Properties of CFRP Unidirectional Sheets

Composite CFRP Sheet	Tensile Strength (ksi)	Tensile Modulus (ksi)	Elongation at Break (%)
CFRP Sheet for C1	143	13900	1.0
CFRP Sheet for C2	128	14200	0.9

Although CFRP anchors are constructed using same carbon fibers and epoxy, laminated properties of the CFRP sheets cannot be used for design purposes because of the construction details of the CFRP anchors. As the construction of the anchors requires to splay fibers onto the substrate surface, the fibers diverge from the primary direction, as shown in Figure 5.6, and cured material properties changes. In this study, estimation on the capacity of the 1 and 1-1/4 in. CFRP anchors were based on the experimental data available. As discussed in the third chapter, several tests were conducted on 1 in. diameter CFRP anchors and a stress-strain curve, shown Figure 5.7, was obtained. Although direct tension tests were conducted on the anchors which had the fibers in the primary direction, an estimation was done using the stress-strain curve obtained from these pull tests.

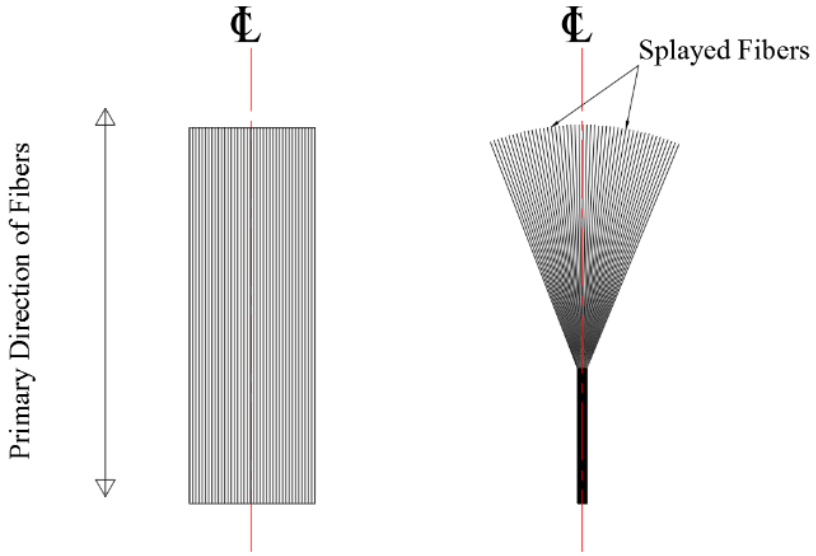

Figure 5.6: Fiber direction in CFRP Sheet and CFRP Anchors

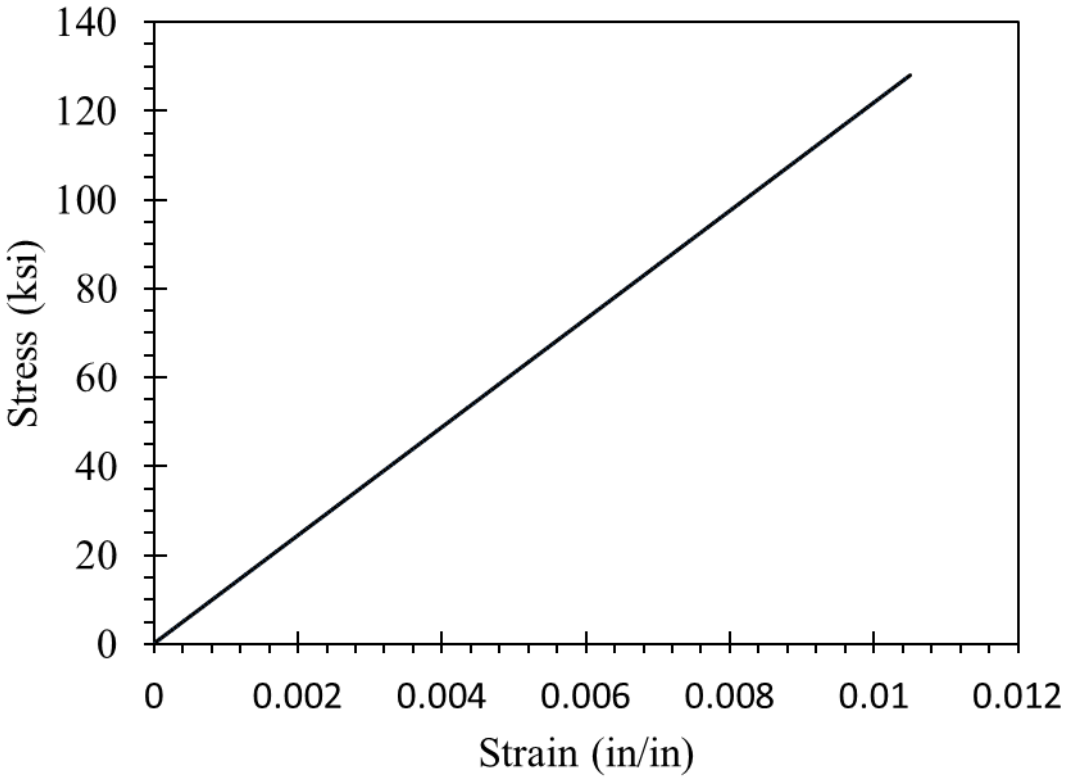

Figure 5.7: Stress-Strain Curve of CFRP Anchors in Primary Direction

5.2.4.2 Moment-Curvature Analysis for Repair Design

It was found that sandwiching the CFRP anchor fan between two vertical CFRP sheets is a good practice because having vertical CFRP sheets allows a uniform stress distribution at the CFRP anchor fan. Also, a strong bond can be produced between the concrete substrate and the CFRP anchor fan fibers. Therefore, a minimum of two layers of vertical CFRP sheets is suggested, but the exact number of vertical CFRP sheet layers is determined utilizing a moment-curvature analysis with the assumption that the attached vertical CFRP sheets have the equal capacity or more capacity than the CFRP anchors distributed around the repaired region. This assumption allows to have equal moment capacity through the height of the repaired region. In the case of a shorter CFRP anchor fan length, the vertical CFRP sheet can be extended to the location of the new plastic hinge. Therefore, the location of the new plastic hinge can be controlled by adjusting the length of the vertical CFRP sheets.

In total, two moment-curvature analyses are needed for the design of the repair. The critical section in the column is at the column-footing interface where the moment and shear demand are the highest as shown in Figure 5.8. Moreover, this section shown in Figure 5.8 is critical because CFRP anchor fan fibers enter a drilled hole in the footing. The change in fiber direction at the critical region leads to a stress concentration in the anchor. Thus, a moment-curvature analysis was important for determining details of the CFRP anchors. For the first moment-curvature analysis, the vertical CFRP sheets were removed from the model to avoid any contribution from fibers as shown in Figure 5.8. A second moment-curvature analysis was run assuming that the vertical fibers will have equal capacity to the CFRP anchors. For this model, CFRP anchors were removed from the cross-section. For both moment-curvature analyses, material models for concrete and reinforcing steel were kept same.

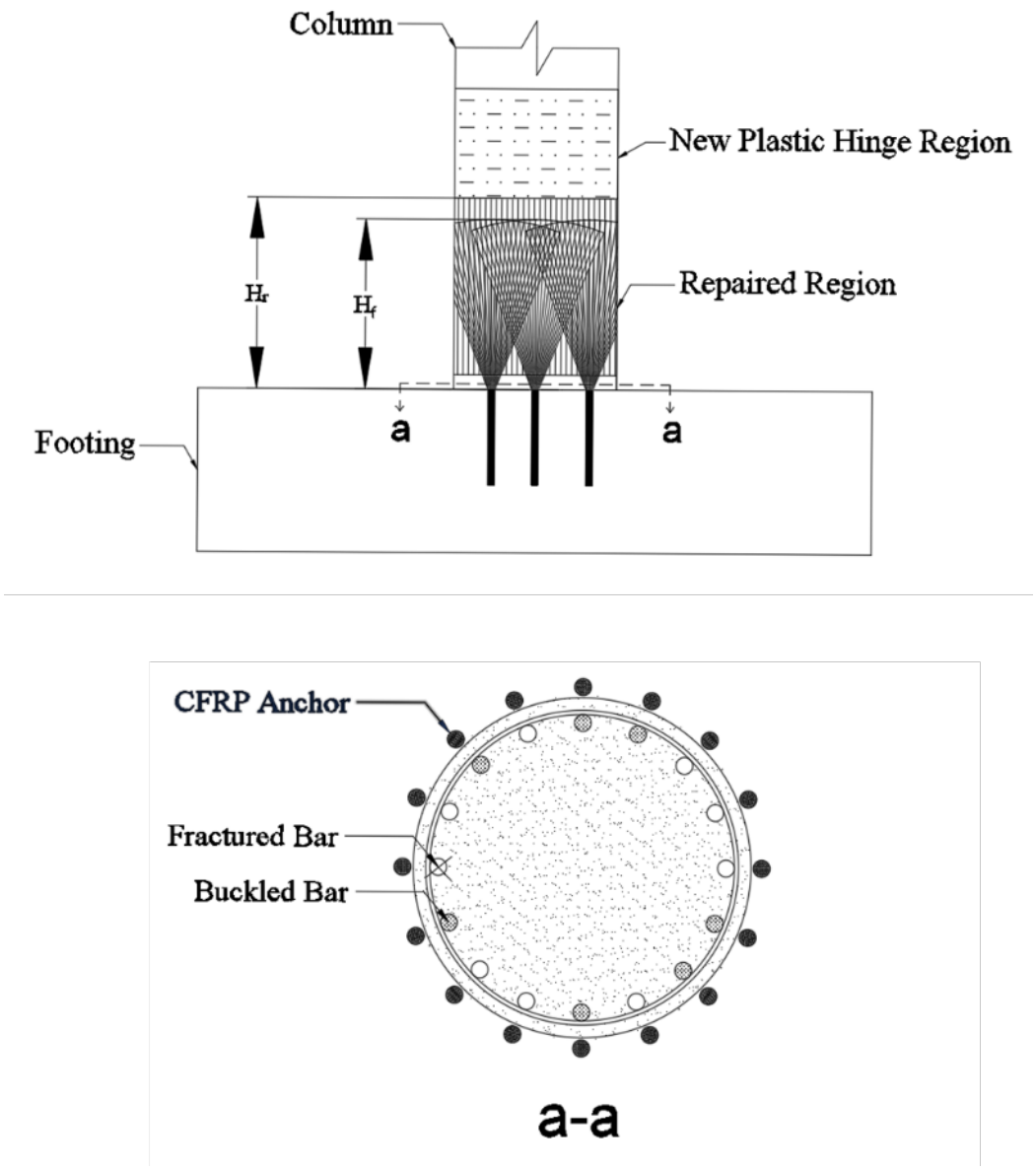

Figure 5.8: Critical Cross-Section at Repair Region

For the moment-curvature analysis, it is essential to model all materials with appropriate material properties and their geometric location with respect to a reference point, typically, the center of the cross-section. A moment-curvature analysis was conducted using Opensees finite element software [26]which includes a wide range of materials. A fiber-based model was developed to represent the repair design. The modeling approach suggested by the developer was used to conduct moment-curvature analyses. Figure 5.9 shows the illustration of the fiber-based

model and zero length element which has the discretized cross-section of the repaired region. A zero-length element requires two nodes which are defined at the same location. Node 1 is restrained against any translational and rotational movements whereas Node 2 was set free only for axial and bending movement. A curvature increment is applied to Node 2 until defined curvature limit is reached. For each curvature increment, force-equilibrium is satisfied, and a moment capacity is determined.

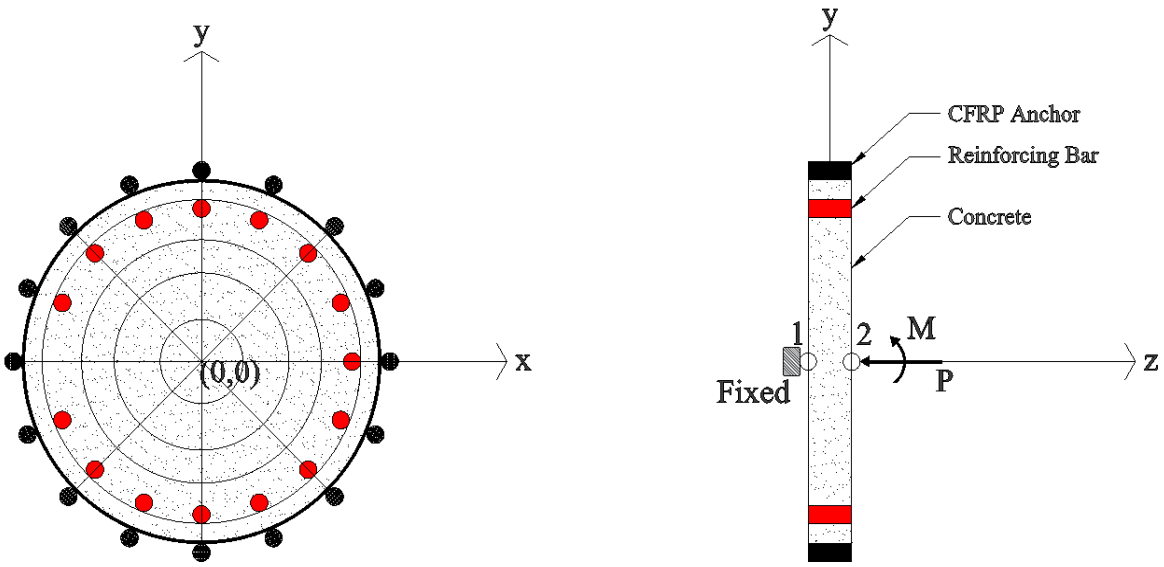

Figure 5.9: An Illustration of Fiber Discretization of Cross-Section for Moment-Curvature Analysis

In the model, confined concrete was modeled using Concrete 01 which has zero tensile strength under tension as shown in Figure 5.10 a. For the steel material, Steel 02 model which incorporates Menegotto-Pinto steel material with isotropic hardening as shown in Figure 5.10 b. An FRP material model has not been included in Opensees, but the elastic uniaxial material model, shown in Figure 5.10 c, can be adapted to represent any CFRP material. Since the model allows the user to independently include compression and tension modulus by assigning a very small compression modulus (close to zero) CFRP material model can be represented. The elastic uniaxial material should be modified in such a way to exhibit the behavior of the CFRP material at ultimate capacity when rupture of material occurs. When CFRP reaches its rupture capacity, FRP should be removed from the model. Min-Max material model can be used to model rupture behavior. This

material model enables the user to define a maximum and minimum strain limits. Once the strain in the discretized element in the model is reached to maximum defined strain level, it is automatically removed from the model.

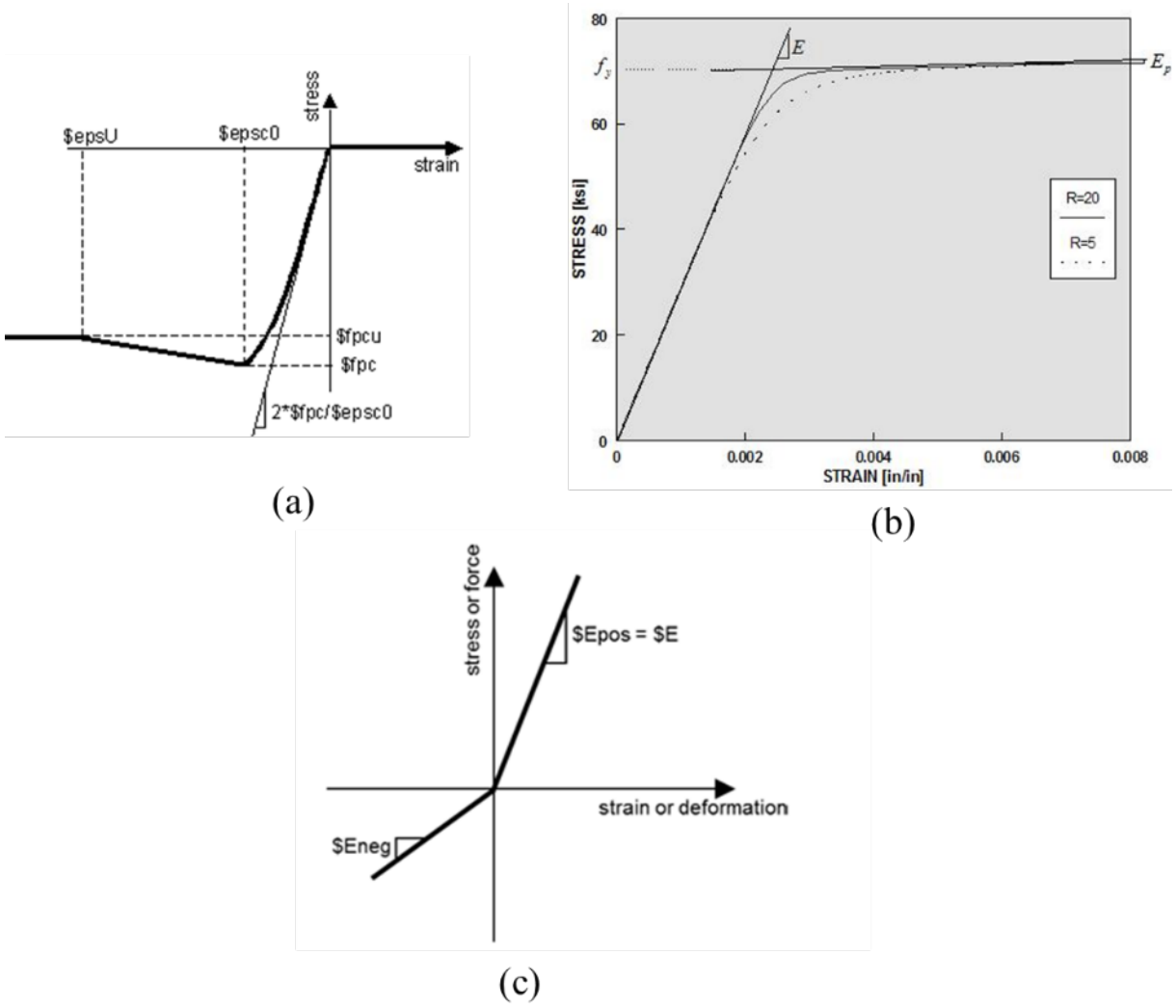

Figure 5.10: Material Models Used in Moment-Curvature Analysis a) Concrete 01 b) Steel 02 c) Elastic Uniaxial Material [26]

Figure 5.11 shows an example of moment-curvature analysis conducted for repair design of a column. As it can be seen, moment increases until rupture of extreme CFRP anchor occurs, and a sudden drop takes places due to a loss of the strength. As the repair region is designed to be elastic, during cyclic loading, it is expected to have a small magnitude of curvatures. As stated before, a moment-curvature analysis is needed to determine the number of vertical sheet layers which was determined using the same moment-curvature analysis methodology.

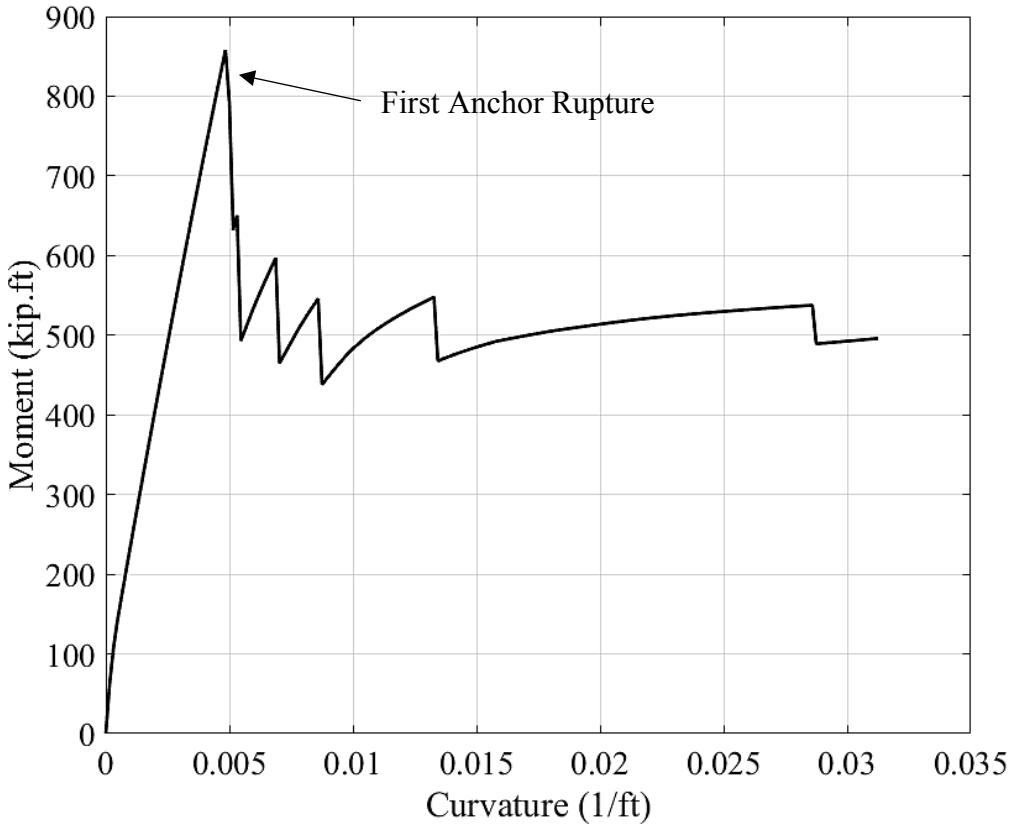

Figure 5.11: An Example for Moment-Curvature Analysis of CFRP Repaired Column

5.2.4.3 Design of Hoop Fibers

A conservative approach was followed to determine the required number of hoop fiber sheets to prevent debonding of CFRP anchors. As mentioned in the fourth chapter, a shear friction model was suggested to prevent debonding of the single CFRP anchor. Using same logic, the model was used to determine the required number of hoop fibers by calculating the required hoop pressure needed to resist rupture capacity of vertical CFRP sheets as shown in Figure 5.12. In the model, it was assumed that the neutral axis at the center of the section and vertical CFRP sheets on the tension side reaches its ultimate capacity.

It should be noted that the capacity of CFRP anchors and vertical CFRP sheet were assumed to be equal. Assuming coefficient of friction of 1 for grout material, and limiting hoop strain at 0.0058, five layers of hoop fibers were required. Since the moment-curvature analyses

resulted in 3 layers of vertical CFRP sheets for each column specimen tested in the program, five layers of hoop fibers were used in the repair of both column specimens.

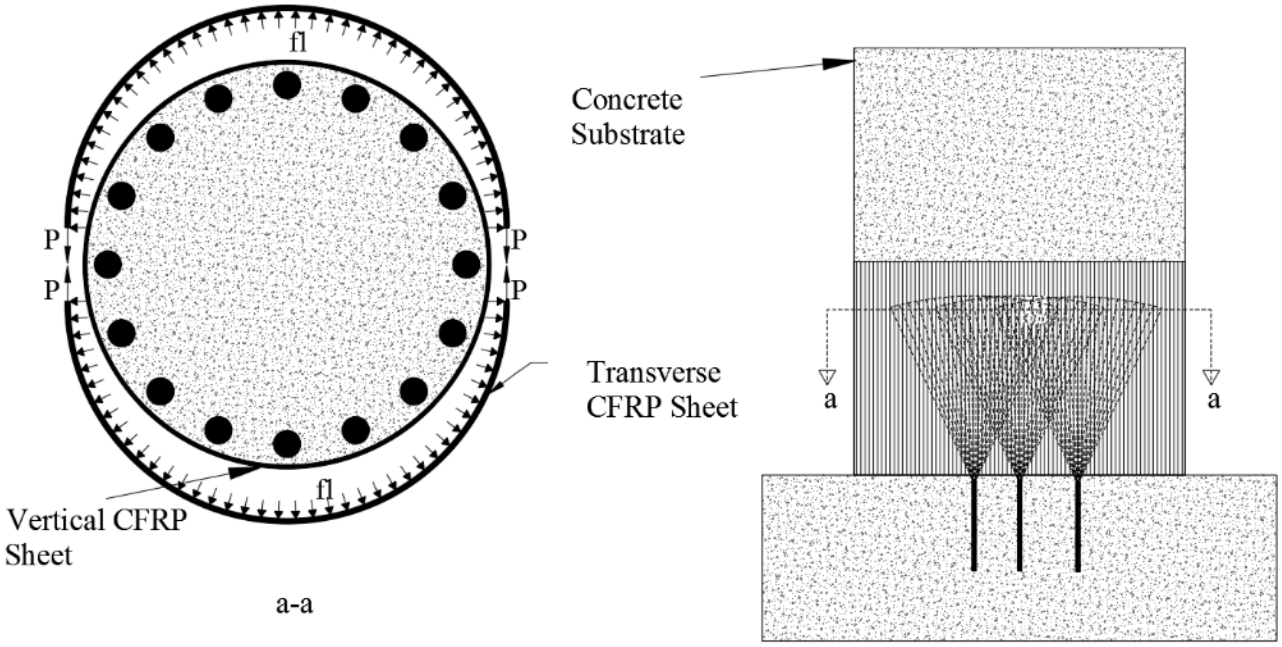

Figure 5.12: Hoop Fiber

5.2.5 Strengthening Procedure

The original columns were intentionally constructed without a cover concrete due to instrumentation method was used in the testing procedure. Due to the absence of the cover concrete and damage level in the columns, patching the tested columns was not possible to produce a concrete substrate as the CFRP application is an externally-bonded application. As a result, the partial restoration of the cross section was required. The restoration process began with removing loose concrete as shown in Figure 5.13. Due to the bi-directional loading procedure, core concrete was crushed in all sides of the columns. Thus, the amount of the loose concrete removed from columns was excessive. Furthermore, to create a bond between grout, which was used to restore section, and reinforcing bars, at least one-inch-thick core concrete was chipped off.

Figure 5.13: A Column after Removal of Loose Concrete

Repair procedure was continued with drilling holes into the footing. Figure 5.14 shows the detail of footing and drilled holes. Although details of the footing were known at the time of drilling, the concrete cover was removed, so that the location of reinforcing bars was easily determined. Also, drilling was interrupted by the rods that were holding form work together. Therefore, removal of cover concrete eased to cut out the formwork rods. Since the concrete cover was removed, drilling started at about 4 inches below the concrete surface. Total of twenty holes was drilled into footing for both columns. Drill bit sizes were 1-1/4 inches and 1-1/2 inches for one inch-diameter and 1-1/4 inch-diameter CFRP anchors, respectively. Holes were drilled to be close enough to restored column concrete surface. For both columns, the depth of the holes varied from 14 inches to 18 inches due to the orientation of J-hooks that were used as shear reinforcement. Also, for a few cases, holes were drilled with an angle to avoid J-hooks. Once chipping and drilling of concrete was completed, dust was washed off from repaired region to ensure that grout bonded

to concrete and bars. Water in the drilled holes was vacuumed out, and the drilled holes were aired to ensure that they get dried before CFRP application.

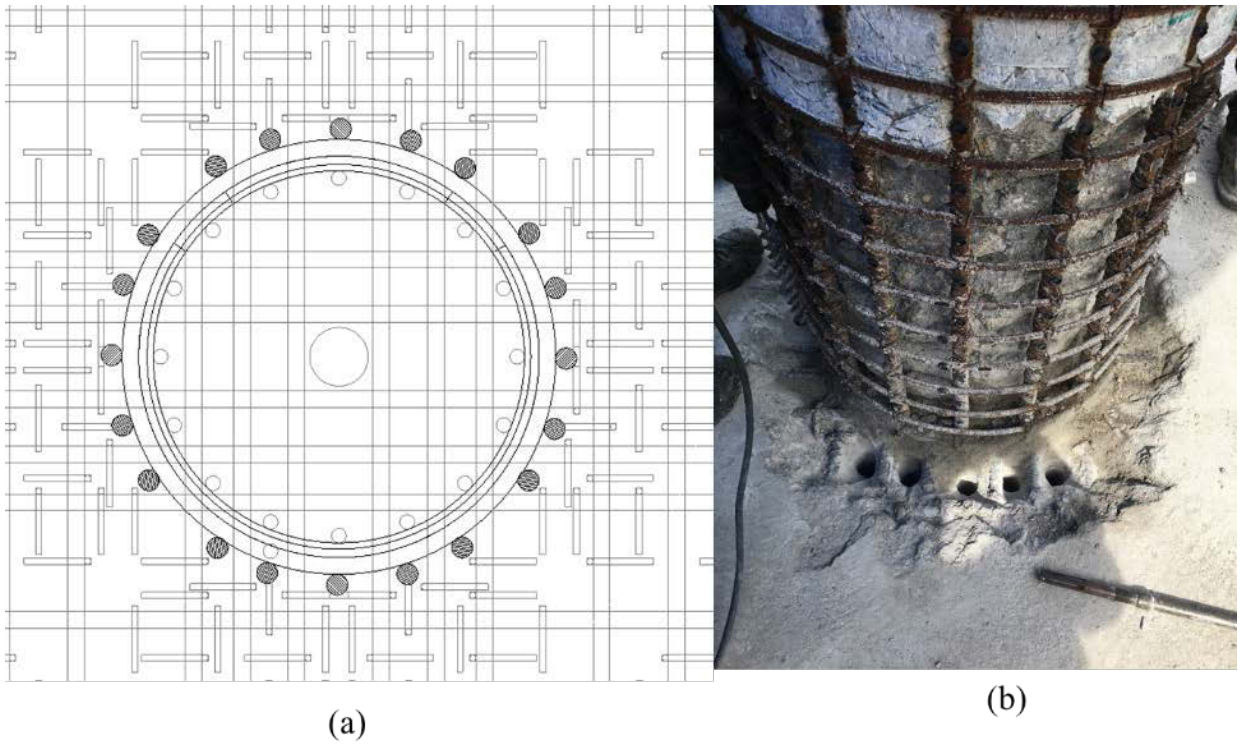

Figure 5.14: a) Anchor Location for C1 and C2 Column Specimens b) Drilled Holes for C2 Column Specimen

As the footing concrete cover was removed, it was necessary to restore concrete cover to have a leveled concrete surface for from work. As shown in Figure 5.15, PVC pipes were cut and located at the top of the drilled hole with silicone to seal the hole to prevent leaking of grout. After curing of silicone, grout was poured to create a leveled concrete surface for formwork as shown in Figure 5.16. After two days of pouring, PVC pipes were removed, and the holes were vacuumed out.

Figure 5.15: PVC Pipe Placed at the top of Anchor Holes with Silicone

Figure 5.16: Restoration of Footing Cover Concrete with Grout

Since some of the reinforcing bars were buckled outward, it was required to restore a larger concrete cross section. Therefore, Flex-board was used to restore cross-section as shown in Figure 5.17. The diameter of the new cross-section was 25 inches, and the height was 24 inches. The inside of the board was covered with plastic sheet to ensure that at the time of removal of formwork a clean grout surface was obtained. Also, since the flex-board was made of plywood, it was possible that flex-board may absorb water in the grout. Thus, a grout with a lower compressive strength may be produced. Sharp edges of the anchor holes were rounded with drill bit provided by the CFRP anchor manufacturer. Rounding of edges was done to ensure that a smooth transition of fiber from anchor dowel to anchor fan was established. Figure 5.18 shows the rounding procedure conducted during the preparation of the column specimens.

Figure 5.17: Form Work Application

Figure 5.18: Rounding Edges of Anchor Holes

For a typical externally bonded CFRP application surface of the substrate should be rough enough to create a good bond between CFRP and substrate. After removal of formwork a smooth surface was obtained as shown in Figure 5.19. Thus, a roughing procedure was followed by using a needle gone. Since the scale of the application is small needle gun was adequate. For real field application, sandblasting or pressurized water can be used to roughen the surface of the concrete. After completion of the roughening procedure of restored surface, all dust from the surface was removed by compressed air. Next, the drilled holes were brushed to remove any loose concrete pieces, and all dust and small concrete pieces were removed with compressed air and vacuum cleaner. This process was repeated for four times which was a recommendation of the CFRP manufacturer.

Figure 5.19: Grout Surface Before and After Roughening

After preparation of concrete surface and anchor holes, application of vertical CFRP sheets, CFRP anchors and CFRP hoop sheets were completed in two stages.

5.2.5.1 Stage 1: Application of vertical CFRP Sheets and CFRP Anchors

As the surface of the grout was roughened, several voids occurred on the surface. Thus, voids should be filled. Before filling up the voids, two-component epoxy was mixed, and the surface of the grout was fully saturated with a roller brush. Later, two-component epoxy was mixed with Cab-O-Sil TS-720 to thicken up the epoxy to fill the voids. A putty knife was used to apply a thin layer of thickened epoxy. As the thickness epoxy increases, shear lag issues arise. Thus, a thin layer of epoxy should be applied. The length of the vertical fibers were 23 inches which were less than the repair height. CFRP sheets were saturated with a roller brush by following the instruction of the manufacturer. The first layer of saturated vertical CFRP fibers was applied onto the substrate one-inch above the footing. After attachment of sheets, a ribbed roller was used to remove air behind the CFRP sheets as shown in Figure 5.20. It should be noted that the first layer

of vertical CFRP sheet was applied to the concrete substrate and the remaining sheets were applied after applying CFRP anchors. An hour break was given before the CFRP anchors application.

Figure 5.20: Air Removal with a Rib Roller

Most of the time challenges with the application of CFRP anchors is to insertion of the anchor dowel into drilled holes. To ease the installation process, anchor looped ends were cured a day before installation. During the saturation process of the looped end, 1/8” inches diameter steel rod was attached to the loop end. Later, the steel rod was used to insert anchor dowels into holes. The looped end diameter of anchors was constructed to be smaller than the anchor hole diameter in order ease the installation. Zip ties were used to adjust the diameter of looped ends of the anchors. Figure 5.21 shows a CFRP anchor utilized in the repair of columns.

Figure 5.21: Preparation of Anchor Ends

Determination of anchor geometry was based on the tests which were conducted in a fourth and third chapter of this report. Figure 5.22 shows the geometric details of CFRP anchors. Anchor fan length, H_f, for C1 and C2 were 22 inches. The anchor fan width, ψ, was around 15 inches for C1 and C2 column specimens. As mentioned before, the depth of the holes was various due to difficulties faced during drilling. Thus, total anchor length was adjusted for each hole. Before installation of anchors, the surface of vertical CFRP sheets was saturated again with a roller brush. All CFRP anchors were saturated with the same epoxy, which was used during the repair procedure. The amount of epoxy was used to saturate anchor fibers was about 20 oz. and 27 oz. for 1 inch and 1-1/4 inch-diameter anchors, respectively.

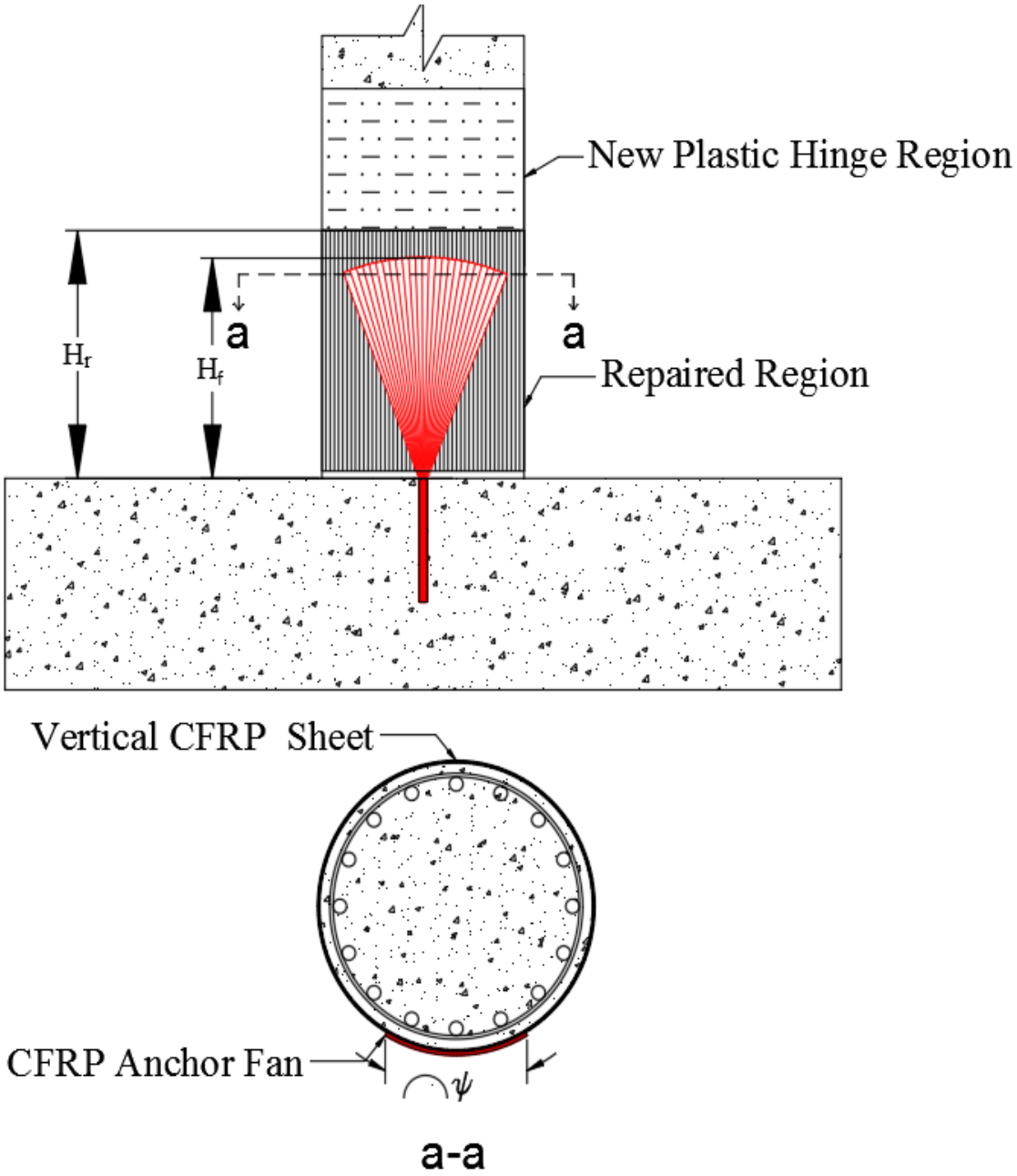

Figure 5.22: Geometric Detail of Anchors

After saturation of each anchor, anchor dowel was pushed into anchor hole via steel rod. While steel rod was held steady, anchor fan was splayed onto the surface of vertical CFRP sheets, and fan fibers were stretched with a putty knife as shown in Figure 5.23. Later, the epoxy was poured into holes. As the installation of CFRP anchors was completed, the remaining layers of vertical CFRP sheets were bonded onto CFRP anchors. Before applying the second and the third

layers of vertical CFRP sheets, anchor fan surfaces were saturated again, and then the second layer vertical CFRP sheets were bonded. Finally, the third layer of vertical CFRP sheets was applied to the second layer.

Figure 5.23: Splayed Anchor Fan Fibers

5.2.5.2 Stage 2: Application of Hoop Fiber Sheets

The role of the hoop CFRP sheets was to prevent debonding any vertical CFRP sheets and anchors from the concrete substrate. As discussed above, the number of vertical CFRP sheet layers were determined based on a shear-friction model suggested in the previous chapter. For this testing program, five layers of hoop fibers were needed for both C1 and C2 column specimens. Since it was not practical to apply a continuous wrapping, each fiber were applied individually. All five layers of hoop fibers were applied one day after completing the first stage. Each hoop fiber were

wrapped around the column with a ten-inch overlap. Overlapped region were removed at a different side of the columns to prevent progressive debonding of hoop fibers. Figure 5.24 shows the application of a hoop fiber sheet. The repair procedure was completed with the installation of all hoop fibers. After three days of curing time, the column specimens were ready for testing. Figure 5.25 shows C2 column specimen before testing.

Figure 5.24: Application of Hoop Fiber for C1 Column Specimen

Figure 5.25: C2 Column Specimen before Testing

5.2.6 Instrumentation

To measure the strains within in the plastic hinge and repaired regions, OPTOTRAK CERTUS® HD Dynamic Measuring systems were used. Since a bidirectional loading was applied to the columns, it was required to collect strain readings from all sides of the column specimens. Thus, a total of three OPTOTRAK cameras was located aroun the columns. LED markers were located on the reinforcing bars and hoop fibers of the C1 column specimen as shown in Figure 5.26. For C2 column specimen, LED markers on the hoop fibers were reduced in number as the C1 column specimen test results indicated that strain reading for a given number of hoop layers was within the expected range. Later, displacement reading from LED markers was used to calculate axial and hoop strain in the column specimens.

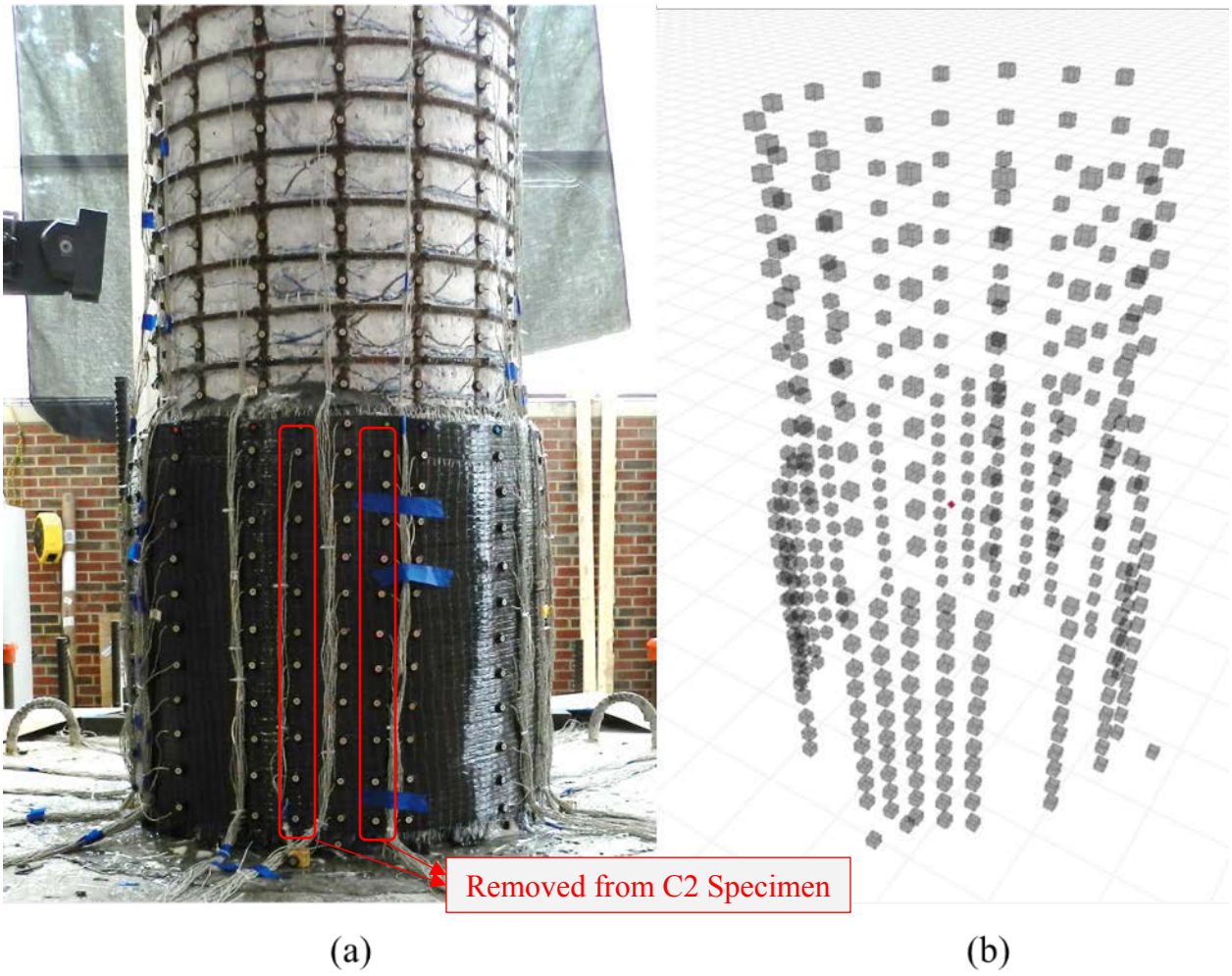

Figure 5.26: a) LED Markers Layout b) 3D View of LED Markers on C1 Column Specimens

String pots were located at North and West side of the columns and attached at the mid-height of the cap beam of the columns as in Figure 5.27. Also, linear potentiometers were attached to all four sides of the footing to collect displacement data to calculate slip and rotation of the footing, if any exist. The applied axial load was controlled using UTM; axial load level was checked at each ductility level to ensure that a constant axial load was applied.

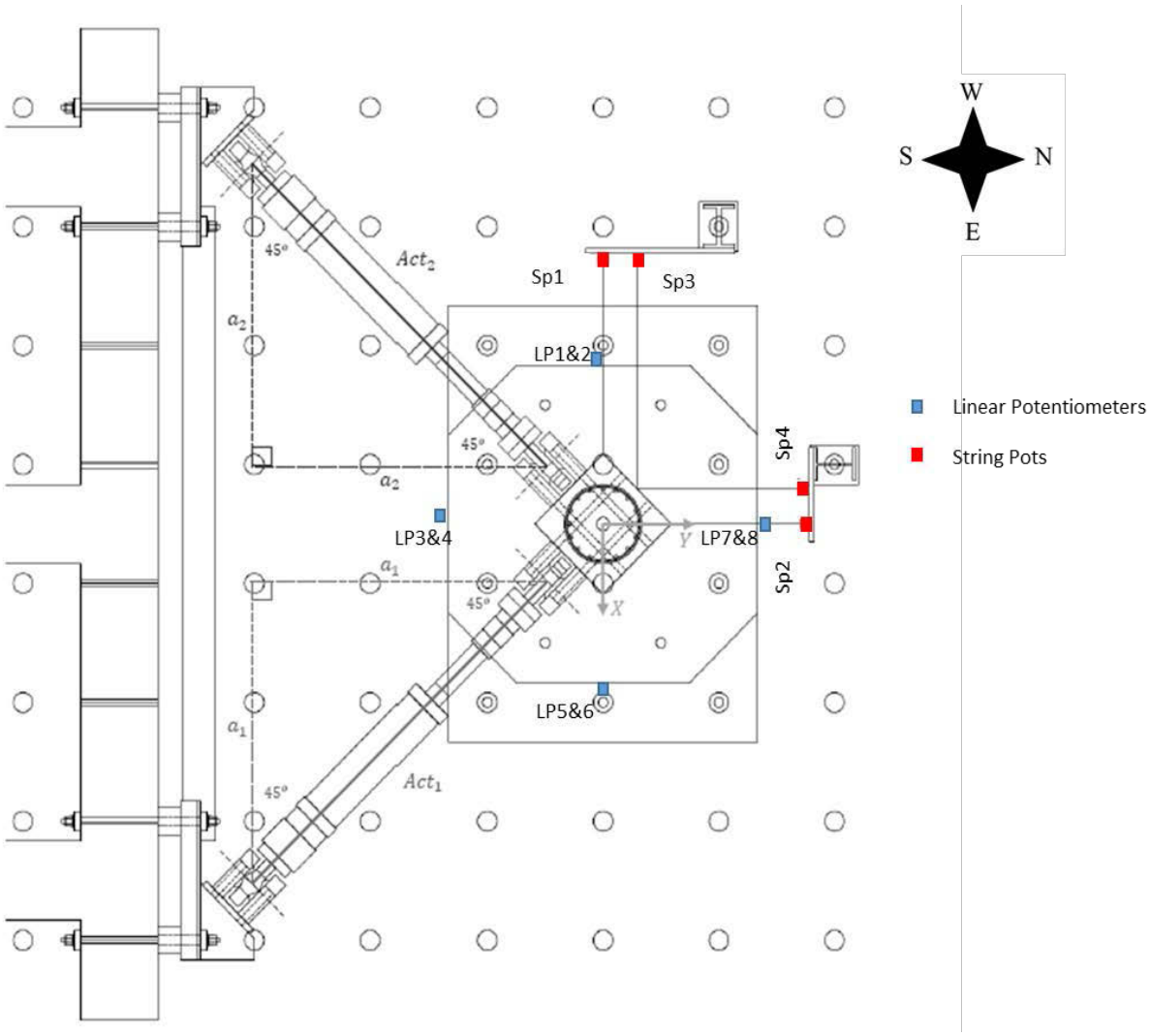

Figure 5.27: String Pots Location

5.2.7 Loading Protocol

A two-cycle set loading protocol, based on yield displacement of the original columns, was applied to both column specimens. Displacement history, which was applied to the original column, was applied to the repaired columns to make a direct comparison of repair. Cycles begin with elastic cycles until first yield force (F_y') and proceed with displacement increment for each ductility level as shown in Figure 5.28a. Asymmetrical load path, shown in Figure 5.28a, was followed. The experiments began with loading columns in +y and –y directions for two cycle of

each ductility level, then continue with +x and –x-direction until a given damage limit states were reached.

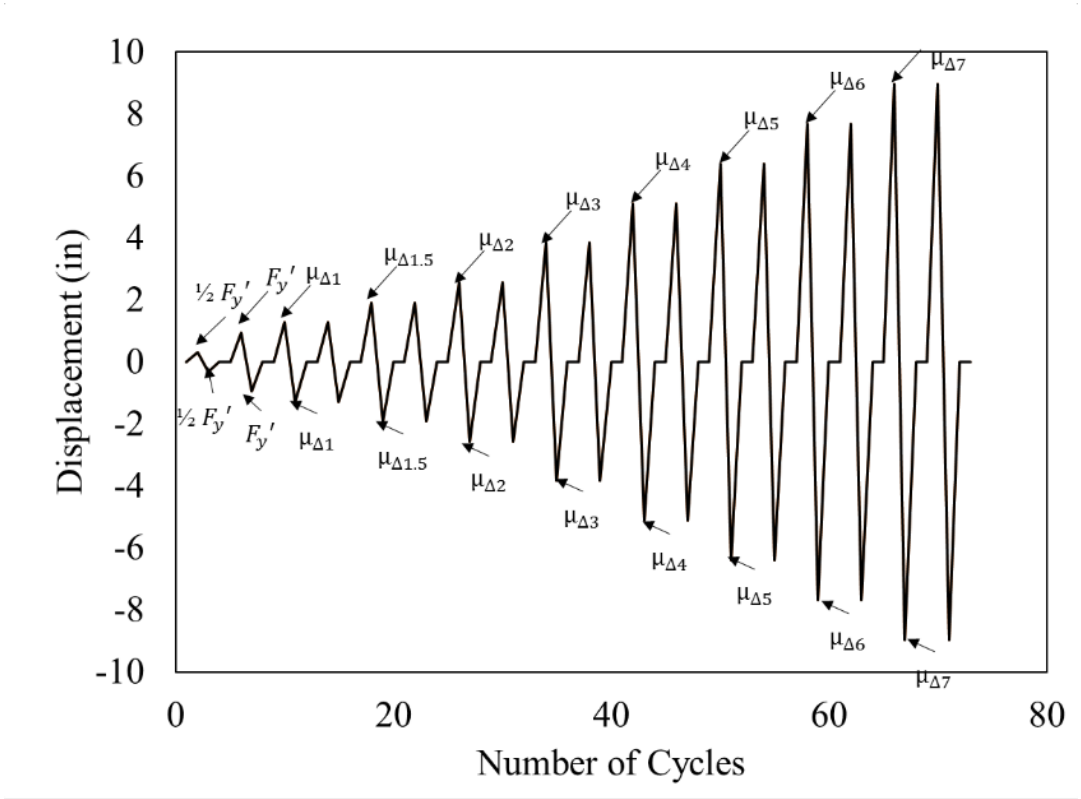

(a)

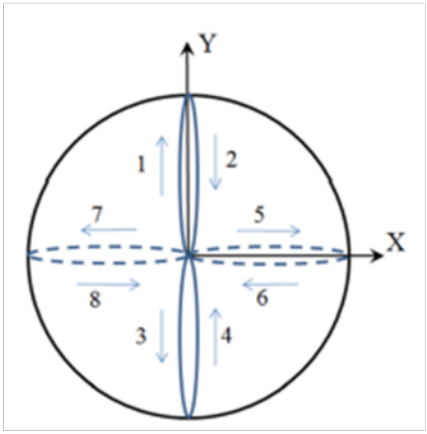

(b)

Figure 5.28: a) Typical Loading Protocol for Specimen C1 and C2 b) Asymmetric Two-Cycle-Set Biaxial Load History

5.3 Column Tests

This section of the chapter focuses on repair design of C1 and C2 column specimens and discussion of the experimental results.

5.3.1 C1 Column Specimen

As discussed before, the design procedure of the column began with the determination of based demand. The new location of the plastic hinge was determined to be one column diameter length above the footing where the level of strains in longitudinal reinforcing bars less than the half of the buckling strain of the reinforcing bars. Although longitudinal reinforcing bars exceeded yield strength at the new location of the plastic hinge, moment capacity was calculated assuming that all bars had original longitudinal reinforcing bar properties. Original column details, shown in Table 5-6, was used to conduct a moment-curvature analysis to get the ultimate moment capacity of the column section. Figure 5.29 shows the moment-curvature curve of the original column. Ultimate moment was 553 kip.ft. Demand at column based was calculated by extrapolating the moment demand at the new hinge to column base. From similar triangles, extrapolation coefficient, which is the ratio of the clear height of the column to a height of column above repair, was calculated as 1.28. Demand at column base was 708 kip.ft.

Table 5-6: Original Column Details for C1

Load History	Asymmetrical Two-Cycle Set
Length, Diameter, and Aspect Ratio	L=109.44 in, D=24 in, (L/D=4.56)
Long. Steel Detail	16#6 for ρ_l = 1.6 %
Long. Steel Properties	f_y= 70.33 ksi, f_u= 98.68 ksi, ε_y= 0.00283 ksi,
Transverse Steel Detailing	#3 @ 2.75in. for ρ_s=0.7%
Column Concrete Strength	f_c= 6.29 ksi
Axial Load	191 kips
Δ_y	1.28 in.

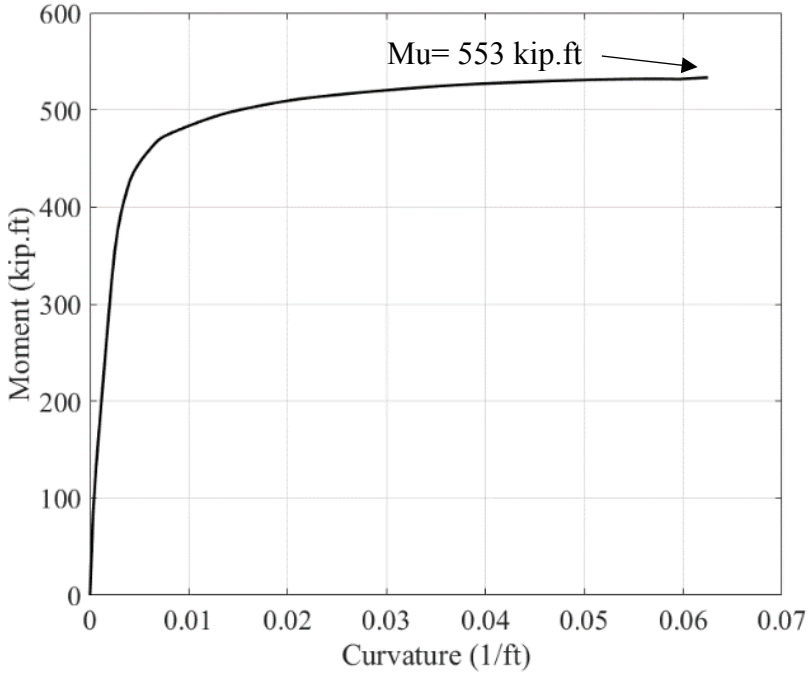

Figure 5.29 : Moment-Curvature Plot for Original C1 Column

As stated before, damage level of the original column at original plastic hinge was a single bar fracture and buckling of most of the bars. In the design procedure, for moment-curvature analysis, the fractured bar was not included into the model since the capacity contribution of the bar is zero. All of the remaining fifteen bars were modeled as buckled, using material model suggested in section 5.2.4.1. As mentioned before, a maximum number of the anchor can be installed into footing was twenty. For the design, all twenty anchors were evenly distributed around the column with the detail shown in Figure 5.30. The capacity of the anchors was estimated around 62 kips. The capacity estimation was based on the best knowledge obtained from the data collected before the time of the test. Using material model suggested for CFRP anchors in section 5.2.4.1, a moment-curvature analysis was conducted. Again, it was assumed that CFRP wraps did not affect the confined concrete properties of the concrete at the repaired region. Figure 5.31 shows the moment-curvature curve of the cross-section at the base of the repaired region. The moment capacity of the section was 857 kip.ft which was higher than the demand at the column base.

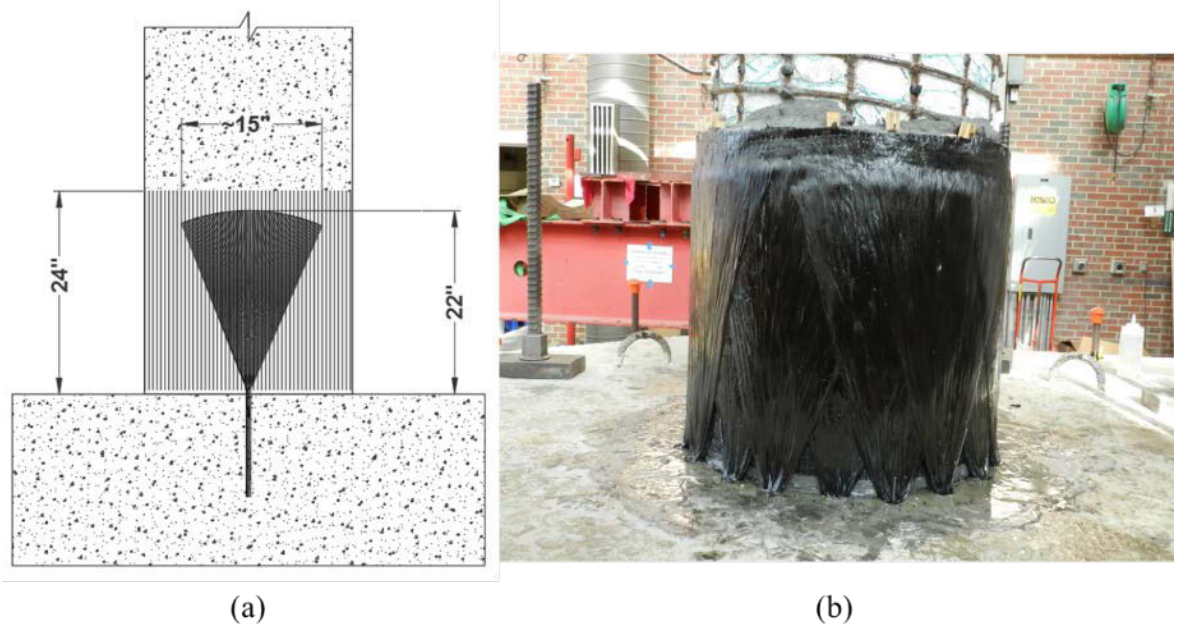

Figure 5.30 : a) CFRP Anchor Detail b) A view of Installed CFRP Anchors

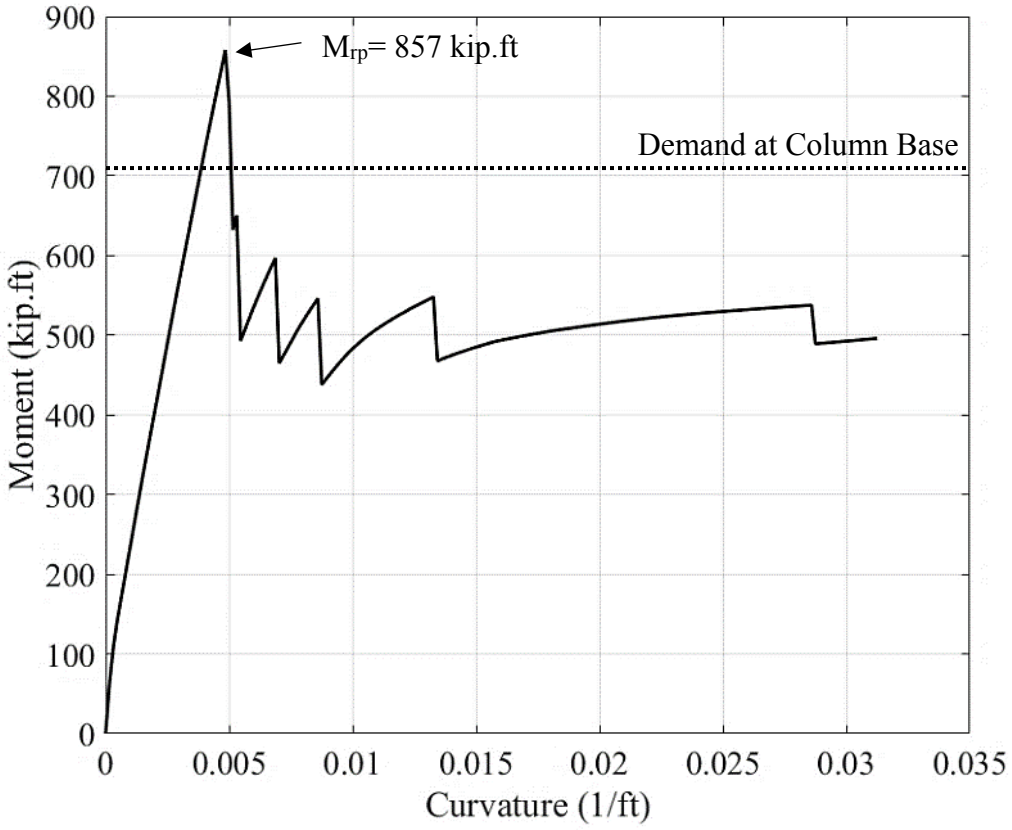

Figure 5.31 : Moment-Curvature Plot for Repaired Region Cross-Section with CFRP Anchors

A second moment-curvature analysis was conducted to determine the number of the required vertical CFRP sheets. The number of vertical CFRP sheet layers were determined to assume that the moment capacity of the section is constant through the height of the repair. The total thickness of the vertical CFRP sheet can be reduced since residual strain in the reinforcing steel reduces towards the top of repair. Also, demand also reduces. Thus, the required capacity can be reduced towards the top of repair. As sandwiching CFRP anchors were shown to be useful to produce uniform stress distribution at the anchor fan, using the same length of vertical sheets were logical. The required number of vertical CFRP sheet layer was determined to utilize cross-section at the bottom of the repaired region which was also used for moment-curvature analysis of the section with CFRP anchors. When three layers of vertical CFRP sheet were used, the moment capacity of the section reached 982 kip.ft which was more significant than the demand due to plastic hinge relocation. Figure 5.32 shows the moment-curvature curve of the section designed with vertical CFRP sheets. Table 5-7 summarizes the detail of the repaired column.

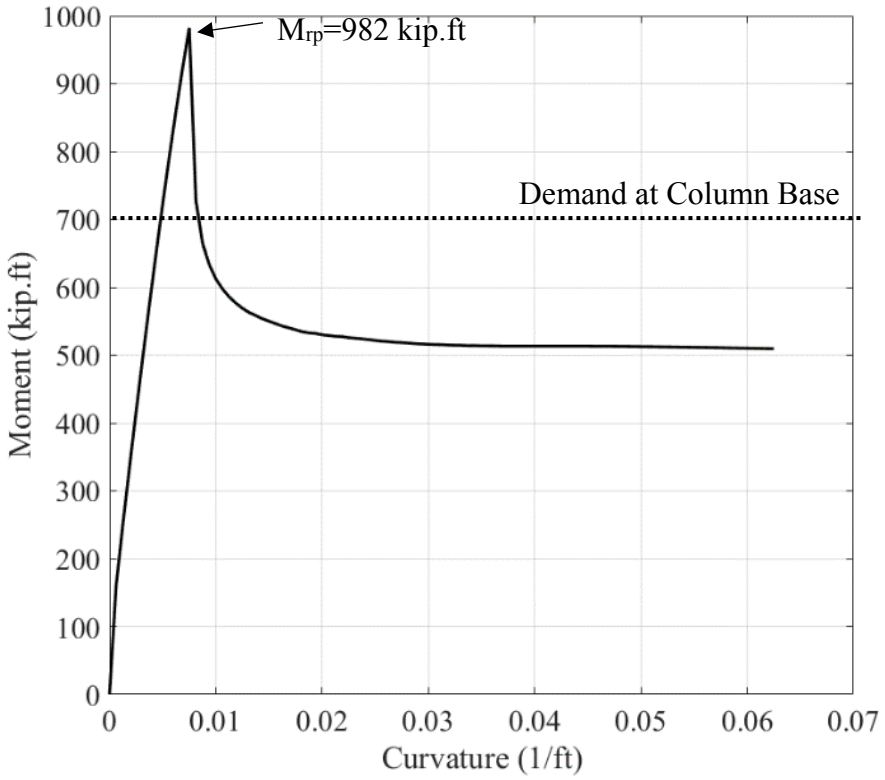

Figure 5.32: Moment-Curvature Plot for Repair Region Cross-Section with Vertical CFRP Sheet Layers

Table 5-7: Details of Repaired Column

Load History	Asymmetrical Two-Cycle Set
Repaired Height	24 in.
Number of CFRP Anchors	20
Anchor Diameter	1 in.
Anchor Fan Width	15 in.
Anchor Fan Length	22 in.
Number of Vertical CFRP Layers	3 (thickness= 0.12 in)
Number of Hoop Fibers	5 (thickness = 0.2 in)

5.3.1.1 Large Scale Testing

This section presented observations made throughout the large-scale testing of the C1 column specimen. Ductility levels were defined using yield displacement of the original column, and each ductility level was used to describe events. To describe the ductility level and direction of loading, an example of cycle labeling system is given in Figure 5.33. Figure 5.34 shows the column cross-section at the new plastic hinge region and the repaired region with the designation of each reinforcing bar and CFRP anchor.

5.3.1.2 Observation during Experiment

Testing of the column began with recording data before applying axial load. 191 kips of the axial load was applied using a self-regulating system described in the first volume of this report. Asymmetrical Two-Cycle Set load history was applied to start with +y direction displacements. Displacement control loading was started with displacement corresponds to force level ½ F_y' in +y and –y directions and continue with the same displacement cycle in +x and –x directions. There were no visible cracks observed. The loading was continued with displacement corresponds to force level F_y' for both ±y and ±x direction. No damage was observed at any part of the column. Hairline cracks were observed in the grout at original column-repair grout interface at the end of the first cycle of ductility level one. Until the end of the second cycle of ductility level one, epoxy around the anchor holes was cracked at the far side of the column, but no damage was observed in CFRP anchors. After the completion of $\mu_{1\Delta}^{+x2}$, crack in the grout at original column-repair grout

interfaces was wider, as show in Figure 5.35a. The crack width was above 0.04 in. In addition, hairline cracks on the core concrete got wider at the end of the loading cycle.

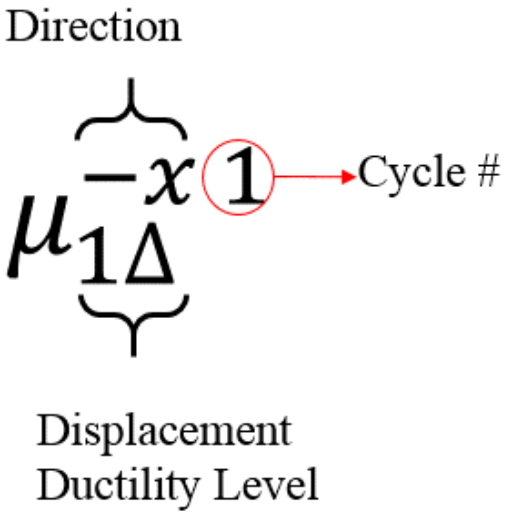

Figure 5.33: Displacement Ductility Cycle Labeling System

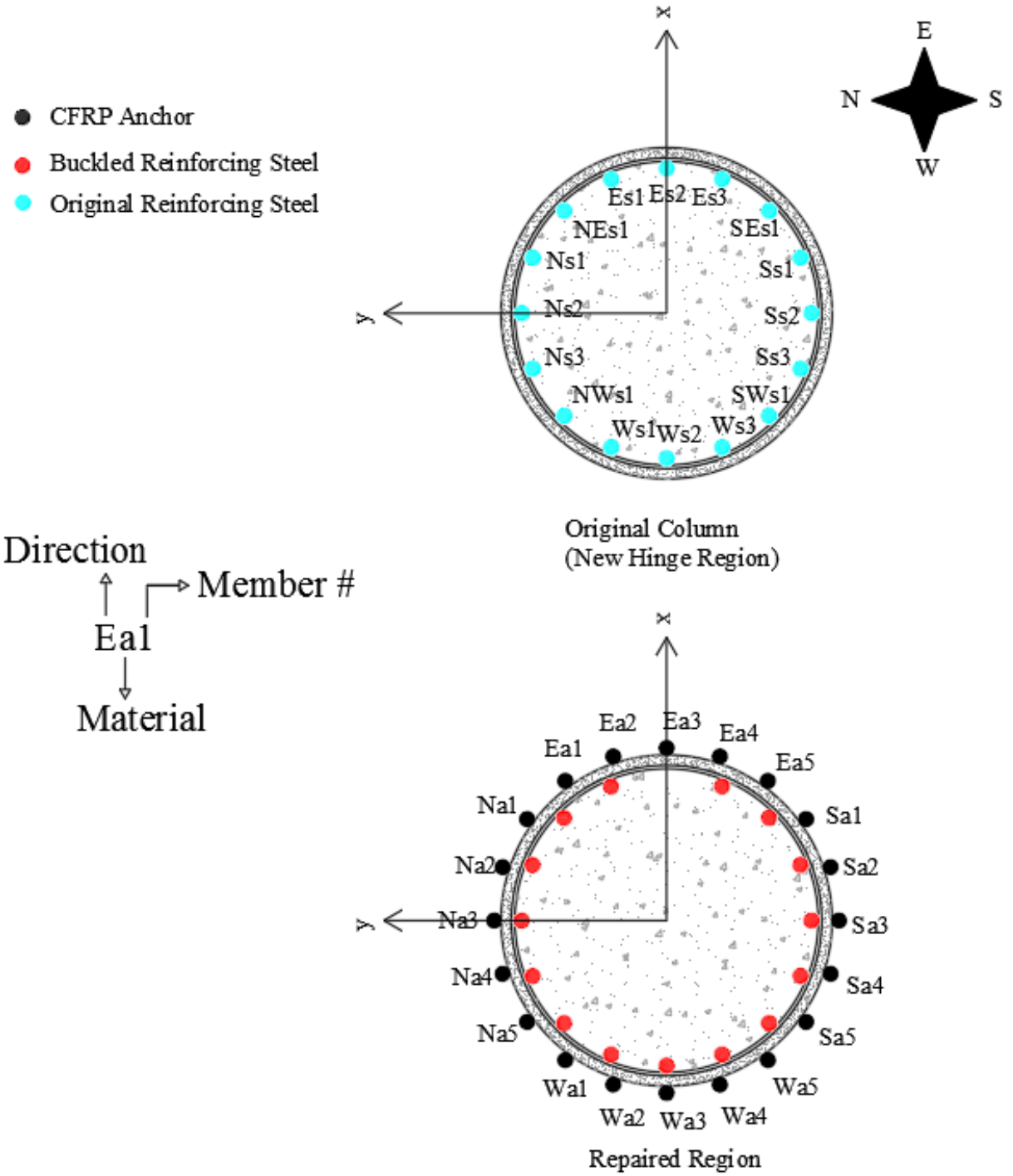

Figure 5.34: Column Cross-Section at a) the New Plastic Hinge Region b) the Bottom of the Repaired Region

When $\mu_{1\Delta}^{-x2}$ completed, crack in the grout at the top of the repair propagated towards the CFRP hoop fibers, as shown in Figure 5.35b. Cracks in the repair grout continued spreading as the loading was advanced. After completion of $\mu_{1.5\Delta}^{-x1}$, cracks at the grout and core concrete widened, and new hairline cracks were formed at core concrete as shown in Figure 5.35c. During the first cycle of $\mu_{1.5\Delta}^{+y2}$, core concrete edge scaled off, as shown in Figure 5.35d, and previously formed cracks widened. Even though cracking of epoxy was heard, no sign of damage in CFRP anchors was found.

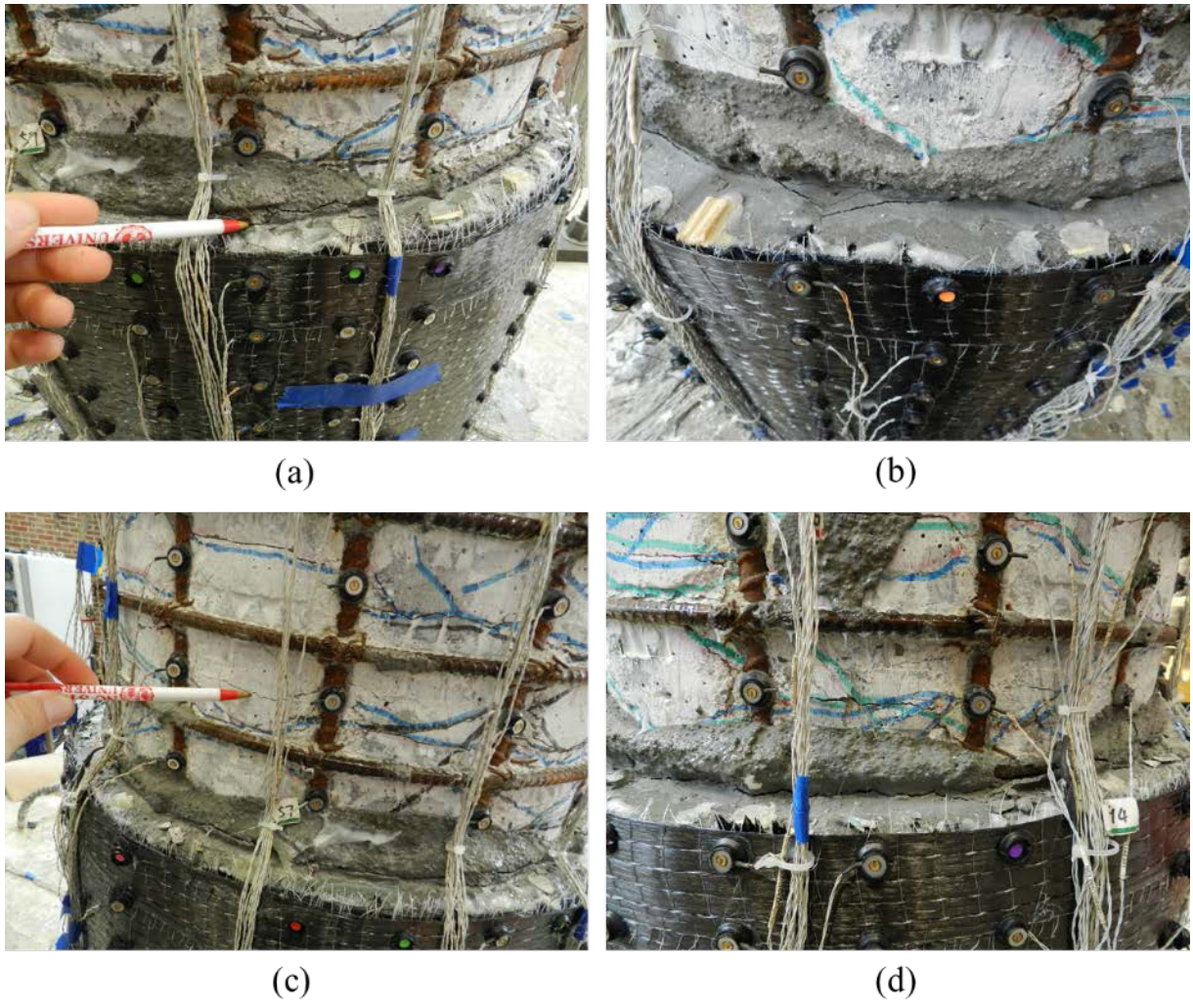

Figure 5.35: a) Wide Crack in Repair Grout b) Crack Propagation in Repair Grout c) New Hairline Cracks in Core Concrete d) Core Concrete Edge Scaled off

At ductility level two, cracking of core concrete continued, and cracking of epoxy was heard, but no signs of damage were observed in CFRP anchors. Previously formed cracks widened till the end of the ductility level two. At the end of $\mu_{3\Delta}^{+y1}$, rupture of anchor fibers was heard. At the west side of the column, Sa3 and Sa4 CFRP anchors were partially ruptured as shown in Figure 5.36a. The most extreme fibers were ruptured, but most of the fiber area was intact for both Sa3 and Sa4. Crack in the core concrete got wider. Column was pulled back to center, and then pushed to in the negative direction of the same ductility level. For $\mu_{3\Delta}^{-y1}$, partial rupture of Na2, Na3 and Na4 anchors was observed as shown in Figure 5.36b. Partial rupture of Wa3 was observed at $\mu_{3\Delta}^{+x1}$ as shown in Figure 5.36c. Then the column was pushed back, and then loaded to reach $\mu_{3\Delta}^{-x1}$. Ea2, Ea3 and Ea4 CFRP anchors partially ruptured. Figure 5.36d shows partial rupture of Ea3, since Ea3 had the most damage on the east side of the column. Experiment continued with second cycle of the ductility level three. When the column pushed to displacement corresponds to $\mu_{3\Delta}^{+y2}$, no additional damage was observed in previously damage south side CFRP anchors. Concrete core crushing was more apparent. The partial rupture of Na5 occurred at $\mu_{3\Delta}^{-y2}$, and previously damaged anchors sustained the loading without having further damage. As the column pushed in positive direction with a displacement corresponds to $\mu_{3\Delta}^{+x2}$, Wa4 anchor partially ruptured. As the column was pushed in negative x direction, no additional fibers ruptured in CFRP anchors on the east side of the column. It was observed that column was rotating about the new plastic hinge as shown in Figure 5.37. At the end of ductility level three cycles concrete core was heavily crushed. The loading was progressed with next set of cycles for same the ductility level. At the end of $\mu_{4\Delta}^{+y1}$, Sa3, Sa4 and Sa5 continued rupturing, but still some amount fibers were undamaged. Moreover, Sa2 partially ruptured. The partly ruptured Na2, Na3, Na4 and Na5 were fully ruptured at $\mu_{4\Delta}^{-y1}$. When the displacement in positive x direction at first cycle the of ductility level of four were reached, Wa1, Wa2 and Wa5 partially ruptured. In addition, Wa3 and Wa4 full ruptured. As the column pulled in negative direction, full rupture of Ea2, Ea3 and Ea4 occurred. Ea1 and Ea5 partially ruptured at this ductility level. At the end of the second cycle of ductility level four, all of the anchors fully ruptured, leading to loss in lateral force in both directions. The test was continued till the end of the first cycle of ductility level six. Since all CFRP anchors were ruptured,

previously buckled reinforcing bars started carrying more load. The column started rotating about its bottom end as shown in Figure 5.38. The loading was continued with the second cycle of the ductility level five. Till the end of the second cycle of ductility level five, only damage was crushing of cover concrete at the repair region near to the bottom end of the column as shown in Figure 5.39. As the column was push in positive y direction for the first cycle of ductility level six, rupturing sound was heard. It was concluded that previously buckled reinforcing still was ruptured. The rupture led to loss in lateral force capacity. The loading was ended when the column pushed in negative x direction of displacement ductility level six, and a reinforcing bar was ruptured.

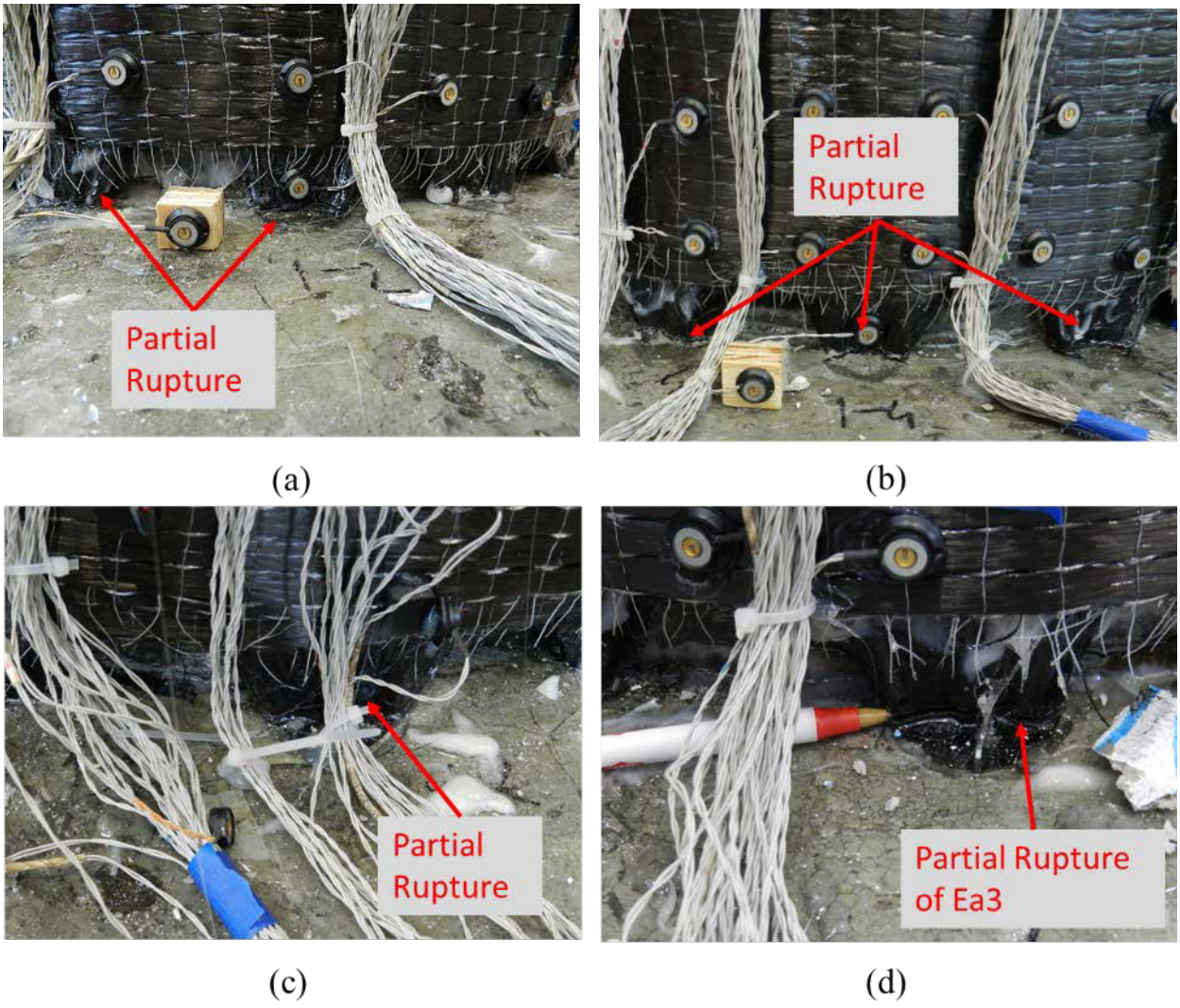

Figure 5.36: a) Partial Rupture of Sa3 and Sa4 b) Partial Rupture of Na2, Na3 and Na4 c) Partial Rupture Wa3 d) Partial Rupture of Ea3

Figure 5.37 : Plastic Hinge Formation above Repair

Figure 5.38 : Column Rotation about its Bottom End

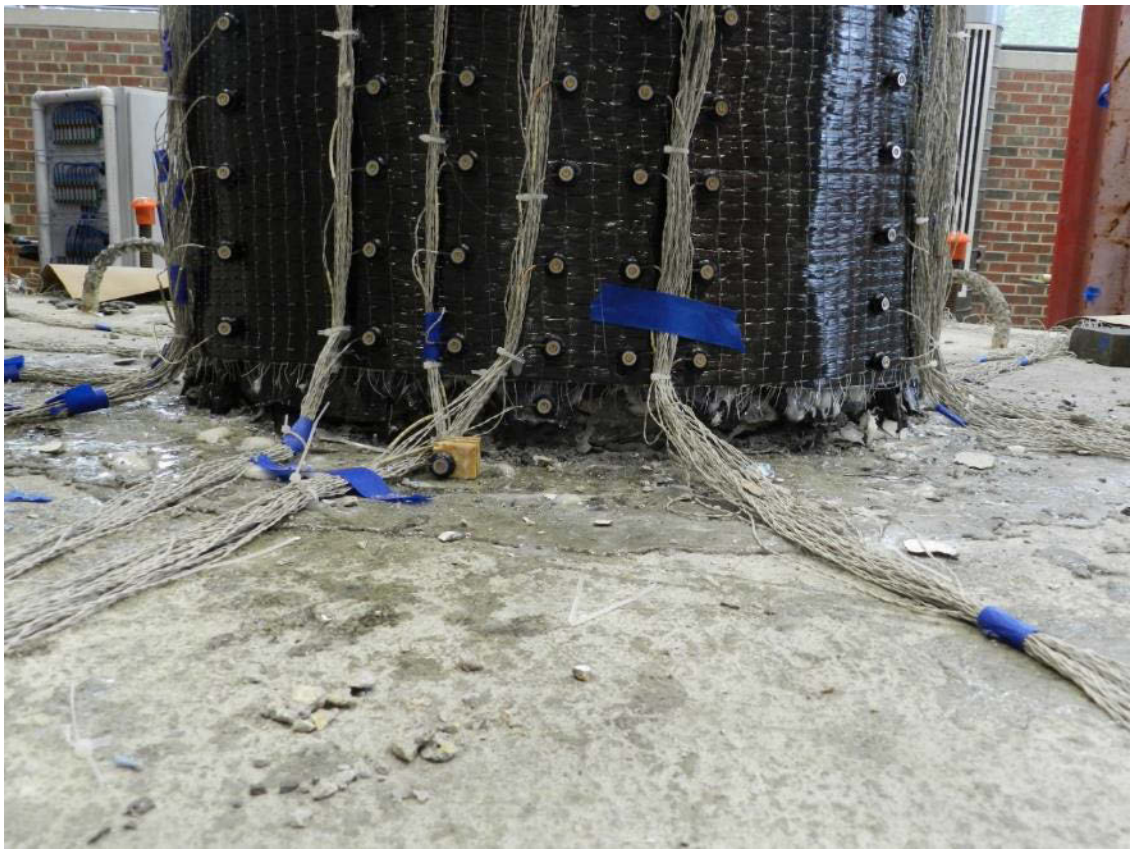

Figure 5.39 : Crushing of Confined Cover Concrete at the Bottom of Repair Region

5.3.1.3 Strain History of Extreme Fiber Reinforcing Bars and Vertical Strain Profiles

Although all reinforcing bars in the new plastic hinge region was instrumented with LED OPTOTRAK markers and data was collected during the test. Figure 5.40 shows designation of the reinforcing bars in the new plastic hinge region. Displacement history data for extreme fiber bars Ns2, Ss2, Es2 and Ws2 was presented in this section. As the plastic deformations were pushed above the repair, strain in the reinforcing bars increased. As shown in Figure 5.41a, Figure 5.41b, Figure 5.42a and Figure 5.42b, tensile strain of the reinforcing bars increased till full rupture of the CFRP anchors at the first cycle ductility level four. Since the anchor on all side of the column continued rupturing, strain degradation become more obvious. As it was mentioned, extreme fiber bar Es2 was ruptured in the original experiment. It can be seen in Figure 5.42a, drop in the strain

is more severe in this bar because Es2 bar started slipping from repair grout. It can be concluded with enough confinement pressure; ruptured bars can be developed.

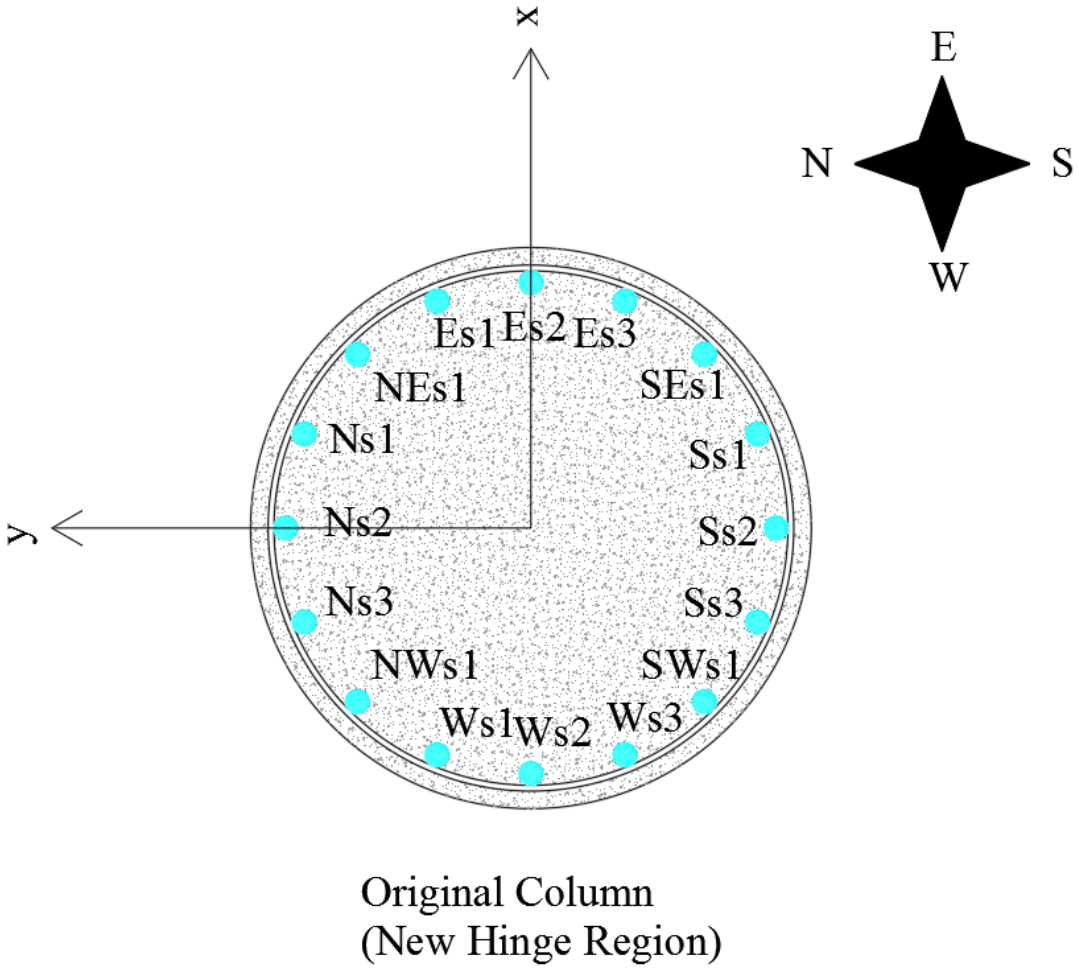

Figure 5.40 : Designation of Reinforcing Bars at New Hinge

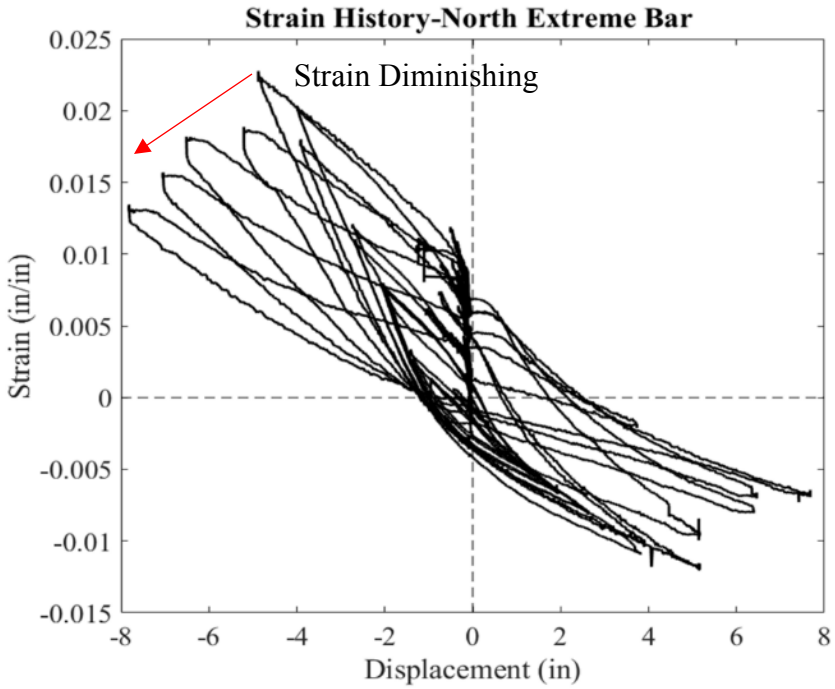

(a)

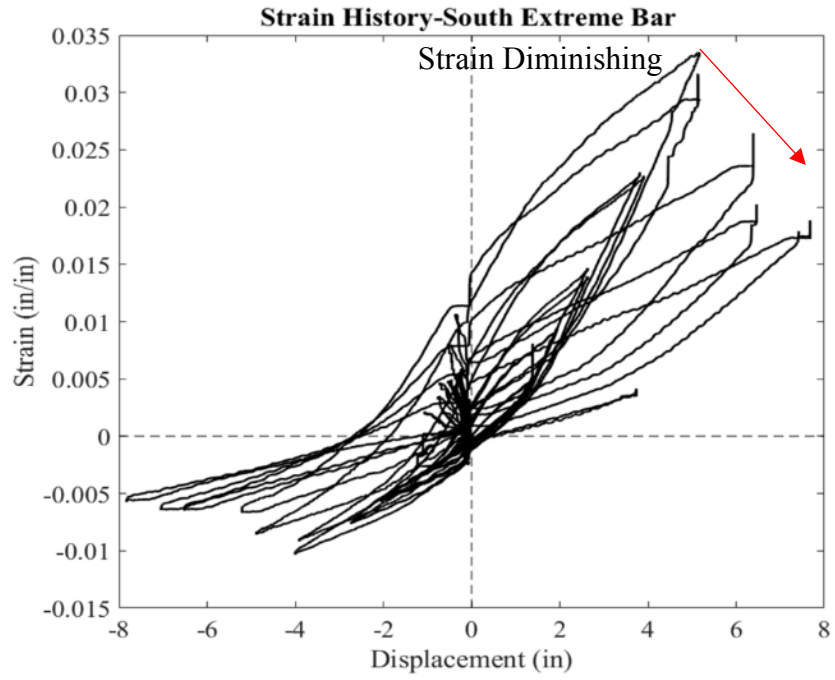

(b)

Figure 5.41 : Strain History of a) North Extreme Bar b) South Extreme Bar

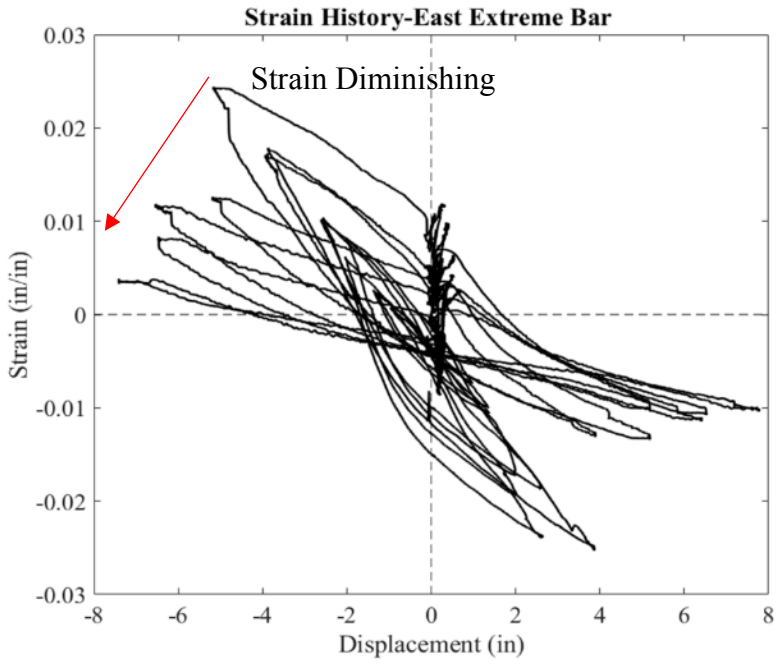

(a)

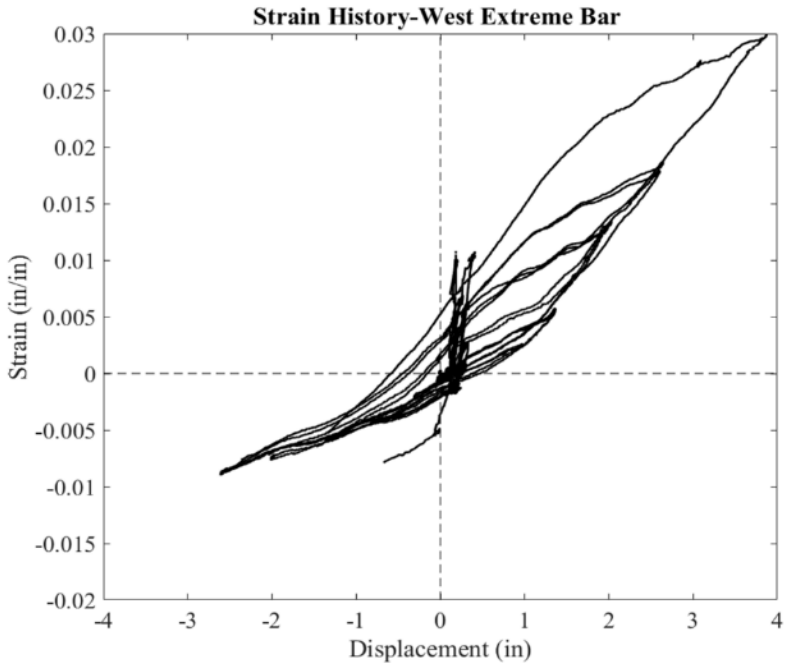

(b)

Figure 5.42 : Strain History of a) East Extreme Bar b) West Extreme Bar

Axial strain profile of extreme fiber reinforcing bars was obtained through led markers which were placed along the repair height as well as 20 inches above the repair. Figure 5.43, Figure 5.44, Figure 5.45 and Figure 5.46 show the axial strain in extreme fiber bars on each side of the column. Vertical strain in the CFRP repair less then yield strain of the reinforcing bars. As the column was pushed in higher ductility levels, strain in Ns2 increases till ductility level four. As the full rupture of the CFRP anchors took place, degradation in the strain was observed. These results suggested that plastic hinge in the new location was started forming but due to strength loss in the repair, relocation was not completed. Same behavior can be observed in all other three extreme fiber reinforcing bars.

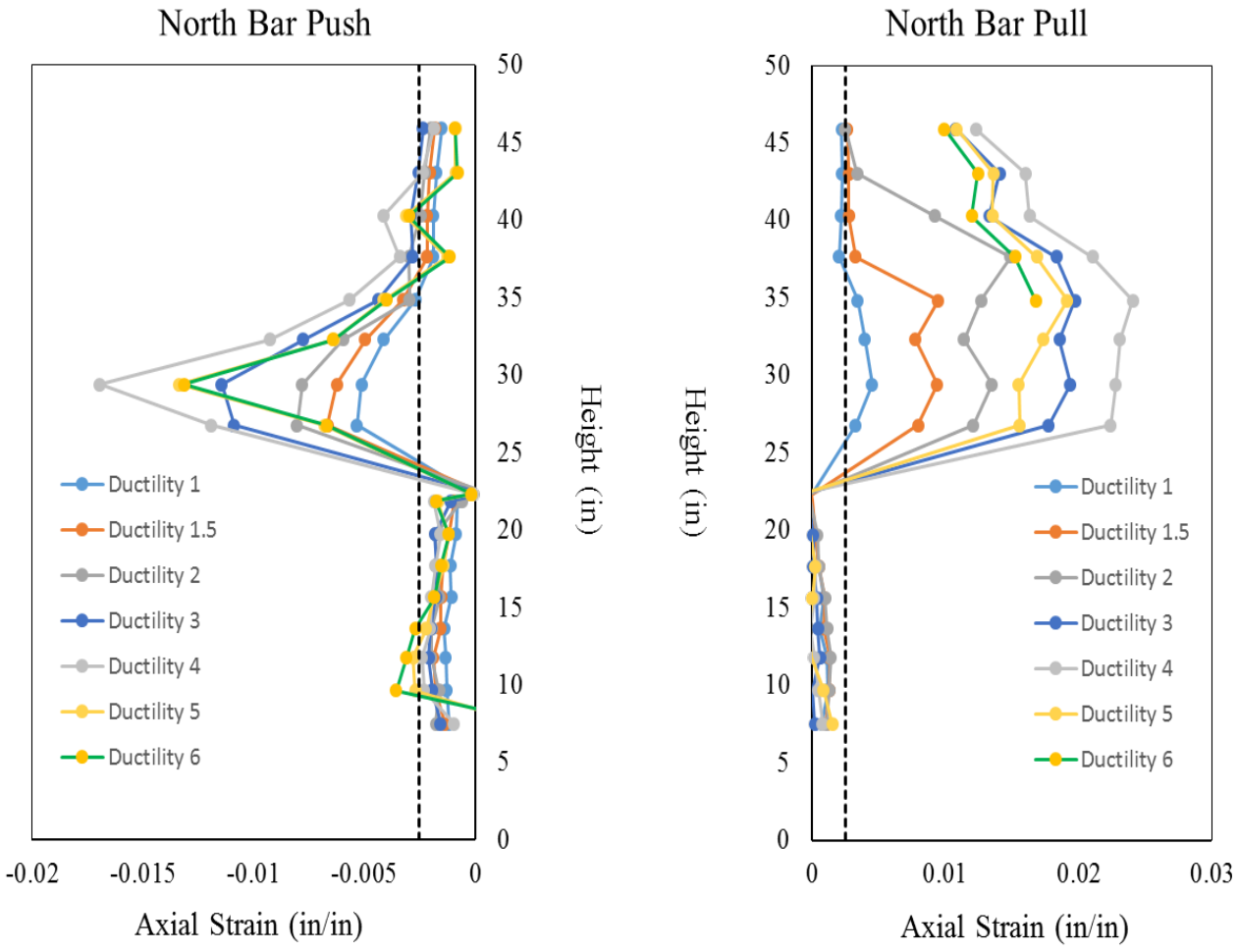

Figure 5.43 : Axial Strain in Ns2 Reinforcing Bar

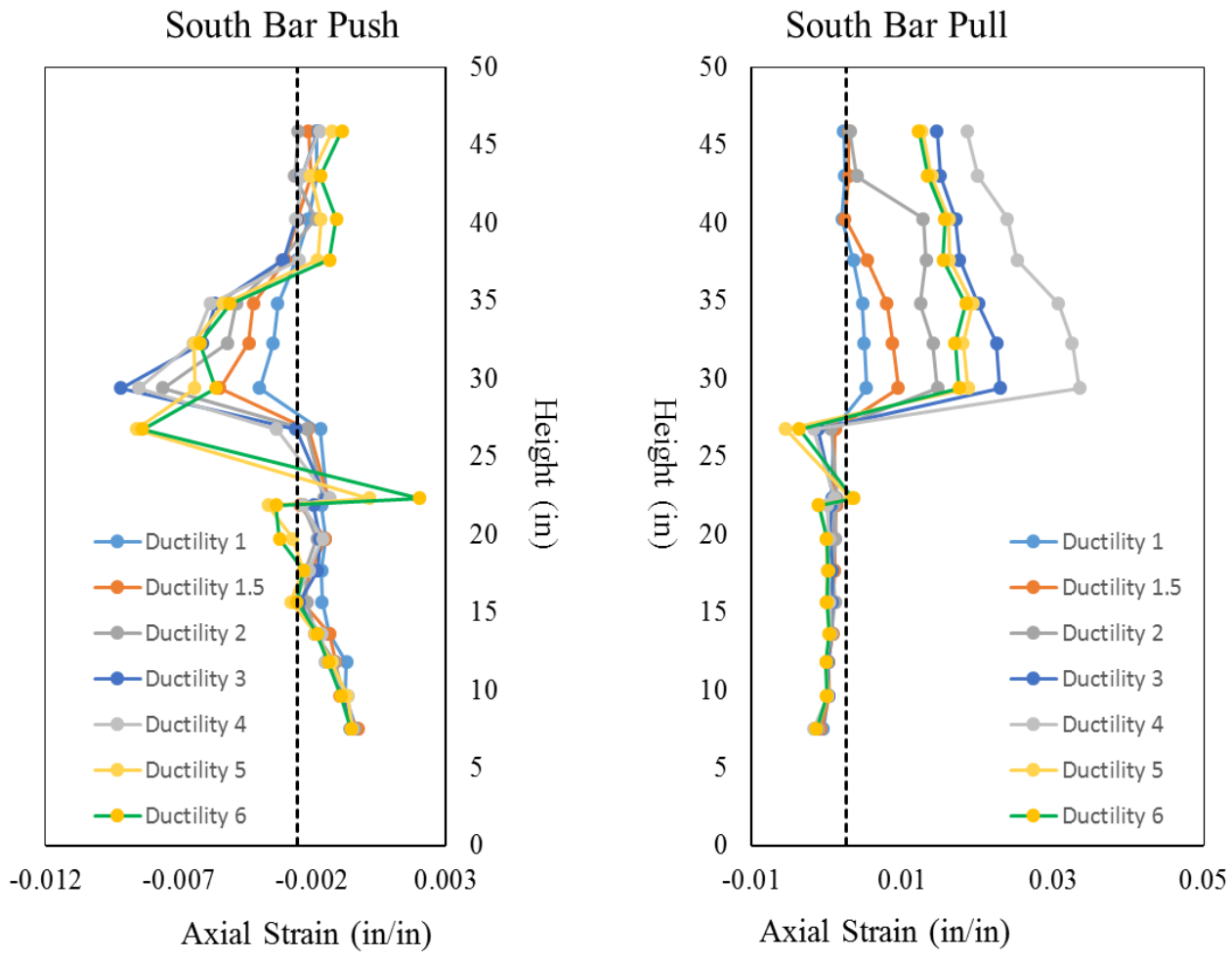

Figure 5.44 : Axial Strain in Ss2 Reinforcing Bar

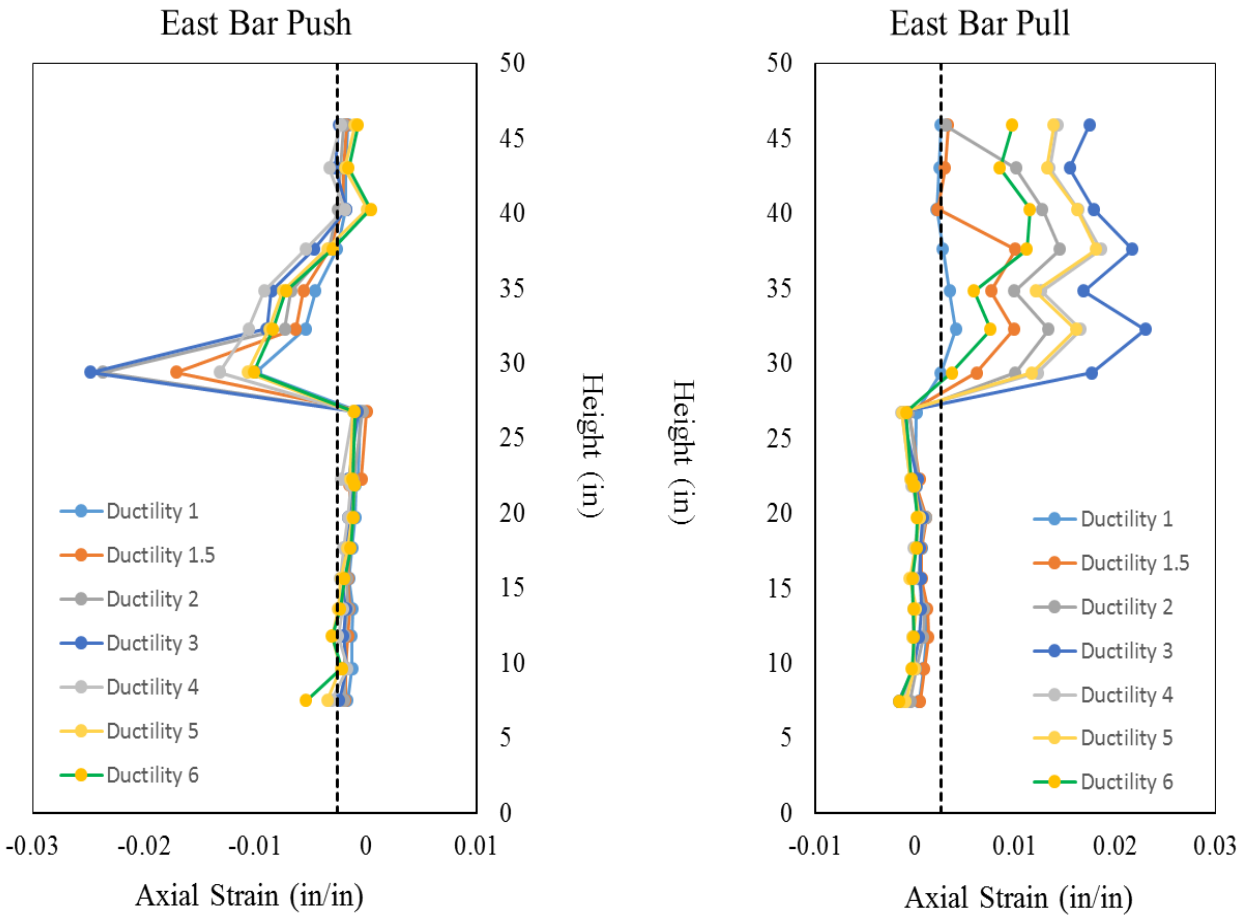

Figure 5.45 : Axial Strain in Es2 Reinforcing Bar

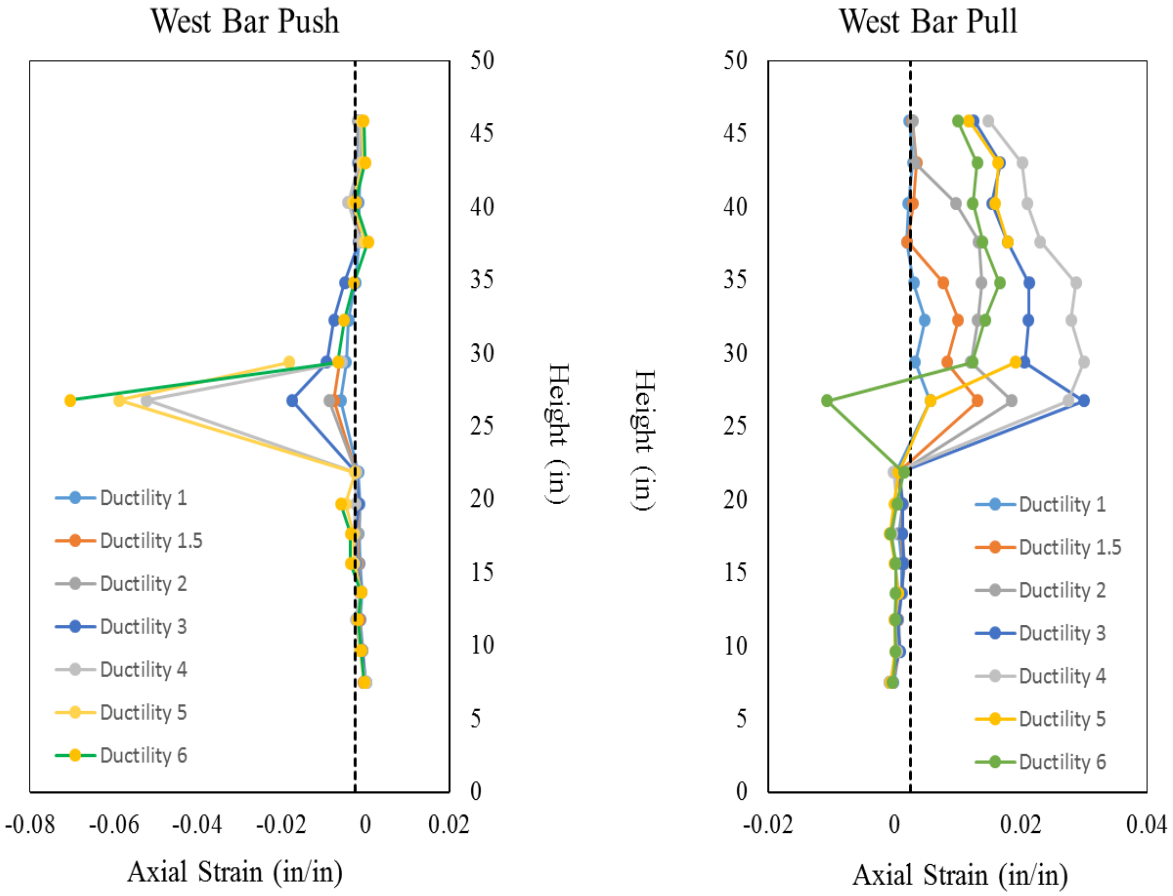

Figure 5.46 : Axial Strain in Ws2 Reinforcing Bar

5.3.1.4 Force-Displacement Response of the Column

Force-displacement response of the C1 column specimen for x and y-directions are given in Figure 5.47. The force capacity of the column was substantially increased. The ultimate lateral force in x direction was 76 kips whereas in y direction lateral force reached to 80 kips at the first displacement cycle of ductility level four. Load increase was about 31 % and 33 % for repaired column in +x and +y direction, respectively. Even though anchor fibers started rupturing at first cycle of ductility three, load continued increased. The increase in load was attributed the area of fibers which were intact before ductility four was larger than the area of fibers ruptured at the second displacement cycle of ductility level three. As it can be seen in Figure 5.48, for both direction, column initial stiffness increased. Due to the rupture of fibers through the testing, load began to reduce for the second displacement cycle of the ductility, but still lateral load was larger than the original column. As the all anchors at four sides of column was totally ruptured, load substantially decreased but this was less than 20 % for both direction of the column. At the loading was continued, due full rupture of all anchors around the column, buckled bars in original columns at the repaired region began to resist until rupture of the bars took place.

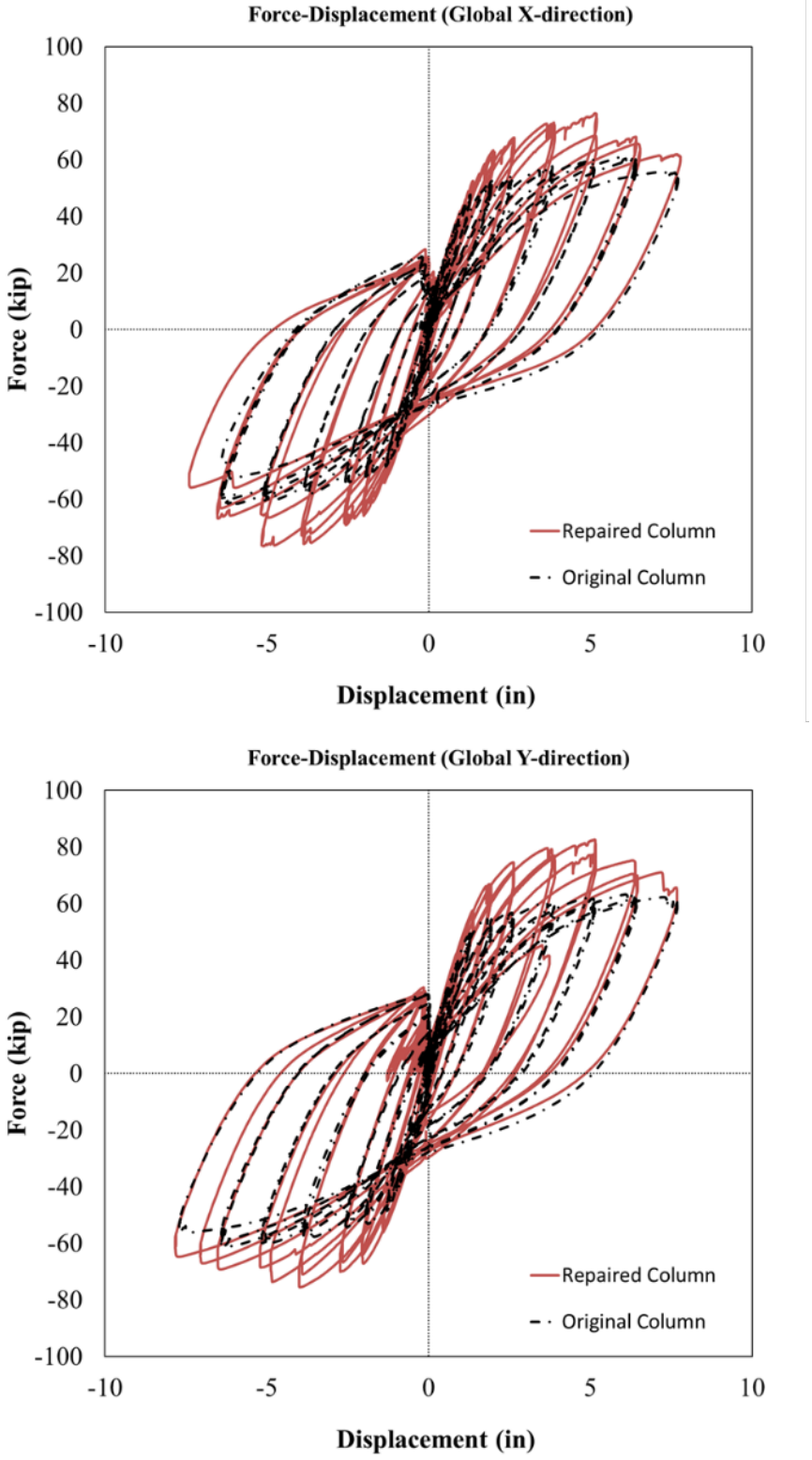

Figure 5.47 : Force-Displacement Curve of C1 Column in X and Y-direction

5.3.2 Conclusion for C1 Column Test

Since the rupture of the CFRP anchors were not expected, it was concluded that the capacity estimation for 1 inch-diameter CFRP anchors was overestimated. A moment-curvature analysis was conducted to estimate capacity of 1 inch-diameter CFRP anchors using same material properties used for the repair design of C1 column specimen. Moment demand at the column base was 744 kip.ft. To resist the demand, the required capacity of the anchor was around 53 kips. Figure 5.48 shows the moment-curvature curve of the column with updated anchor capacity.

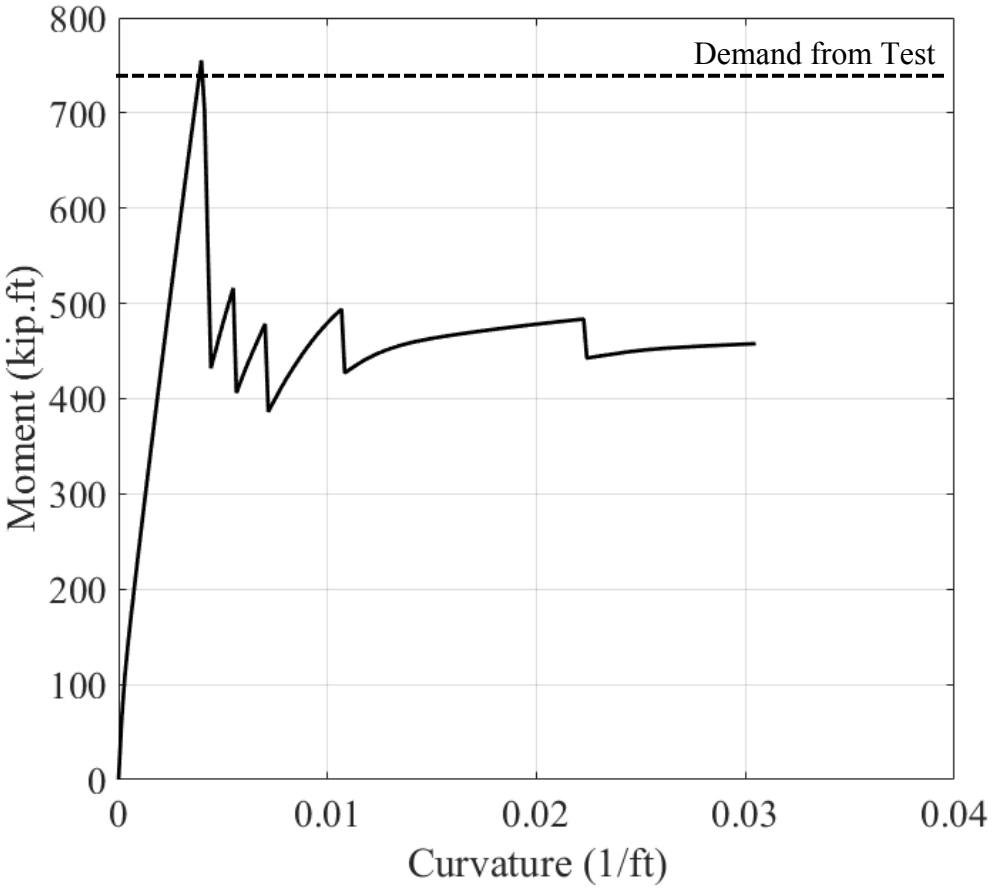

Figure 5.48 : Moment-Curvature Curve of the Section with Updated CFRP Anchor Capacity

Sandwiching CFRP anchor fan between vertical CFRP sheets was a reasonable approach distributed stress along CFRP anchor fan length. The number of vertical CFRP layers were adequate to develop full capacity of the anchors. Although length of CFRP sheet was 2 inches longer than the CFRP anchor fan, there was no development issue due to provided confinement

from hoop fibers. It was concluded that number of CFRP hoop fiber layers were adequate to prevent debonding of the CFRP anchor fans. Figure 5.49 shows the hoop strain develop in the repair at the south side of the column. The maximum hoop strain was 0.0043 in/in, suggesting that design assumption for strain limit of 0.0058 in was appropriate. Only hoop strain data for south side of repair was given because the largest hoop strain developed at this side of the column. Strain at the top of the repair increased until last cycle of ductility three. Since the formation of plastic deformation continued until rupture of anchor fibers, the largest hoop strain developed at the top of the repair. Strain demand at the top of the repair substantially dropped when the anchors fully ruptured. The rotation of column moves from new plastic hinge to column base. Thus, hoop strain at column base started to increase. The result signifying that relocation of plastic hinge into new region can be done through:

- Use of larger CFRP anchors
- Increase the number of CFRP anchors around the column.

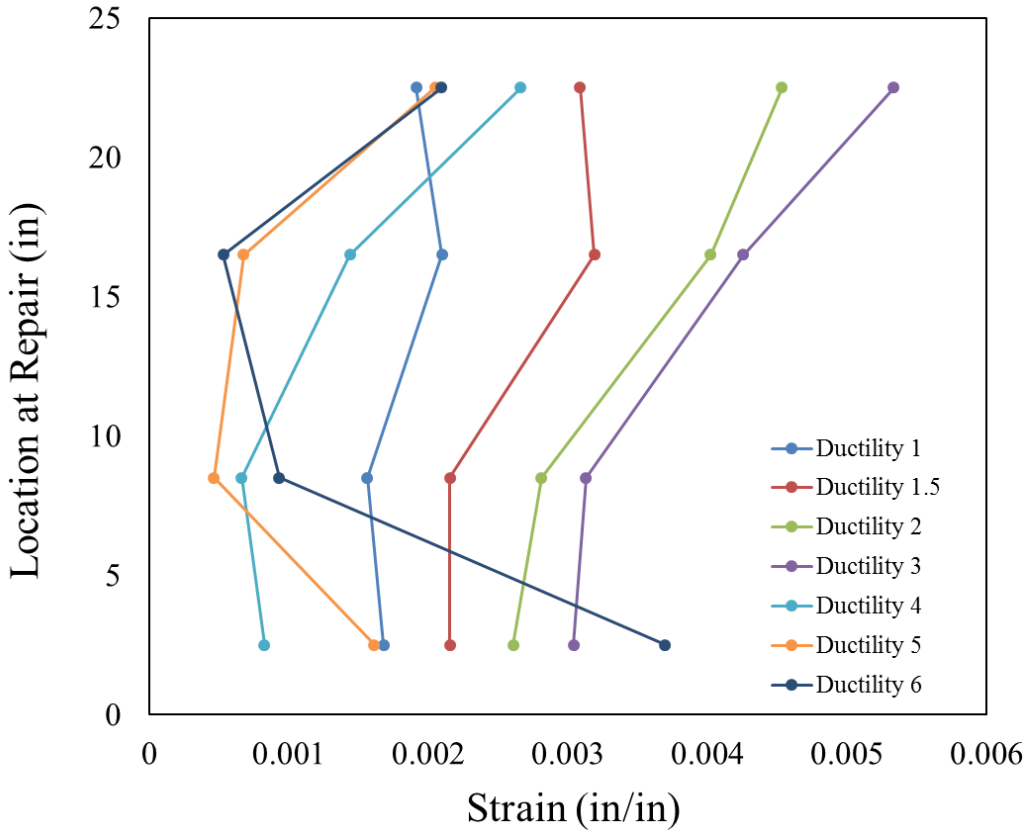

Figure 5.49 : Hoop Strain on South Side of Repair

5.3.3 C2 Column Specimen

Since the rupture of the CFRP anchors were not desired outcome for the repair design, a column test was conducted to show a repair scenario where plastic hinge can be moved above the repair region. In order to compare C1 and C2 column specimens, base demand of C2 was required to be reduced. Therefore, four of the longitudinal reinforcing bars at new plastic hinge region was intentionally severed. As show in Figure 5.50 a, four extreme fiber bars, Ns2, Ss2, Es2, and Ws2, were cut. The reinforcing bars were cut above the repair region as shown in Figure 5.50b.

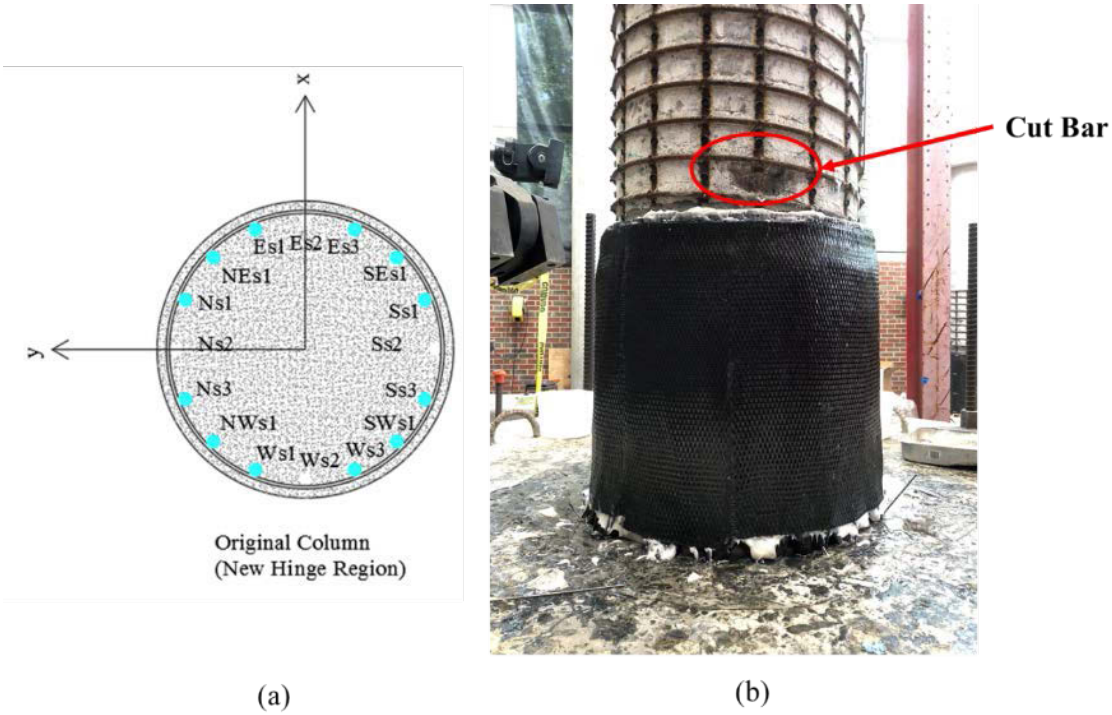

Figure 5.50 : a) Designation of Reinforcing Bars in C2 Column Specimen b) Location of Bar Cut

Using details given in Table 5-8, a moment-curvature analysis was conducted. As it can be seen in Figure 5.51, ultimate moment capacity of both columns was close. Ultimate moment capacity of the C2 column was about 560 kip.ft. Repair height for C2 column specimen was 24 inches because the level strain was less than the half of buckling at 24 inches above the footing. Extrapolation coefficient for this column test was 1.28. Thus, demand at column base was 716.8 kip.ft.

Table 5-8: Column Details for C2

Load History	Asymmetrical Two-Cycle Set
Length, Diameter, and Aspect Ratio	L=109.44 in, D=24 in, (L/D=4.56)
Long. Steel Detail	16#7 for ρ_l = 2.1 %
Long. Steel Properties	f_y= 71.2 ksi, f_u= 97.9 ksi, ε_y= 0.00254 ksi,
Transverse Steel Detailing	#3 @ 2.75in. for ρ_s=0.7%
Column Concrete Strength	f_c= 6.24 ksi
Axial Load	191 kips
Δ_y	1.47 in.

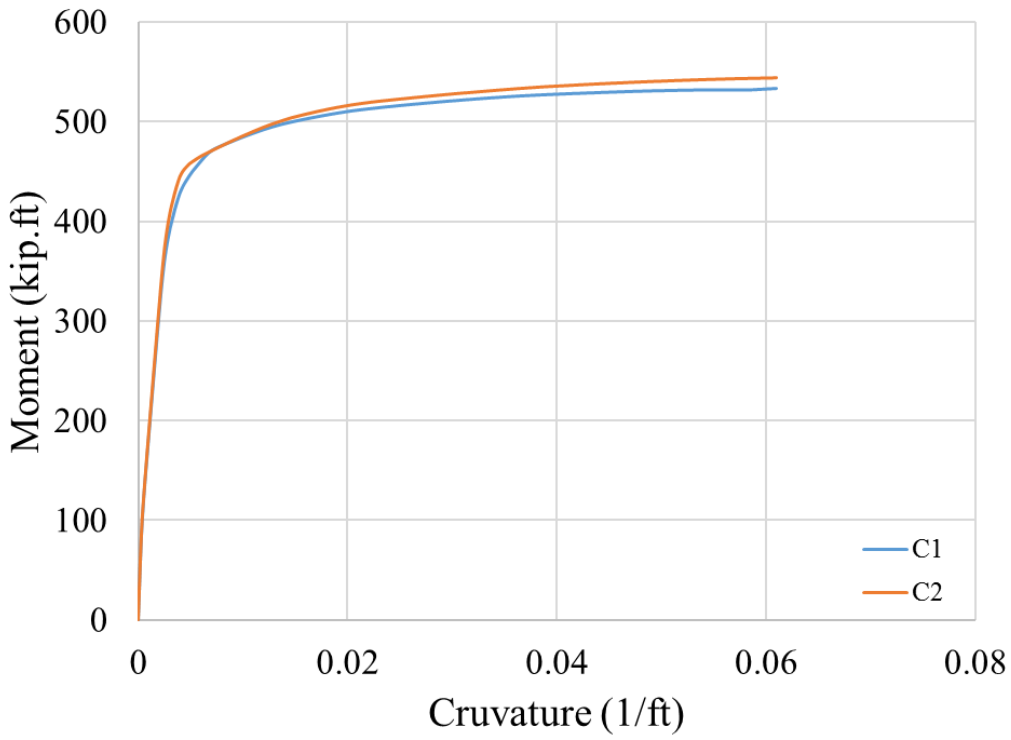

Figure 5.51 : Moment-Curvature Curve of C1 and C2

Since maximum number of anchors can be installed into footing was twenty and the demand at column base was close to the demand in C1 column specimen, using 1-inch diameter anchors would resulted in failure of anchor. Thus, the next larger diameter anchor, which had diameter of 1-1/4 inches, was used to repair the column. To make a direct comparison, same anchor detail was used for column C2 as shown in Figure 5.52.

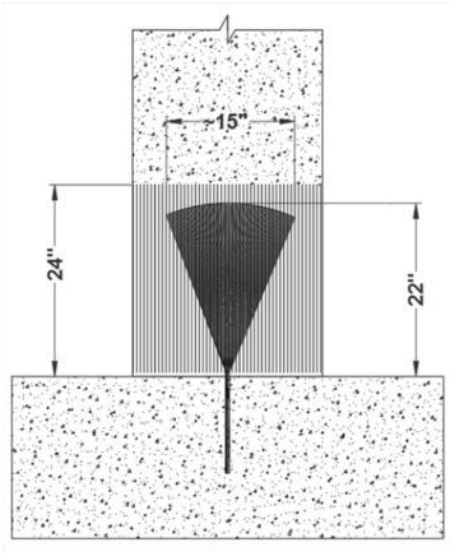

Figure 5.52 : Detail of CFRP Anchor for C2 Column Specimen

Due to limited available data for 1-1/4 in diameter CFRP anchors, the capacity of an anchor was estimated using data collected from the first column test. The capacity of 1inch-diameter was estimated around 52 kips. Through linear extrapolation, the capacity of 1-1/4-inch diameter anchor was estimated around 65 kips. It should be noted that efficiency of anchors reduces with increasing fiber volume fraction. Thus, there is no linear correlation between capacity and anchor diameter, but it was assumed that capacity estimation was reasonable enough to repair the column. Using pull-out test results, tensile modulus of 1-1/4-inch anchors were calculated. Figure 5.53 shows the material property for 1-1/4 inch-diameter CFRP anchors. With modified material model, a

moment-curvature analysis was conducted. Cross-section of the column at repair base is shown in Figure 5.54. Four extreme fiber bars were also removed from the cross-section although provided confinement was large enough to develop force in those bars except east extreme fiber bar which was fractured at column base. Confinement of CFRP wraps were excluded in the analysis since repair section was designed to remain elastic during a seismic event. The moment capacity of the repaired column was 883 kip.ft which was larger than the demand. A second moment curvature analysis was conducted to determine vertical CFRP sheet layers. Analysis resulted in three layers of vertical CFRP sheets. Number of Hoop fibers were determine using shear friction model, which was discussed previously. The required number of hoop fiber layers were five for the repair of this column. Table 5-9 shows the detail of the repaired column.

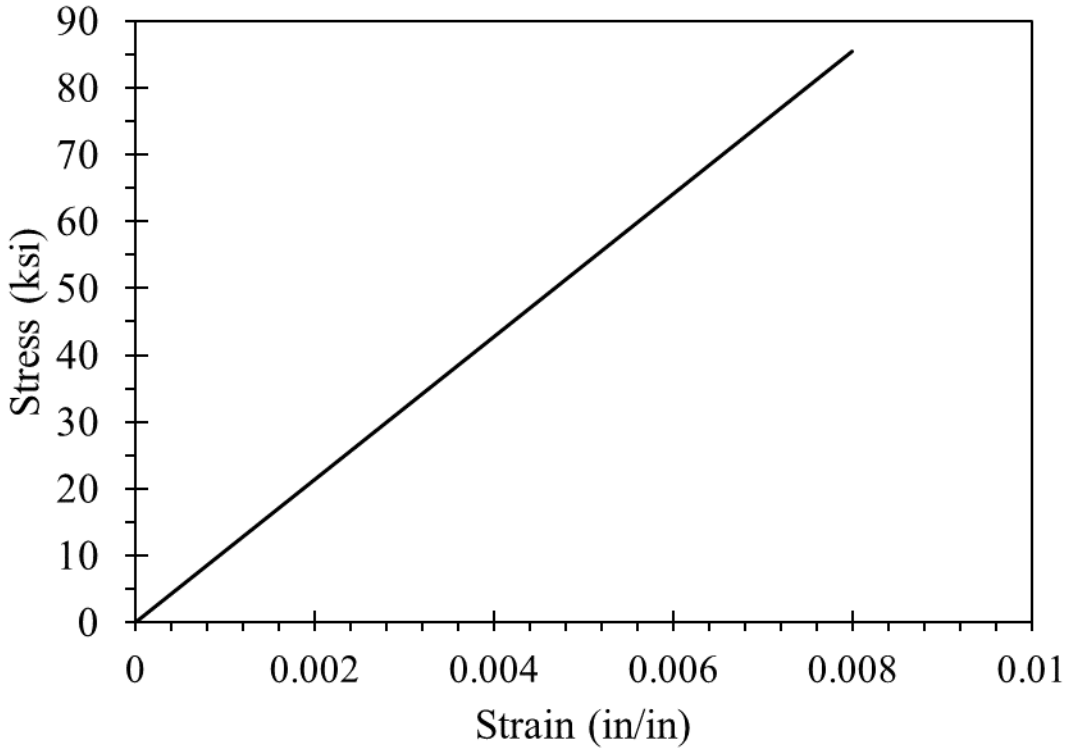

Figure 5.53 : Stress-Strain Curve for 1-1/4 inch-diameter Anchors

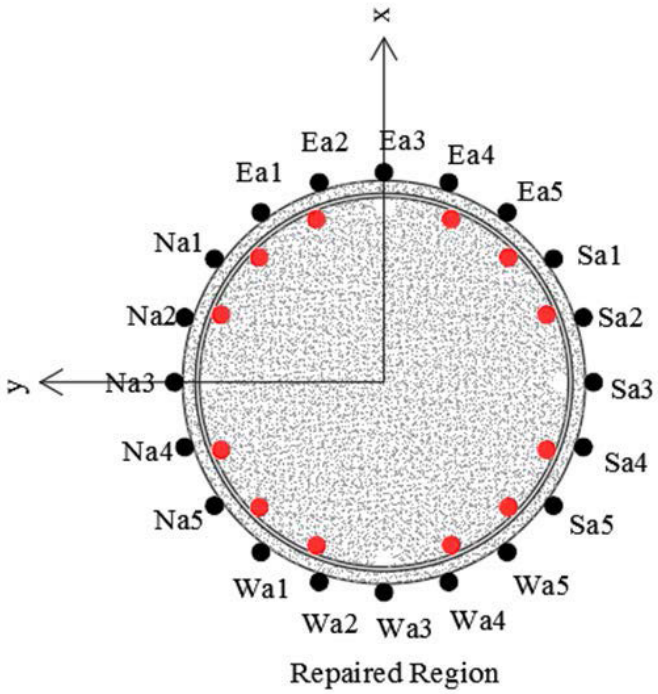

Figure 5.54 : Designation of CFRP Anchors in Repair Region

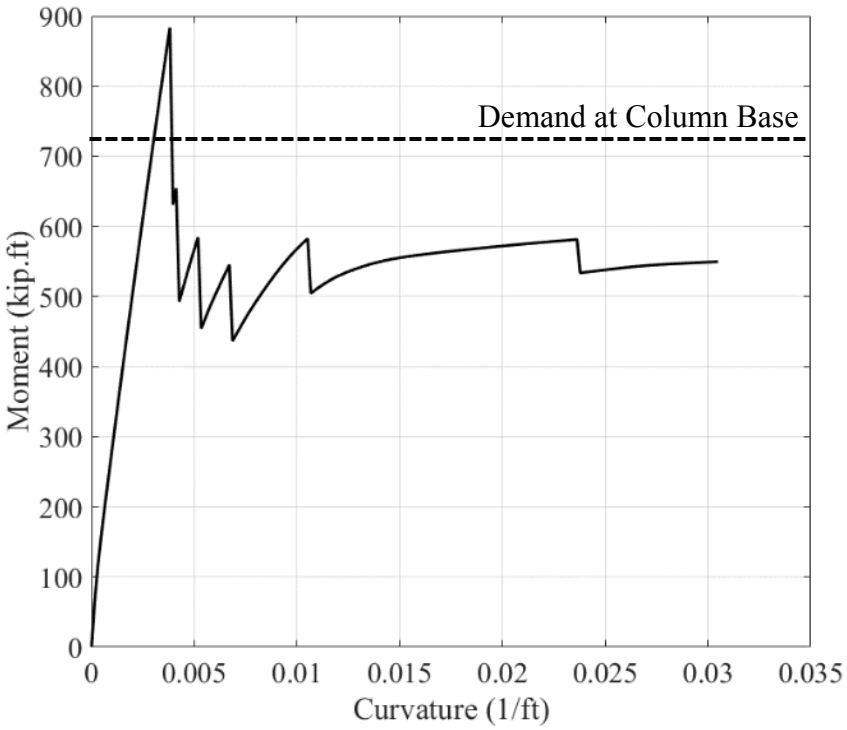

Figure 5.55 : Moment-Curvature Curve for C2 with CFRP Anchors

Table 5-9: Details of Repaired Column C2

Load History	Asymmetrical Two-Cycle Set
Repaired Height	24 in.
Number of CFRP Anchors	20
Anchor Diameter	1-1/4 in.
Anchor Fan Width	15 in.
Anchor Fan Length	22 in.
Number of Vertical CFRP Layers	3 (total thickness= 0.12 in)
Number of Hoop Fibers	5 (total thickness = 0.2 in)

5.3.3.1 Observations during Experiments

Before applying displacement in any direction, data collection was started. After applying 191 kips axial load, testing of the column was started. Asymmetrical two cycle set loading protocol was applied to the column. The column was first pushed in +y direction to reach ½ F_y and then pulled in –y direction to reach half yield force. Same displacement was applied in + x and –x direction. Displacement control loading was continued until first yield force (F_y') reached in both x and y direction. As shown in Figure 5.56a, a continuous crack at repair grout occurred. Using yield displacement of the original column, displacement at each ductility level was calculated. The column was pushed in +y direction for the first cycle of ductility level one, and loading was continued with next cycle. Due to removal of core concrete around the extreme fiber bars, previously formed cracks were enlarged as shown Figure 5.56b. Although cracking of epoxy was heard, no damage was observed in CFRP anchors. As the loading progressed, cracking of core concrete around severed extreme fiber bars became more apparent at the end of $\mu_{1.5\Delta}^{+y1}$ as shown in Figure 5.56c. It was observed that concrete was stared spalling at the north face of the column as shown in Figure 5.56d.

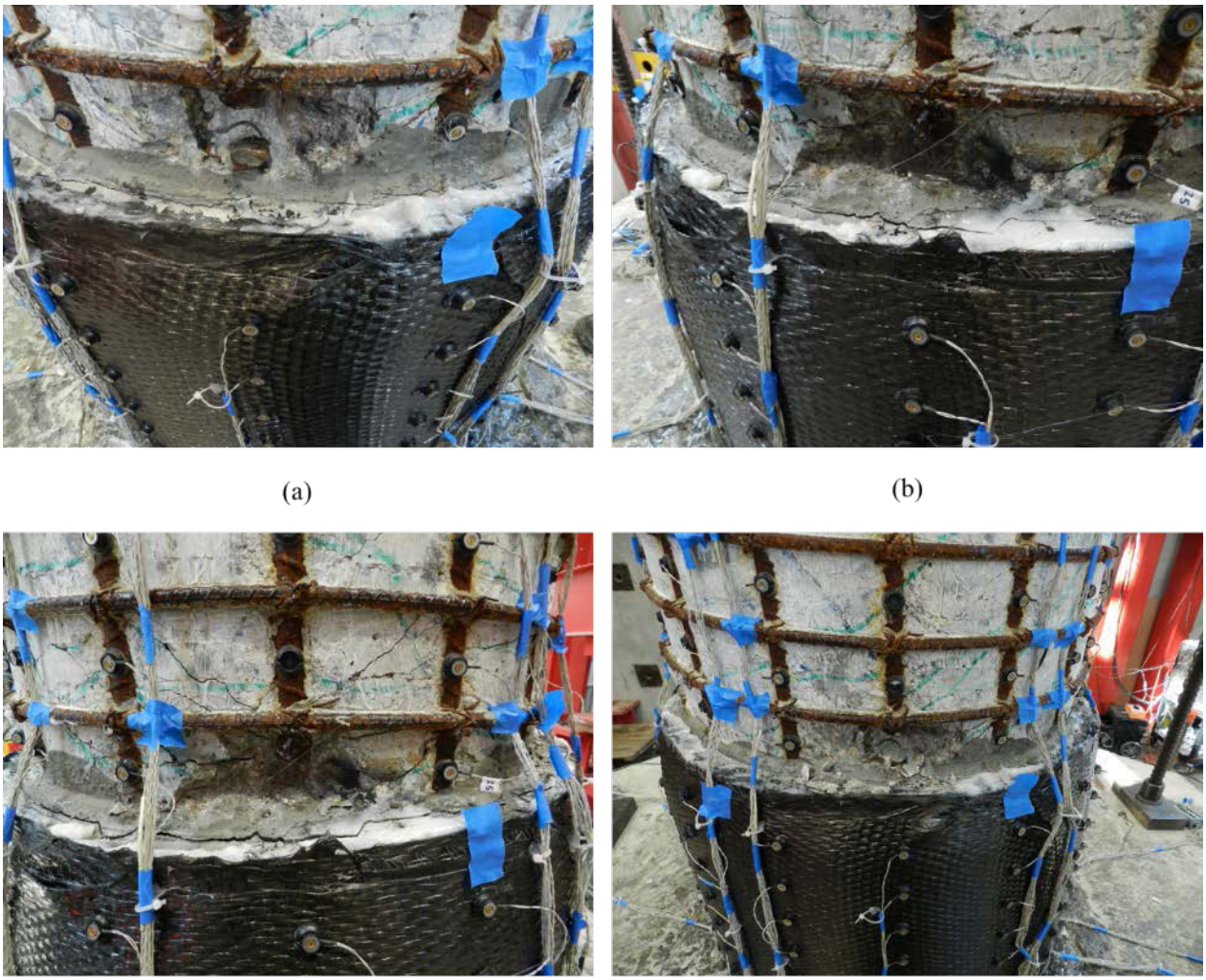

(a) (b)

(c) (d)

Figure 5.56 : Observed Damage in C2 Column before $\mu_{1.5\Delta}^{+y1}$

Spalling of core concrete was observed at west side of the column at the end of $\mu_{1.5\Delta}^{-x1}$ as shown in Figure 5.57a, and flaking of core concrete edge away from cut bars was observed as shown Figure 5.57b. At the end of $\mu_{2\Delta}^{+y1}$, crack width enlarged around the extreme bars, and concrete stated spalling at south-west and south-east side of column as shown Figure 5.57c. Rotation of the column above repair became more recognizable as shown in Figure 5.58. Concrete core crushing was noticeable at the end of $\mu_{2\Delta}^{+y2}$ as shown in Figure 5.59a and Figure 5.59b. Distribution of plastic deformations above the repair can be observed through crack distribution

as shown in Figure 5.59c. Although cracking in repair grout enlarged as the testing continued, no damage observed in hoop fibers. The amount of the core concrete above severed bar began crushing as shown in Figure 5.60a. An extreme fiber bar on the north side of the column was slightly buckled out at the end of $\mu_{4\Delta}^{+y1}$ as can be seen in Figure 5.60b. As the column pull back in –y direction, extreme fiber bar buckled, as shown in Figure 5.60c. When the column was displaced in +x direction, two extreme fiber bars slightly buckled as shown in Figure 5.61a and Figure 5.61b. Rotation of the column above repair became more apparent, as shown in Figure 5.61c. As the column was pulled in –x direction for the first cycle of ductility level four, two extreme fiber bars on west side of column buckled out as shown in Figure 5.62a-b. For the second cycle of ductility level four in +y direction, buckling of two extreme fiber bars were significant as can be seen in Figure 5.62c. Buckled bar on the north side of the column straightened and no bar fracture observed as the column move in –y direction as can be seen in Figure 5.63a. When the column reached displacement corresponds to $\mu_{4\Delta}^{-x2}$, extreme fiber bar fractured, shown in Figure 5.63b. Once the column pushed in +y direction for the first cycle of ductility level five, one of the extreme fiber bar fractured before reaching target displacement. Testing was ended as one of extreme fiber bar fractured on the north side of the column as the column was pulled back in –y direction.

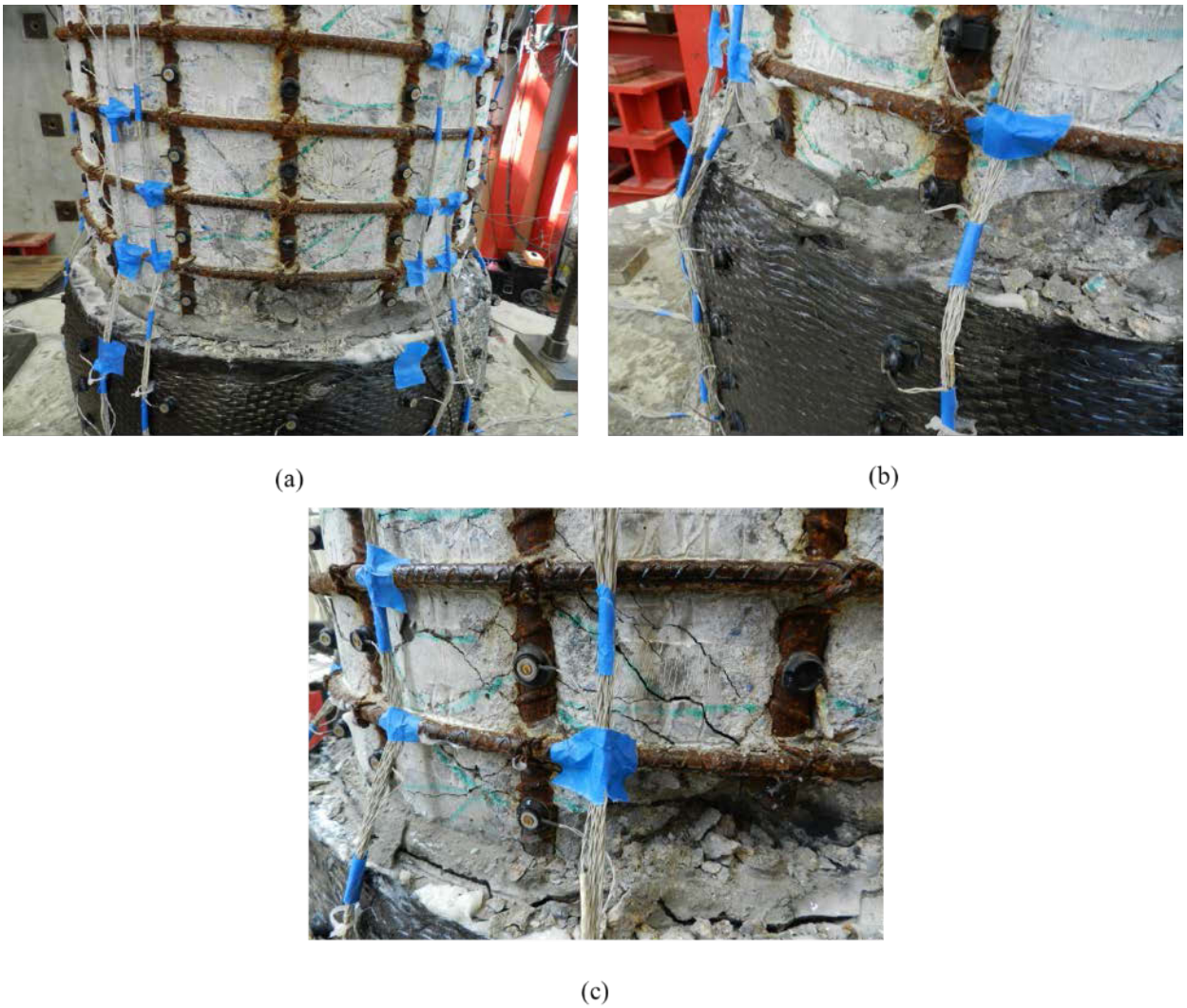

Figure 5.57 : Observed Damage in C2 Column during $\mu_{1.5\Delta}^{2}$

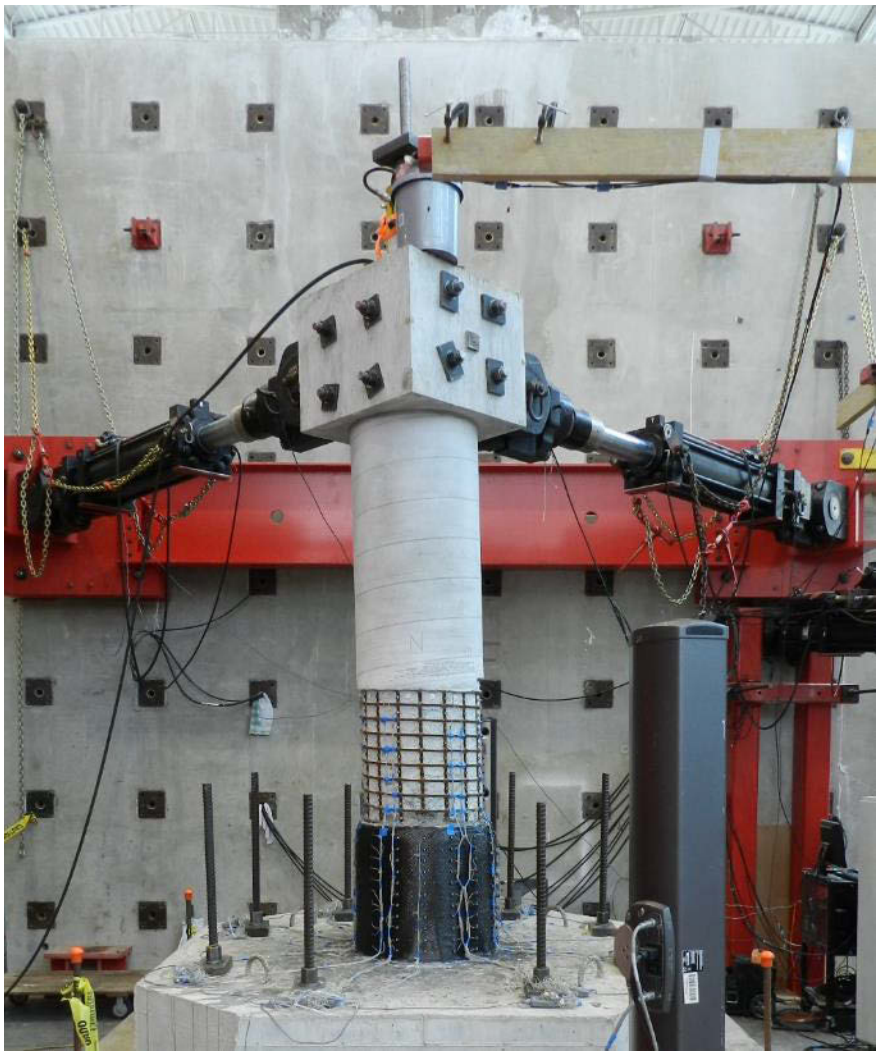

Figure 5.58 : Column Rotation above Repair at $\mu_{2\Delta}^{+x1}$

(a) (b)

(c)

Figure 5.59 : Damage During $\mu_{3\Delta}$

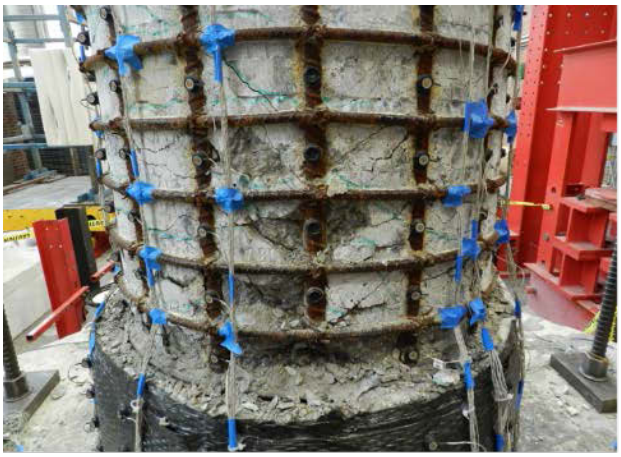

(a)

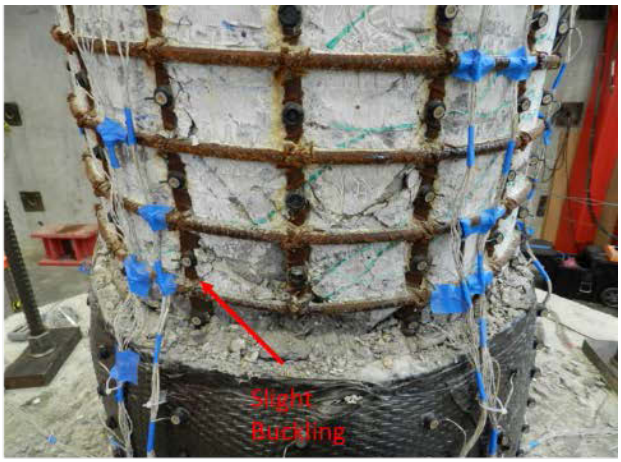

(b)

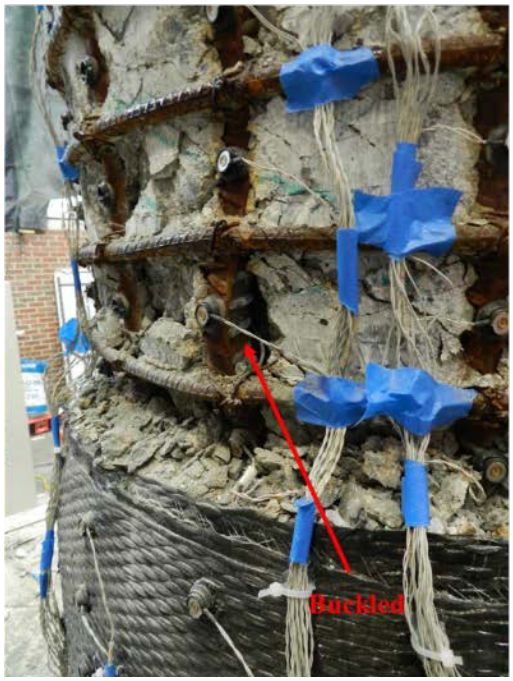

Figure 5.60 : Damage During $\mu_{4\Delta}$

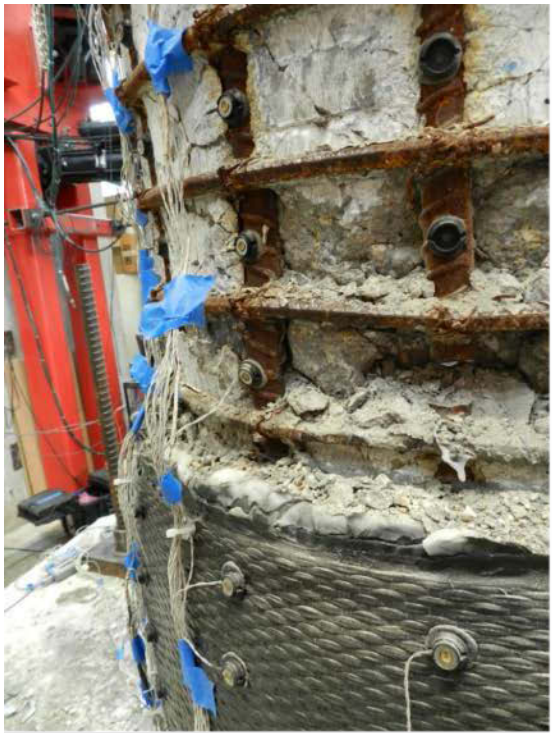

(a)

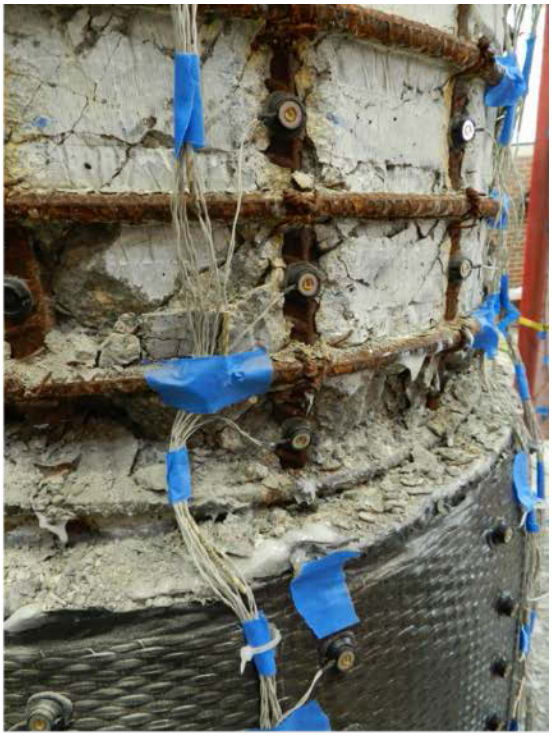

(b)

(c)

Figure 5.61 : Damage During $\mu_{4\Delta}^{1}$

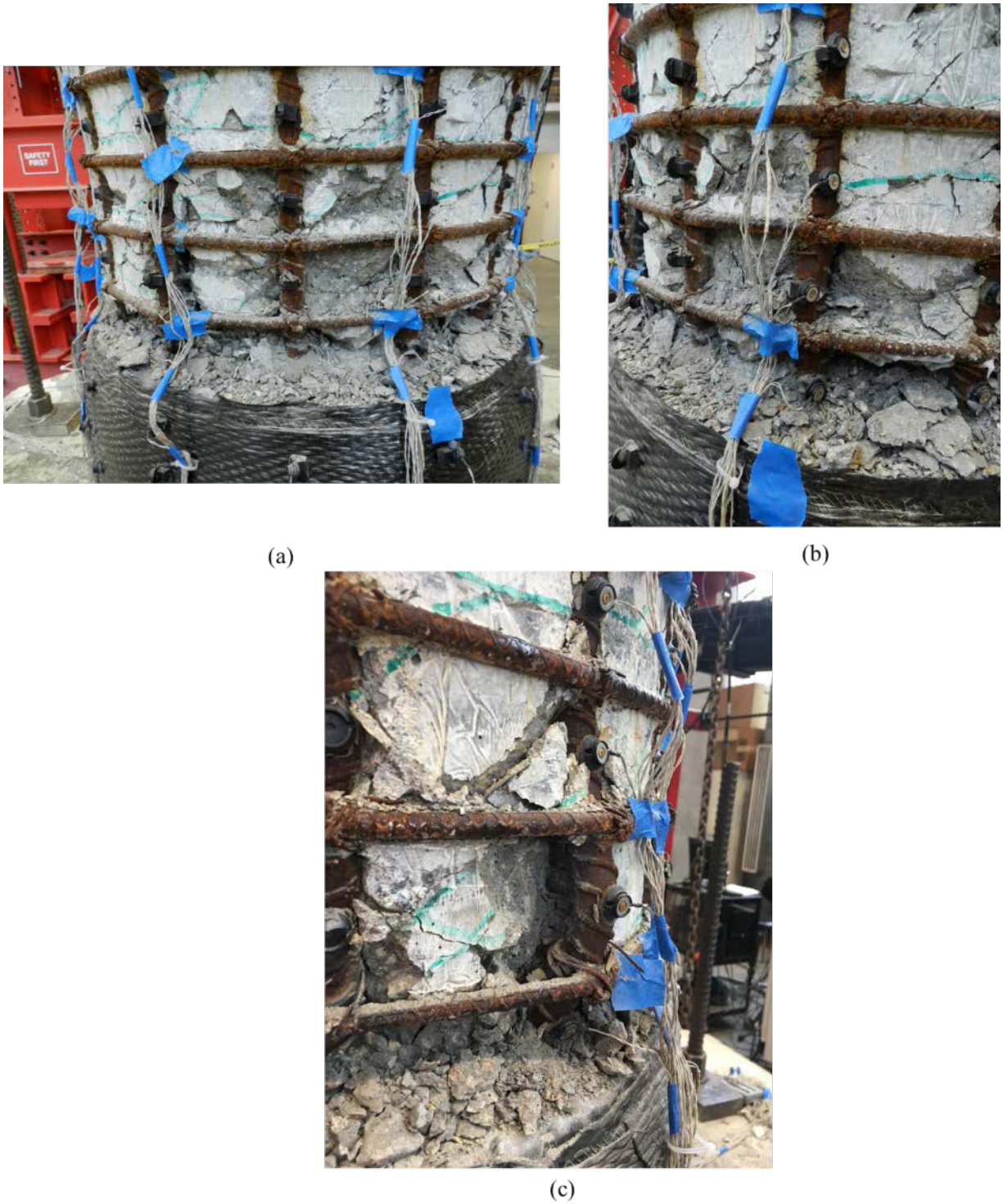

Figure 5.62 : Damage During $\mu_{4\Delta}^{1-2}$

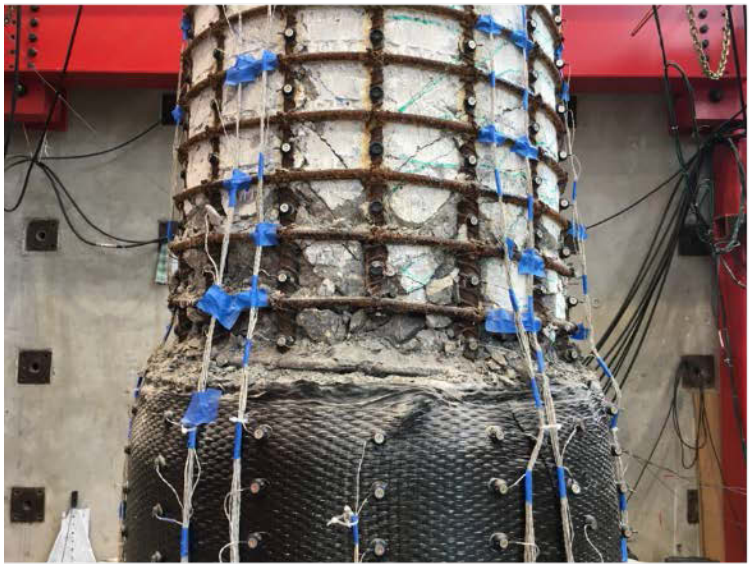

(a)

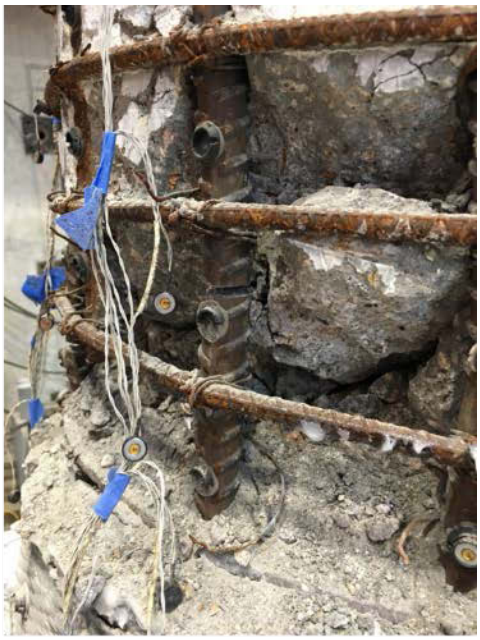

(b)

(c)

Figure 5.63 : Damage During $\mu_{4\Delta-}^{2}\ \mu_{5\Delta}^{\pm y1}$

5.3.3.2 Strain History of Extreme Fiber Reinforcing Bars and Vertical Strain Profiles

Since extreme fiber bars (Ns2, Ss2, Es2 and Ws2) at each side of the column was severed to reduced demand on the columns, OPTOTRAK Led markers were only placed on the bars which were intact at the new plastic hinge region. In addition, LED markers were placed on the repair to collect data during experiment. Designation of reinforcing bars in new hinge region is shown in Figure 5.64. Strain history of each reinforcing bar on the left of each extreme bars were shown in Figure 5.65 and Figure 5.66. Each bar reached substantial strain and showed visible buckling at the end of displacement ductility level four which corresponded to 6 inches of lateral displacement. Figure 5.67 and Figure 5.68 show the axial strain profile of the column for Ns3, Ss3, and Es3 and Ws3. Axial strain profile of the column indicates that plastic hinge formed just above the repair, and column went through large amount of rotation at the end of testing.

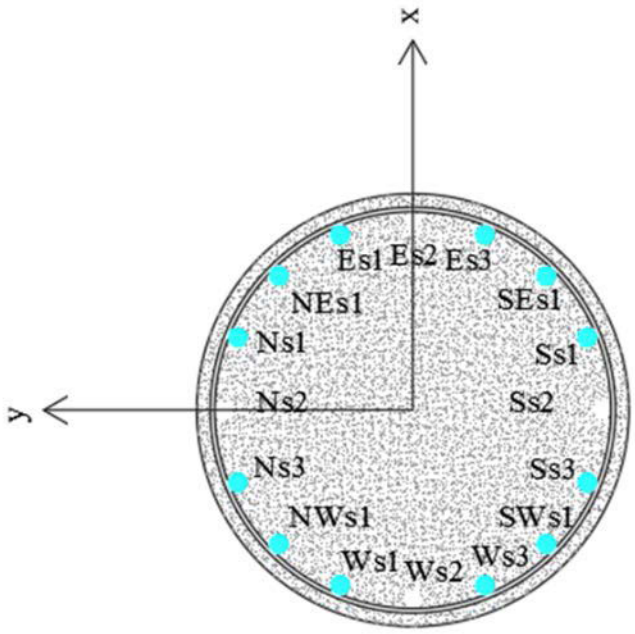

Figure 5.64 : Designation of Reinforcing Bars in New Plastic Hinge Region

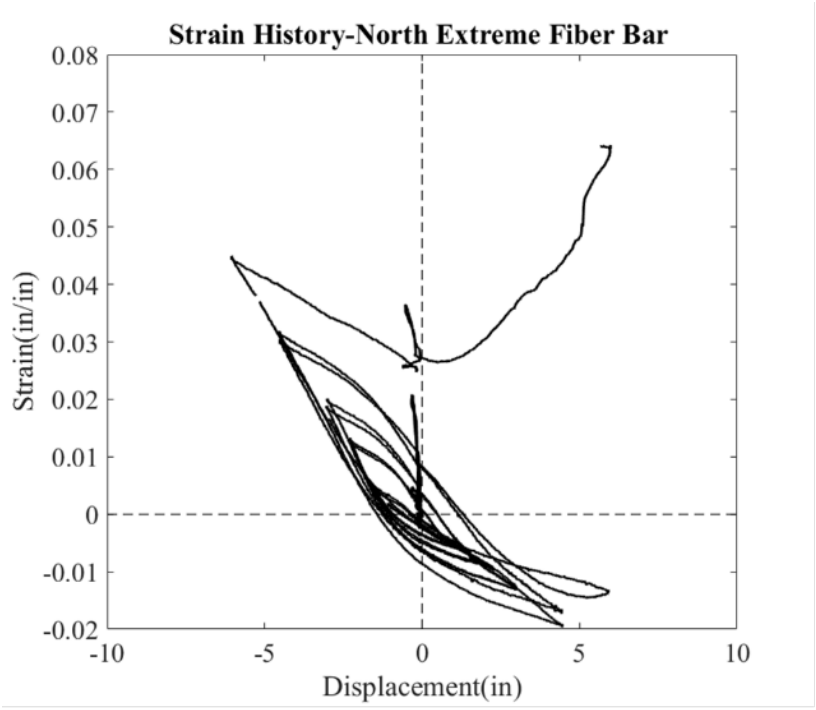

(a)

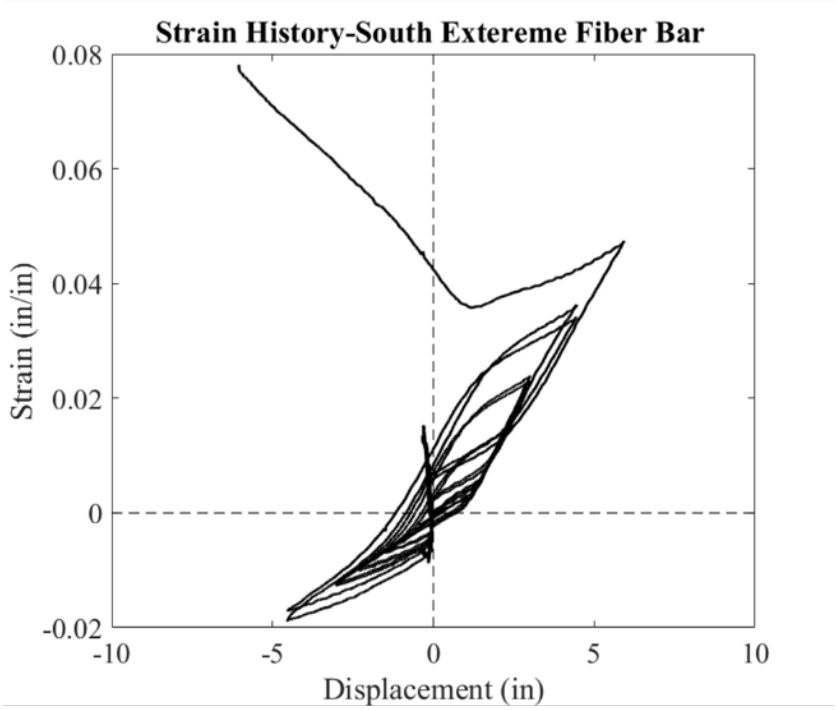

(b)

Figure 5.65 : Strain History of Extreme a) Ns3 b) Ss3

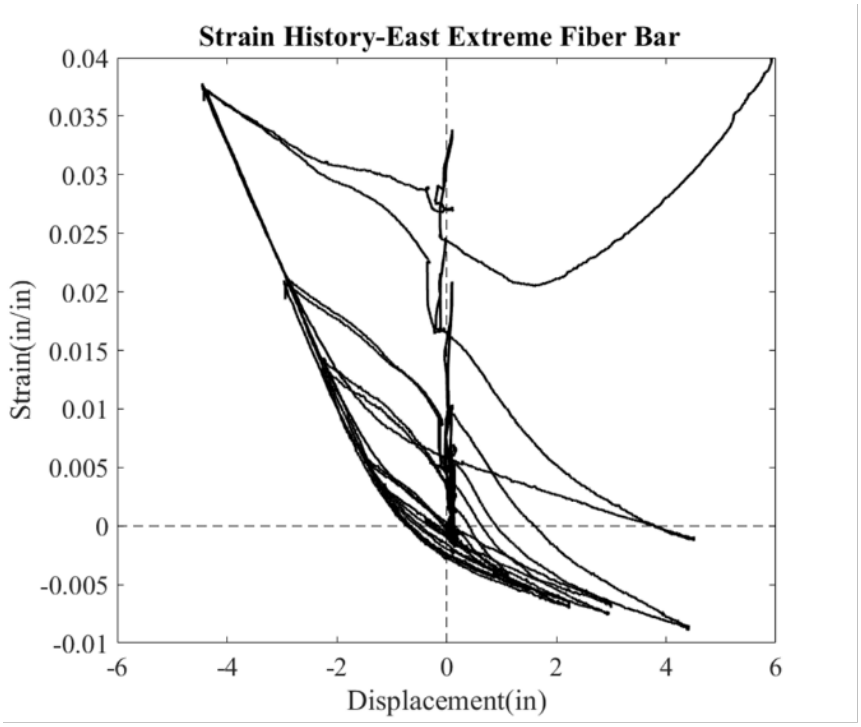

(a)

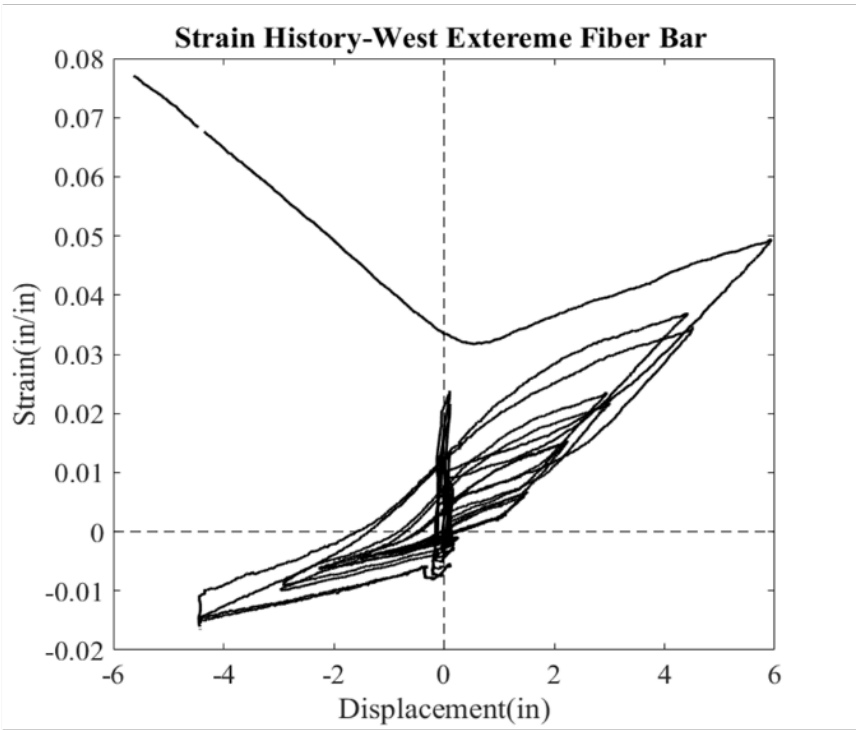

(b)

Figure 5.66 : Strain History of Extreme a) Es3 b) Ws3

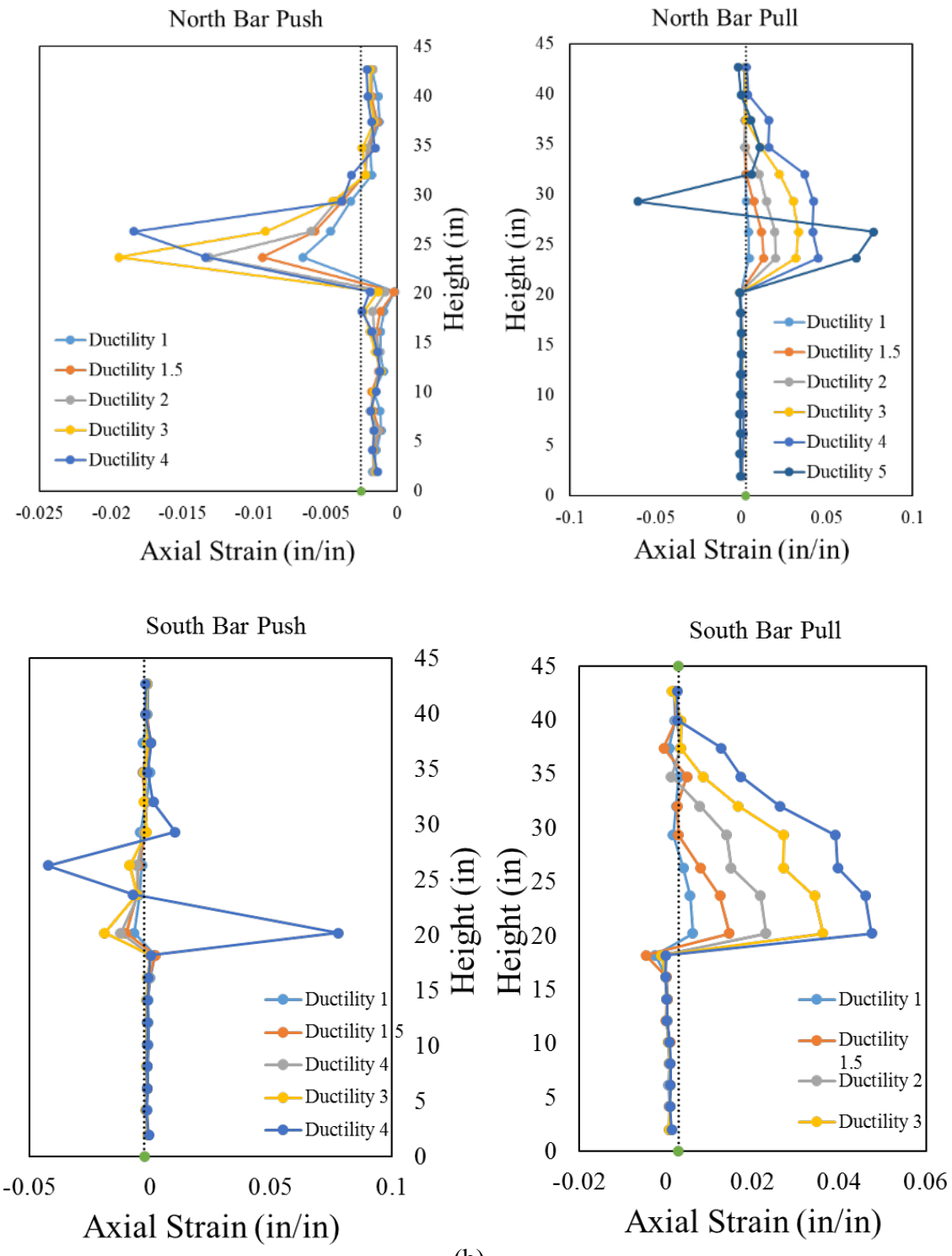

(b)

Figure 5.67 : Axial Strain Profile of Extreme a) Ns3 b) Ss3

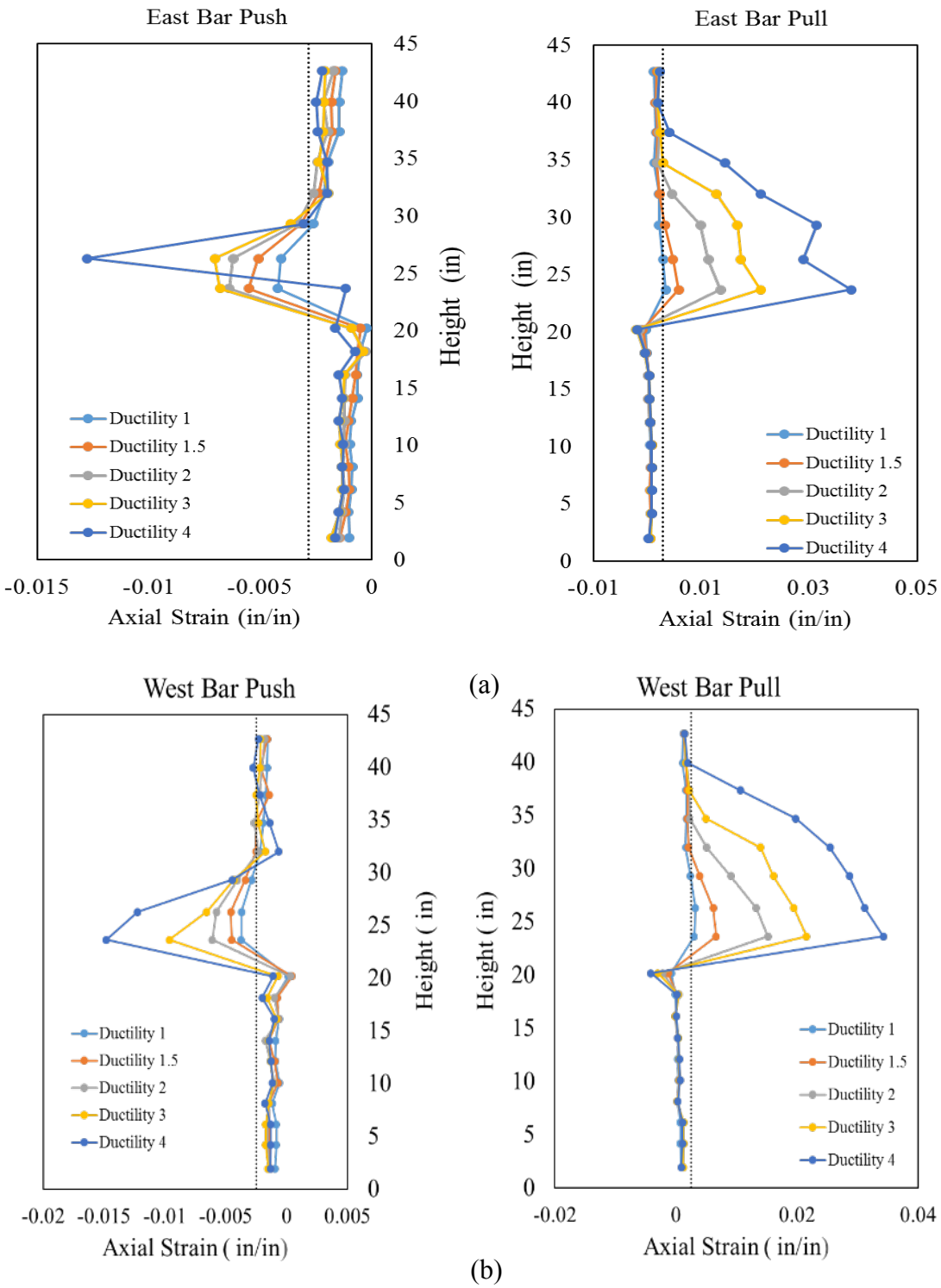

Figure 5.68 : Axial Strain Profile of Extreme a) Es3 b) Ws3

5.3.3.3 Force-Displacement Response of C2 Column

Force-displacement response of the C2 column specimen for x and y-directions are given in Figure 5.69 and Figure 5.70. Force in the column in both directions was slightly larger than the original column till ductility level four. As it can be seen in Figure 5.69 and Figure 5.70, for both direction, column initial stiffness increased. Due to the buckling of reinforcing bars, strength substantially dropped for +x direction for the second cycle of displacement ductility four. Due to the rupture of reinforcing, target displacement was not reached. Thus, lateral load was substantially small at the second cycle of displacement ductility level four. Similarly, strength loss was observed in the + y and – y direction, due to buckling of reinforcing bars in the new hinge region at the second cycle of displacement ductility level four. Rupture of the reinforcing bars occurred when the column was pushed and pulled in + y and –y direction for the first cycle of ductility level five. It can be seen in Figure 5.70, rupture of the reinforcing bar occurred before reaching target displacement. In conclusion, moment strength of the column was noticeably restored for both direction of the column.

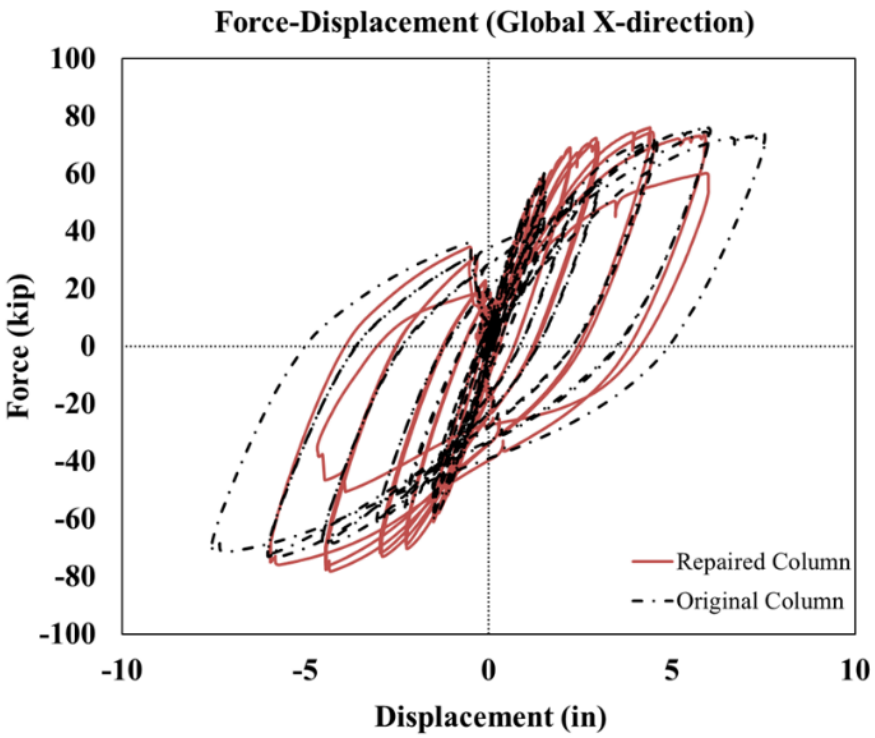

Figure 5.69 : Force-Displacement Response in X direction

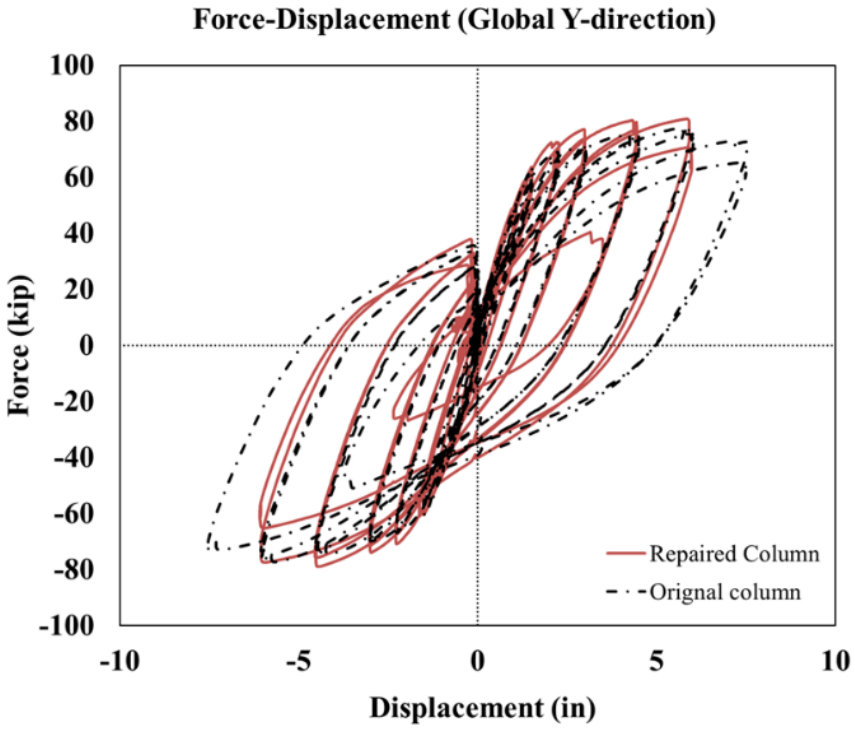

Figure 5.70 : Force-Displacement Response in Y direction

5.3.4 Conclusion for C2 Column Test

Several conclusions were drawn from the column test:

- Plastic hinge was relocated above the repair region without inducing damage to the CF anchors.
- The estimation of the capacity of the 1-1/4 CFRP anchors was reasonable for given CF anchor details.
- The length of the vertical sheet was adequate for design.
- Five layers of hoop fibers were enough to prevent debonding of anchor. Moreover, confinement provided by hoop fibers were adequate to prevent any failure that may lead to failure of the repair system.
- Material models, which were adopted for sectional analysis, was appropriate.

Chapter 6: Summary, Conclusions and Recommendations

6.1 Summary

Initially, an understanding on CF anchors were developed to produce a reasonable approach for a repair design. The direct tension test showed that capacity of the anchor varied as the preparation method improved. In addition, it was observed that efficiency of anchors decreases for larger diameter. Thus, there is no linear correlation between diameter and anchor capacity. Anchor fan angle was found to be an important parameter since capacity of the anchor primarily depends on the width of the fan. The test conducted on fanned anchor showed that debonding is inevitable for the repaired of the columns. Thus, an anchorage method was needed to prevent debonding of CF anchors from column surface. Providing hoop fibers was shown to be a reasonable approach. Moreover, the method used to determine the required layer of hoop fibers were promising although a refined solution is needed. The repair of reinforced concrete circular columns with buckled and fractured bars were conducted using the CFRP sheets and the CF anchors. Using plastic relocation concept, the moment and displacement capacity was shown to be restored. The capacity of 1 and 1-1/4 inch-diameter CFRP anchors was estimated using direct tension test results. Although the capacity estimation for one-inch-diameter CF anchor was slightly off, the moment capacity of the column was restored, but due to the rupture of the CF anchors, the repair was deemed to be failed. For the second test, with appropriate material properties, it was shown that plastic hinge relocation was achieved. A complete and effective methodology was developed to repair flexural failed modern reinforced concrete bridge columns.

6.2 Conclusions and Recommendations

The experimental program led to following conclusion.

1. More direct tension tests are required to determine design stress limits for the CF anchors.
2. More column tests are needed to determine an optimum anchor fan width and anchor fan length.
3. Columns with a single fractured bar can be effectively repaired using CFRP sheets and anchors.
4. Plastic hinge relocation enables restoration of moment and displacement capacity of original column.
5. One column diameter height is an appropriate repaired height.
6. The shear friction model can be used to determine number of hoop fiber to prevent debonding of CFRP anchor fan. Ten inches overlapped is enough to prevent debonding of hoop fibers. A design strain of 0.0058 for determination of the number of hoop fiber layers is reasonable.
7. Vertical CFRP sheets should be used to sandwich CFRP anchors to produce a uniform stress distribution around circumference of the column, and to control location of new plastic hinge.
8. The CFRP anchor fan length is important for the development of full capacity of the CFRP anchor by preventing debonding of anchor fan. Thus, the suggested fan length is 22 in for 15 in fan width for 1 in and 1-1/4 in diameter CF anchors.
9. The length of vertical CFRP sheets should be equal to repair height and should extend beyond the height of the CF anchor fan.
10. Minimum embedment length for 1-inch-diameter and 1-1/4-inch-diameter are 15 inches and 18 inches, respectively.

6.3 Future Work

Based on the results of testing program presented in this report, several topics are recommended for future study include:

1. Perform more direct tension tests to determine design limit states.
2. Perform more direct tension tests with different fanning angle to determine capacity of an anchor for a given diameter.
3. Perform more column bending tests to determine minimum fan length for a given angle.
4. Improve shear friction model to determine optimum number of hoop fibers with more column test.
5. Perform columns tests with fractured bars to determine limit where repair is feasible.

References

[1] S. T. Rutledge, M. J. Kowalsky, R. Seracino, and J. M. Nau, "Repair of reinforced concrete bridge columns containing buckled and fractured reinforcement by plastic hinge relocation," *J. Bridg. Eng.*, vol. 19, no. 8, p. A4013001, 2014.

[2] K. Kobayashi, F. S., Y. Y., T. H., and S. T., "Advanced wrapping system with CF anchor – Stress Transfer Mechanism of CF Anchor," *5th Int. Symp. Fiber-Reinforced Polym. Reinf. Concr. Struct.*, pp. 379–388, 2001.

[3] J. G. Teng, J. F. Chen, S. T. Smith, and L. Lam, "FRP : Strengthened RC Structures," *Front. Phys.*, p. 266, 2002.

[4] I. Vrettos, E. Kefala, and T. C. Triantafillou, "Innovative Flexural Strengthening Of Reinforced Concrete Columns Using Carbon-Fiber Anchors_Vrettos et al_2013.pdf," no. 110, 2013.

[5] R. He, L. H. Sneed, and A. Belarbi, "Rapid Repair of Severely Damaged RC Columns with Different Damage Conditions: An Experimental Study," *Int. J. Concr. Struct. Mater.*, vol. 7, no. 1, pp. 35–50, 2013.

[6] M. R. Ehsani, H. Saadatmanesh, and S. Tao, "Design Recommendations for Bond of GFRP Rebars to Concrete," *J. Struct. Eng.*, vol. 122, no. 3, pp. 247–254, 1996.

[7] A. Vosooghi and M. S. Saiidi, "Design Guidelines for Rapid Repair of Earthquake-Damaged Circular RC Bridge Columns Using CFRP," *J. Bridg. Eng.*, no. September, p. 120725052316002, 2012.

[8] Y. Yang, L. H. Sneed, A. Morgan, M. S. Saiidi, and A. Belarbi, "Repair of RC bridge columns with interlocking spirals and fractured longitudinal bars - An experimental study," *Constr. Build. Mater.*, vol. 78, pp. 405–420, 2015.

[9] E. del R. Castillo, R. Rogers, M. C. Griffith, and J. M. Ingham, "Tensile Strength of Straight Frp Anchors in Rc Structures," no. December, pp. 14–16, 2015.

[10] E. del Rey Castillo, M. C. Griffith, and J. M. Ingham, "Fibre Rupture Tensile Capacity of FRP Straight Anchors," *Proc. New Zeal. Concr. Ind. Conf.*, no. October, 2016.

[11] E. del Rey Castillo, M. Griffith, and J. M. Ingham, "Force-Based Model for Straight FRP Anchors Exhibiting Fibre Rupture Failure Mode," *Proc. 8th Int. Conf. Fibre-Reinforced Polym. Compos. Civ. Eng. (CICE 2016)*, no. December, 2016.

[12] S. J. Kim and S. T. Smith, "Behaviour of Handmade FRP Anchors under Tensile Load in Uncracked Concrete," *Adv. Struct. Eng.*, vol. 12, no. 6, pp. 845–865, 2010.

[13] G. Ozdemir and U. Akyuz, "Tensile capacities of CFRP anchors," *Adv. Earthq. Eng. Urban Risk Reduct.*, pp. 471–487, 2006.

[14] T. Ozbakkaloglu and M. Saatcioglu, "Tensile Behavior of FRP Anchors in Concrete," *J. Compos. Constr.*, vol. 13, no. April, pp. 82–92, 2009.

[15] D. A. Bournas, A. Pavese, and W. Tizani, "Tensile capacity of FRP anchors in connecting FRP and TRM sheets to concrete," *Eng. Struct.*, vol. 82, pp. 72–81, 2015.

[16] S. Rutledge, R. Seracino, M. Kowalsky, and S. Witt, "FRP repair of damaged large-scale circular reinforced concrete columns," *Proc. 6th Int. Conf. FRP Compos. Civ. Eng. CICE 2012*, pp. 1–8, 2012.

[17] ASTM, "D7205," *Stand. Test Method Tensile Prop. Fiber Reinf. Polym. Matrix*, vol. i, no. Reapproved 2011, pp. 1–13, 2011.

[18] J. C. Goodnight, Y. Feng, M. J. Kowalsky, and J. M. Nau, "The effects of load history and design variables on performance limit states of circular bridge columns - Volume 1," vol. 4000, no. January, 2015.

[19] H. W. S. Inc and 10, "Discussion of 'Bond Behavior of Fiber Reinforced Polymer Bars under Direct Pullout Conditions' by Zenon...," *J. Compos. Constr.*, vol. 9, no. 1, pp. 101–104, 2005.

[20] M. K. Leo Barcley, "Seismic Behavior of Grade 80 RC Bridge Columns," 2017.

[21] H. Rasheed, B. Decker, A. Esmaeily, R. Peterman, and H. Melhem, "The Influence of CFRP Anchorage on Achieving Sectional Flexural Capacity of Strengthened Concrete Beams," *Fibers*, vol. 3, no. 4, pp. 539–559, 2015.

[22] ACI Committee 440, *ACI 440.2R-08 Guide for the Design and Construction of Externally Bonded FRP Systems*. 2008.

[23] J. C. Goodnight, M. J. Kowalsky, and J. M. Nau, "Seismic Load Path Effects in Reinforced Concrete Bridge Columns and Wall Piers," 2017.

[24] J. Garcia, W. Sun, C. Kim, W. M. Ghannoum, and J. O. Jirsa, "Procedures for the

Installation and Quality Control of Anchored CFRP Sheets for Shear Strengthening of Concrete Bridge Girders," vol. 7, p. 41, 2014.

[25] J. B. Mander, M. J. N. Priestley, and R. Park, "THEORETICAL STRESS-STRAIN MODEL FOR CONFINED CONCRETE," *J. Struct. Eng.*, 1988.

[26] "OpenSees Command Language Manual." [Online]. Available: http://opensees.berkeley.edu/OpenSees/manuals/usermanual/OpenSeesCommandLanguageManualJune2006.pdf.